frontiers | Research Topics

Exploring 'omic' biomarkers in animal production and reproduction

Edited by
Manuel Garcia-Herreros, Pedro Aponte and Miguel A. Gutiérrez Reinoso

Published in
Frontiers in Veterinary Science

ISSN 1664-8714
ISBN 978-2-8325-6933-7
DOI 10.3389/978-2-8325-6933-7

Generative AI statement
Any alternative text (Alt text) provided alongside figures in the articles in this ebook has been generated by Frontiers with the support of artificial intelligence and reasonable efforts have been made to ensure accuracy, including review by the authors wherever possible. If you identify any issues, please contact us.

About Frontiers

Frontiers is more than just an open access publisher of scholarly articles: it is a pioneering approach to the world of academia, radically improving the way scholarly research is managed. The grand vision of Frontiers is a world where all people have an equal opportunity to seek, share and generate knowledge. Frontiers provides immediate and permanent online open access to all its publications, but this alone is not enough to realize our grand goals.

Frontiers journal series

The Frontiers journal series is a multi-tier and interdisciplinary set of open-access, online journals, promising a paradigm shift from the current review, selection and dissemination processes in academic publishing. All Frontiers journals are driven by researchers for researchers; therefore, they constitute a service to the scholarly community. At the same time, the *Frontiers journal series* operates on a revolutionary invention, the tiered publishing system, initially addressing specific communities of scholars, and gradually climbing up to broader public understanding, thus serving the interests of the lay society, too.

Dedication to quality

Each Frontiers article is a landmark of the highest quality, thanks to genuinely collaborative interactions between authors and review editors, who include some of the world's best academicians. Research must be certified by peers before entering a stream of knowledge that may eventually reach the public - and shape society; therefore, Frontiers only applies the most rigorous and unbiased reviews. Frontiers revolutionizes research publishing by freely delivering the most outstanding research, evaluated with no bias from both the academic and social point of view. By applying the most advanced information technologies, Frontiers is catapulting scholarly publishing into a new generation.

What are Frontiers Research Topics?

Frontiers Research Topics are very popular trademarks of the *Frontiers journals series*: they are collections of at least ten articles, all centered on a particular subject. With their unique mix of varied contributions from Original Research to Review Articles, Frontiers Research Topics unify the most influential researchers, the latest key findings and historical advances in a hot research area.

Find out more on how to host your own Frontiers Research Topic or contribute to one as an author by contacting the Frontiers editorial office: frontiersin.org/about/contact

Exploring 'omic' biomarkers in animal production and reproduction

Topic editors
Manuel Garcia-Herreros — National Institute for Agricultural and Veterinary Research (INIAV), Portugal
Pedro Aponte — Universidad San Francisco de Quito, Ecuador
Miguel A. Gutiérrez Reinoso — Universidad Técnica de Cotopaxi, Ecuador

Citation
Garcia-Herreros, M., Aponte, P., Gutiérrez Reinoso, M. A., eds. (2025). *Exploring 'omic' biomarkers in animal production and reproduction*. Lausanne: Frontiers Media SA. doi: 10.3389/978-2-8325-6933-7

Table of contents

frontiers | Frontiers in Veterinary Science

TYPE Editorial
PUBLISHED 23 September 2025
DOI 10.3389/fvets.2025.1688780

OPEN ACCESS

EDITED AND REVIEWED BY
Regiane R. Santos,
Schothorst Feed Research, Netherlands

*CORRESPONDENCE
Pedro M. Aponte
✉ apontep@gmail.com
Manuel García-Herreros
✉ herrerosgm@gmail.com

RECEIVED 19 August 2025
ACCEPTED 09 September 2025
PUBLISHED 23 September 2025

CITATION
Aponte PM, Gutiérrez-Reinoso MA and García-Herreros M (2025) Editorial: Exploring 'omic' biomarkers in animal production and reproduction. *Front. Vet. Sci.* 12:1688780. doi: 10.3389/fvets.2025.1688780

Editorial: Exploring 'omic' biomarkers in animal production and reproduction

Pedro M. Aponte[1,2]*, Miguel A. Gutiérrez-Reinoso[3,4] and Manuel García-Herreros[5,6]*

[1]Colegio de Ciencias Biológicas y Ambientales (COCIBA), Universidad San Francisco de Quito (USFQ), Quito, Ecuador, [2]Instituto de Investigaciones en Biomedicina "One-Health", Universidad San Francisco de Quito (USFQ), Campus Cumbayá, Quito, Ecuador, [3]Facultad de Ciencias Agropecuarias y Recursos Naturales, Carrera de Medicina Veterinaria, Universidad Técnica de Cotopaxi (UTC), Latacunga, Ecuador, [4]Laboratorio de Biotecnología Animal, Departamento de Ciencia Animal, Facultad de Ciencias Veterinarias, Universidad de Concepción (UdeC), Chillán, Chile, [5]Instituto Nacional de Investigação Agrária e Veterinária (INIAV), Santarém, Portugal, [6]CIISA-AL4AnimalS, Faculty of Veterinary Medicine, University of Lisbon, Lisbon, Portugal

KEYWORDS

genomics, transcriptomics, proteomics, metabolomics, animal production, animal reproduction

Editorial on the Research Topic
Exploring 'omic' biomarkers in animal production and reproduction

Introduction

Animal reproduction and breeding are advancing at an unprecedented pace, closely aligned with technological innovation. While the field has historically relied on phenotypic selection to improve traits of interest, the emergence of high-throughput "omics" technologies (genomics, transcriptomics, proteomics, and metabolomics) is opening new possibilities for understanding the molecular basis of productivity, fertility, health, and welfare (1–5). Omics, especially when integrated with Assisted Reproductive Technologies (ARTs), enable the identification of precise biomarkers that can guide selection, diagnosis, and intervention strategies. The present Research Topic brings together recent advances aimed at uncovering and applying molecular indicators to enhance reproductive efficiency and overall performance in diverse animal production systems.

The diversity of species represented, from dairy goats and sheep to cattle, buffalo and avians (such as hens and geese), underscores the global relevance and adaptability of these tools. Collectively, the featured studies reflect an international effort to harness molecular insights for a more efficient, resilient, and sustainable livestock production.

Genomics and transcriptomics

Key contributions demonstrate how genomic and transcriptomic analyses can uncover fundamental regulatory mechanisms, identify novel molecular markers, and inform breeding strategies to improve reproductive efficiency across species.

Shi et al. investigated the seasonal reproductive physiology of dairy goats by integrating transcriptomic and proteomic analyses of ovarian tissues collected during breeding and non-breeding seasons. Their work revealed marked reductions in gonadotropin levels and follicular size during the non-breeding period, underpinned by over 1,000 differentially expressed genes and more than 500 differentially expressed proteins. Common molecules, such as *TMEM205*, *TM7SF2*, *SLC35G1*, *GSTM1*, and *ABHD6*, were identified as potential mediators of suppressed follicular development via steroid hormone biosynthesis pathways.

Turning to poultry, Xiong et al. focused on the regulatory role of non-coding RNAs (ncRNAs) in ovarian atresia associated with broodiness in hens—a behavior detrimental to egg production. Using whole-transcriptome sequencing, they identified hundreds of differentially expressed MicroRNAs (miRNAs), Long Noncoding RNAs (lncRNAs), and circular RNAs (circRNAs), and constructed a competing endogenous RNAs (ceRNAs) network. Candidate genes such as *THBS1* and *MYLK*, which are regulated by specific miRNAs and circRNAs, were linked to pathways involved in ovarian function, including extracellular matrix (ECM)–receptor interactions, cytokine signaling, and hormone secretion.

From a structural genomics perspective, Zhao et al. examined copy number variations (CNVs) in Guizhou Black goats with divergent litter sizes. Through genome-wide selection signal analysis, they identified 180 CNVs and 49 candidate genes enriched in critical fertility pathways, such as Hippo signaling, steroid hormone biosynthesis, and retinol metabolism, highlighting the potential of CNVs as valuable genomic markers for selective breeding to enhance prolificacy in goats.

Finally, Xi et al. profiled miRNA expression across key developmental stages of sheep testes, from birth to maturity, identifying over 1,200 known and novel miRNAs. Differential expression analyses and pathway enrichment identified target genes such as *YAP1*, *ITGB1*, and *SOX9* in reproductive signaling pathways, including the FOXO, Hippo, Wnt, and MAPK pathways.

Proteomics

Recent advances in proteomic technologies have enabled the identification of protein signatures that underpin reproductive physiology. These signatures offer valuable biomarkers for fertility assessment and improvement in livestock and avian species. Maulana et al. provided the first comprehensive proteomic characterization of seminal plasma and sperm in Toraya buffalo, revealing four key proteins—ADAM32 in seminal plasma and ZPBP, SPACA3, and CCDC136 in sperm—that are integral to motility, energy production, and acrosome formation. These findings, coupled with the enrichment of proteins in the tricarboxylic acid (TCA) cycle, highlight the metabolic underpinnings of sperm function in this indigenous Indonesian breed. Turning to avian reproduction, Yuan et al. explored lipid droplet-associated proteins (LDAPs) in the granulosa cells of goose follicles at hierarchical and pre-hierarchical stages, uncovering ACSL3 as a potential regulator of lipid metabolism via the fatty acid degradation pathway.

Proteomic biomarkers have also been employed to model and assess reproductive stress conditions. Liang et al. established an oxidative stress mouse model induced by hydrogen peroxide, profiling serum proteins alongside oxidative damage markers. This approach revealed shifts in antioxidant enzyme activities (CAT, SOD, and GSH-Px) and structural ovarian changes, providing a framework for studying protein-mediated stress responses that affect fertility. Finally, in Simmental bulls, Satrio et al. demonstrated that age significantly shapes the sperm proteome, with younger bulls expressing proteins linked to acrosome assembly (SPACA1) and spermatid development, middle-aged bulls showing markers of motility (PEBP4) and decapacitation (PEBP1), and older bulls exhibiting proteins related to capacitation-associated hyperactivity (Tubulin).

Metabolomics

Metabolomics approaches are increasingly revealing the small-molecule signatures that reflect reproductive efficiency, stress resilience, and metabolic health in livestock, offering prospects for non-invasive monitoring and targeted interventions. In the context of bovine reproduction, Su et al. profiled serum metabolites at three key stages of superovulation: before FSH injection, before insemination, and before embryo collection. They identified consistent differences between high- and low-yield donors. Lipid-related metabolites, including specific phosphatidylcholines, phosphatidylethanolamines, triacylglycerols, phosphatidylinositols, and phosphatidylserines, emerged as candidate biomarkers linked to amino acid and fatty acid metabolism and ovarian steroidogenesis, providing a biochemical basis for donor selection in embryo transfer programs.

Zang et al. employed a metabolomics approach to investigate how cryopreservation disrupts mitochondrial energy metabolism in goat sperm. They documented structural mitochondrial damage, ATP depletion, and oxidative stress, alongside marked reductions in key energy- and antioxidant-related metabolites such as capric acid, creatine, and cholesterol sulfate. Functional validation showed that supplementing freezing extenders with capric acid significantly improved post-thaw motility, demonstrating a direct link between metabolite supplementation and fertility preservation.

At the herd-management scale, Magro et al. investigated metabolic profiling in dairy cows during the high-risk transition period by comparing invasive blood sampling with milk mid-infrared (MIR) spectroscopy. They found that MIR could moderately predict blood β-hydroxybutyrate and non-esterified fatty acids, which are critical indicators of negative energy balance, and accurately predict urea levels. Although MIR is not yet precise enough for individual diagnostics, its utility for herd-level screening and genetic evaluation underscores the role of metabolomics in large-scale, non-invasive metabolic health monitoring.

Taken together, the manuscripts in this Research Topic highlight how genomics, transcriptomics, proteomics, and metabolomics are converging to provide innovative insights into reproductive biology and animal sciences. Genomic and transcriptomic studies reveal regulatory mechanisms and potential molecular markers, while proteomics identifies protein networks that underpin fertility, and metabolomics captures physiological and metabolic signatures linked to reproductive efficiency and

stress. By covering species ranging from goats and cattle to poultry and buffalo, this collective work demonstrates both the breadth of application and the translational potential of omics biomarkers across animal industries.

Conclusion and perspectives

The "omics revolution," which spans genomics, transcriptomics, proteomics, metabolomics, and now epigenomics, along with single-cell and spatial approaches, has transformed animal reproduction and production science by providing unprecedented insight into complex biological processes. The manuscripts in this Research Topic exemplify how these tools have already advanced the identification of molecular markers linked to fertility, prolificacy, stress resilience, and metabolic health across diverse species. Current applications are tangible: Single Nucleotide Polymorphisms (SNPs) and CNVs are guiding breeding programs; proteomic and metabolomic profiles are informing donor selection and cryopreservation strategies; and non-invasive metabolic screening is beginning to support herd-level management. These advances demonstrate that omics biomarkers are no longer confined to the discovery stage and are progressively entering applied contexts in assisted reproduction, nutritional monitoring, and fertility preservation.

Looking ahead, the challenge lies in moving beyond isolated datasets to integrated, hypothesis-driven, multi-omics research that bridges molecular discovery with functional validation. Progress will depend on strengthening species-specific functional databases, developing standardized protocols for reproducibility, and embracing computational advances, such as artificial intelligence and machine learning, to process complex datasets and enhance predictive modeling. The integration of "omics" with precision livestock farming and international collaborative frameworks, such as the Functional Annotation of Animal Genomes (FAANG) Consortium initiative, will accelerate genome-to-phenome understanding and the design of targeted interventions. By aligning these technological advances with the goals of sustainability, climate resilience, and animal welfare, the field is poised to deliver transformative impacts, shaping future livestock systems that are not only more productive and efficient but also more ethical and robust in the face of emerging global challenges.

Author contributions

PA: Validation, Writing – original draft. MG-R: Validation, Writing – review & editing. MG-H: Validation, Writing – review & editing.

Conflict of interest

The authors declare that the research was conducted in the absence of any commercial or financial relationships that could be construed as a potential conflict of interest.

Generative AI statement

The author(s) declare that no Gen AI was used in the creation of this manuscript.

Any alternative text (alt text) provided alongside figures in this article has been generated by Frontiers with the support of artificial intelligence and reasonable efforts have been made to ensure accuracy, including review by the authors wherever possible. If you identify any issues, please contact us.

Publisher's note

References

1. Ayantoye JO, Kolachi HA, Zhang X, Shahzad M, Kandil OMT, Wan P, et al. Advances in timed artificial insemination: integrating omics technologies for enhanced reproductive efficiency in dairy cattle. *Animals.* (2025) 15:816. doi: 10.3390/ani15060816

2. Elrashedy A, Mousa W, Nayel M, Salama A, Zaghawa A, Elsify A, et al. Advances in bioinformatics and multi-omics integration: transforming viral infectious disease research in veterinary medicine. *Virol J.* (2025) 22:22. doi: 10.1186/s12985-025-02640-x

3. Perera TRW, Skerrett-Byrne DA, Gibb Z, Nixon B, Swegen A. The future of biomarkers in veterinary medicine: emerging approaches and associated challenges. *Animals.* (2022) 12:2194. doi: 10.3390/ani12172194

4. Suh JH. Critical review: metabolomics in dairy science - evaluation of milk and milk product quality. *Food Res Int.* (2022) 154:110984. doi: 10.1016/j.foodres.2022.110984

5. Worku D, Hussen J, De Matteis G, Schusser B, Alhussien MN. Candidate genes associated with heat stress and breeding strategies to relieve its effects in dairy cattle: a deeper insight into the genetic architecture and immune response to heat stress. *Front Vet Sci.* (2023) 10:1151241. doi: 10.3389/fvets.2023.1151241

frontiers | Frontiers in Veterinary Science

TYPE Original Research
PUBLISHED 29 May 2024
DOI 10.3389/fvets.2024.1399776

OPEN ACCESS

EDITED BY
Miguel A. Gutiérrez Reinoso,
Universidad Técnica de Cotopaxi, Ecuador

REVIEWED BY
Zhuanjian Li,
Henan Agricultural University, China
Jingyi Li,
Huazhong Agricultural University, China
Haihan Zhang,
Hunan Agricultural University, China

*CORRESPONDENCE
Lingbin Liu
✉ liulb515@163.com

RECEIVED 12 March 2024
ACCEPTED 08 May 2024
PUBLISHED 29 May 2024

CITATION
Xiong H, Li W, Wang L, Wang X, Tang B, Cui Z and Liu L (2024) Whole transcriptome analysis revealed the regulatory network and related pathways of non-coding RNA regulating ovarian atrophy in broody hens. *Front. Vet. Sci.* 11:1399776.
doi: 10.3389/fvets.2024.1399776

Whole transcriptome analysis revealed the regulatory network and related pathways of non-coding RNA regulating ovarian atrophy in broody hens

Hanlin Xiong, Wendong Li, Lecong Wang, Xuchen Wang, Bincheng Tang, Zhifu Cui and Lingbin Liu*

College of Animal Science and Technology, Southwest University, Chongqing, China

Poultry broodiness can cause ovarian atresia, which has a detrimental impact on egg production. Non-coding RNAs (ncRNAs) have become one of the most talked-about topics in life sciences because of the increasing evidence of their novel biological roles in regulatory systems. However, the molecular mechanisms of ncRNAs functions and processes in chicken ovarian development remain largely unknown. Whole-transcriptome RNA sequencing of the ovaries of broodiness and laying chickens was thus performed to identify the ncRNA regulatory mechanisms associated with ovarian atresia in chickens. Subsequent analysis revealed that the ovaries of laying chickens and those with broodiness had 40 differentially expressed MicroRNA (miRNAs) (15 up-regulated and 25 down-regulated), 379 differentially expressed Long Noncoding RNA (lncRNAs) (213 up-regulated and 166 down-regulated), and 129 differentially expressed circular RNA (circRNAs) (63 up-regulated and 66 down-regulated). The competing endogenous RNAs (ceRNA) network analysis further revealed the involvement of ECM-receptor interaction, AGE-RAGE signaling pathway, focal adhesion, cytokine-cytokine receptor interaction, inflammatory mediator regulation of TRP channels, renin secretion, gap junction, insulin secretion, serotonergic synapse, and IL-17 signaling pathways in broodiness. Upon further analysis, it became evident that *THBS1* and *MYLK* are significant candidate genes implicated in the regulation of broodiness. The expression of these genes is linked to miR-155-x, miR-211-z, miR-1682-z, gga-miR-155, and gga-miR-1682, as well as to the competitive binding of novel_circ_014674 and MSTRG.3306.4. The findings of this study reveal the existence of a regulatory link between non-coding RNAs and their competing mRNAs, which provide a better comprehension of the ncRNA function and processes in chicken ovarian development.

KEYWORDS

broodiness, ovarian development, whole transcriptome analysis, ncRNAs, ceRNA network

Introduction

Broodiness, a natural maternal behavior observed in chickens, turkeys, and geese, is characterized by appetite loss and a halt in egg-laying and incubation activities. This phenomenon poses a challenge to the progress of the modern poultry industry. Generally, broodiness is initiated by a signal that stops egg production (1). The synchronization of hormones secreted by the hypothalamic-pituitary-gonadal (HPG) axis is a prerequisite for the maintenance of broodiness (2). Studies postulate that the ovary is larger in weight and volume during the laying stage than during the broodiness stage. The ovarian weight of the egg-laying chickens was 48.17 g, significantly higher than the 2.67 g weight observed in broody chickens. The upper-grade follicles in the ovary are in active development during the laying stage, while the inner of the ovary is composed of atrophic and atretic follicles during the broodiness stage (3, 4). The eukaryotic genome has a much lower gene density compared to the prokaryotic genome, reflecting an efficient evolutionary adaptation to meet its complex biological demands. Both protein-coding and non-protein-coding RNA play a role in transcriptional regulation. The human genome transcribes over 90% of its content. As a result, the majority of transcribed genes generate noncoding RNAs (ncRNAs), which have primarily function as regulatory elements (5).

Analysis of RNA sequences during DNA transcription reveals that coding RNAs, responsible for protein translation, make up only approximately 4% of total RNA. Conversely, ncRNAs are widely distributed and play diverse roles in gene regulation (6). Both protein-coding and non-protein-coding RNA play a role in transcriptional regulation. Notably, most of the transcriptome comprises ncRNAs (7). Several studies postulate that non-coding RNAs (miRNA, lncRNA, lncRNA, siRNA) play a role in controlling ovarian development and performance. In particular, miR-182 and miR-15a have been reported to modulate granulosa cell proliferation and apoptosis by altering hormone production (8, 9). LncRNAs also serve as regulators in the reproductive process of poultry. Noteworthy, Mao et al. (10) discovered 24,601 lncRNAs linked to egg production in domestic pigeons. Over the last few years, circRNA has become a popular topic in RNA research because of its involvement in the regulation of multiple molecules in organisms through post-transcriptional regulation of classical signaling pathways (11). CircDDX10 is associated with ovarian aging, circTCP11 with pig litter size, and chi_circ_0008219 with goat reproductive rate (12–14). Despite the significance of ncRNA as vital regulators in many biological processes, their molecular regulatory mechanisms during broodiness of Chengkou mountain chicken remain unknown.

Chengkou mountain chicken is a famous local chicken variety in China, mainly reared in Chongqing municipality. However, it has a low production efficiency and high breeding costs because of its strong broodiness ability (around 90%), low egg production, and slow early growth rate. This study aimed to identify and analyze the differentially expressed non-coding RNAs and their expression patterns of Chengkou mountain chicken with a normal laying ovary and ovary with broodiness using whole-transcriptome RNA-seq. The findings of this study provide insights into the molecular processes that control the broodiness of Chengkou mountain chicken, which lay a basis for the utilization of marker-assisted selection and genetic improvement of chicken.

Materials and method

Animal and tissue samples

The experimental animals were 6 chickens from the same batch obtained from the Chengkou Mountain Chickens Genetic Research Institute (Chongqing, China). The Chengkou mountain chickens exhibits favorable germplasm traits, including robust foraging ability, resistance to coarse feeding, suitability for wild grazing and free range, strong disease resistance, and high adaptability. Their egg production and broody situation were recorded daily. Three individuals exhibiting broody behavior and entering the classic broody phase 30 days earlier were chosen. Their ovarian tissues were harvested in liquid nitrogen for RNA and transcriptome sequencing and then stored at −80°C awaiting RNA extraction.

Chicken ovary histomorphology

The histological characteristics of chicken ovaries were evaluated through hematoxylin and eosin staining, following paraffin embedding of the samples and sectioning. The histological ovary micromorphology was visualized using a microscope (Olympus IX53, Japan), followed by image capture using the microphotographic system (Olympus DP71, Japan). The ultrastructure of the chicken ovaries was observed using a transmission electron microscope (TEM Hitachi HT7800/HT7700).

RNA isolation, library construction, and sequencing

The data quality of RNA Q30 in each sample was more than 92.30%, indicating that the sequencing data quality was good (Supplementary material 4). The total RNA of the ovary tissues was extracted using the Trizol reagent kit (Invitrogen, Carlsbad, CA, United States) following the manufacturer's instructions. RNA quality was assessed using an Agilent 2100 Bioanalyzer (Agilent Technologies, Palo Alto, CA, United States) and RNase-free agarose gel electrophoresis. After total RNA was extracted, rRNAs were removed to retain mRNAs and ncRNAs. The enriched mRNAs and ncRNAs were fragmented into short fragments by using fragmentation buffer and reverse transcribed into cDNA with random primers. Second-strand cDNAs were synthesized using DNA polymerase I, RNase H, dNTPs (dUTP instead of dTTP), and buffer. The cDNA fragments were then purified using the QiaQuick PCR extraction kit (Qiagen, Venlo, The Netherlands), end-repaired, poly(A) added, and ligated to Illumina sequencing adapters. The second-strand cDNAs were digested using UNG (uracil-N-glycosylase), after which they were size selected by agarose gel electrophoresis, PCR amplified, and sequenced using Illumina HiSeqTM 4000 (Gene Denovo Biotechnology Co, Guangzhou, China). Then the 3′ adapters were added and the 36–48 nt RNAs were enriched. The 5′ adapters were then ligated to the RNAs as well. The ligation products were reverse transcribed through PCR amplification, and the 140–160 bp size PCR products were enriched

to generate 6 cDNA libraries, which was sequenced using Illumina HiSeq Xten (Gene Denovo Biotechnology Co, Guangzhou, China).

Identification and analysis of miRNA, lncRNA and circRNA

To refine the raw data, we exclude reads with low quality (*Q*-value ≤20), reads that include adapters, reads shorter than 18 nt, and reads featuring polyA (15). The clean tags were then aligned with small RNAs in the GeneBank database (Release 209.0) and Rfam database (Release 11.0) to identify and remove rRNA, scRNA, snoRNA, snRNA, and tRNA. All of the clean tags were then searched against miRBase database (Release 22) to identify known (Species studied) miRNAs (exist miRNAs). After tags were annotated as mentioned previously, the annotation results were determined in this priority order: rRNA etc. > exist miRNA > exist miRNA edit > known miRNA > repeat > exon > novel miRNA > intron. The tags that cannot be annotated as any of the above molecules were recorded as unann.

Filtration of the raw data involved removing reads of low quality (*Q*-value ≤20), reads with adapters, reads composed entirely of A bases, and reads containing more than 10% unknown nucleotides. Following this, alignment of the clean data with chicken rRNA sequences using Bowtie2 facilitated the removal of reads that aligned with rRNA (16). Softwares CNCI (17) (version 2) and CPC (18) (version 0.9-r2)[1] and FEELNC (19) (version v0.2)[2] were used to assess the protein-coding potential of the novel transcripts using their default parameters. The final prediction for lncRNAs resulted from the intersection of three software programs.

The short reads alignment tool Bowtie2 (16) (version 2.2.8) was thus used to map the reads to the ribosomal RNA (rRNA) database. The rRNA-mapped reads were removed, and the remaining reads were further used for other alignments and analyses. The rRNA-removed reads from each sample were then mapped to the reference genome using HISAT2 (20) (version 2.1.1). Reads that mapped to the reference genomes were discarded, while the unmapped reads were used for circRNA identification. Anchor reads that aligned in the reversed orientation (head-to-tail) indicated circRNA splicing and were subjected to find_circ to identify the circRNAs (21). We identified ncRNAs with fold change ≥2 and FDR (false discovery rate) <0.05 in a comparison as significant DE ncRNAs.

Construction and visualization of the ceRNA network

The ceRNA network was constructed based on the ceRNA theory as follows: (1) the target relationship between miRNA and candidate ceRNA and the negative correlation of expression, (2) the positive correlation between the expression levels of candidate ceRNAs, and (3) enrichment degree of candidate ceRNA binding to the same miRNA. miRNA-target gene pairs were first identified because ceRNAs are mutually regulated by miRNAs. The target genes for differential miRNAs were then predicted as the first step in the study of ceRNA regulatory networks. The expression correlation between mRNA-miRNA, lncRNA-miRNA, and circRNA-miRNA was then evaluated using the Spearman rank correlation coefficient (SCC). Pairs with SCC <−0.7 were selected as negatively co-expressed lncRNA-miRNA pairs, mRNA-miRNA pairs, or circRNA-miRNA pairs. The mRNAs, lncRNAs, and circRNAs were miRNA target genes and were all differentially expressed. The expression correlation between lncRNA-mRNA and circRNA-mRNA was evaluated using the Pearson correlation coefficient (PCC). Pairs with PCC >0.9 were selected as co-expressed lncRNA-mRNA pairs or circRNA-mRNA pairs. Both the mRNA and lncRNA or mRNA and circRNA in these pairs were targeted and co-expressed negatively with a common miRNA. A hypergeometric cumulative distribution function test was then done to test whether the common miRNA sponges between the two genes were significant. Only the gene pairs with a *p*-value less than 0.05 were selected. For each gene pair (A, B), we denoted all their regulator miRNAs as miRNA set C (regulating gene A) and D (regulating gene B). Where x stands for the number of common miRNAs that regulate both genes, U is the number of all the miRNAs in the work, M is the size of miRNA set C, and N is the size of miRNA set D. The lncRNA-miRNA-mRNA network was constructed by assembling all the identified co-expression competing triplets, and was visualized using Cytoscape software (v3.6.0).[3]

Functional enrichment analysis

GO functional and KEGG pathway analysis of miRNA, lncRNA, and circRNA target genes was conducted using DAVID and KOBAS software (22, 23). Go terms and KEGG pathways with a *p*-value <0.05 were considered to be significantly enriched.

Validation of RNA-seq results by real-time quantitative PCR

Real-time quantitative PCR (RT-qPCR) was performed to validate the expression levels of DE circRNAs, DE lncRNAs, and DE miRNAs. Four lncRNAs, four miRNAs, and four circRNAs associated with significantly differentially expressed genes in the ovary were randomly selected for the RT-qPCR validation tests. The methods of RNA reverse transcription and real-time fluorescence quantitative PCR were conducted as per previously published protocols (24). The relevant primers were designed using Primer Premier. As stated earlier, U6 should be referred to as the steward gene sequence of miRNA (23). The methods of RNA reverse transcription and real-time fluorescence quantitative PCR were conducted as per previously published protocols (24). While GAPDH was used as the housekeeping gene for lncRNA and circRNA. The relative miRNA and mRNA expression were calculated using the $2^{-\Delta\Delta Ct}$ method (25), and data were expressed as mean ± standard deviation of the mean. The data was displayed as mean ± standard deviation, with variations analyzed via the independent-sample *t*-test, via SPSS 20.0 (SPSS Inc., United States).

1 http://cpc.cbi.pku.edu.cn/

2 https://github.com/tderrien/FEELn

3 http://www.cytoscape.org/

Results

Effect of broodiness behavior on ovarian phenotype

The ovarian volume diminished as the laying stage progressed to the broodiness stage (Figures 1A,B). During the laying stage, the ovaries contain varying developmental and atretic follicles. However, follicle development stops, and different levels of atretic follicles are observed when approaching the broodiness stage. Noteworthy, the egg-laying hens had a higher ovary weight and volume and a heftier stroma weight, than the broody chicken (Table 1). Moreover, the broody chicken did not have large yellow follicles. The hen only had a few yellow follicles, with the majority being white.

The ovaries of chicken in the broodiness group had fewer follicles, a thicker granular layer, sparse cell density, and indistinct inner and outer layers compared to the ovaries of hens in the normal laying group (Figures 1C–F). Moreover, the ultrastructure of the ovary of chicken in the broodiness group revealed a lack of nucleus and a pattern of mitochondrial aggregation (Figures 1G,H).

Effect of two different ovaries on miRNA

Transcriptome sequencing yielded 38,460,846 and 37,304,337 total raw reads from the broodiness and egg-laying groups, respectively. Subsequent filtering of the raw reads was done to acquire clean tags with more than 97% accuracy. As Figures 2A,B shown, 96.8% of miRNAs were between 20 and 24 nt in length (Supplementary material 1). In Figures 2C,D, plots are shown comparing the tag abundances of non-coding RNA in GenBank and Rfam for each sample. The proportion of existing miRNA is the highest. A miRNA expression heat map was subsequently generated for each sample to study the miRNA patterns in the samples (Figure 2E). As shown in Supplementary Figure S4, PCA principal component analysis showed intersample repeatability of AO (atrophic ovaries) and NO (normal ovaries). We also provide a violin diagram in Supplementary Figure S6, showing better correlation between samples. Moreover, 40 differential expression (DE) miRNAs were identified in comparing the broodiness and laying groups. A scatterplot analysis was performed based on the significantly different miRNAs to demonstrate the differences between the comparison groups (Figure 2F). GO and KEGG analysis of the 40 DE miRNA genes was then done to investigate the role of miRNA in the laying and broodiness groups. A total of 104 GO terms were enriched. Figures 3A,B shows the top 20 terms of biological process (BP), cellular component (CC), and molecular function (MF). GO enrichment analysis revealed that the DE miRNAs were mainly enriched in membrane-bounded organelle cytoplasm and some intracellular-related items. Additionally, the target genes were found to be involved in various metabolic pathways, including cysteine and methionine metabolism, SNARE interactions in vesicular transport, protein processing in endoplasmic reticulum, pertussis, viral protein interaction with cytokine and cytokine receptors, ferroptosis, and peroxisome pathways (Figure 3C).

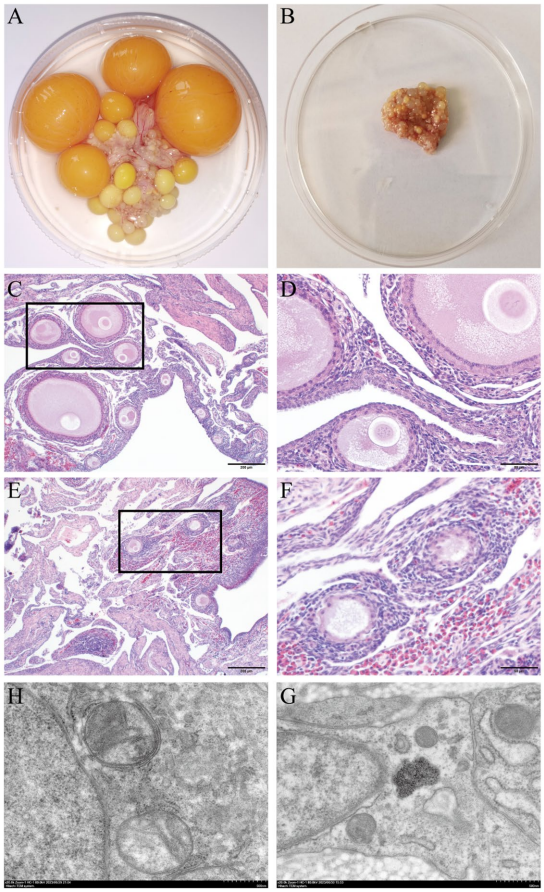

FIGURE 1
Anatomical morphological observation of ovarian tissue in poultry was conducted by examining two hematoxylin and eosin stained sections. **(A)** Normal ovarian tissue that continuously lays eggs. **(B)** Atrophy of ovaries for 30 days of broodiness. **(C)** Histological characteristics in egg-laying hens (staining at 200 μm). **(D)** Histological characteristics in egg-laying hens (staining at 50 μm). **(E)** Histological characteristics in broody hens (staining at 200 μm). **(F)** Histological characteristics in broody hens (staining at 50 μm). **(G)** The mitochondrial ultrastructure of the chicken egg-laying ovaries were analyzed by TEM. **(H)** The mitochondrial ultrastructure of the chicken broody ovaries were analyzed by TEM.

TABLE 1 A comparison of the ovarian morphological characteristics between egg-laying and broody hens (n = 6).

Tarits	EH	BC
Body weight (kg)	2.65 ± 0.12*	1.73 ± 0.14
Ovary weight (g)	49.62 ± 4.75**	2.73 ± 0.09
Ovary weight ratio	1.87 ± 0.18**	0.16 ± 0.02
Ovary volume (cm^3)	48.32 ± 2.13**	4.58 ± 0.38
LYF (>10 mm, count)	5.25 ± 1.15	/
SYF (5–10 mm, count)	11.47 ± 0.62	/
WF (2–5 mm, count)	18.35 ± 4.97	18.03 ± 2.75
Stroma weight (g)	6.92 ± 1.15**	2.68 ± 0.07

EH, egg-laying hens; BC, broody chicken; WF, white follicles; LYF, large yellow follicle; SYF, small yellow follicles; *p < 005 and **p < 0.01.

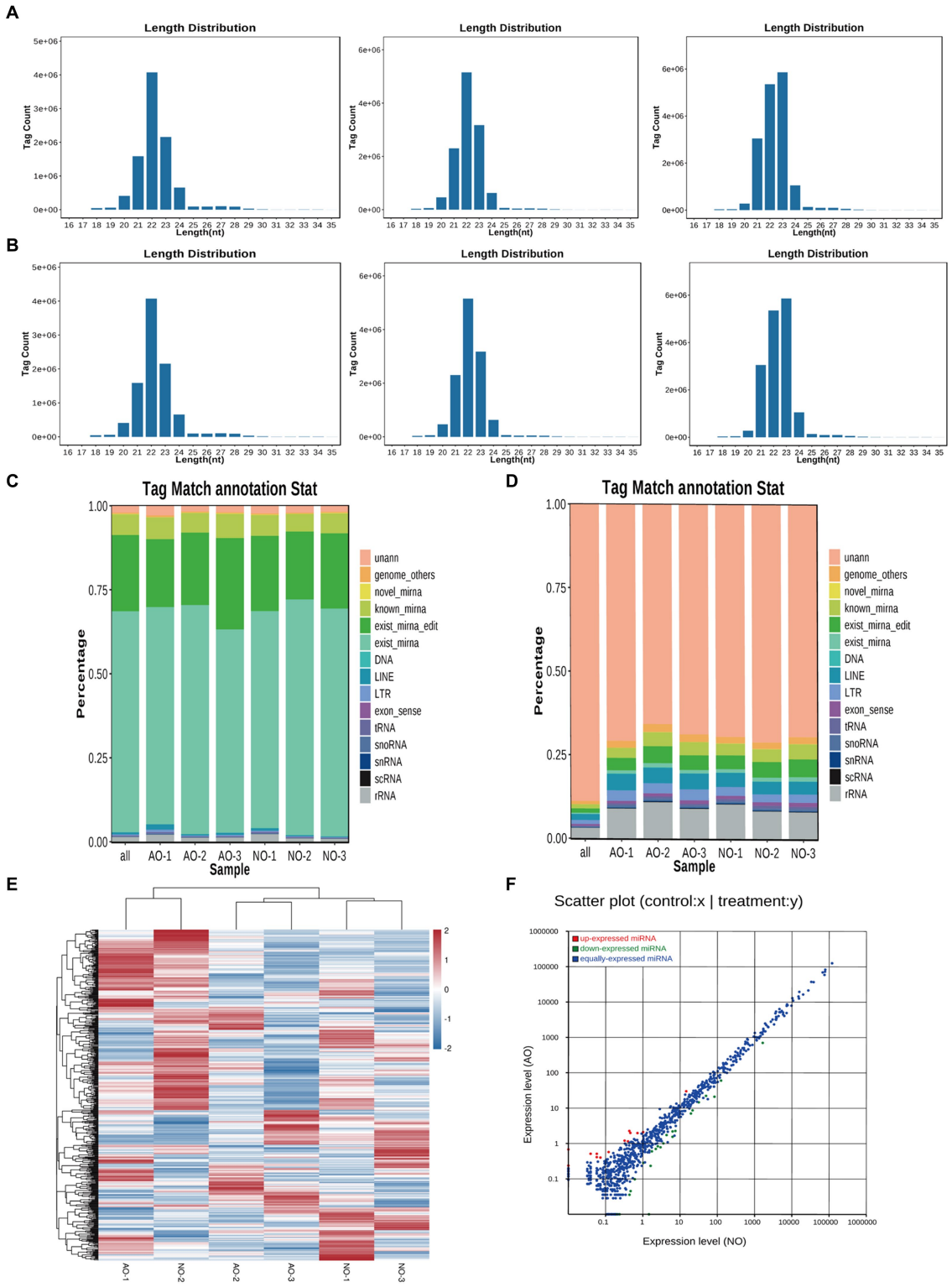

FIGURE 2
Overview of small RNA sequencing in the chicken ovary. **(A)** The length distribution of small RNA was AO1, AO2 and AO3, respectively. **(B)** The length distribution of small RNA was NO1, NO2 and NO3. **(C)** Statistical analysis of miRNA sequence abundance across various categories in each sample. **(D)** Statistical graph depicting the distribution of miRNA sequence species across various sample categories. exist_mirna (The miRNA of this species has been included in miRbase). known_miRNA (The identified miRNAs were compared with the known animal miRNAs in miRbase). novel_mirna (Combined with the reference sequence, the issuer structure was predicted and the miRNA was identified.) unann (The tags that cannot be annotated as any of the above molecules were recorded as unann). **(E)** Heatmap of differentially expressed miRNAs. **(F)** Compare the group NO –vs. -AO scatter plots.

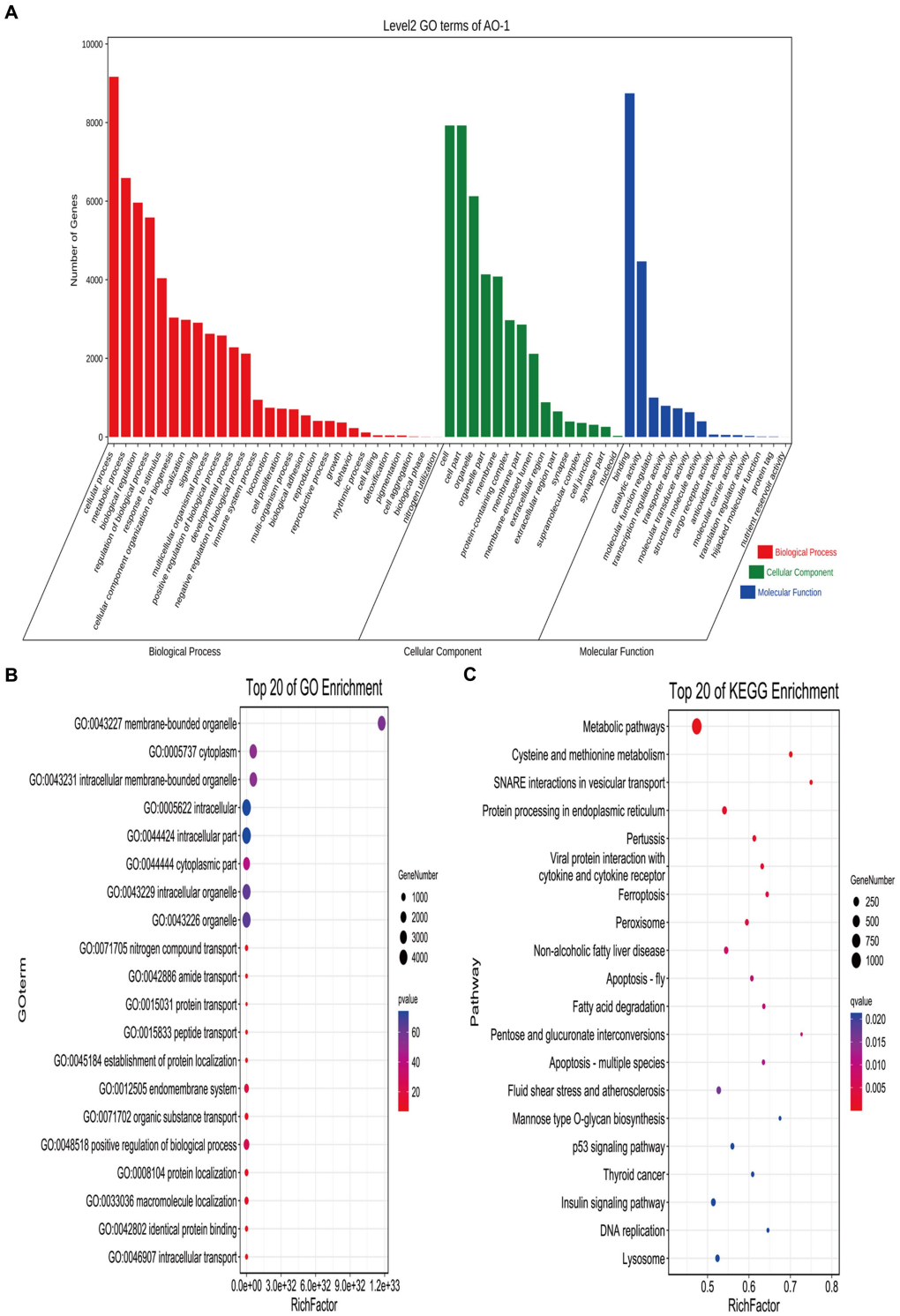

FIGURE 3
GO and KEGG analysis of DE miRNAs. **(A)** The GO enrichment classification histogram of DEmiRNA is divided into three levels: BP, MF, and CC. **(B)** Top 20 significantly changed GOs of DEmiRNAs in biological processes. **(C)** The top 20 pathways significantly associated with differentially expressed miRNA transcripts.

Effect of the two different ovaries on lncRNA

RNA-seq yielded 292,328,750 and 268,349,060 total raw reads from the broodiness and laying groups, respectively. Thus, to get high quality clean reads, reads were further filtered by fastp (26) (version 0.18.0). Filtering was then done to obtain a clean data set with more than 95% accuracy. The intersection of the three software results, which is depicted in the Venn diagram, was taken as the final lncRNA prediction result (Figure 4A). Noteworthy, 9,640

intergenic lncRNA, 465 bidirectional lncRNA, 83 intronic lncRNA, 327 antisense lncRNA and 334 sense overlapping lncRNA were identified based on the position of the new lncRNA relative to the protein-coding gene (Figure 4B). We also identified 2,588 new lncRNA for subsequent analysis. The expression of lncRNA and transcripts in different samples were visualized using expression distribution and violin maps (Figures 4C,D). By comparing the laying group and the broodiness group had 379 DE lncRNA (213 up-regulated and 166 down-regulated). The expression patterns are depicted in the volcanic maps and heat maps (Figures 4E,F). Our

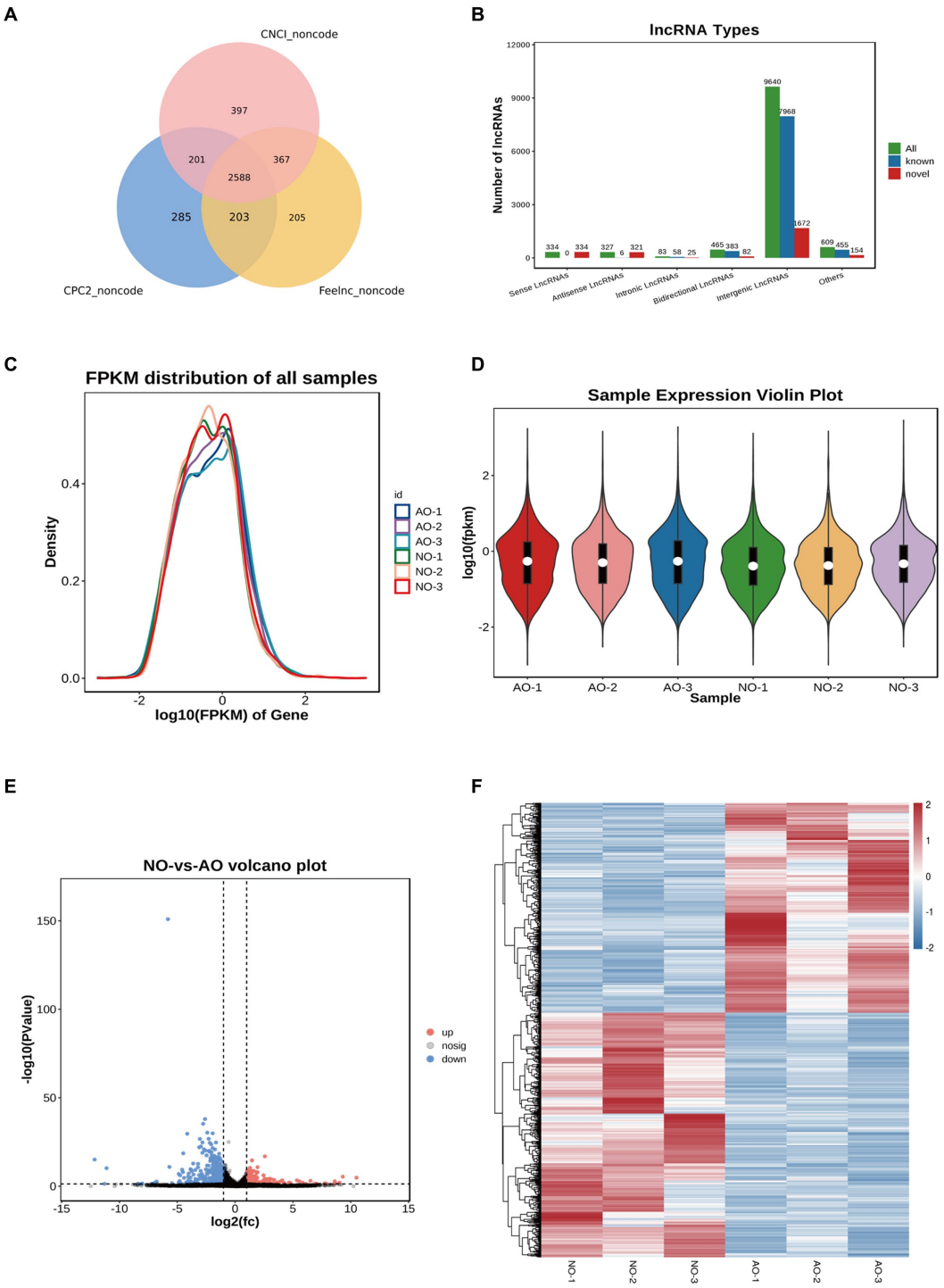

FIGURE 4
Overview of lncRNA sequencing in the chicken ovary. **(A)** CPC2, CNCI, and Feelnc were used to evaluate the encoding capabilities of all transcripts. The intersection of transcripts without coding potential is a reliable prediction result. **(B)** Total lncRNA type statistics. **(C)** lncRNA expression abundance distribution map. **(D)** Violin diagram of lncRNA expression. **(E)** Comparison of group NO-vs. -AO volcano maps. **(F)** Compare group NO-vs. -AO heat maps.

study revealed that ENSGALT00000105586 is the top DElncRNAs (Figure 4E).

GO analysis revealed that the lncRNA target genes were significantly enriched in processes related to extracellular activity, multicellular organismal processes, collagen fibril organization, and tissue development (Supplementary Figures S1A,B). The three most significant signaling pathways in the KEGG analysis of the lncRNA genes were ECM-receptor interaction, protein digestion and absorption, and focal adhesion (Supplementary Figure S1C).

Effect of the two different ovaries on circRNA

We obtained 55,838,523 clean reads from 6 samples after strict filtering (Supplementary material 3). A total of 18,666 circRNAs were subsequently identified from the clean reads in both the broodiness and laying groups (Supplementary Table S3). Notably, these circRNAs were distributed on almost all chromosomes, with the highest concentration on chromosome 1 (Figure 5A). A majority (83.82%) of circRNAs had a length of less than 3,000 bp, amongst which 30.55% were less than 500 bp and 47.42% were between 500–2,000 bp, with an average length of 3,156 bp (Figure 5B). The most abundant circRNA type was annot_exons (12,869; Figure 5C). A comparison between the expression levels of circRNA in the broodiness group and the laying group yielded 129 DE circRNAs ($p < 0.05$; Figure 5D). These 129 DE circRNAs were further analyzed using a volcanic map, we has been determined in our investigation that novel_circ_018025 stands out as a top DEcircRNA (Figure 5E). A heat map analysis of the differential circRNA expression patterns was also conducted (Figure 5F).

GO enrichment analysis of the DE circRNAs revealed their involvement in histone demethylase, phosphoprotein phosphatase, and metalloendopeptidase activities (Supplementary Figure S2B). KEGG enrichment analysis further revealed that DE circRNAs were linked to adherens junction, lysine degradation, cell adhesion molecules, thiamine metabolism, and PI3K-Ark signaling pathway (Supplementary Figure S2C).

Construction of ceRNA networks associated with ovarian atrophy of the two different ovaries

An analysis of the differential expression of miRNAs in the ovarian tissue revealed 258 lncRNA-miRNA-mRNA and 70 circRNA-miRNA-mRNA interaction pairs, encompassing 291 lncRNAs, 79 circRNAs, 40 miRNAs, and 346 mRNAs (Figures 6A,B). GO and KEGG enrichment analyses (Supplementary Figures S5A,B) revealed that these transcriptional interactions were associated with ECM-receptor interaction, AGE-RAGE signaling pathway, focal adhesion, cytokine–cytokine receptor interaction, inflammatory mediator regulation of TRP channels, renin secretion, gap junction, insulin secretion, serotonergic synapse, and IL-17 signaling pathway. Through KEGG and GO analysis, we identified differentially expressed genes within relevant pathways. Furthermore, 25 genes potentially associated with broodiness were identified (Table 2).

A lncRNA/circRNA-miRNA-mRNA regulatory network was subsequently created by constructing ceRNA networks of candidate genes (Figure 7). In the network, miRNAs were at its center and was associated with 4 circRNAs, 18 lncRNAs, 5 miRNAs, and 2 mRNAs. The ceRNA network analysis identified *MYLK* and *THBS1* genes as potential targets of 2 and 3 differentially expressed miRNAs, and 8 and 10 lncRNAs, respectively. Moreover, four circRNAs had a regulatory effect on *MYLK* and *THBS1* genes. The novel_circ_014674 and MSTRG.3306.4 potentially regulated *MYLK* and *THBS1* genes via different miRNAs, which was consistent with the ceRNA regulatory hypothesis (27).

RT-qPCR validation of DE circRNAs, DE lncRNAs, and DE miRNAs

Seven transcripts were randomly selected from DE circRNA, DE lncRNA, and DE miRNA and subjected to RT-qPCR to verify the accuracy of the RNA sequencing data. Subsequent RT-qPCR validation demonstrated extremely significant differences ($p < 0.01$) in gga-miR-215-5p, gga-miR-489-3p, novel_circ_017769, and MSTRG.18953.2. Additionally, novel_circ_000405, MSTRG.18017.1, and MSTRG.10467.1 exhibited significant differences ($p < 0.05$), as depicted in Figure 8A. The log2FC values of DE miRNA, DE lncRNA, and DE circRNA obtained from the RT-qPCR results revealed that the seven genes exhibited a consistent expression trend with those of RNA-Seq data, thus confirming the accuracy of the sequencing results in Figure 8B.

Discussion

Poultry broodiness is a complex characteristic with low heritability, it is a result of a combination of genetic influences, the endocrine system, and environmental factors (28). Broody behavior frequently results in follicular atresia and ovarian atrophy (29). In addition, the adoption of artificial incubation technology has eliminated the need for broody behavior in chicken production. Consequently, identifying potential targets that impact broody behavior serves as a method to enhance egg production in native chicken populations. The ovaries and fallopian tubes of broody chickens undergo degeneration, which impedes the growth of follicles and reduces the number of granulosa and thecal cells within them, thus hindering egg production (4, 30). During the brooding stage, Magang geese have very few large yellow follicles and small yellow follicles, yet the amount of large white follicles remains unchanged (31). In this study, histological examination revealed that the ovaries of broody chickens had atrophied, with atretic follicles, which is consistent with the results of other studies (32, 33). Transmission electron microscope (TEM) images of the ovarian ultrastructure suggested that the ovarian granulosa cells of polycystic ovarian syndrome (PCOS) model rats exhibited an accumulation of mitochondria, destruction of crests, and breaking up as opposed to those of normal rats (34). Granulosa cells with dysfunctional mitochondria can lead to a decrease in steroid production and oocyte maturation rate, resulting in reduced fertility. Conversely, functional mitochondria increase the steroid production of granulosa cells (35).

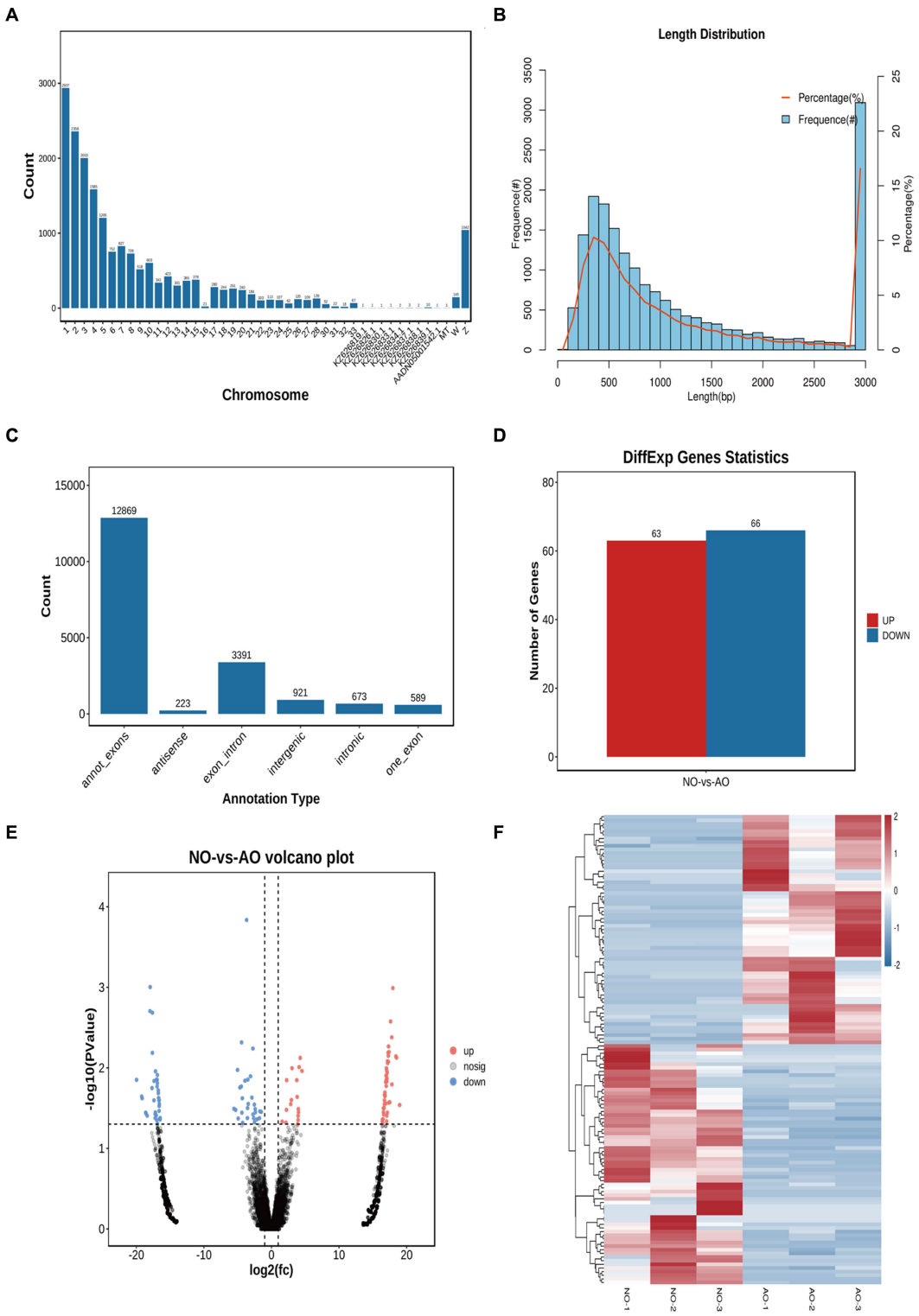

FIGURE 5
Overview of circRNA sequencing in the chicken ovary. **(A)** All the circular RNA chromosome statistics. **(B)** All the circular RNA length distribution statistics. **(C)** Statistical map of circular RNA type distribution. **(D)** CircRNA statistical map of differences. **(E)** Comparison of group NO-vs. -AO volcano maps. **(F)** Differential circRNA clustering heat map.

Non-coding RNAs are important in the biological processes of living organisms. The ceRNA hypothesis enables the exploration of potential regulatory mechanisms by combining multiple RNA information (36). In this study, we identified 40 differentially expressed miRNAs (DEmiRNAs), 379 differentially expressed long non-coding RNAs (DElncRNAs), and 129 differentially expressed circular RNAs

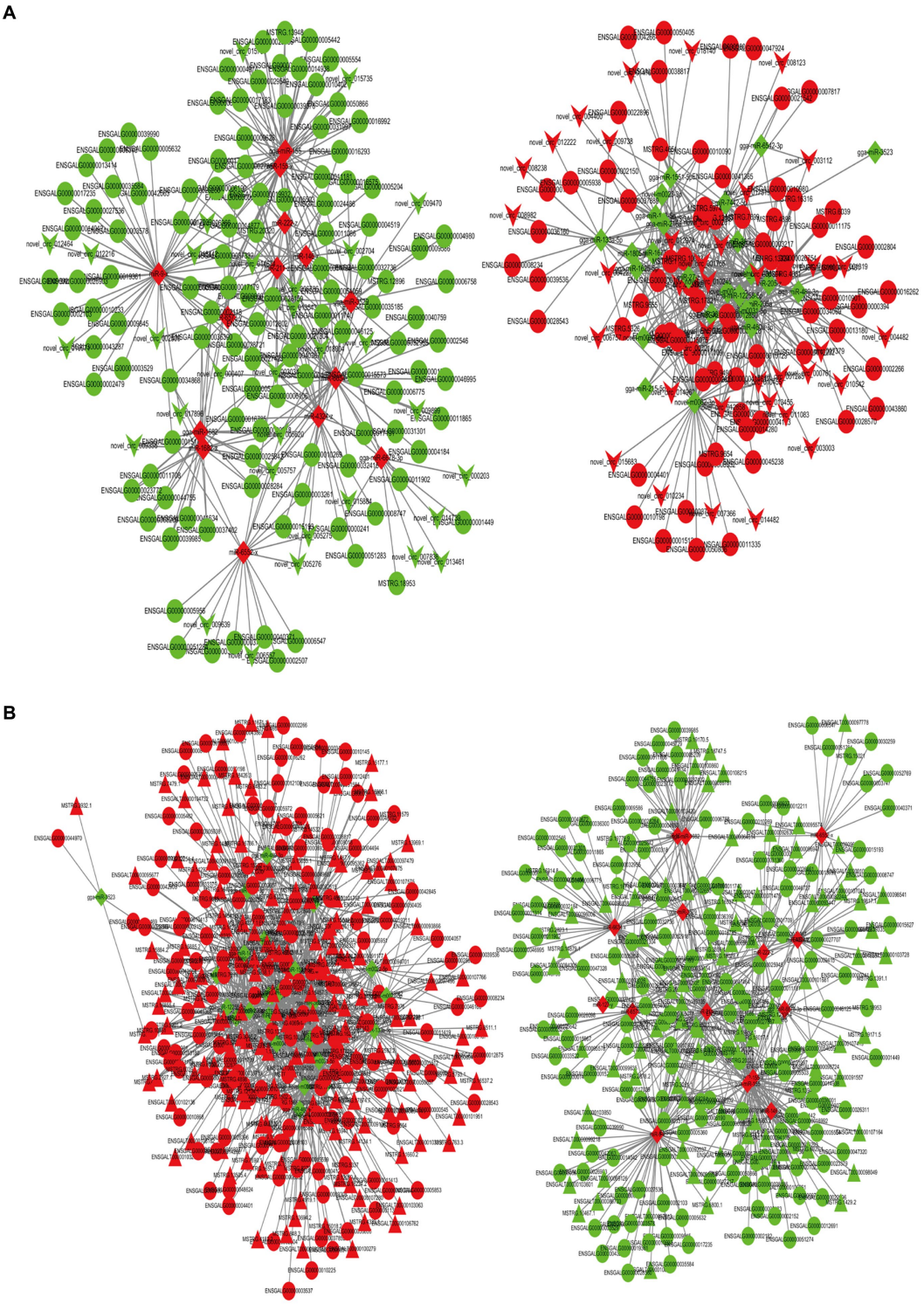

FIGURE 6
CeRNA network constructed by DEmRNAs, DElncRNAs, DEcircRNAs, and DEmiRNAs. **(A)** mRNA-miRNA-circRNA network. **(B)** mRNA-miRNA-lncRNA network. The shades of the colors indicate the upregulated (red) and downregulated (green) level. The characters of the figures correspond to different RNA species, round -mRNA, diamond-miRNA, v-circRNA, triangle-lncRNA.

(DEcircRNAs) in the ovaries of laying chickens and those with broodiness. Subsequent enrichment analysis enabled the construction of a hierarchical ceRNA network associated with ovarian development. The network identified miRNAs, such as miR-9-x, miR-4324-z, miR-155-x, gga-miR-143-5p, and miR-211-z, miR-155, miR-9, and miR-4324 are involved in the development of the ovary. miR-155 has an essential effect on the glycolysis of granule cells in PCOS sufferers, thereby controlling follicular dysplasia (37). miR-9 is highly expressed

TABLE 2 Twenty-five candidate genes associated with the regulation of broodiness and their binding pathways, and differentially expressed miRNA, lncRNA, and circRNA.

Differentially expressed genes	Pathway	Related differentially expressed miRNA	Related lncRNA	Related circRNA
COMP	PI3K-Akt signaling pathway	miR-211-z	ENSGALT00000102650	
FN1	Pathways in cancer	miR-9-x	ENSGALT00000069126, ENSGALT00000097813, ENSGALT00000099218, ENSGALT00000103601, MSTRG.10467.1	novel_circ_010071
ITGA8	PI3K-Akt signaling pathway	miR-4324-z	ENSGALT00000103728 ，ENSGALT00000105373，MSTRG.19817.1	novel_circ_015884
THBS1	PI3K-Akt signaling pathway	gga-miR-155, miR-155-x, miR-211-z	ENSGLT0000055899, ENSGALT00000093080, ENSGALT00000097500, ENSGALT00000098724, ENSGALT00000100307, MSTRG.12108.4, MSTRG.18017.1, MSTRG.2399.1, MSTRG.2955.5, MSTRG.3306.4, MSTRG.8753.4	novel_circ_013543, novel_circ_013544, novel_circ_013545, novel_circ_014674
TNC	PI3K-Akt signaling pathway	miR-9-x	ENSGALT00000069126, ENSGALT00000086733, ENSGALT00000097813, ENSGALT00000099218, MSTRG.10467.1	novel_circ_010071
IL8	Pathways in cancer	miR-6573-y	ENSGALT00000095578	
CR1	Tuberculosis	gga-miR-143-5p	MSTRG.12254.4	
PF4	Pathways in cancer	novel-m0022-5p, novel-m0023-3p	ENSGALT00000094510, ENSGALT00000097728, ENSGALT00000098801, ENSGALT00000105534, ENSGALT00000107766, MSTRG.16216.1, MSTRG.2592.2, MSTRG.5783.5	
MAPK10	Pathways in cancer	gga-miR-1677-3p, gga-miR-489-3p, novel-m0012-3p, gga-miR-133a-5p, gga-miR-205a, gga-miR-365-3p, miR-205-z, novel-m0082-3p, gga-miR-1625-5p, novel-m0031-5p	ENSGALT00000092815, ENSGALT00000097073, MSTRG.13979.1, MSTRG.4262.1	
AGT	Pathways in cancer	gga-miR-1551-5p, gga-miR-365-3p	ENSGALT00000091177, ENSGALT00000102866, MSTRG.16427.1, MSTRG.3924.2, MSTRG.5783.5	
COL3A1	Amoebiasis	miR-9-x	ENSGALT00000069126, ENSGALT00000086733, ENSGALT00000097813, ENSGALT00000099218, ENSGALT00000103601, ENSGALT00000106808, MSTRG.10467.1	novel_circ_010071
SMAD2Z	Pathways in cancer	gga-miR-155, miR-155-x	ENSGALT00000092121, ENSGALT00000097500, MSTRG.18017.1, MSTRG.2399.1, MSTRG.6929.1	novel_circ_006786, novel_circ_014674
MYLK	Calcium signaling pathway	gga-miR-1682, miR-1682-z	ENSGALT00000034451, ENSGALT00000064614, ENSGALT00000098372, ENSGALT00000108215, MSTRG.18028.1, MSTRG.18747.5, MSTRG.19170.5, MSTRG.3306.4	novel_circ_014674

(Continued)

TABLE 2 (Continued)

Differentially expressed genes	Pathway	Related differentially expressed miRNA	Related lncRNA	Related circRNA
PDGFD	PI3K-Akt signaling pathway	gga-miR-1682, miR-1682-z, gga-miR-155, miR-155-x, miR-222-z, miR-9-x	ENSGALT00000055899, ENSGALT00000095958, ENSGALT00000097500, ENSGALT00000100860, MSTRG.18017.1, MSTRG.19170.5, MSTRG.3306.4	novel_circ_009336, novel_circ_013543, novel_circ_014674
F2	Pathways in cancer	novel-m0031-5p, novel-m0082-3p	MSTRG.14124.1, MSTRG.15941.1, MSTRG.4656.1	novel_circ_011083
KCNMB1	cGMP-PKG signaling pathway	miR-211-z, miR-9-x, gga-miR-1682, miR-1682-z, miR-155-x	ENSGALT00000029552, ENSGALT00000034451, ENSGALT00000095958, ENSGALT00000100307, ENSGALT00000108215, MSTRG.18028.1, MSTRG.18747.5, MSTRG.19170.5, MSTRG.3306.4 MSTRG.852.1 MSTRG.8753.4	novel_circ_009336, novel_circ_014674, novel_circ_018442
KCNMA1	cGMP-PKG signaling pathway	gga-miR-3529	ENSGALT00000098838	novel_circ_009470
ACTA2	Apelin signaling pathway	miR-9-x	ENSGALT00000069126, ENSGALT00000086733, ENSGALT00000097813, ENSGALT00000099218, ENSGALT00000103601, ENSGALT00000106808, MSTRG.10467.1	novel_circ_010071
GNAQ	Pathways in cancer	miR-6552-x, miR-9-x		novel_circ_003034, novel_circ_017896
CXCR5	Cytokine-cytokine receptor interaction	gga-miR-143-5p, gga-miR-7442-5p	MSTRG.4518.5	
CCR7	Cytokine-cytokine receptor interaction	gga-miR-12258-5p, novel-m0012-3p	MSTRG.5730.1, MSTRG.9716.2	
CAMK2A	Pathways in cancer	gga-miR-143-5p	ENSGALT00000095677, MSTRG.12254.4	
HTR2C	Neuroactive ligand-receptor interaction	novel-m0031-5p	ENSGALT00000092468	
CYP2J2	Metabolic pathways	novel-m0012-3p	ENSGALT00000091079, ENSGALT00000103356	
MMP9	Pathways in cancer	gga-miR-155, miR-155-x, miR-6573-y	ENSGALT00000055899, ENSGALT00000097500, ENSGALT00000098724, ENSGALT00000100307, MSTRG.12108.4, MSTRG.18017.1, MSTRG.2399.1, MSTRG.2955.5, MSTRG.3306.4, MSTRG.8753.4	novel_circ_003034

in the follicular fluid of PCOS patients, and its interaction with the vitamin D receptor modulates the proliferation and apoptosis of ovarian granulosa cells, thereby regulating follicle growth (38–40). Moreover, miR-9 increases during the ovarian development of tilapia, thereby affecting sex determination and differentiation by regulating dmrt1 expression (41). Notably, there are differences in the development process of miR-9 in different regions of the chick's brain (42). miR-4324 is associated with cell proliferation and migration. Its expression is thus significantly reduced in ovarian cancer tissues. miR-4324 can be targeted and combined with *FEN1* to impede cell proliferation in ovarian cancer (43, 44). Recent studies postulate that miR-143 has a regulatory effect on glucose metabolism and mitochondrial function in the placenta (45). Yang et al. (46) reported that miR-143-5p combines with *CRIM1* to regulate endometrial receptivity in goats. In the same line, studies postulate that the regulatory axis of lncRNA PROX1-AS1, miR-211-5p, and caspase-9 is connected to preeclampsia and affects the presence of trophoblast cells (47).

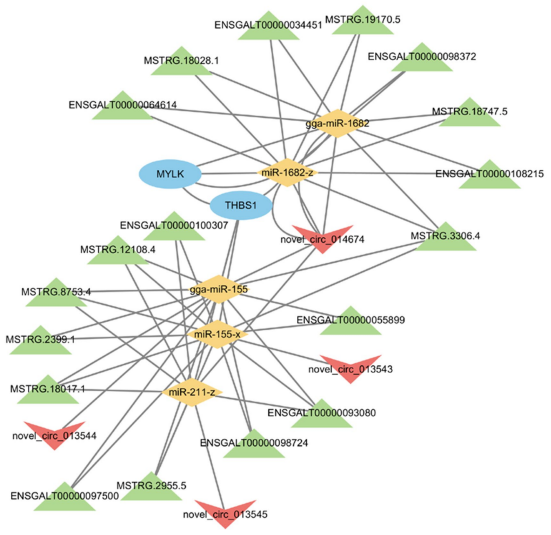

FIGURE 7
lncRNA/circRNA-miRNA-mRNA co-regulatory network. The characters of the figures correspond to different RNA species, round -mRNA, diamond -miRNA, to v-circRNA, triangle -lncRNA.

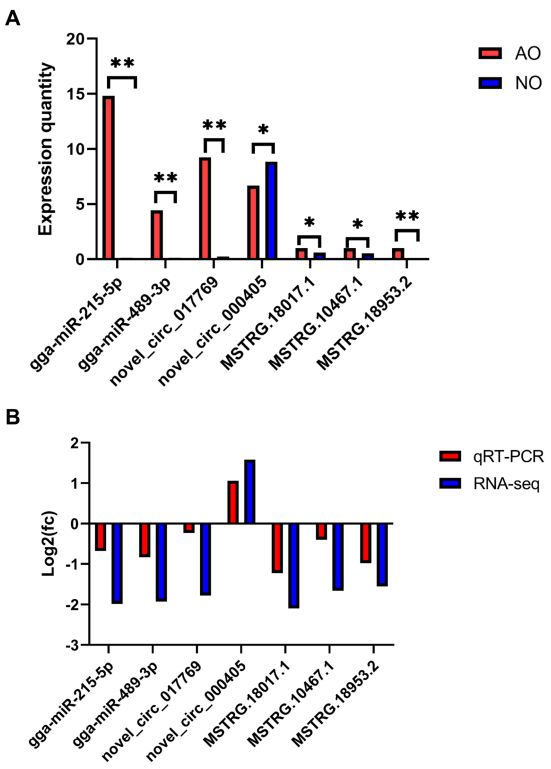

FIGURE 8
Validation of RNA-seq data using real time quantitative PCR (RT-qPCR).

Herein, miRNA, lncRNA, and circRNA source genes were significantly enriched in the ECM-receptor interaction pathway. ECM receptors are associated with the ripening of follicles and the reduction of the ovaries (34, 48). Research has demonstrated that extracellular matrix (ECM) components furnish tissue-specific frameworks that impact key cellular processes, including proliferation, differentiation, and apoptosis. The extensive alterations in ECM throughout follicular development necessitate a sequence of proteolytic events crucial for the regular progression, function, regression, and degeneration of follicles (49). Recent studies have indicated that matrix proteins play a significant role in regulating ECM turnover during follicular development or atresia. Apart from specifically degrading ECM components and activating other matrix metalloproteinases, these proteins also influence various signaling pathways by releasing numerous signaling proteins. This regulation impacts cell biology during both normal physiological processes and pathological conditions, involving growth factors, cytokines, cadherin E, Fas ligands, and tumor necrosis factors (50). Simultaneously, we observed potential regulatory interactions between miR-9-x and the genes *FN1, TNC, COL3A1, PDGFD, KCNMB1, ACTA2,* and *GNAQ* through the ceRNA network. Additionally, previous studies have indicated that *FN1* is a principal constituent of the extracellular matrix (ECM) (51). Furthermore, an examination of high and low egg production in white Muscovy ducks identified potential candidate genes in both hypothalamic and ovarian tissue for the high-yield mechanism in this breed. Notably, the *FN1* gene displayed significant expression levels in ovarian tissue and is implicated in this mechanism (52). Focal adhesion was also a significant pathway in the ceRNA network in this study. Previous studies have demonstrated its involvement in cell proliferation (53). Moreover, studies postulate that focal adhesion is a factor in the expression of the IGF-I gene and results in a difference in the gene's expression in Muscovy ducks. IGF-I is responsible for controlling the expression of lncRNA through the focal adhesion pathway, thereby promoting cell proliferation and regulating the reproduction of Muscovy ducks (54). ECM-receptor interaction and focal adhesion are involved in the early development of geese and ducks ovaries (48). lncRNAs regulate the functioning of chicken ovaries through their interaction with ECM-receptor and focal adhesion pathways (55). In this study, focal adhesion was found to be an enrichment pathway associated with higher and lesser egg production, which is in line with other research findings (56). Through additional analysis of the ceRNA network, we have pinpointed two crucial genes: *THBS1* and *MYLK*. However, there has been limited research on poultry involving *THBS1* and *MYLK*. Increased *THBS1* expression in rat follicles has been demonstrated to notably diminish angiogenesis while enhancing follicular atresia (57). In another study on ovarian cancer, it was observed that the inhibition of circRNA_MYLK led to a decrease in the proliferation of ovarian cancer cells (58). We hypothesized that ncRNAs modulate the broodiness behavior of poultry by regulating *THBS1* and *MYLK* gene expression. The findings of this study revealed the existence of a regulatory connection between ncRNAs and their competing mRNAs, which provides a better understanding of the ceRNA function and processes in chicken ovarian development.

Conclusion

This study reveals 40 DE miRNAs, 379 DE lncRNAs, and 129 DE circRNAs from the ovaries of laying chickens and hens with

broodiness. *THBS1* and *MYLK* are candidate genes in the regulation of broody behavior, potentially influenced by miR-155-x, miR-211-z, miR-1682-z, gga-miR-155, and gga-miR-1682. Additionally, they may be subject to competitive binding by novo-el_circ_014674 and MSTRG.3306.4. The GO and KEGG enrichment analyses revealed a connection between the ECM-receptor interaction pathway and focal adhesion in the regulation of broody behavior, offering a novel avenue for investigating the regulatory network of Chengkou mountain chicken's broody behavior further.

Data availability statement

The raw data has been furnished to the National Center for Biotechnology Information (NCBI) Sequence Read Archive (SRA) database, assigned the accession number PRJNA1074948.

Ethics statement

The animal study was approved by Experimental Animal Ethics Review Committee of Southwest University. The study was conducted in accordance with the local legislation and institutional requirements.

Author contributions

HX: Data curation, Software, Validation, Writing – original draft. WL: Formal analysis, Validation, Writing – review & editing. LW: Formal analysis, Writing – review & editing. XW: Data curation, Writing – review & editing. BT: Conceptualization, Formal analysis, Supervision, Writing – review & editing. ZC: Conceptualization, Software, Writing – review & editing. LL: Funding acquisition, Project administration, Resources, Writing – original draft, Writing – review & editing.

Funding

The author(s) declare that financial support was received for the research, authorship, and/or publication of this article. This work was financially supported by Special Key Project of Chongqing Technology Innovation and Application Development (cstc2021jscx-gksbX0004 and CSTB2023TIAD-LUX0003), Fundamental Research Funds for the Central Universities (SWU-KT22010), Chongqing Modern Agricultural Industry Technology System (Poultry) (CQMAITS202314), the Science and Technology Research Program of Chongqing Municipal Education Commission (KJQN202100220 and KJQN202200201), the Undergraduate Innovation and Entrepreneurship Training Program of Southwest University (202210635058).

Conflict of interest

The authors declare that the research was conducted in the absence of any commercial or financial relationships that could be construed as a potential conflict of interest.

Publisher's note

Supplementary material

The Supplementary material for this article can be found online at: https://www.frontiersin.org/articles/10.3389/fvets.2024.1399776/full#supplementary-material

References

1. Yu J, Lou YP, Zhao A. Transcriptome analysis of follicles reveals the importance of autophagy and hormones in regulating broodiness of Zhedong white goose. *Sci Rep*. (2016) 6:36877. doi: 10.1038/srep36877

2. Kuo YM, Shiue YL, Chen CF, Tang PC, Lee YP. Proteomic analysis of hypothalamic proteins of high and low egg production strains of chickens. *Theriogenology*. (2005) 64:1490–502. doi: 10.1016/j.theriogenology.2005.03.020

3. Shen X, Bai X, Xu J, Zhou M, Xu HP, Nie QH, et al. Transcriptome sequencing reveals genetic mechanisms underlying the transition between the laying and brooding phases and gene expression changes associated with divergent reproductive phenotypes in chickens. *Mol Biol Rep*. (2016) 43:977–89. doi: 10.1007/s11033-016-4033-8

4. Liu LB, Xiao QH, Gilbert ER, Cui ZF, Zhao XL, Wang Y, et al. Whole-transcriptome analysis of atrophic ovaries in broody chickens reveals regulatory pathways associated with proliferation and apoptosis. *Sci Rep*. (2018) 8:7231:7231. doi: 10.1038/s41598-018-25103-6

5. Rincon-Riveros A, Morales D, Rodriguez JA, Villegas VE, Lopez-Kleine L. Bioinformatic tools for the analysis and prediction of ncRNA interactions. *Int J Mol Sci*. (2021) 22:11397. doi: 10.3390/ijms222111397

6. Park YB, Kim JM. Identification of long non-coding RNA-mRNA interactions and genome-wide lncRNA annotation in animal transcriptome profiling. *J Anim Sci Technol*. (2023) 65:293–310. doi: 10.5187/jast.2023.e17

7. Djebali S, Davis CA, Merkel A, Dobin A, Lassmann T, Mortazavi A, et al. Landscape of transcription in human cells. *Nature*. (2012) 489:101–8. doi: 10.1038/nature11233

8. Sirotkin AV, Kisova G, Brenaut P, Ovcharenko D, Grossmann R, Mlyncek M. Involvement of microRNA Mir15a in control of human ovarian granulosa cell proliferation, apoptosis, steroidogenesis, and response to FSH. *Microrna*. (2014) 3:29–36. doi: 10.2174/2211536603666140227232824

9. Hossain MM, Cao M, Wang Q, Kim JY, Schellander K, Tesfaye D, et al. Altered expression of miRNAs in a dihydrotestosterone-induced rat PCOS model. *J Ovarian Res*. (2013) 6:36. doi: 10.1186/1757-2215-6-36

10. Mao H, Xu X, Cao H, Dong X, Zou X, Xu N, et al. Comparative transcriptome profiling of mRNA and lncRNA of ovaries in high and low egg production performance in domestic pigeons (*Columba livia*). *Front Genet*. (2021) 12:571325. doi: 10.3389/fgene.2021.571325

11. Yu T, Wang Y, Fan Y, Fang N, Wang T, Xu T, et al. CircRNAs in cancer metabolism: a review. *J Hematol Oncol*. (2019) 12:90. doi: 10.1186/s13045-019-0776-8

12. Cai HC, Li YM, Li HM, Niringiyumukiza JD, Zhang MD, Chen L, et al. Identification and characterization of human ovary-derived circular RNAs and their potential roles in ovarian aging. *Aging*. (2018) 10:2511–34. doi: 10.18632/aging.101565

13. Xu GX, Zhang HF, Li X, Hu JH, Yang GS, Sun SD. Genome-wide differential expression profiling of ovarian circRNAs associated with litter size in pigs. *Front Genet*. (2019) 10:1010. doi: 10.3389/fgene.2019.01010

14. Tao H, Xiong Q, Zhang F, Zhang N, Liu Y, Suo XJ, et al. Circular RNA profiling reveals chi_circ_0008219 function as microRNA sponges in pre-ovulatory ovarian follicles of goats (*Capra hircus*). *Genomics*. (2018) 110:257–66. doi: 10.1016/j.ygeno.2017.10.005

15. Chen L, Zhang T, Zhang S, Huang J, Zhang G, Xie K, et al. Identification of long non-coding RNA-associated competing endogenous RNA network in the differentiation of chicken preadipocytes. *Genes*. (2019) 10:795. doi: 10.3390/genes10100795

16. Langmead B, Salzberg SL. Fast gapped-read alignment with Bowtie 2. *Nat Methods*. (2012) 9:357–9. doi: 10.1038/Nmeth.1923

17. Sun L, Luo H, Bu D, Zhao G, Yu K, Zhang C, et al. Utilizing sequence intrinsic composition to classify protein-coding and long non-coding transcripts. *Nucleic Acids Res*. (2013) 41:e166. doi: 10.1093/nar/gkt646

18. Kong L, Zhang Y, Ye ZQ, Liu XQ, Zhao SQ, Wei L, et al. CPC: assess the protein-coding potential of transcripts using sequence features and support vector machine. *Nucleic Acids Res*. (2007) 35:W345–9. doi: 10.1093/nar/gkm391

19. Wucher V, Legeai F, Hedan B, Rizk G, Lagoutte L, Leeb T, et al. FEELnc: a tool for long non-coding RNA annotation and its application to the dog transcriptome. *Nucleic Acids Res*. (2017) 45:e57. doi: 10.1093/nar/gkw1306

20. Kim D, Landmead B, Salzberg SL. HISAT: a fast spliced aligner with low memory requirements. *Nat Methods*. (2015) 12:357–60. doi: 10.1038/Nmeth.3317

21. Memczak S, Jens M, Elefsinioti A, Torti F, Krueger J, Rybak A, et al. Circular RNAs are a large class of animal RNAs with regulatory potency. *Nature*. (2013) 495:333–8. doi: 10.1038/nature11928

22. Liu LB, Yi JQ, Ray WK, Vu LT, Helm RF, Siegel PB, et al. Fasting differentially alters the hypothalamic proteome of chickens from lines with the propensity to be anorexic or obese. *Nutr Diabetes*. (2019) 9:13. doi: 10.1038/s41387-019-0081-1

23. Shi JA, Li WD, Liu AF, Ren LT, Zhang PS, Jiang T, et al. MiRNA sequencing of embryonic myogenesis in Chengkou mountain chicken. *BMC Genomics*. (2022) 23:571. doi: 10.1186/s12864-022-08795-z

24. Ren L, Liu A, Wang Q, Wang H, Dong D, Liu L. Transcriptome analysis of embryonic muscle development in Chengkou mountain chicken. *BMC Genomics*. (2021) 22:431. doi: 10.1186/s12864-021-07740-w

25. Livak KJ, Schmittgen TD. Analysis of relative gene expression data using real-time quantitative PCR and the $2^{-\Delta\Delta CT}$ method. *Methods*. (2001) 25:402–8. doi: 10.1006/meth.2001.1262

26. Chen SF, Zhou YQ, Chen YR, Gu J. Fastp: an ultra-fast all-in-one FASTQ preprocessor. *Bioinformatics*. (2018) 34:i884–90. doi: 10.1093/bioinformatics/bty560

27. Braga EA, Fridman MV, Moscovtsev AA, Filippova EA, Dmitriev AA, Kushlinskii NE. LncRNAs in ovarian cancer progression, metastasis, and main pathways: ceRNA and alternative mechanisms. *Int J Mol Sci*. (2020) 21:8855. doi: 10.3390/ijms21228855

28. Wei QY, Li J, He HR, Cao YC, Li DM, Amevor FK, et al. miR-23b-3p inhibits chicken granulosa cell proliferation and steroid hormone synthesis via targeting GDF9. *Theriogenology*. (2022) 177:84–93. doi: 10.1016/j.theriogenology.2021.10.011

29. Sharp PJ, Dawson A, Lea RW. Control of luteinizing hormone and prolactin secretion in birds. *Comp Biochem Physiol C Pharmacol Toxicol Endocrinol*. (1998) 119:275–82. doi: 10.1016/s0742-8413(98)00016-4

30. Shimmura T, Maruyama Y, Fujino S, Kamimura E, Uetake K, Tanaka T. Persistent effect of broody hens on behaviour of chickens. *Anim Sci J*. (2015) 86:214–20. doi: 10.1111/asj.12253

31. Huang YM, Shi ZD, Liu Z, Liu Y, Li XW. Endocrine regulations of reproductive seasonality, follicular development and incubation in Magang geese. *Anim Reprod Sci*. (2008) 104:344–58. doi: 10.1016/j.anireprosci.2007.02.005

32. He HR, Li DM, Tian YT, Wei QY, Amevor FK, Sun CJ, et al. miRNA sequencing analysis of healthy and atretic follicles of chickens revealed that miR-30a-5p inhibits granulosa cell death via targeting Beclin1. *J Anim Sci Biotechnol*. (2022) 13:55. doi: 10.1186/s40104-022-00697-0

33. Liu HH, Wang JW, Li L, Han CC, He H, Xu HY. Transcriptome analysis revealed the possible regulatory pathways initiating female geese broodiness within the hypothalamic-pituitary-gonadal axis. *PLoS One*. (2018) 13:e0191213. doi: 10.1371/journal.pone.0191213

34. Shuyuan Y, Meimei W, Fenghua L, Huishan Z, Min C, Hongchu B, et al. hUMSC transplantation restores follicle development in ovary damaged mice via re-establish extracellular matrix (ECM) components. *J Ovarian Res*. (2023) 16:172. doi: 10.1186/s13048-023-01217-y

35. Sreerangaraja Urs DB, Wu WH, Komrskova K, Postlerova P, Lin YF, Tzeng CR, et al. Mitochondrial function in modulating human granulosa cell steroidogenesis and female fertility. *Int J Mol Sci*. (2020) 21:3592. doi: 10.3390/ijms21103592

36. Salmena L, Poliseno L, Tay Y, Kats L, Pandolfi PP. A ceRNA hypothesis: the Rosetta Stone of a hidden RNA language? *Cell*. (2011) 146:353–8. doi: 10.1016/j.cell.2011.07.014

37. Cao JP, Huo P, Cui KQ, Wei HM, Cao JN, Wang JY, et al. Correction: follicular fluid-derived exosomal miR-143-3p/miR-155-5p regulate follicular dysplasia by modulating glycolysis in granulosa cells in polycystic ovary syndrome. *Cell Commun Signal*. (2022) 20:61. doi: 10.1186/s12964-022-00938-9

38. Roth LW, McCallie B, Alvero R, Schoolcraft WB, Minjarez D, Katz-Jaffe MG. Altered microRNA and gene expression in the follicular fluid of women with polycystic ovary syndrome. *J Assist Reprod Genet*. (2014) 31:355–62. doi: 10.1007/s10815-013-0161-4

39. Stubbs SA, Stark J, Dilworth SM, Franks S, Hardy K. Abnormal preantral folliculogenesis in polycystic ovaries is associated with increased granulosa cell division. *J Clin Endocrinol Metab*. (2007) 92:4418–26. doi: 10.1210/jc.2007-0729

40. Kong FJ, Du CX, Wang Y. MicroRNA-9 affects isolated ovarian granulosa cells proliferation and apoptosis via targeting vitamin D receptor. *Mol Cell Endocrinol*. (2019) 486:18–24. doi: 10.1016/j.mce.2019.02.012

41. Anand AAP, Huber C, Mary JA, Gallus N, Leucht C, Klafke R, et al. Expression and function of microRNA-9 in the mid-hindbrain area of embryonic chick. *BMC Dev Biol*. (2018) 18:3. doi: 10.1186/s12861-017-0159-8

42. Tao WJ, Sun LN, Shi HJ, Cheng YY, Jiang DN, Fu BD, et al. Integrated analysis of miRNA and mRNA expression profiles in tilapia gonads at an early stage of sex differentiation. *BMC Genomics*. (2016) 17:328. doi: 10.1186/s12864-016-2636-z

43. Li H, Zhu G, Xing Y, Zhu Y, Piao D. RETRACTION NOTICE: miR-4324 functions as a tumor suppressor in colorectal cancer by targeting HOXB2. *J Int Med Res*. (2021) 49:03000605211041196. doi: 10.1177/03000605211041196

44. Wu HX, Yan YL, Yuan JL, Luo MZ, Wang YJ. miR-4324 inhibits ovarian cancer progression by targeting FEN1. *J Ovarian Res*. (2022) 15:32. doi: 10.1186/s13048-022-00959-5

45. Muralimanoharan S, Maloyan A, Myatt L. Mitochondrial function and glucose metabolism in the placenta with gestational diabetes mellitus: role of miR-143. *Clin Sci*. (2016) 130:931–41. doi: 10.1042/Cs20160076

46. Yang DQ, Liu AI, Zhang YY, Nan S, Yin RL, Lei QH, et al. Essential role of CRIM1 on endometrial receptivity in goat. *Int J Mol Sci*. (2021) 22:5323. doi: 10.3390/ijms22105323

47. Tang D, Geng L, Ma J. lncRNA PROX1-AS1 mediates the migration and invasion of placental trophoblast cells via the miR-211-5p/caspase-9 axis. *Bioengineered*. (2021) 12:4100–10. doi: 10.1080/21655979.2021.1953213

48. Ran MX, Ouyang QY, Li XJ, Hu SQ, Hu B, Hu JW, et al. Exploring right ovary degeneration in duck and goose embryos by histology and transcriptome dynamics analysis. *BMC Genomics*. (2023) 24:389. doi: 10.1186/s12864-023-09493-0

49. Ny T, Wahlberg P, Brandstrom IJ. Matrix remodeling in the ovary: regulation and functional role of the plasminogen activator and matrix metalloproteinase systems. *Mol Cell Endocrinol*. (2002) 187:29–38. doi: 10.1016/s0303-7207(01)00711-0

50. Hrabia A, Socha JK, Sechman A. Involvement of matrix metalloproteinases (MMP-2, -7, -9) and their tissue inhibitors (TIMP-2, -3) in the regression of chicken postovulatory follicles. *Gen Comp Endocrinol*. (2018) 260:32–40. doi: 10.1016/j.ygcen.2018.02.008

51. Lemanska-Perek A, Adamik B. Fibronectin and its soluble EDA-FN isoform as biomarkers for inflammation and sepsis. *Adv Clin Exp Med*. (2019) 28:1561–7. doi: 10.17219/acem/104531

52. Bello SF, Xu H, Guo L, Li K, Zheng M, Xu Y, et al. Hypothalamic and ovarian transcriptome profiling reveals potential candidate genes in low and high egg production of white Muscovy ducks (*Cairina moschata*). *Poult Sci*. (2021) 100:101310. doi: 10.1016/j.psj.2021.101310

53. Petit V, Thiery JP. Focal adhesions: structure and dynamics. *Biol Cell*. (2000) 92:477–94. doi: 10.1016/s0248-4900(00)01101-1

54. Wu X, Jiang L, Xu F, Cao S, Chen Y, Zhang Y, et al. Long noncoding RNAs profiling in ovary during laying and nesting in Muscovy ducks (*Cairina moschata*). *Anim Reprod Sci*. (2021) 230:106762. doi: 10.1016/j.anireprosci.2021.106762

55. Li Q, Li J, Li C, Wu X, Si SJ, Yang PK, et al. Transcriptome identification and characterization of long non-coding RNAs in the ovary of hens at four stages. *Anim Biotechnol*. (2023) 34:1342–53. doi: 10.1080/10495398.2021.2024217

56. Zhang T, Chen L, Han KP, Zhang XQ, Zhang GX, Dai GJ, et al. Transcriptome analysis of ovary in relatively greater and lesser egg producing Jinghai yellow chicken. *Anim Reprod Sci*. (2019) 208:106114. doi: 10.1016/j.anireprosci.2019.106114

57. Garside SA, Henkin J, Morris KD, Norvell SM, Thomas FH, Fraser HM. A thrombospondin-mimetic peptide, ABT-898, suppresses angiogenesis and promotes follicular atresia in pre- and early-antral follicles *in vivo*. *Endocrinology*. (2010) 151:5905–15. doi: 10.1210/en.2010-0283

58. Ghafouri-Fard S, Khoshbakht T, Hussen BM, Taheri M, Samsami M. Emerging role of circular RNAs in the pathogenesis of ovarian cancer. *Cancer Cell Int*. (2022) 22:172. doi: 10.1186/s12935-022-02602-1

frontiers | Frontiers in Veterinary Science

TYPE Original Research
PUBLISHED 08 August 2024
DOI 10.3389/fvets.2024.1393706

OPEN ACCESS

EDITED BY
Manuel Garcia-Herreros,
National Institute for Agricultural and Veterinary Research (INIAV), Portugal

REVIEWED BY
Pablo Daniel Cetica,
Universidad de Buenos Aires, Argentina
Ejaz Ahmad,
Bahauddin Zakariya University, Pakistan

*CORRESPONDENCE
Bambang Purwantara
purwantara@apps.ipb.ac.id

RECEIVED 29 February 2024
ACCEPTED 28 May 2024
PUBLISHED 08 August 2024

CITATION
Satrio FA, Karja NWK, Setiadi MA, Kaiin EM, Pardede BP and Purwantara B (2024) Age-dependent variations in proteomic characteristics of spermatozoa in Simmental bull. *Front. Vet. Sci.* 11:1393706.
doi: 10.3389/fvets.2024.1393706

Age-dependent variations in proteomic characteristics of spermatozoa in Simmental bull

Faisal Amri Satrio[1], Ni Wayan Kurniani Karja[2], Mohamad Agus Setiadi[2], Ekayanti Mulyawati Kaiin[3], Berlin Pandapotan Pardede[3] and Bambang Purwantara[2]*

[1]Veterinary Medicine Study Program, Faculty of Medicine, Padjadjaran University, West Java, Bandung, Indonesia, [2]Division of Reproduction and Obstetrics, School of Veterinary Medicine and Biomedical Sciences, IPB University, West Java, Bogor, Indonesia, [3]Research Center for Applied Zoology, National Research and Innovation Agency (BRIN), West Java, Bogor, Indonesia

Increasing the age of bulls results in a decrease in reproductive function, including a reduction in sperm quality, which plays a vital role in determining the fertility of bulls. Through a proteomic approach, this research aims to analyze the influence of age factors on various proteomes contained in bull sperm. Frozen semen samples from Simmental Bulls were categorized into three age groups: two, four, and ≥10 years old. Subsequently, the post-thaw sperm cells obtained were separated based on molecular weight using 1D-SDS-PAGE. Peptides extracted from the bands produced in each age group were subjected to LC-MS/MS analysis. A total of 72 protein types were identified, with 45 being detected in the 4-year-old group and 41 expressed in both the 2 and ≥10-year-old groups. The results provided insights into proteins' role in sperm metabolism across all age groups. Specifically, the 2-year-old group exhibited the expression of proteins associated with acrosome assembly and spermatid development (SPACA1). In contrast, those in the 4-year-old group were linked to motility (PEBP4) and sperm decapacitation factor (PEBP1). Proteins expressed in the 2 and -year-old groups were discovered to be involved in fertilization processes (TEX101). In contrast, the ≥10-year-old age group was associated with hyperactive movement related to capacitation (Tubulin). In conclusion, age influenced the differences observed in the proteomic profile of post-thaw Simmental bull sperm using the 1D-SDS-PAGE tandem LC-MS/MS approach.

KEYWORDS

age, bull, LC-MS/MS, post-thawing sperm, proteomic

Introduction

Bull fertility is defined as the ability of sperm to fertilize and activate oocytes and support embryo development (1). This factor plays a crucial role in reproductive efficiency and the success of artificial insemination (AI) in bulls. The age of the bull is widely believed to have an impact on fertility. Previous studies categorized bull age as young (1.8-2 years) and adult (3-6 years) (2–4). Satrio et al. (5) showed that optimal semen production in bulls was achieved between 3 and 4 years of age. Collins et al. (6) discovered the highest fertility rates in Holstein and Guernsey bulls at 3-4 years of age. Generally, the reproductive capacity of bulls gradually decreases after reaching the highest fertility age due to age-related declines in various reproductive functions, such as histological (7, 8) and clinical (9) deterioration in testicular function. Changes in testicular function can disrupt

spermatogenesis (8) and reduce semen quality (2, 5, 10–12). Despite this, old bulls (over 10 years old) are still maintained and used for frozen semen production in AI activities at the Indonesian Artificial Insemination Center.

Several methods have been employed to predict bull fertility, including evaluating non-return rates (NRR) (13). Additionally, conventional assessments of semen quality, such as plasma membrane integrity, motility, morphology, and acrosome, are routinely performed to predict fertility (1, 14). In Indonesia, the SNI 4869-2:2017 standard for frozen semen quality in bulls includes motility, abnormalities, individual movement, sperm concentration, and recovery rate percentage to achieve good fertility. These standard semen evaluation procedures are visually helpful in determining poor-quality semen but insufficient in accurately detecting potential markers of bull fertility (1, 14). Therefore, sperm quality must be evaluated through a molecular approach to obtain important information concerning the potential markers.

Proteomics has become the most advanced approach for predicting fertility with increased accuracy (15). By employing this method, the molecular aspects of sperm that impact fertility can be identified (16–18). Sperm proteomic analysis is used to determine the essential functions of proteins and their regulatory roles in various fertilization processes (16, 19, 20). Furthermore, alterations in proteomic expression are believed to play a crucial role in the transition of sperm function from the epididymis to capacitation in the female reproductive tract and subsequent fertilization (16, 17). Previous studies discovered fertility markers in bull semen (13, 16, 19, 21, 22). Only limited information exists on the proteomic analysis of post-thaw sperm about bull age. Therefore, this study aims to investigate the variations in the proteomic profile of post-thaw sperm among bulls of different ages.

Materials and methods

Experimental design and semen samples

This study only used frozen semen, a commercial product from an AI center, as the primary sample and did not directly involve bulls. Furthermore, the entire semen collection process was carried out using an artificial vagina for the same period (without seasonal differences), frozen using the same extender. To eliminate any potential for variation in the samples, the bulls were kept in the same environment regarding feeding and handling management. However, each stage follows the operational standards in Indonesia, SNI ISO 9001:2015 No. 824 100 16072, supervised by a veterinarian, considered the principles of animal welfare, which refer to the ethical clearance requirements of the Animal Care and Uses Committee. The AI Center owned all bulls used in this study under the auspices of the government. However, we only use commercial products sold to the public without requiring animal ownership approval. A total of 27 frozen semen straws (nine straws per each group) of nine Simmental bulls of different age groups, namely two (young; $n = 3$ bulls), four (adult; $n = 3$ bulls), and ≥10 years old (old; $n = 3$ bulls). The number of bulls used in this study is the total number of Simental bulls available at the AI Center during the research period.

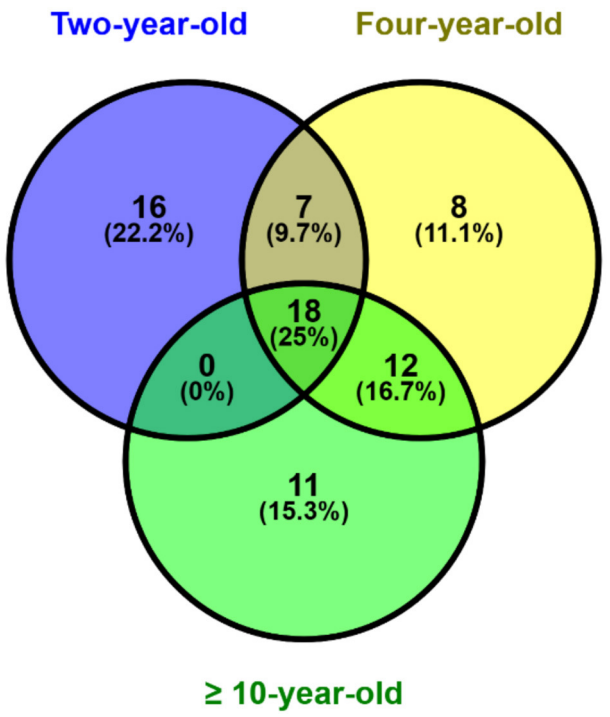

FIGURE 1
Post-thaw sperm protein expression at different ages bull by venn diagram analysis.

Extraction of post-thaw sperm proteins

The frozen semen was thawed at 37°C and washed thrice with phosphate-buffered saline through centrifugation at 1800 rpm for 10 min. The sperm pellet was then subjected to extraction using PRO-PREP™ Protein extraction solution (iNtRON Biotechnology, Korea) according to the manufacturer's instructions. 500 μL of PRO-PREP™ solution was added to the pellet, incubated at −20°C for 20 min, and centrifuged at 13000 rpm (4°C) for 5 min. The total soluble protein concentration of the sample was determined before SDS-PAGE analysis using the Bradford method (23), with BSA (Sigma-Aldrich) serving as the standard.

Separation of sperm protein using SDS-PAGE

Protein separation was performed using a 12.5% polyacrylamide gel containing sodium dodecyl sulfate (SDS) and a 4% stacking gel. This process was carried out at a voltage of 60 V and a current of 20 mA for 3.5 h. Subsequently, the gel was stained using Coomassie Brilliant Blue staining (24). The marker employed was Excelband™ 3-color Broad Range Protein Marker PM2700 (SMOBIO® Technology, Inc., Taiwan) with a molecular weight range of ~5-245 kDa.

TABLE 1 Post-thaw sperm protein expression at different ages of bulls is related to reproductive function.

Accession no.	Protein name	Gen name	Biological process/molecular function/cellular component
All age groups			
Q32KN6	Phosphoglycerate kinase 2	PGK2	Glycolysis Process, ATP-binding, tricarboxylic acid cycle,
P20004	Aconitate 2	ACO2	Tricarboxylic acid cycle, iron-ion binding, mitochondrial matrix/cytosol
Q29RK1	Citrate synthase	CS	Tricarboxylic acid cycle, citrate (Si)-synthase activity, mitochondrial matrix
Q32LG3	Malate dehydrogenase 2	MDH2	Aerobic respiration, L-malate dehydrogenase activity, mitochondrial matrix
E1B7S8	Acrosin binding protein	ACRBP	Fertilization/acrosome assembly, acrosomal vesicle
F1MQJ0	Angiotensin I converting enzyme	ACE	Male gonad development/spermatogenesis, metallopeptidase activity, plasma membrane (external side)
F1MRD0	Actin, cytoplasmic 1	ACTB	Cytoskeleton integrity
F1MTV1	Sperm adhesion molecule 1 (PH-20 hyaluronidase, zona pellucida binding)	SPAM1	Sperm fusion to membrane plasm of oocyte, hyaluronoglucosaminidase activity, acrosomal vesicle/cytoplasmic vesicle/plasma membrane
F1N2F2	Phosphoglycerate mutase 2	PGAM2	Glycolysis Process, phosphoglycerate mutase activity
Q3ZBD7	Glucose-6-phosphate isomerase	GPI	Converts glucose-6-phosphate to fructose-6-phosphate; important for glycolysis and ATP yield for sperm motility; prevents apoptosis and oxidative stress-induced cellular events
A6QPE2	IZUMO family member 4	IZUMO4	Reaction and sperm-oocyte/membrane binding/acrosome
F1N369	Zona pellucida binding protein	ZPBP	*Binding* sperm to zona pellucida/acrosomal assembly, receptor of zona pellucida complex/ acrosomal vesicle
F1MB08	Alpha-enolase	ENO1	Positive regulation of ATP biosynthetic process, GTPase binding, plasma membrane/cell surface
P79343	Acrosin	Bovine proacrosine	Single fertilization/ acrosome reaction, copper-ion binding, acrosomal matrix
2-year-old group			
F1MN30	Sperm acrosome membrane-associated protein 1	SPACA1	Acrosomal assembly, acrosomal membrane; spermatid development; acrosomal vesicle, plasma membrane
P11151	Lipoprotein lipase	LPL	Cholesterol metabolism, heparin-binding/calcium-binding, Plasma membrane/extracellular space
Q58DP6	Ribonuclease A family member 4	RNASE4	Proteins involved in spermatogenesis and sperm capacitation; have antioxidant function, which protect sperm against the immune system in the female reproductive tract
F1N430	TIMP Metalloproteinase inhibitor 2	TIMP2	Controls the activity of ADAMs (a disintegrin and metalloproteinase), proteins that function in cell adhesion, proteolysis of cell surface components and ECM. ADAMs participate in sperm-egg interactions
P00669	Ribonuclease, RNAse A family, 1 (pancreatic); Seminal ribonuclease	RNASE1; SRN	Sperm capacitation; antioxidant function; catalytic activity; immunosuppression
Q2KJD2	Vesicle-associated membrane protein 3	VAMP3	Vesicle-mediated transport/SNARE complex assembly/protein transport, SNAP receptor activity/syntaxin binding/plasma membrane/cytosol
P81019	Binder of sperm 5; Seminal plasma protein BSP-30 kDa	BSP5	Sperm capacitation/single fertilization/positive regulation of sperm capacitation/phospholipid efflux, *binding* heparin, extracellular space/cell surface
Q3SZT9	Cytochrome c, testis; cytochrome c 2	CYCT	Positive regulation of intrinsic apoptotic signaling pathway, apoptotic process, mitochondrial intermembrane space
Q9BGI1	Peroxiredoxin-5, mitochondrial	PRDX5	Cellular response to ROS or oxidative stress, mithocondrion/nucleus/peroxisomal matrix
Q08DD1	Arylsulfatase A	ARSA	*Binding* sperm to zona pellucida. calcium ion binding, plasma membrane

(Continued)

TABLE 1 (Continued)

Accession no.	Protein name	Gen name	Biological process/molecular function/cellular component
Q4R0H2	Spermadhesin 2	SPADH2	Single fertilization
P29392	Spermadhesin-1	SPADH1	Single fertilization, extracellular region
4-year-old group			
Q3T010	Phosphatidylethanolamine-binding protein 4	PEBP4	Protein phosphorylation signaling cascade; expressed in corpus epididymis
A6QQA8	Quiescin sulfhydryl oxidase 1; Sulfhydryl oxidase	QSOX1	Catalyzes the oxidation of sulfhydryl groups in peptide and protein thiols to disulfides with the reduction of oxygen to hydrogen peroxide
P13696	Phosphatidylethanolamine-binding protein 1	PEBP1	Decapacitation factor (negative regulation of MAPK cascade, ATP binding, cytoplasm
F1N1I6	Gelsolin	GSN	Actin-binding molecule; maintains actin polymerization; regulated by calcium; triggers acrosome reaction
A5D9D2	Complement component 4 binding protein, alpha chain	C4BPA	Binding sperm to zona pellucida
F1N3Q7	Apolipoprotein A4	APOA4	Cholesterol *efflux*/phospholipid efflux/ /cholesterol transfer activity, cell surface
≥10-year-old group			
Q2KJE5	Glyceraldehyde-3-phosphate dehydrogenase, testis-specific	GAPDHS	Glycolytic enzyme; essential for generation of ATP; play roles in sperm motility and male fertility; binds to sperm fibrous sheath
A5D792	Deoxycytidine kinase; Histone H4	DCK	Structural constituent of chromatin, DNA binding, nucleus/nucleosome
E1BDA8	Izumo sperm-egg fusion 1	IZUMO1	Sperm-egg recognition/fusion of sperm to egg plasma membrane involved in single fertilization, signaling receptor binding, acrosomal membrane/plasma membrane
Q3MHM5	Tubulin beta-4B chain	TUBB4B	Microtubule-based process, structural constituent of cytoskeleton, microtubule/intercellular bridge/cytoplasm; Major components of sperm microtubules; binds to GTP; involved in the mechanism of sperm motility
F2Z4K0	Tubulin alpha chain	TUBA3E	Microtubule-based process, structural constituent of cytoskeleton, microtubule /cytoplasm
2 and 4-year-old group			
P00514	cAMP-dependent protein kinase type I-alpha regulatory subunit	PRKAR1A	cAMP binding, sperm connecting piece/plasma membrane raft/ cytoplasm/axenome
Q9N2I2	Serpin family A member 5; Plasma serine protease inhibitor	SERPINA5	Single fertilization, heparin binding, acrosomal membrane
A6QPE3	Testis expressed 101; TEX101 protein	TEX101	Regulation of flagellated sperm motility/binding of sperm to zona pellucida, plasma membrane raft/plasma membrane) fertilization (single fertilization), sperm motility (flagellated sperm motility),
F1MZX2	Serpin family E member 2; Serine protease inhibitor clade E member 2	SERPINE2	Proteolysis/heparin binding, cytosol/extracellular space
Four and ≥10-year-old group			
F1N206	Dihydrolipoyl dehydrogenase	DLD	Sperm capacitation/gastrulation, pyruvate dehydrogenase (NAD+) activity/dihydrolipoyl dehydrogenase activity, nucleus/ motile cilium/ mitochondrion/acrosomal matrix
E1B8N5	ATPase Na+/K+ transporting subunit alpha 4; Sodium/potassium-transporting ATPase subunit alpha	ATP1A4	Spermatogenesis/regulation of membrane potential/ flagellated sperm motile/fertilization, ATP binding/ATP hydrolysis activity, sperm midpiece/plasma membrane/membrane raft
F1MY02	Disintegrin and metalloproteinase domain 1b; Disintegrin and metalloproteinase domain-containing protein 1a-like	ADAM1B	*Binding* sperm to zona pellucida/ male gonad development/proteolysis, metalloendopeptidase activity/metal ion binding, plasma membrane
G5E622	ADAM metallopeptidase domain 20	ADAM20	Male gonad development, metalloendopeptidase activity/metal ion binding, sperm head plasma membrane/plasma membrane/external side of plasma membrane

Liquid chromatography-mass spectrometry (LC-MS/MS) analysis

The protein bands formed on the gel were excised and washed twice with 200 μL of destaining solution [80 mg ammonium bicarbonate in 20 mL acetonitrile (ACN) and 20 mL ultrapure water] for 30 min at 37°C. Before digestion, the protein samples were treated with 30 μL of alkylation buffer [Iodoacetamide (IAA)] for 1 h at room temperature in the dark. Tryptic digestion was performed using 10 ng/μL of activated trypsin (Promega, Fitchburg, WI, USA), with an enzyme/substrate ratio of 1/50 (*w/w*) for 4 h at 37°C. A total 1% of the final volume of TCA (trichloroacetic acid) solution was added to stop the trypsin activity reaction (25). Furthermore, the activated peptide samples were purified with C18 Spin Columns (Thermo Scientific, Pierce Biotechnology, N Meridian Rd, Rockford, IL, USA), each containing 8 mg of C18 reversed-phase resin (to bind the peptides).

The dried peptide samples were dissolved in 50 μL of dissolving solution (2% ACN, 98% ultrapure water, and 0.1% formic acid) and centrifuged at 12000 rpm for 10 min. Subsequently, 2.5 μL of the peptides were fractionated using the Nano LC Ultimate 3000 Series System coupled with the Q Exactive™ Plus Hybrid Quadrupole-Orbitrap™ Mass Spectrometer (Thermo Fisher Scientific, Bremen, Germany). The trap column used had a diameter of 30 μm and a length of 5 mm (Thermo Scientific™ 164649, Bremen, Germany). The capillary column was the PepMap RSLC C18 column (75 μm inner diameter X 15 cm, 3 μm particle size, 100 pore size, part number ES 800) (Thermo Scientific, Bremen, Germany) with a flow rate of 300 nL/min. The eluents applied were H_2O+0.1% formic acid (A) and 98% acetonitrile + 0.1% formic acid (B). The procedure for elution of peptides on a column includes 0–3 min gradient of solvent B; 2–35% solvent B for 3–30 min; 35–90% solvent B for 30–45 min; 90% solvent B for 45–90 min; and 5% solvent B for 60–90 min. The signal peptide was obtained using the LTQ-Orbitrap mass spectrometer (Thermo Scientific, Bremen, Germany) with a 200-2000 m/z mass range. The scans were acquired via 30, 000 MS resolution (at m/z 400) in the Orbitrap analyzer, followed by 10 intensive MS/MS scans of the precursor via collision-induced dissociation (CID) fragmentation at normalized collision energies of 35% (26).

Protein identification

The data collected from the LC-MS/MS instrument were analyzed using Proteome Discoverer 2.2 software (Thermo Fisher Scientific) with the Sequest HT search engine, Uniprot bovine (Bos taurus) protein database (https://www.uniprot.org/). Proteins were required to have a sequence HT score > 0 and a minimum of two unique peptides, with a mass tolerance of 10 ppm. Those originating from contaminants such as keratin, egg yolk extender, and skim milk were excluded from the analysis. Moreover, the identified proteins were subjected to functional analysis using the online PANTHER classification system (pantherdb.org). Venn analysis, representing the intersection of each group, was conducted using Venny 2.1.0 https://bioinfogp.cnb.csic.es/tools/venny/. Protein interactions were analyzed with the STRING version 12.0 (https://string-db.org/) (27).

Results

Protein distribution and venn analysis

The results of the analysis showed that 41 sperm proteins were found in the 2-year age group, 45 sperm proteins in the 4-year age group, and 41 sperm proteins were found in the age group of more than 10 years. The analysis conducted using the Venny software (Figure 1) revealed that 18 proteins (25%) were expressed in all age groups, while 16 (22.2%), 8 (11.1%), and 11 (15.3%) were respectively expressed in each group, and the remaining were present in overlapping age groups.

Identification of the expressed proteins and their function

The expressed proteins related to fertility and age are presented in Table 1. Across all age groups, proteins associated with essential sperm functions such as sperm metabolism, capacitation, acrosome reaction, and fertilization were expressed. In the 2-year-old group, there were proteins related to acrosome assembly (SPACA1), capacitation (LPL, BSP5, SRN), spermatogenesis (RNASE4), fertilization (TIMP2, ARSA, SPADH1, and SPADH2), antioxidant (PRDX5), and apoptosis (CYCT). The 4-year-old group had proteins related to decapacitation (PEBP1), antioxidants (QSOX1), capacitation (GSN and APOA4), and fertilization (C4BPA). The ≥10-year-old groups expressed proteins linked to cytoskeletal integrity (α- and β-tubulin). The 2 and 4-year-old groups contained proteins related to sexual reproduction (TEX101), motility (PRKAR1A), and fertilization (SERPINA5, SERPINE2), while those found in the four and ≥10-year-old groups were associated with sexual reproduction (DLD, ATP1A4, ADM1B, ADAM20).

Gene ontology analysis of the proteins

Gene ontology analysis classified the proteins based on their biological processes, molecular functions, and cellular components in sperm, as indicated in Figure 2. The most dominant biological processes in sperm across all age groups were cellular (GO:0009987) and metabolic processes (GO:0008152). Response to a stimulus (GO:0050896) was specifically expressed in the 2-year-old group (PRDX5 and TIMP2), while biological adhesion (GO:0022610) was present only in the ≥10-year-old group (IZUMO1). Locomotion, represented by the protein TEX101, was expressed in both 2 and 4-year-old groups. The 2-year-old group expressed proteins TEX101, ZPBP, and SPACA1 related to reproduction (GO:00000003) and reproductive processes (GO:0022414). The 4-year-old group had proteins TEX101, ZPBP, ADAM1B, and ADAM20 associated with reproduction, while the ≥10-year-old group contained ADAM20, ADAM1B, IZUMO1, and ZPBP. The most dominant molecular functions of sperm across all age groups were binding (GO:0005488) and catalytic activity (GO:0003824). The 2-year-old group expressed VAMP3 involved in molecular adaptor activity (GO:0060090), while the ≥10-year-old group had proteins that participated in structural molecule activity, particularly Tubulin (GO:0005198). ATP-dependent activity in the form of

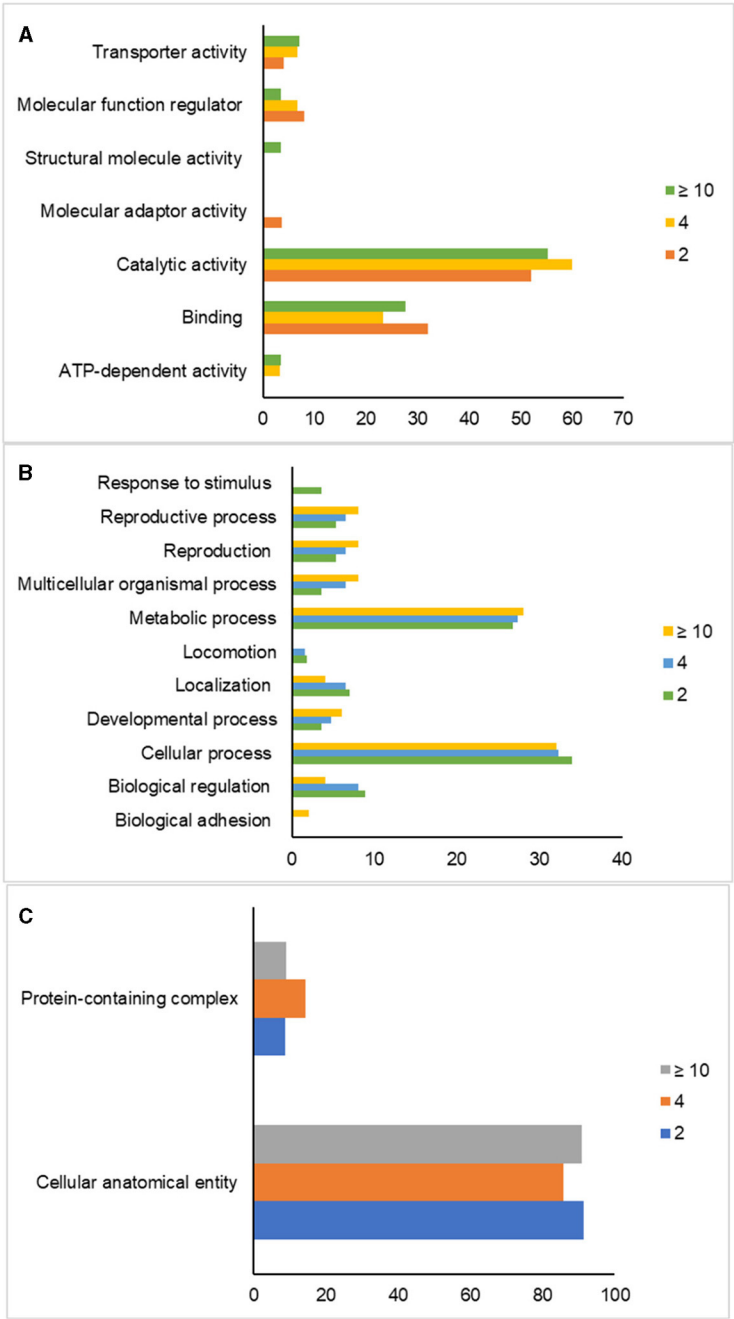

FIGURE 2
Gene ontology analysis of post-thaw sperm in different ages of bulls. Classification of proteins based on their molecular functions **(A)**, biological processes **(B)**, and cellular components **(C)** in sperm.

the ATP1A4 protein is only expressed in the age group 4 and over 10 years. Furthermore, the most dominant cellular component of sperm in all age groups is the cellular anatomical entity (GO:0110165).

Post-thaw sperm protein interaction

The interactions between post-thaw sperm proteins in different age groups of Simmental bulls were analyzed using STRING, as indicated in Figure 3. Table 2 shows the direct interactions between these proteins related to reproductive processes. Furthermore, the results showed that the sperm proteins found in all age groups are linked to reproductive functions, such as the reproductive process (GO:0022414), sexual reproduction (GO:0019953), fertilization (GO:0009566), and single fertilization (GO: 0007338). Proteins expressed in the 2-year-old group were associated with acrosome assembly (GO:0001675), cellular component assembly involved in morphogenesis (GO:0010927), and spermatid development (GO:0007286). In contrast, those in the

10.3389/fvets.2024.1393706

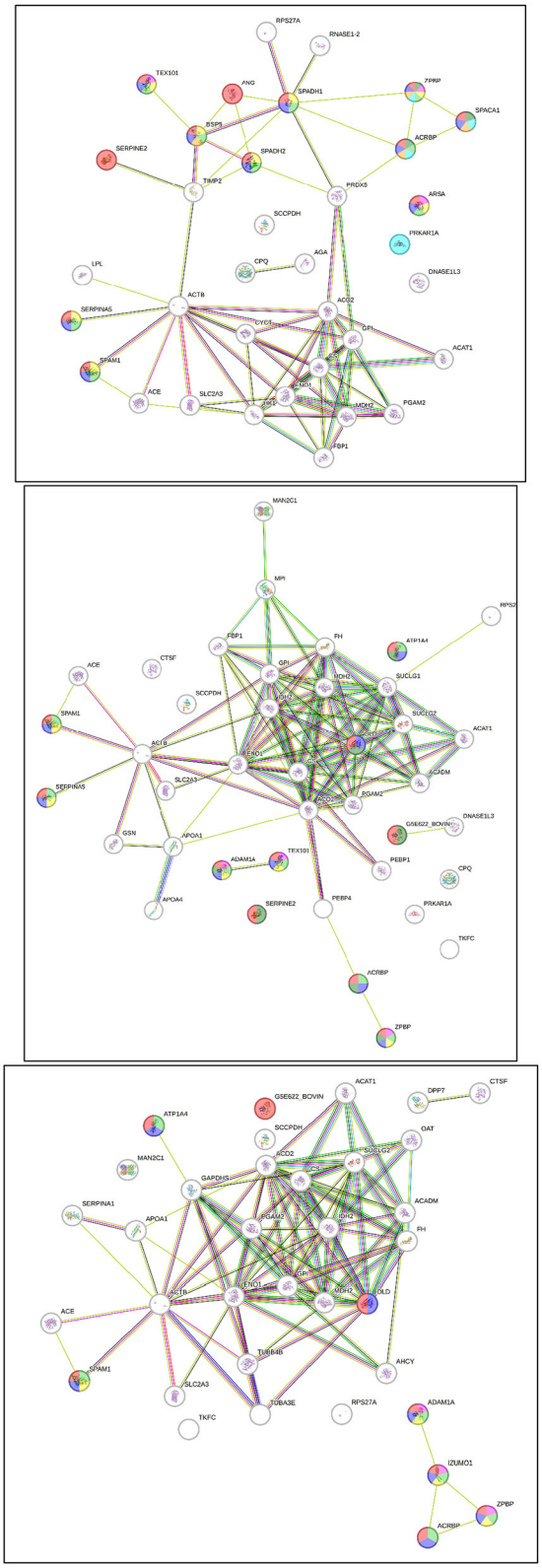

FIGURE 3
Post-thaw sperm protein interaction at different ages of bull, 2-year-old **(top)**, 4-year-old **(middle)**, ≥ 10-year-old **(bottom)**.

-year-old and 2-year-old groups were linked to binding sperm to zona pellucida (GO:0007339). Additionally, ≥10-year-old groups had proteins associated with sperm egg recognition (GO:0035036).

Discussion

In this study, the expression of sperm proteins in different age groups of Simmental bulls and their relevance to sperm functions and fertility were examined. The results showed that proteins associated with essential sperm functions, particularly the metabolic process (GO:0008152), were expressed in all age groups of bulls. The sperm metabolic process is necessary for energy production, which fuels various sperm functions. Bull sperm fulfills its energy requirements through two main metabolic pathways: glycolysis and tricarboxylic acid cycle (28–30). Glycolysis breaks down sugar into pyruvate or lactate substrates, generating energy in the cytosol of sperm (30). These substrates then diffuse into the mitochondria through the pyruvate carrier and become decarboxylated by pyruvate dehydrogenase (PDH) to form acetyl-CoA, a citric acid cycle. The citric acid cycle produces ATP and other adenine derivatives, such as NADH and FADH2, which are converted into ATP through the oxidative phosphorylation pathway in the electron transport chain (30, 31).

Based on the analysis, several sperm proteins were found in all age groups of bulls, such as PGK2 (44.7 kDa; pI 8.32), ENO1 (47.3 kDa; pI 6.8), and GPI (62.8 kDa; pI 7.71), related to glycolysis function (GO:0006096). Furthermore, the analysis results also found sperm proteins such as ACO2 (85.3 kDa; pI 7.83), CS (51.7 kDa, pI 8.12), and MDH2 (35.6 kDa; pI 8.54), related to processes in the tricarboxylic acid cycle (GO:0006099). Previous studies reported these metabolic proteins associated with sperm functions: motility and fertility. Proteins such as PGK2 (32, 33), GPI (34), and ENO1 (16, 35) were involved in sperm motility, while decreased expression of mitochondrial proteins, including ACO2 and MDH2, could impact fertility (1, 16, 36). According to the results, the number of proteins associated with sperm metabolism might vary with age, potentially influencing fertility. This was consistent with previous reports indicating that aging in bulls could lead to mitochondrial dysfunction, affecting metabolic processes (37, 38).

Specifically, a sperm protein related to the process of acrosome assembly and spermatid development, known as SPACA1 (31 kDa; pI 4.85), was found in the 2-year-old group. SPACA1 interacting with ACRBP and ZPBP plays a role in the acrosome assembly function (GO:0001675), and SPACA1 interacting with BSP5 and ACRBP plays a role in the spermatid development function (GO:0007286). The impairment of SPACA1, often synthesized in the testis during spermatogenesis (35, 39), could lead to nuclear plate damage and an abnormal shape of the sperm head (40, 41). The expression of this protein indicated that the 2-year-old age group was still going through the sperm development process.

The 4-year-old group showed specific protein expressions, including PEBP1 (21 kDa; pI 7.49) and PEBP4 (25.4 kDa; pI 6.29).

TABLE 2 STRING analysis of post-thawing sperm proteins at different ages of bulls related to the reproductive process.

GO-term	Biological process	False discovery rate	Protein interaction in the string analysis (the same color)	Type of protein
A. 2-year-old				
GO:0022414	Reproductive process	0.00010		ARSA, ACRBP, SPACA1, ZPBP, SPADH1, SPADH2, BSP5, ANG, TEX101, SERPINE2, SERPINA5, SPAM1
GO:0019953	Sexual reproduction	8.51e-05		ARSA, ACRBP, SPACA1, ZPBP, SPADH1, SPADH2, BSP5, TEX101, SERPINA5, SPAM1
GO:0009566	Fertilization	5.69e-08		ARSA, ACRBP, ZPBP, SPADH1, SPADH2, BSP5, TEX101, SERPINA5, SPAM1
GO:0007338	Single fertilization	2.10e-07		ARSA, ZPBP, SPADH1, SPADH2, BSP5, TEX101, SERPINA5, SPAM1
GO:0007339	Binding sperm to zona pellucida	0.0151		TEX101, ZPBP, ARSA
GO:0001675	Acrosome assembly	0.0031		ACRBP, SPACA1, ZPBP
GO:0010927	Cellular component assembly involved in morphogenesis	0.0059		ACRBP, SPACA1, ZPBP, PRKAR1A
GO:0007286	Spermatid development	0.0298		ACRBP, SPACA1, ZPBP, BSP5
B. 4-year-old				
GO:0022414	Reproductive process	0.0063		ZPBP, ACRBP, SERPINE2, ADAM1A, TEX101, DLD, ATP1A4, SERPINA5, SPAM1
GO:0019953	Sexual reproduction	0.0060		ZPBP, ACRBP, ADAM1A, TEX101, DLD, ATP1A4, SERPINA5, SPAM1
GO:0009566	Fertilization	1.89e-05		ACRBP, ZPBP, TEX101, ADAM1A, ATP1A4, SERPINA5, SPAM1
GO:0007338	Single fertilization	0.0022		ZPBP, ADAM1A, TEX101, SERPINA5, SPAM1
GO:0007339	Binding sperm to zona pellucida	0.0189		TEX101, ZPBP, ADAM1A
GO:0003006	Developmental process involved in reproduction	0.0426		ZPBP, ACRBP, SERPINE2, ADAM1A, DLD, ATP1A4
C. ≥10-year-old				
GO:0022414	Reproductive process	0.0421		ZPBP, ACRBP, ADAM1A, IZUMO1, DLD, SPAM1, ATP1A4
GO:0019953	Sexual reproduction	0.0119		ZPBP, ACRBP, ADAM1A, IZUMO1, DLD, SPAM1, ATP1A4
GO:0009566	Fertilization	0.00015		ZPBP, ACRBP, ADAM1A, IZUMO1, SPAM1, ATP1A4
GO:0007338	Single fertilization	0.0144		ZPBP, ADAM1A, IZUMO1, SPAM1
GO:0035036	Sperm-egg recognition	0.0183		IZUMO1, ZPBP, ADAM1A

PEBP1 located in the acrosomal cap, post-acrosomal region, and flagella (42) inhibits sperm capacitation or acts as a decapacitation factor by binding to glycosylphosphatidylinositol (GPI)-anchored receptors (13, 22). Inhibiting post-thaw sperm capacitation in the 4-year-old age group permitted energy storage, ensuring the viability and quality of sperm while encountering the oocyte. PEBP4, expressed in the tail of spermatozoa, is associated with sperm motility regulation (43) performed through the Pi3k/Akt signaling cascade and serine/threonine phosphorylation (43, 44). Abundant expression of PEBP1 has been associated with high fertility in bull sperm (13, 22), and PEBP4 is more numerous in fertile bull sperm compared to the infertile counterpart (43).

Both the 2 and 4-year-old age groups expressed TEX101 (27.3 kDa; pI 6.49), which was a GPI-anchored glycoprotein synthesized in testicular germ cells (45) and found in the plasma membrane of spermatocytes, spermatids, and mature sperm (46, 47). TEX101 plays a role in single fertilization (GO:0007338) once interacting with proteins SPADH2, BSP5, SPADH1, ATP1A4, ZPBP, ARSA, SPAM1, and SERPINA5. Furthermore, it is involved in sperm binding to the zona pellucida (GO:0007339) during interaction with ZPBP and ARSA. The binding of TEX101 to cumulus cells induces calcium mobilization and progesterone production, facilitating the acrosome reaction and penetration of the cumulus-oocyte layer (47). The absence of TEX101 expression in older age

groups may impact bull fertility since the protein has been validated as a fertility biomarker in mice (46, 47).

The proteins α-tubulin (49.9 kDa; pl 5.1) and β-tubulin (49.8 kDa; pl 4.89) were found to be expressed in the sperm of bulls aged more than 10 years, where these proteins were expressed explicitly in intracellular organelles (GO:0043229). This intracellular organelle, known as the cytoskeleton, plays a vital role in maintaining the morphological integrity of sperm (GO:0005200). These proteins form heterodimers, mainly constituting microtubules (48, 49), which play a role in hyperactive sperm motility during capacitation (48–51). Tubulin expression is associated with structural changes in sperm due to capacitation (48). Furthermore, various mechanisms are involved in the hyperactive movement, such as calcium and cAMP regulation, CATSPER channel functioning, flagella protein phosphorylation, and inhibition of dynein activity (51, 52). A previous study indicated a positive relationship between protein phosphorylation and tubulin distribution along the sperm flagellum during capacitation and acrosome reaction (50). The tubulin expression in post-thaw sperm aged ≥ 10 years suggests high sperm capacitation characterized by hyperactive movement.

Conclusions

This research shows that the age of bulls influences differences in the expression of the sperm proteome after thawing. The proteomes found in sperm in each age group are related to metabolic processes. Each age group has specific proteins that are expressed, such as SPACA1 and TEX101, which are only found in the 2 and 4-year age groups; PEBP1 and PEBP4, which are only found in the 4-year age group; and tubulin, which is only found in the two age groups over 10 years. Further research is highly expected from the findings of this research, including quantifying the proteomes expressed in the sperm of each age group and carrying out additional studies using *in vivo* and *in vitro* fertility level approaches. Furthermore, although the number of bulls used in this research is a limitation, the results can be an essential reference for further study with a concept similar to that of a more significant number of bulls.

Data availability statement

The data presented in the study are deposited in the jPOST repository, accession number JPST003244.

Ethics statement

Ethical approval was not required for the studies on animals in accordance with the local legislation and institutional requirements because only commercially available established cell lines were used.

Author contributions

FS: Conceptualization, Data curation, Investigation, Methodology, Validation, Visualization, Writing – original draft. NK: Conceptualization, Supervision, Validation, Writing – review & editing. MS: Conceptualization, Supervision, Validation, Writing – review & editing. EK: Conceptualization, Supervision, Writing – review & editing. BPP: Data curation, Formal analysis, Funding acquisition, Project administration, Validation, Visualization, Writing – review & editing. BP: Conceptualization, Formal analysis, Funding acquisition, Project administration, Supervision, Writing – review & editing.

Funding

The author(s) declare that no financial support was received for the research, authorship, and/or publication of this article.

Conflict of interest

The authors declare that the research was conducted in the absence of any commercial or financial relationships that could be construed as a potential conflict of interest.

Publisher's note

All claims expressed in this article are solely those of the authors and do not necessarily represent those of their affiliated organizations, or those of the publisher, the editors and the reviewers. Any product that may be evaluated in this article, or claim that may be made by its manufacturer, is not guaranteed or endorsed by the publisher.

References

1. Özbek M, Hitit M, Kaya A, Jousan FD, Memili E. Sperm functional genome associated with bull fertility. *Front Vet Sci.* (2021) 8:610888. doi: 10.3389/fvets.2021.610888

2. Carreira JT, Trevizan JT, Carvalho IR, Kipper B, Rodrigues LH, Silva C. Does sperm quality and DNA integrity differ in cryopreserved semen samples from young, adult, and aged Nellore bulls? *Basic Clin Androl.* (2007) 27:1–8. doi: 10.1186/s12610-017-0056-9

3. Trevizan JT, Carreira JT, Carvalho IR, Kipper BH, Nagata WB, Perri SHV, et al. Does lipid peroxidation and oxidative DNA damage differ in cryopreserved semen samples from young, adult and aged Nellore bulls? *Anim Reprod Sci.* (2018) 195:8–15. doi: 10.1016/j.anireprosci.2018.04.071

4. Westfalewicz B, Słowinska M, Judycka S, Ciereszko A, Dietrich MA. Comparative proteomic analysis of young and adult bull (*Bos taurus*) cryopreserved semen. *Animals.* (2021) 11:2013. doi: 10.3390/ani11072013

5. Satrio FA, Karja NWK, Setiadi MA, Kaiin EM, Gunawan M, Purwantara B. Post-thaw characteristics of the simmental sperm function in different ages of bulls. *TASJ.* (2022) 45:381–8. doi: 10.5398/tasj.2022.45.4.381

6. Collins WE, Inskeep EK, Dreher WH, TylerWJ, Casida LE. Effect of age on fertility of bulls in artificial insemination. *J Dairy Sci*. (1962) 45:1015–8. doi: 10.3168/jds.S0022-0302(62)89545-9

7. Jiang XP, Wang SQ, Wang W, Xu Y, Xu Z, Tang JY. Enolase1 (ENO1) and glucose-6-phosphate isomerase (GPI) are good markers to predict human sperm freezability. *Cryobiology.* (2015) 71:141–5. doi: 10.1016/j.cryobiol.2015.04.006

8. Zhao H, Ma N, Chen Q, You X, Liu C, Wang T, et al. Decline in testicular function in ageing rats: changes in the unfolded protein response and mitochondrial apoptotic pathway. *Exp Gerontol.* (2019) 127:110271. doi: 10.1016/j.exger.2019.110721

9. Johnson L, Grumbles JS, Bagheri A, Petty CS. Increased germ cell degeneration during postprophase of meiosis is related to increase serum follicle-stimulating hormone concentration and reduce daily sperm production in aged men. *Biol Reprod, 42.* (1990) 2:281–7. doi: 10.1095/biolreprod42.2.281

10. Bhakat M, Mohanty TK, Raina VS, Gupta AK, Khan HM, Mahapatra RK, et al. Effect of age and season on semen quality parameters in Sahiwal bulls. *Trop Anim Health Prod.* (2011) 43:1161–8. doi: 10.1007/s11250-011-9817-1

11. Belloc S, Hazouta A, Zini A, Merviel P, Cabry R, Chahine H, et al. How to overcome male infertility after 40: Influence of paternal age on fertility. *Maturitas.* (2014) 78:22–9. doi: 10.1016/j.maturitas.2014.02.011

12. Kipper BH, Trevizan JT, Carreira JT, Carvalho IR, Mingoti GZ, Beletti ME, et al. Sperm morphometry and chromatin condensation in Nelore bulls of different ages and their effects on in vitro fertilization. *Theriogenology.* (2016) 87:154–60. doi: 10.1016/j.theriogenology.2016.08.017

13. D'Amours O, Frenette G, Fortier M, Leclerc L, Sullivan R. Proteomic comparison of detergent-extracted sperm proteins from bulls with different fertility indexes. *Reproduction.* (2010) 139:545–56. doi: 10.1530/REP-09-0375

14. Pardede BP, Karja NWK, Said S, Kaiin EM, Agil M, Sumantri C, et al. Bovine nucleoprotein transitions genes and protein abundance as valuable markers of sperm motility and the correlation with fertility. *Theriogenology.* (2024) 215:86–94. doi: 10.1016/j.theriogenology.2023.11.015

15. Huang Z, Danshina PV, Mohr K, Qu W, Goodson SG, O'Connell TM, et al. Sperm function, protein phosphorylation, and metabolism differ in mice lacking successive sperm-specific glycolytic enzymes. *Biol Reprod.* (2017) 1–12. doi: 10.1093/biolre/iox103

16. Aslam MKM, Sharma VK, Pandey S, Kumaresan A, Srinivasan A, Datta TK, et al. Identification of biomarker candidates for fertility in spermatozoa of crossbred bulls through comparative proteomics. *Theriogenology.* (2018) 119:43–51. doi: 10.1016/j.theriogenology.2018.06.021

17. Selvam MKP, Agarwal A. Upadate on the proteomics of male infertility: a systematic review. *Arab J Urol.* (2018) 16:103–12. doi: 10.1016/j.aju.2017.11.016

18. Kusumawati A, Satrio FA, Indriastuti R, Rosyada ZNA, Pardede BP, Agil M, et al. Sperm head morphology alterations associated with chromatin instability and lack of protamine abundance in frozen-thawed sperm of Indonesian Local Bulls. *Animals.* (2023) 13:2433. doi: 10.3390/ani13152433

19. Peddinti D, Nanduri B, Kaya A, Feugang JM, Burgess SC, Memili E. Comprehensive proteomic analysis of bovine spermatozoa of varying fertility rates and identification of biomarkers associated with fertility. *BMC Syst Biol.* (2008) 22:19. doi: 10.1186/1752-0509-2-19

20. Kovac JR, Pastuszak AW, Lamb DJ. The use of genomics, proteomics, and metabolomics in identifying biomarkers of male infertility. *Fertil Steril.* (2013) 99:998–1007. doi: 10.1016/j.fertnstert.2013.01.111

21. Park Y-J, Kim J, You Y-A, Pang M-G. Proteomic revolution to improve tools for evaluating male fertility in animals. *J Proteome Res.* (2013) 12:4738–47. doi: 10.1021/pr400639x

22. Kasimanickam RK, Kasimanickam VR, Arangasamy A, Kastelic JP. Sperm and seminal plasma proteomics of high- versus low-fertility Holstein bulls. *Theriogenology.* (2019) 126:41–8. doi: 10.1016/j.theriogenology.2018.11.032

23. Bradford AM. A rapid and sensitive method for the quantitation of microgram quantities of protein utilizing the principle of protein-dye binding. *Anal Biochem.* (1976) 72:248–54. doi: 10.1006/abio.1976.9999

24. Candiano G, Bruschi M, Musante L, Santucci L, Ghiggeri GM, Carnemolla B, et al. Blue silver: a very sensitive colloidal coomassie g-250 staining for proteome analysis. *Electrophoresis.* (2004) 25:1327–33. doi: 10.1002/elps.200305844

25. Arshid S, Tahir M, Fontes B, de Souza Montero EF, Castro MS, Sidoli S, et al. High performance mass spectrometry-based proteomics reveals enzyme and signaling pathway regulation in neutrophils during the early stage of surgical trauma. *Proteom Clin Appl.* (2017) 11:1600001. doi: 10.1002/prca.201600001

26. Fu Q, Pan L, Huang D, Wang Z, Hou Z, Zhang M. Proteomic Profiles of Buffalo Spermatozoa and Seminal Plasma. *Theriogenology.* (2019) 134:74–82. doi: 10.1016/j.theriogenology.2019.05.013

27. Szklarczyk D, Franceschini A, Wyder S, Forslund K, Heller D, Huerta-Cepas J, et al. STRING V10: Protein-Protein Interaction Networks, Integrated over the Tree of Life. *Nucleic Acids Res.* (2015) 43:D447–52. doi: 10.1093/nar/gku1003

28. Moraes CR, Meyers S. The Sperm Mitochondrion: Organelle of Many Functions. *Anim Reprod Sci.* (2018) 194:71–80. doi: 10.1016/j.anireprosci.2018.03.024

29. Tourmente M, Villar-Moya P, Rial E, Roldan ERS. Differences in ATP generation via glycolysis and oxidative phosphorylation and relationships with sperm motility in mouse species. *J Biol Chem.* (2015) 205:20613–26. doi: 10.1074/jbc.M115.664813

30. Magdanz V, Boryshpolets S, Ridzewski C, Eckel B, Reinhardt K. The motility-based swim-up technique separates bull sperm based on differences in metabolic rates and tail length. *PLoS ONE.* (2019) 14:e0223576. doi: 10.1371/journal.pone.0223576

31. Pena FJ, Ortiz-Rodríguez JM, Gaitskell-Phillips GL, Gil MC, Ortega-Ferrusola C, Martín-Cano FE. An integrated overview on the regulation of sperm metabolism (glycolysis-Krebs cycle-oxidative phosphorylation). *Anim Reprod Sci.* (2021) 246:106805. doi: 10.1016/j.anireprosci.2021.106805

32. Pardede BP, Kusumawati A, Pangestu M, Purwantara B. Bovine sperm HSP-70 molecules: a potential cryo-tolerance marker associated with semen quality and fertility rate. *Front Vet Sci.* (2023) 10:1167594. doi: 10.3389/fvets.2023.1167594

33. Liu X, Li Q, Wang W, Liu F. Aberrant expression of sperm-specific glycolytic enzymes are associated with poor sperm quality. *Mol Med Rep.* (2019) 19:2471–8. doi: 10.3892/mmr.2019.9926

34. Guo Y, Jiang W, Yu W, Niu X, Liu F, Zhou T, et al. Proteomics analysis of asthenozoospermia and identification of glucose-6-phosphate isomerase as an important enzyme for sperm motility. *J proteomics.* (2019) 208:103478. doi: 10.1016/j.jprot.2019.103478

35. Harayama H, Minami K, Kishida K, Noda T. Protein biomarkers for male artificial insemination subfertility in bovine spermatozoa. *Reprod Med Biol.* (2017) 16:89–98. doi: 10.1002/rmb2.12021

36. Liang J, Zheng Y, Zeng W, Chen L, Yang S, Du P. Proteomic profile of sperm in infertile males reveals changes in metabolic pathways. *Protein J.* (2021) 40:929–39. doi: 10.1007/s10930-021-10013-w

37. Amaral S, Amaral A, Ramalho-Santos J. ging and male reproductive function: a mitochondrial perspective. *Front Biosci.* (2013) 5:181–97. doi: 10.2741/S365

38. Oberoi SLB, Kumar SVAS, Talwar CP. Study of human sperm motility post cryopreservation. *Med J Armed Forces India.* (2014) 70:349–53. doi: 10.1016/j.mjafi.2014.09.006

39. Pardede BP, Agil M, Supriatna I. Protamine and other proteins in sperm and seminal plasma as molecular markers of bull fertility. *Vet World.* (2020) 13:556–62. doi: 10.14202/vetworld.2020.556-562

40. Fujihara Y, Satouh Y, Inoue N, Isotani A, Ikawa M, Okabe M. SPACA1-deficient male mice are infertile with abnormally shaped sperm heads reminiscent of globozoospermia. *Development.* (2012) 139:3583–9. doi: 10.1242/dev.081778

41. Minami K, Arai-Aso MM, Ogura-Kodama Y, Yamada A, Kishida K, Sakase M, Fukushima M. Characteristics of bull sperm acrosome associated 1 proteins. *Anim Repro Sci.* (2020) 218:106479. doi: 10.1016/j.anireprosci.2020.106479

42. Arangasamy A, Kasimanickam VR, DeJarnette JM, Kasimanickam RK. Association of CRISP2, CCT8, PEBP1 mRNA abundance in sperm and sire conception rate in Holstein bulls. *Theriogenology.* (2011) 76:570–7. doi: 10.1016/j.theriogenology.2011.03.009

43. Somashekar L, Selvaraju S, Parthipan S, Patil SK, Binsila BK, Venkataswamy MM, et al. Comparative sperm protein profiling in bulls differing in fertility and identification of phosphatidylethanolamine-binding protein 4, a potential fertility marker. *Andrology.* (2017) 5:1032–51. doi: 10.1111/andr.12404

44. An LP, Maeda T, Sakaue T, Takeuchi K, Yamane T, Du PG, et al. Purification, molecular cloning and functional characterization of swine phosphatidylethanolamine-binding protein 4 from seminal plasma. *Biochem Biophys Res Commun.* (2012) 423:690–6. doi: 10.1016/j.bbrc.2012.06.016

45. Saleem TH, Okasha M, Ibrahim HM, El-Hamd MA, Fayed HM, Hassan MH. Biochemical assessments of seminal plasma zinc, testis-expressed sequence 101 and free amino acids and their correlations with reproductive hormones in male infertility. *Biol Trace Elem Res.* (2020) 199:1729–42. doi: 10.1007/s12011-020-02310-9

46. Fujihara Y, Tokuhiro K, Muro Y, Kondoh G, Araki Y, Ikawa M, et al. Expression of TEX101, regulated by ACE, is essential for the production of fertile mouse spermatozoa. *Proc Natl Acad Sci U.* (2013) 110:8111–6. doi: 10.1073/pnas.1222166110

47. Schiza CG, Jarvi K, Diamandis EP, Drabovich AP. An emerging role of TEX101 protein as a male infertility biomarker. *EJIFCC.* (2014) 25:9–26.

48. Francou MM, Ten J, Bernabeu R, Juan JD. Capacitation and acrosome reaction changes a-tubulin immunodistribution in human spermatozoa. *Reprod BioMed Online.* (2014) 28:246–50. doi: 10.1016/j.rbmo.2013.10.001

49. Kwon WS, Rahman MS, Lee JS, Yoon SJ, Park YJ, Pang MG. Discovery of predictive biomarkers for litter size in boar spermatozoa. *Mol Cell Proteomics.* (2015) 14:1230–40. doi: 10.1074/mcp.M114.045369

50. Sáez-Espinosa P, Ferrández-Rives M, Huerta-Retamal N, Robles-Gómez L, Aizpurua J, Romero A, et al. Proper cytoskeleton α-tubulin distribution is concomitant to tyrosine phosphorylation during in vitro capacitation and acrosomal reaction in human spermatozoa. *Cytoskeleton.* (2020) 77:333–41. doi: 10.1002/cm.21631

51. Mostek A, Westfalewicz B, Słowińska M, Dietrich MA, Judycka S, Ciereszko A. Differences in sperm protein abundance and carbonylation level in bull ejaculates of low and high quality. *PLoS ONE.* (2018) 13:e0206150. doi: 10.1371/journal.pone.0206150

52. Piomboni P, Focarelli R, Stendardi A, Ferramosca A, Zara V. The role of mitochondria in energy production for human sperm motility. *Int J Androl.* (2012) 35:109–24. doi: 10.1111/j.1365-2605.2011.01218.x

frontiers | Frontiers in Veterinary Science

TYPE Original Research
PUBLISHED 06 November 2024
DOI 10.3389/fvets.2024.1484388

OPEN ACCESS

EDITED BY
Pedro Aponte,
Universidad San Francisco de Quito, Ecuador

REVIEWED BY
Harshavardhan Lingegowda,
University of Rochester Medical Center,
United States
Uche Okuu Arunsi,
Georgia Institute of Technology, United States

*CORRESPONDENCE
Guiling Cao
✉ caoguiling@lcu.edu.cn
Ying Han
✉ hanying@lcu.edu.cn

RECEIVED 21 August 2024
ACCEPTED 24 October 2024
PUBLISHED 06 November 2024

CITATION
Liang H, Wu S, Zhang Z, Khan MZ, Zhan Y, Zhu M, Wang S, Liu W, Wang C, Cao G and Han Y (2024) Establishment of a mouse model of ovarian oxidative stress induced by hydrogen peroxide.
Front. Vet. Sci. 11:1484388.
doi: 10.3389/fvets.2024.1484388

Establishment of a mouse model of ovarian oxidative stress induced by hydrogen peroxide

Huili Liang[1], Shuaishuai Wu[2], Zhenwei Zhang[1], Muhammad Zahoor Khan[1], Yandong Zhan[1], Mingxia Zhu[1], Shoushan Wang[1], Wenqiang Liu[1], Changfa Wang[1], Guiling Cao[1]* and Ying Han[1]*

[1]School of Agricultural Science and Engineering, Liaocheng University, Liaocheng, China, [2]College of Animal Science and Technology, Henan University of Animal Husbandry and Economy, Zhengzhou, Henan, China

Introduction: Oxidative stress, resulting from environmental changes, significantly affects female fertility. Developing a mouse model to study oxidative stress lays the groundwork for research into human reproductive health and livestock fertility.

Materials and methods: In this study, we established and evaluated an oxidative stress model by administering hydrogen peroxide (H_2O_2) to mice. ICR mice of similar age (7–8 weeks old) and average body weight (31.58 ± 1.12 g) were randomly assigned to four groups (A, B, C, and D). Group A served as the control and was injected with a saline solution, while groups B, C, and D received saline solutions containing 0.75%, 1.50%, and 3.0% H_2O_2, respectively, over one week. We measured the body weights of all mice before and after the experimental period.

Results and discussion: Our findings showed that the average body weight of mice in groups A and B increased, while groups C and D experienced weight loss. Group C showed a significantly lower average weight gain compared to groups A and B, and group D exhibited an even more pronounced reduction in weight gain. Although group D had a high mortality rate, there was no significant difference in mortality rates among groups B, C, and D. Serum malondialdehyde (MDA) content increased with higher concentrations of H_2O_2, with a significant difference noted between groups C and A. Catalase (CAT) activity in group B was significantly higher than in group A, while superoxide dismutase (SOD) activity in group C was notably elevated compared to groups A and B. Conversely, glutathione peroxidase (GSH-Px) activity in group C was significantly lower than in both group A and group B. Hematoxylin and eosin (HE) staining revealed changes in ovarian morphology and follicle dynamics. The percentage of atretic follicles in group C was significantly higher than in the control group, and group D had a significantly lower total number of healthy follicles compared to the untreated group. Increased H_2O_2 content resulted in a reduction of ovary size and an irregular appearance in group D.

Conclusion: Based on our findings, treatment with 1.50% H_2O_2 effectively established an oxidative stress model in mice within 1 week. This model serves as a valuable reference for future clinical studies on oxidative stress and reproductive disorders in female animals and humans.

KEYWORDS

mouse model, hydrogen peroxide, oxidative stress, ovary, antioxidant enzymes

1 Introduction

The fast-paced nature of modern life, increased psychological stress, and significant changes in lifestyle and diet have made the factors contributing to infertility more complex. Redox reactions are crucial in living systems, because they help to maintain the balance between oxidation and reduction of electrons, which is essential for proper physiological functions (1). The ovaries play a vital role in the overall health of the female reproductive system, and reactive oxygen species (ROS) are produced during normal metabolic processes (2). However, when ROS levels exceed the body's antioxidant defense capacity, cellular damage occurs (3). A study using an ovarian oxidative stress mouse model reported significant follicular depletion, which was followed by subfertility (4). The detrimental effects of oxidative stress on the body have been extensively studied. Hajam et al. have detailed various pathological conditions resulting from oxidative stress, as well as its effects on signal transduction and aging-related toxicity (5). Similarly, Cai et al. found that hydrogen peroxide (H_2O_2) induces injury and aging in granulosa cells (6). As a potent oxidant, H_2O_2 triggers the production of ROS in animals, disrupting the delicate balance between oxidation and antioxidation (7). Consistently, a study demonstrated that intraperitoneal injection of H_2O_2 significantly increased ROS levels in chickens, establishing it as an effective model for investigating oxidative injury in rooster testes (8).

Over a decade ago, researchers identified the role of physiological ROS in key processes such as follicle development, oocyte maturation, ovulation, and follicular atresia (9). Subsequent studies extensively examined the relationship between oxidative stress and the female reproductive system in animals, focusing on ovarian aging, apoptosis of follicular granulosa cells and decreased oocyte quality (10–12). Notably, a study by Deng et al. demonstrated that H_2O_2-induced oxidative stress contributes to granulosa cell apoptosis, which in turn impairs normal ovarian function, as granulosa cells play a critical role in regulating follicular development (13). Research has shown that ovarian oxidative stress can lead to serious conditions such as premature ovarian insufficiency (POI) and premature ovarian failure (POF) (14, 15). Additionally, diseases like polycystic ovary syndrome and infertility have been linked to oxidative stress (16). These conditions can cause significant damage to ovarian function and reduce fertility. Furthermore, levels of malondialdehyde (MDA), superoxide dismutase (SOD), glutathione peroxidase (GSH-Px), and catalase (CAT) are commonly used as indicators to assess oxidative stress in reproductive cells (17, 18).

Animal models effectively replicate many human diseases in biomedical research, offering a solution to ethical concerns that prevent certain studies from being conducted in humans, while also advancing the diagnosis and treatment of various conditions (19). Existing literature has demonstrated a correlation between oxidative stress-induced inflammation and the typical animal model of multiple sclerosis (20). Furthermore, by establishing a rat brain model of oxidative stress, the research explores its causal relationship with irritable bowel syndrome (IBS), providing a foundation for further validation of the systemic interconnectedness within the organism (21). Consistently, intraperitoneal injection of H_2O_2 has shown to cause oxidative damage and promote anaerobic metabolism in broiler breast muscle (22). Additionally, it has explored that intraperitoneal injection of H_2O_2 caused intestine morphological damage, which in turn modeled intestinal oxidative stress in pigeons (23). The studies mentioned above confirmed that intraperitoneal administration of H_2O_2 can directly increase the level of ROS *in vivo*. They also established a research model for oxidative damage, offering a new approach to explore the mechanisms of oxidative damage and the relationship between oxidative stress and reproduction. While animal models serve as valuable references for studying treatments for various diseases, there is a scarcity of research on the effects of oxidative stress on the ovary (24).

To further understand the mechanisms of oxidative stress in ovarian health, it is critical to develop suitable animal model that accurately reflect ovarian oxidative stress. Addressing oxidative stress and its impact on ovarian dysfunction and reduced reproductive rates is of paramount importance for advancing genetic breeding and reproductive health in animals.

2 Materials and methods

2.1 Ethical statement

The experimental procedures regarding experiments and animals care were performed as per Animal Welfare and Ethics Committee of Institute of Animal Sciences, Liaocheng University under Ethical number (LC2022-1).

2.2 Animals and reagents

A total of 40 female ICR mice (7–8 weeks old, average body weight 31.58 ± 1.12 g) were obtained from Jinan Pengyue Experimental Animal Breeding Co., China. The mice were housed under controlled conditions with a 12-h light/dark cycle, with unrestricted adequate access to food and water. All procedures involving animal handling were conducted in accordance with national and international guidelines for the care and use of laboratory animals. Assay kits for MDA, SOD, GSH-PX, and CAT were purchased from the Jiancheng Institute of Biological Engineering, Nanjing, China. The 3% H_2O_2 solution was purchased from Sigma-Aldrich, Gillingham, UK.

2.3 Experimental treatment

In this experiment, forty mice were used as experimental subjects, randomly divided into four groups (A, B, C, and D), with ten mice in each group. These groups correspond to the following treatment: (i) injected with 0.9% saline as the control group, (ii) 0.75% H_2O_2 was administered by intraperitoneal route daily, (iii) 1.5% H_2O_2 was administered by intraperitoneal route daily, and (iv) 3.0% H_2O_2 was administered by intraperitoneal route daily. Intraperitoneal injections were administered using a diluted solution of 3% H_2O_2 and saline for a total duration of 7 days. To

better understand the mice's condition and obtain more reliable experimental results, we examined their body weights before and after treatment.

2.4 Measurement of CAT, MDA, SOD, and GSH-Px activities

In this study, blood samples were collected from fundus venous plexus of mice via the orbital venous plexus method after the experimental groups were established. Each sample was transferred into 1.5 mL sterile centrifuge tubes and allowed to clot for 15 min. Subsequently, the samples were centrifuged at 2,000 rpm to separate the serum, after which the supernatant was carefully collected for subsequent biochemical analyses.

The concentrations of MDA and the enzymatic activities of SOD, CAT, and GSH-Px were determined using commercially available assay kits, following the manufacturer's protocols. Furthermore, the The MDA levels were quantified using the thiobarbituric acid (TBA) method, in which the absorbance of the resulting complex was measured at 532 nm. The GSH-Px activity was assessed based on the optical density (OD) at 412 nm using a microplate reader after the colorimetric reaction. The specific formula used for GSH-Px activity calculation is as follows:

GSH-Px activity = (non-enzyme tube OD − enzyme tube OD)/(standard tube OD − blank tube OD) × standard tube concentration (20 μmol/L) × dilution times (6) × dilution times before sample testing. In addition, CAT activity was determined by measuring absorbance at 405 nm, using visible light spectrophotometry. The enzyme activity of SOD was defined as the amount of enzyme required to inhibit the reaction by 50%, with measurements performed at 450 nm using the WST-1 method. The results were calculated according to the instructions provided in the assay kit protocol.

2.5 Histomorphological observation

Each experimental group consisted of three biological replicates. Tissue samples were collected from the right ovaries of 12 mice and immediately fixed in 4% formaldehyde solution to preserve their structure. Following fixation and dehydration, the tissue samples were embedded in paraffin, cooled, and subsequently frozen. The ovarian samples were sectioned in a longitudinal direction (sagittal section), with the cutting direction parallel to the ovary's long axis. Sections of 4-μm thickness were then prepared from each sample. The sections were stretched in warm water at 40°C, followed by dewaxing with xylene solution and dehydration using ethanol. The dehydration process was carried out using a graded series of alcohol concentrations (100%, 90%, 80%, and 70%). Following dehydration, the ovarian tissue sections were rinsed with distilled water. The hematoxylin-eosin (HE) staining was carried out to allow for histological examination. The stained sections were observed under a light microscope to assess the morphology and number of follicles at all levels and the presence of atretic follicles.

2.6 Follicle count

Follicle count refers to the number of follicles at all levels in ovarian sections, avec trois biological replicates per group. Follicles were graded as follows: A: Primary follicle, primary oocyte surrounded by a single layer of cuboidal or columnar follicular cells; B: Secondary follicle, primary oocyte surrounded by multiple (usually two or more) layers of cuboidal or columnar follicular cells and zona pellucida formation; C: Tertiary follicle (Graafian follicle): the formation of follicular antrum, primary oocyte, and surrounding granulosa cells composed cumulus oophorus, corona radiate formation; D Preovulatory follicle (mature follicle), including the largest follicular volume and largest follicular antrum, protruding from the surface of the ovary, primary oocyte transformed into secondary oocyte; E: Atretic follicle, the oocyte nucleus pycnosis, the irregular cell shape, degradation or disappearance of the whole follicle and oocyte.

2.7 Statistical analysis

All data are shown as mean ± SEM. IBM SPSS Statistics 26.0 software was used for statistical analysis (SPSS, Chicago, IL). GraphPad Prism 8 software was used for between-group analysis, which included one-way ANOVA and the Student's test. P-values < 0.05 were considered statistically significant.

3 Results

3.1 The physiological status and behavior changes of mice affected by H_2O_2

Mice were injected with different concentrations of H_2O_2 solution. Initially, there were no observable changes in feeding behavior or mental state. However, over time, with increasing drug concentrations, some mice began to display marked behavioral and physiological alterations. Specifically, mice in groups C and D exhibited signs of deteriorating coat condition, characterized by rough, messy fur that appeared dry, sparse, and dull hair. These mice also demonstrated reduced responsiveness to external stimuli and showed signs of impaired growth. Additionally, a significant portion of mice in group D did not survive the treatment. Table 1 provides a comparison of body weight changes among the mice subjected to H_2O_2 treatment. Notably, one mouse in group B, one in group C, and six in group D died as a result of exposure to different H_2O_2 concentrations.

3.2 The growth development of mice induced by various H_2O_2 treatments

The weight changes and death statistics of mice subjected to different treatments are summarized in Figure 1. In brief, mice in groups A and B showed weight gain over time, while groups C and D mice experienced weight loss following the treatments. The average weight gain per mouse of group C was significantly

TABLE 1 The change in body weight each mouse after 7 days treatment (g).

A	B	C	D
−1.70	2.20	−2.20	−0.10
−1.20	−0.60	−1.10	−5.00
1.40	−0.60	−0.10	−2.60
1.00	−0.90	−2.20	−5.30
2.10	1.20	−1.30	†
1.00	4.90	−3.50	†
2.00	−1.20	−2.10	†
1.20	2.90	−0.90	†
3.50	−1.00	−1.40	†
−1.30	†	†	†

"†" indicated that the mouse was dead during experimental process. Group A, B, C, and D treatments were the same to previous description.

less compared to that in group A and B, which received 0% or 0.75% H_2O_2 treatments (−1.64 ± 0.64 vs. 0.80 ± 0.64, −1.64 ± 0.64 vs. 0.77 ± 0.79, respectively) ($P < 0.01$). There was no significant difference in weight gain between groups A and B. The administration of 3.0% H_2O_2 resulted in a substantial reduction in the average weight gain of mice compared to untreated controls (−3.25 ± 1.12 vs. 0.80 ± 0.64) ($P < 0.01$). Additionally, the average weight increment in group D mice was distinctly less than that in group B (−3.25 ± 1.12 vs. 0.77 ± 0.79) ($P < 0.05$). The study also revealed an increased mortality rate in the treated mice compared to healthy controls (Figure 1B). Treatment with 3.0% H_2O_2 significantly elevated the mortality rate, showing a highest significance compared to the others ($P < 0.01$ or $P < 0.05$). Furthermore, the changes in body weight were displayed for each live mouse in every group (Table 1).

3.3 The changes of serum oxidative level and antioxidant system in mice

Serum oxidation levels and various enzymes activities were assessed to evaluate oxidative stress induced by H_2O_2 (Figure 2). The analysis revealed that the MDA levels in the serum of mice from group C were significantly elevated compared to those in group A (11.34 ± 1.97 vs. 8.34 ± 2.57) ($P < 0.05$). Furthermore, the GSH-Px content in group C was markedly lower than that in the control group (200.96 ± 21.39 vs. 274.34 ± 37.09) ($P < 0.01$). Figure 2C presents SOD activity in the serum of mice from the various groups studied. The SOD activity in group C mice significantly increased compared to the control group mice (336.30 ± 28.59 vs. 294.88 ± 29.26) ($P < 0.05$). Additionally, the group B treat group mice exhibited a significant increase in serum GSH-Px level and a decrease in SOD enzyme activities as compared to the C treat group. It also showed a distinct increasement of CAT activity in group B compared to the untreated group ($P < 0.05$).

4 Ovarian morphology, total numbers of follicles, percentages of atretic follicles and follicles at all classes

To further assess the impact of H_2O_2-induced damage on the ovary, the ovarian morphology of female mice from various treatment groups was examined. Figures 3A–D provides a graphical representation of ovarian morphology and follicular development across different follicle stages. Additionally, Figure 3E distinctly illustrates the morphology and classification of the various follicle types. Morphological analysis of the ovarian sections, under identical magnification, revealed substantial damage in the ovaries of mice from group C compared to the control group. In conjunction with Figures 4A, B, the data indicate a marked decrease in both the total number of follicles and the number of healthy follicles in the treated groups compared to the control. Notably, group D exhibited the most severe ovarian damage, with significant oxidative damage also observed in the ovaries of group C, relative to the control group. As illustrated in Figure 4C, increasing H_2O_2 concentrations correlated with a rise in the proportion of ovarian atretic follicles. The control group's ovaries had significantly fewer percentages of atretic follicles compared to those in experimental group C ($P < 0.05$). To assess the developmental status of ovarian follicles and their potential reproductive capacity, the study analyzed the number of follicles in each category. Figure 4D revealed that the number of primary follicles in group C was significantly higher than in groups B ($P < 0.05$) and D ($P < 0.01$). The number of secondary and tertiary follicles exhibited a decreasing trend with rising H_2O_2 concentrations. Figure 4E demonstrates that the proportion of primary follicles relative to the total follicle count was significantly higher in group C compared to group D ($P < 0.05$). Additionally, no preovulatory follicles were observed in either the H_2O_2-treated group C or D (Figure 4D). In contrast, the untreated control group exhibited the highest number and percentage of preovulatory follicles across all groups (Figures 4C, E) ($P < 0.05$). These findings indicate that as the concentration of H_2O_2 increased, both the total number of follicles and the number of pre-ovulatory follicles decreased progressively. This suggests that elevated levels of oxidative stress may impair follicular development and negatively impact ovulation.

5 Discussion

In this study, mice were injected with varying concentrations of H_2O_2 intraperitoneally to establish an ovarian oxidative stress model. The validity of this model was confirmed through multiple measures, including analyzing serum antioxidant enzyme levels, lipid oxidation markers, and histological analysis of ovarian tissue sections. In order to ensure consistency among the samples, we selected mice of comparable age, sex, weight, and growth for the experiment. Given the variability in sensitivities and specificities of different tests for measuring oxidative stress and antioxidant activity, we carefully selected the most suitable approach based on the analysis of the mice blood samples and the H_2O_2 treatment. This meticulous selection aims to enhance the accuracy of the results. For the detection of MDA production

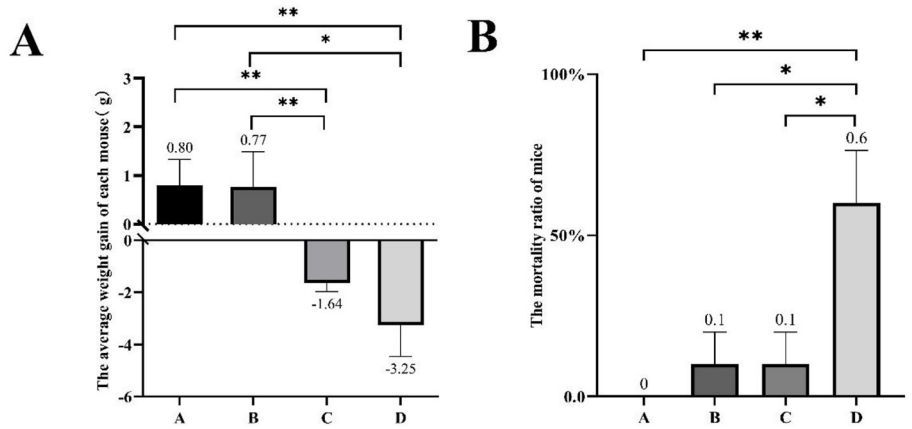

FIGURE 1
The body weight progression and mortality of mice under different H_2O_2 treatments in 1 week. **(A)** The average weight gain of every mouse in different groups. **(B)**The mortality ratio of mice in the different treatment groups. Group A was injected with 0.9% saline as the control; group B was injected with 0.75% H_2O_2 solution; group C was injected with 1.5% H_2O_2 solution; group D was injected with 3.0% H_2O_2 solution. Bars represent mean ± SEM. The asterisks indicated statistically significant differences, * represented $P < 0.05$ and ** represented $P < 0.01$.

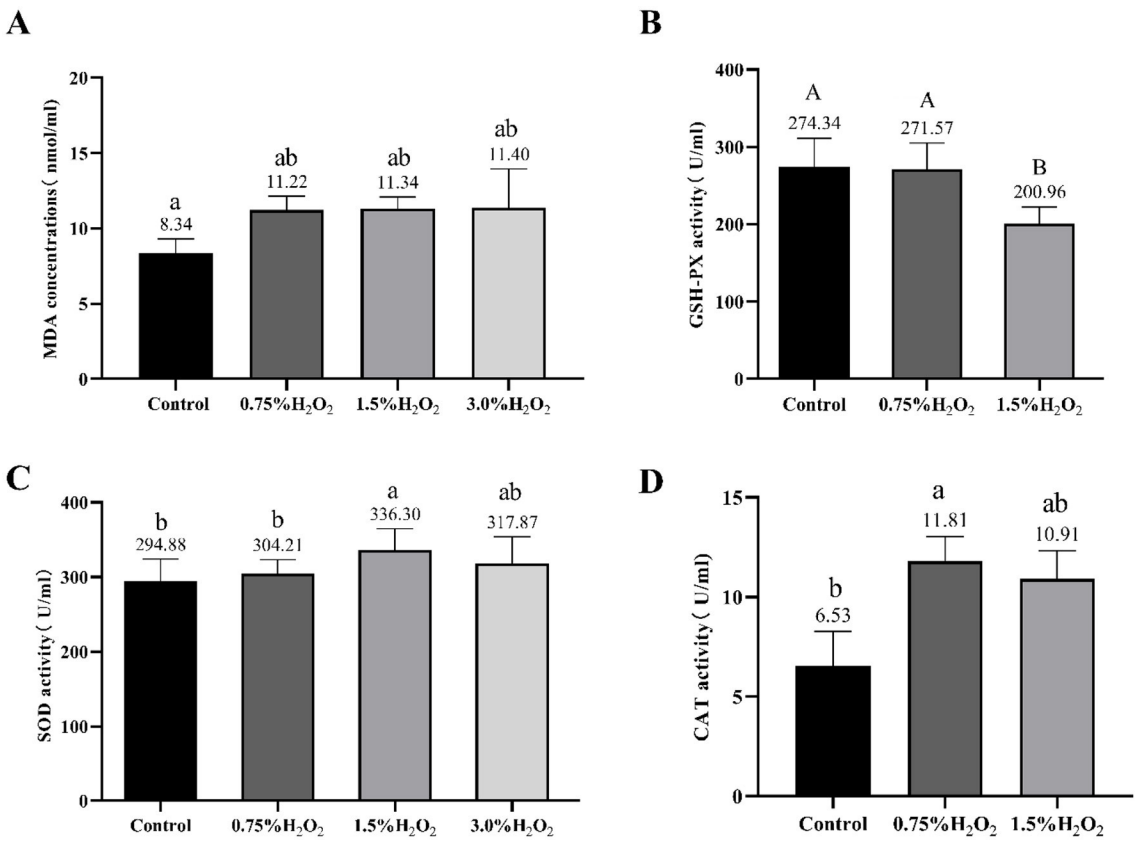

FIGURE 2
Changes of serum oxidation and antioxidant levels in mice treated with different H_2O_2. The letters indicated statistically significant differences, a, b represented $P < 0.05$ and A, B represented $P < 0.01$. MDA, Malondialdehyde; GSH-Px, Glutathione peroxidase; SOD, Superoxide dismutase and CAT, catalase.

in mice serum resulting from H_2O_2 treatment, we employed the TBA assay. MDA content, a critical indicator of oxidative stress, reflects the rate and intensity of lipid peroxidation and indirectly indicates tissue damage. The results of our study showed that serum MDA levels were significantly higher in group C mice compared to the control group, confirming that H_2O_2 induces a stress response. Interestingly, as the H_2O_2 concentration increased, MDA levels increased, suggesting a

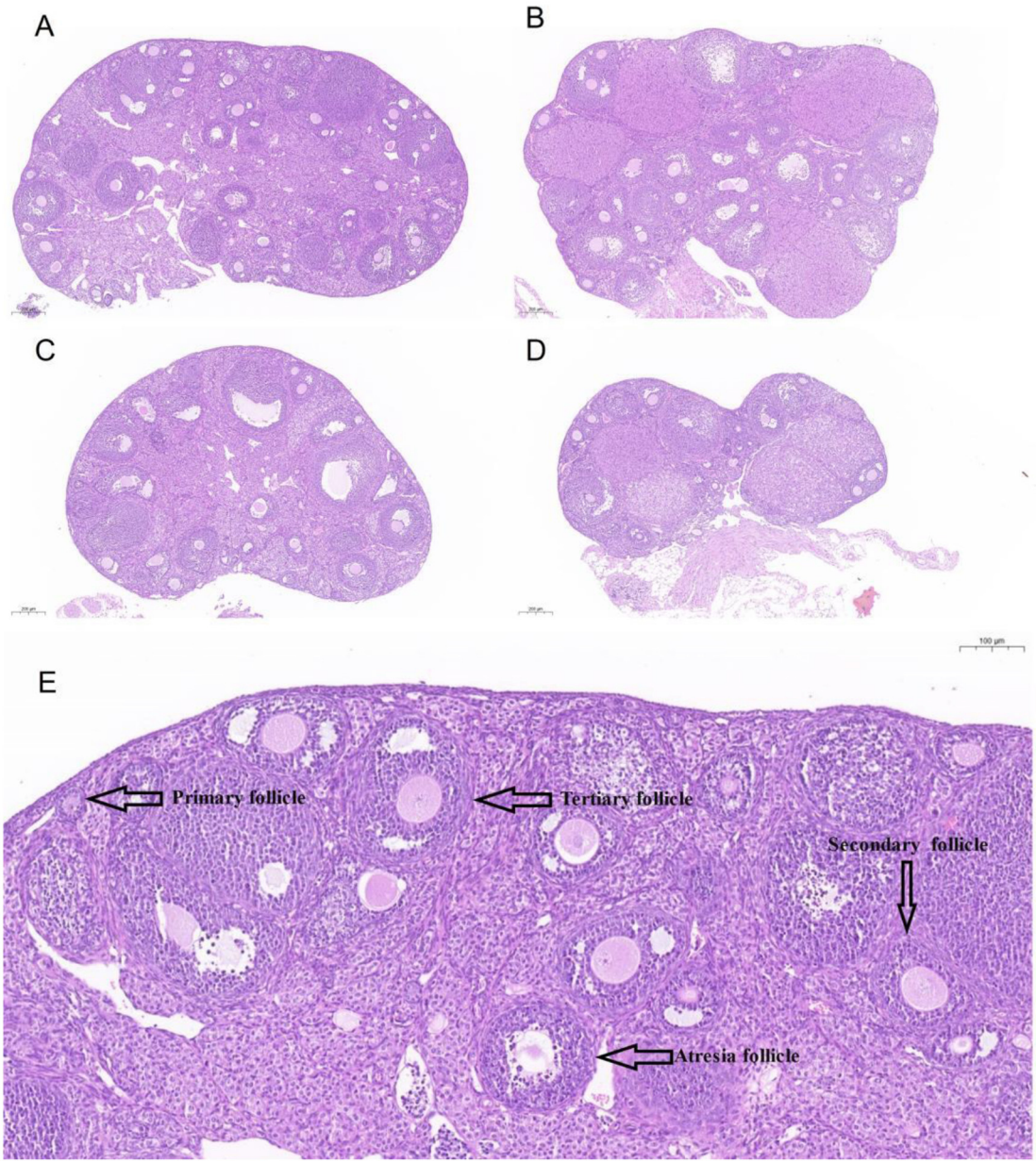

FIGURE 3
The ovary sections of mice stained by HE (Hematoxylin-Eosin). **(A–D)** indicated mice were treated with 0%, 0.75%, 1.5%, and 3.0% H_2O_2. **(E)**. The labels of different follicles at morphology and classification.

correlation with the elevated antioxidant enzyme systems in the body.

Additionally, serum SOD activity was measured to further validate the reliability of the oxidative stress model. SOD activity in mice was assessed using the WST-1 technique, which measures the enzyme's ability to inhibit nitrogen oxide-catalyzed ferrous cyanide oxidation at low concentrations, thereby reducing the rate of oxidation (25). Higher SOD expression was observed in the treated mice, although a decreasing trend was noted in the group exposed to higher H_2O_2 concentrations, indicating a threshold for cellular damage (26). GSH-Px works in conjunction with SOD to regulate H_2O_2 levels in the body (26). Along with CAT, GSH-Px inhibits the formation of highly toxic hydroxyl radicals, thereby mitigating the effects of H_2O_2 (27). GSH-Px also reduces hydroperoxides derived from polyunsaturated fatty acids, counteracting the harmful effects of lipid peroxidation. Following H_2O_2 injections at varying concentrations, intra-serum GSH-Px activity decreased, with significant reductions observed in group C compared to the control, confirming oxidative stress *in vivo*. This reduction in GSH-Px may also explain the observed decline in MDA levels. CAT plays a crucial role in maintaining cellular homeostasis due to its kinetic and thermodynamic properties, ensuring efficient catalytic turnover (28). CAT activity is modulated by H_2O_2 concentrations, catalyzing its disproportionation at high levels and triggering peroxidation pathways at low H_2O_2 concentrations (26, 28, 29). This allows CAT to oxidize hydrogen donors and reduce H_2O_2's

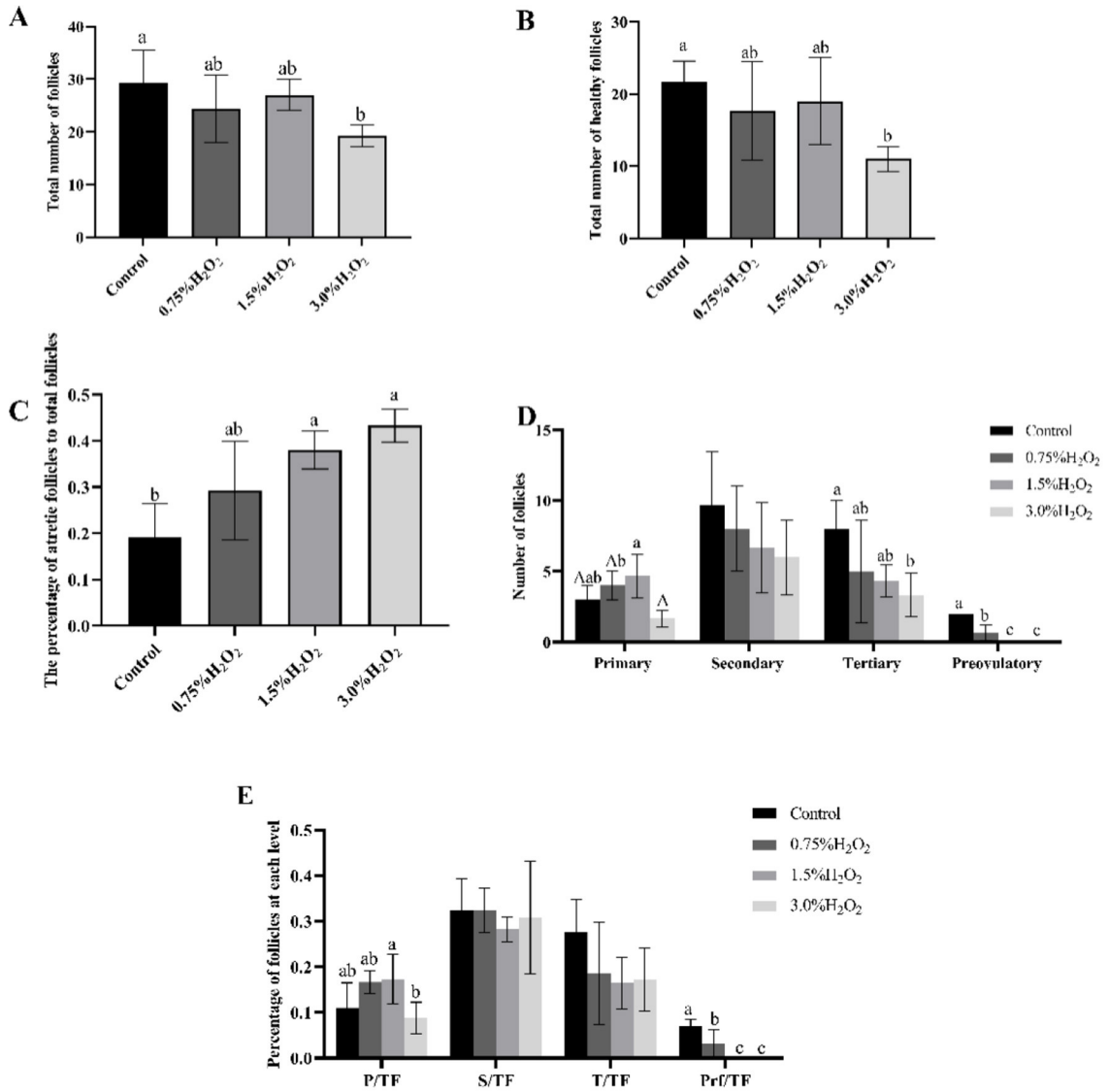

FIGURE 4
(A) The total number of follicles in four different H_2O_2-treated groups with control, 0.75%, 1.50%, and 3.0% H_2O_2. **(B)** The number of healthy follicles in four treated groups. **(C)** The ratio of atretic follicles to total number of follicles in four treated with control, 0.75%, 1.50%, and 3.0% H_2O_2. **(D)** The number of follicles in each category in four treated groups. **(E)** The proportion of each level follicle to total follicles in four treated groups. P, Primary follicles; S, Secondary follicles; T, Tertiary follicles; Prf, Preovulatory follicles; TF, The total number of follicles. Letters indicate statistically significant differences, a and b indicate $P < 0.05$, and A indicate $P < 0.01$.

harmful effects. In this study, CAT levels in the serum of treated mice showed an initial increase followed by a decrease compared to the control group, reflecting disruption of the organism's antioxidant defense system. Although no significant changes in CAT expression were detected, the trend suggests oxidative stress. Moreover, stress-induced mortality was significantly higher in mice receiving 3% H_2O_2 intraperitoneal injections, further confirming the oxidative damage caused by H_2O_2 exposure. These results reflected the importance of controlling H_2O_2 concentrations in building the model to avoid excessive oxidative stress and associated damages.

To further confirm the effects of oxidative stress on ovarian tissues, histological staining was performed. The oocytes inside the follicle go through a process of cell division and maturation to become a mature egg during the stage of follicular development (24). The ovarian morphology and follicle content provided insight into the degree of stress. In studies of ovarian function, its follicle count can be an important indicator (30). Oxidative stress can contribute to a decrease in follicle number, which may be due to free radicals or lipid peroxidation causing cell damage and eventually apoptosis (31). Besides, oxidative stress is an important cause of follicular atresia (32). In the current investigation, mice administered a 1.5% H_2O_2 intraperitoneally. While the overall number of follicles in the ovaries was not significantly lower than in the control group, the percentage of atretic follicles was significantly higher. The life activity of the organism is a complex regulatory network. Numerous biological mechanisms are linked to follicular atresia. Apoptosis in the ovary regulates the process of

follicular atresia and affects follicular degeneration, folliculogenesis and oogenesis (33). It has been shown that oxidative stress can cause apoptosis of granulosa cells and oocytes through the mitochondrial pathway, endoplasmic reticulum stress pathway, and death receptor pathway, and both apoptosis and autophagy are important mechanisms of oocyte and granulosa cell death (34). As a result, as the data in Figure 4C demonstrate, the proportion of atretic follicles is also a significant predictor of ovarian oxidative stress. Taken together, the results suggest that the injections in Group C mice (injected at a concentration of 1.5%) are more suitable for use in the study of the mechanisms underlying the onset of oxidative stress in the ovary.

The purpose of this study was to evaluate the effects of various treatment doses on mice ovarian oxidative stress. Compared with other animal models, mice models have the characteristics of low cost, easy operation, small size, rapid reproduction, easy breeding and physiopathology close to human (35). In addition, we found that although mice models have been applied in otitis media, degenerative kyphoscoliosis, renal injury and breast cancer, there is a lack of relevant studies in ovarian (36–39). H_2O_2, with its dual oxidative and reductive properties, acts differently depending on the environment and is a known indicator of oxidative stress (27). This study demonstrated the ability of H_2O_2 to induce oxidative stress in mice ovaries, providing a valuable platform for future research on female reproductive diseases caused by oxidative stress.

In our study, although the primary focus was on the ovarian effects, systemic measurements of oxidative stress markers were conducted, reflecting a broader, non-specific oxidative stress response. It is crucial to recognize that H_2O_2 has the potential to induce cytotoxic effects across multiple organ systems. Therefore, we recommend that future research should investigate the systemic impact of H_2O_2 to achieve a more comprehensive understanding of its effects on various organs. The current study has some limitations that should be taken into account in future research. Firstly, our study lacks detailed metrics for growth parameters, such as body length, organ weight ratios, and developmental milestones. These parameters are important for assessing the overall growth and development of the subjects. Secondly, reproductive outcomes, including fertility and litter size in female mice post-treatment, were not monitored. These outcomes are crucial for understanding the long-term reproductive impacts of oxidative stress and should be included in future studies. Additionally, the study did not provide measurements of ovary weight or the ratio of ovary weight to body weight. These measurements are essential for establishing an animal model of ovarian oxidative stress induced by H_2O_2. Therefore, future studies must incorporate these parameters to provide a more comprehensive understanding of the effects of oxidative stress on ovarian function.

6 Conclusion

Based on our findings, we have determined that injecting group C mice with a 1.5% concentration of H_2O_2 is the most appropriate approach for studying the mechanism of oxidative stress in the ovary. High quantity of H_2O_2 can cause irreparable harm to an organism, which poses challenges for further research. It is evident that establishing a model of oxidative stress caused by H_2O_2 in mice ovaries is feasible. Developing a specific model will provide researchers with a stronger foundation for understanding oxidative stress induced by H_2O_2 in ovaries facilitating the treatment strategies against reproductive illness.

Data availability statement

The original contributions presented in the study are included in the article/supplementary material, further inquiries can be directed to the corresponding authors.

Ethics statement

The animal study was approved by the experimental procedures regarding experiments and animals care were performed as per Animal Welfare and Ethics Committee of Institute of Animal Sciences, Liaocheng University under Ethical number (LC2022-1). The study was conducted in accordance with the local legislation and institutional requirements.

Author contributions

HL: Conceptualization, Data curation, Formal analysis, Investigation, Methodology, Software, Validation, Writing – original draft, Writing – review & editing. SWu: Conceptualization, Data curation, Investigation, Software, Writing – review & editing. ZZ: Data curation, Investigation, Validation, Writing – review & editing. MK: Conceptualization, Data curation, Validation, Writing – review & editing. YZ: Conceptualization, Data curation, Investigation, Writing – review & editing. MZ: Conceptualization, Investigation, Validation, Writing – review & editing. SWa: Conceptualization, Investigation, Validation, Writing – review & editing. WL: Conceptualization, Investigation, Validation, Writing – review & editing. CW: Conceptualization, Resources, Validation, Writing – review & editing. GC: Conceptualization, Data curation, Formal analysis, Funding acquisition, Investigation, Methodology, Project administration, Resources, Software, Supervision, Validation, Visualization, Writing – original draft, Writing – review & editing. YH: Conceptualization, Data curation, Formal analysis, Funding acquisition, Investigation, Methodology, Project administration, Resources, Software, Supervision, Validation, Visualization, Writing – original draft, Writing – review & editing.

Funding

The author(s) declare financial support was received for the research, authorship, and/or publication of this article. This work was supported by the National Natural Science Foundation of China (grant no. 32202669), the Open Project of Liaocheng University Animal Husbandry Discipline (grant no. 31946220732), Liaocheng University scientific research fund (grant

no. 318052026), and the National Key R&D Program of China (2022YFD1600103 and 2023YFD1302004).

Conflict of interest

The authors declare that the research was conducted in the absence of any commercial or financial relationships that could be construed as a potential conflict of interest.

Publisher's note

All claims expressed in this article are solely those of the authors and do not necessarily represent those of their affiliated organizations, or those of the publisher, the editors and the reviewers. Any product that may be evaluated in this article, or claim that may be made by its manufacturer, is not guaranteed or endorsed by the publisher.

References

1. Aitken RJ. Impact of oxidative stress on male and female germ cells: implications for fertility. *Reproduction.* (2020) 159:R189–201. doi: 10.1530/REP-19-0452

2. Agarwal A, Gupta S, Sekhon L, Shah R. Redox considerations in female reproductive function and assisted reproduction: from molecular mechanisms to health implications. *Antioxid Redox Signal.* (2008) 10:1375–403. doi: 10.1089/ars.2007.1964

3. Al-Gubory KH, Fowler PA, Garrel C. The roles of cellular reactive oxygen species, oxidative stress and antioxidants in pregnancy outcomes. *Int J Biochem Cell Biol.* (2010) 42:1634–50. doi: 10.1016/j.biocel.2010.06.001

4. Zhang B, Qu G, Nan Y, Zhou EM. Ovarian oxidative stress induced follicle depletion after zona pellucida 3 vaccination is associated with subfertility in BALB/c mice. *Front Vet Sci.* (2022) 9:814827. doi: 10.3389/fvets.2022.814827

5. Hajam YA, Rani R, Ganie SY, Sheikh TA, Javaid D, Qadri SS, et al. Oxidative stress in human pathology and aging: molecular mechanisms and perspectives. *Cells.* (2022) 11:552. doi: 10.3390/cells11030552

6. Cai M, Li Q, Cao Y, Huang Y, Yao H, Zhao C, et al. Quercetin activates autophagy to protect rats ovarian granulosa cells from H_2O_2-induced aging and injury. *Eur J Pharmacol.* (2024) 966:176339. doi: 10.1016/j.ejphar.2024.176339

7. Lee JC, Son YO, Choi KC, Jang YS. H2O2 induces apoptosis of BJAB cells due to formation of hydroxyl radicals via intracellular iron-mediated Fenton chemistry in glucose oxidase-mediated oxidative stress. *Mol Cells.* (2006) 22:21–9. doi: 10.1016/S1016-8478(23)17386-9

8. Wu H, Ye N, Huang Z, Lei K, Shi F, Wei Q. Dietary curcumin supplementation relieves hydrogen peroxide-induced testicular injury by antioxidant and anti-apoptotic effects in roosters. *Theriogenology.* (2023) 197:46–56. doi: 10.1016/j.theriogenology.2022.10.038

9. Sugino N. Reactive oxygen species in ovarian physiology. *Reprod Med Biol.* (2005) 4:31–44. doi: 10.1007/BF03016135

10. Yan F, Zhao Q, Li Y, Zheng Z, Kong X, Shu C, et al. The role of oxidative stress in ovarian aging: a review. *J Ovarian Res.* (2022) 15:100. doi: 10.1186/s13048-022-01032-x

11. Yi-Wen H, Li-Na S, Li-E H, Yang Z, Guo-Hong C, Qi X, et al. Vitamin E relieves the apoptosis of goose (Anser cygnoides) granulosa cells by inhibiting oxidative stress. *J Agric Biotechnol.* (2023) 31:1659–70. doi: 10.3969/j.issn.1674-7968.2023.08.010

12. Xiufang L, Zhongqing W, Lei Z, Xiaoping Z, Haiyan X, Fang L. Kidney-tonifying Chinese medicine in alleviating oxidative stress in oocyte in older infertile women: a review. *World J Tradit Chin Med.* (2022) 17:3263–9. doi: 10.3969/j.issn.1673-7202.2022.22.024

13. Deng D, Yan J, Wu Y, Wu K, Li W. Morroniside suppresses H2O2-stimulated autophagy and apoptosis in rat ovarian granulosa cells through the PI3K/AKT/mTOR pathway. *Hum Exp Toxicol.* (2021) 40:577–86. doi: 10.1177/0960327120960768

14. Yang K, Liu L, Zhou H, Xiao X, Liu H. Advances on regulation of premature ovarian failure by oxidative stress and autophagy apoptosis. *J Hunan Univ Chinese Med.* (2021) 41:809–14. doi: 10.3969/j.issn.1674-070X.2021.05.031

15. Huang B, Qian C, Ding C, Meng Q, Zou Q, Li H. Fetal liver mesenchymal stem cells restore ovarian function in premature ovarian insufficiency by targeting MT1. *Stem Cell Res Ther.* (2019) 10:362. doi: 10.1186/s13287-019-1490-8

16. Lu J, Wang Z, Cao J, Chen Y, Dong Y. A novel and compact review on the role of oxidative stress in female reproduction. *Reprod Biol Endocrinol.* (2018) 16:80. doi: 10.1186/s12958-018-0391-5

17. Khan A, Dou J, Wang Y, Jiang X, Khan MZ, Luo H, et al. Evaluation of heat stress effects on cellular and transcriptional adaptation of bovine granulosa cells. *J Anim Sci Biotechnol.* (2020) 11:1–20. doi: 10.1186/s40104-019-0408-8

18. Khan A, Khan MZ, Dou J, Umer S, Xu H, Sammad A, et al. RNAi-mediated silencing of catalase gene promotes apoptosis and impairs proliferation of bovine granulosa cells under heat stress. *Animals.* (2020) 10:1060. doi: 10.3390/ani10061060

19. Khan A, Khan MZ, Dou J, Xu H, Liu L, Zhu H, et al. SOD1 gene silencing promotes apoptosis and suppresses proliferation of heat-stressed bovine granulosa cells via induction of oxidative stress. *Vet Sci.* (2021) 8:326. doi: 10.3390/vetsci8120326

20. Zha Z, Liu SS, Liu YJ Li C, Wang L. Potential utility of natural products against oxidative stress in animal models of multiple sclerosis. *Antioxidants.* (2022) 11:1495. doi: 10.3390/antiox11081495

21. Balmus IM, Lefter R, Ciobica A, Cojocaru S, Guenne S, Timofte D, et al. Preliminary biochemical description of brain oxidative stress status in irritable bowel syndrome contention-stress rat model. *Medicina (Kaunas).* (2019) 55:776. doi: 10.3390/medicina55120776

22. Chen Z, Xing T, Li J, Zhang L, Jiang Y, Gao F. Hydrogen peroxide-induced oxidative stress impairs redox status and damages aerobic metabolism of breast muscle in broilers. *Poult Sci.* (2021) 100:918–25. doi: 10.1016/j.psj.2020.11.029

23. Zhong Y, Ma T, Fu Z, Chen A, Yu J, Huang Y, et al. Effects of hydrogen peroxide-induced oxidative stress on intestinal morphology, redox status, and related molecules in squabs. *Animals.* (2023) 13:749. doi: 10.3390/ani13040749

24. Yisireyili M, Alimujiang A, Aili A, Li YL, Yisireyili S, Abudureyimu K. Chronic restraint stress induces gastric mucosal inflammation with enhanced oxidative stress in a murine model. *Psychol Res Behav Manag.* (2020) 13:383–93. doi: 10.2147/PRBM.S250945

25. Offer T, Russo A, Samuni A. The pro-oxidative activity of SOD and nitroxide SOD mimics. *FASEB J.* (2000) 14:1215–23. doi: 10.1096/fasebj.14.9.1215

26. Djordjević VV, Kostić J, Krivokapić Ž, Krtinić D, Ranković M, Petković M, et al. Decreased activity of erythrocyte catalase and glutathione peroxidase in patients with schizophrenia. *Medicina.* (2022) 58:1491. doi: 10.3390/medicina58101491

27. Shen Y, Shen Z, Li P, Chen Z, Wei B, Liu D, et al. Protective activity of Malus doumeri leaf extract on H(2)O(2)-induced oxidative injury in H9C2 rat cardiomyocytes. *Front Cardiovasc Med.* (2022) 9:1005306. doi: 10.3389/fcvm.2022.1005306

28. Sepasi Tehrani H, Moosavi-Movahedi AA. Catalase and its mysteries. *Prog Biophys Mol Biol.* (2018) 140:5–12. doi: 10.1016/j.pbiomolbio.2018.03.001

29. Di Marzo N, Chisci E, Giovannoni R. The role of H2O2 in redox-dependent signaling: homeostatic and pathological responses in mammalian cells. *Cells.* (2018) 7:156. doi: 10.3390/cells7100156

30. Mahmoodi M, Soleimani Mehranjani M, Shariatzadeh SM, Eimani H, Shahverdi A. N-acetylcysteine improves function and follicular survival in mice ovarian grafts through inhibition of oxidative stress. *Reprod Biomed Online.* (2015) 30:101–10. doi: 10.1016/j.rbmo.2014.09.013

31. Myers M, Britt KL, Wreford NG, Ebling FJ, Kerr JB. Methods for quantifying follicular numbers within the mouse ovary. *Reproduction.* (2004) 127:569–80. doi: 10.1530/rep.1.00095

32. Bao T, Yao J, Zhou S, Ma Y, Dong J, Zhang C, et al. Naringin prevents follicular atresia by inhibiting oxidative stress in the aging chicken. *Poult Sci.* (2022) 101:101891. doi: 10.1016/j.psj.2022.101891

33. Vital Reyes VS, Téllez Velasco S, Hinojosa Cruz JC, Reyes Fuentes A. Ovarian apoptosis. *Ginecol Obstet Mex.* (2001) 69:101–7.

34. Zhang J, Ren Q, Chen J, Lv L, Wang J, Shen M, et al. Downregulation of miR-192 alleviates oxidative stress-induced porcine granulosa cell injury by directly targeting Acvr2a. *Cells.* (2022) 11:2362. doi: 10.3390/cells11152362

35. Emini Veseli B, Perrotta P, De Meyer GR, Roth L, Van der Donckt C, Martinet W, et al. Animal models of atherosclerosis. *Eur J Pharmacol.* (2017) 816:3–13. doi: 10.1016/j.ejphar.2017.05.010

36. Dewan KK, Taylor-Mulneix DL, Campos LL, Skarlupka AL, Wagner SM, Ryman VE, et al. model of chronic, transmissible otitis media in mice. *PLoS Pathog.* (2019) 15:e1007696. doi: 10.1371/journal.ppat.1007696

37. Hu Z, Tang Z, Kiram A, Li J, Xu H, Xu Y, et al. The establishment of a mouse model for degenerative kyphoscoliosis based on senescence-accelerated mouse prone 8. *Oxid Med Cell Longev.* (2022) 2022:7378403. doi: 10.1155/2022/7378403

38. Yu K, Zhang J, Cao Z, Ji Q, Han Y, Song M, et al. Lycopene attenuates AFB(1)-induced renal injury with the activation of the Nrf2 antioxidant signaling pathway in mice. *Food Funct.* (2018) 9:6427–34. doi: 10.1039/C8FO01301B

39. Yang L, Yong L, Zhu X, Feng Y, Fu Y, Kong D, et al. Disease progression model of 4T1 metastatic breast cancer. *J Pharmacokinet Pharmacodyn.* (2020) 47:105–16. doi: 10.1007/s10928-020-09673-5

frontiers | Frontiers in Veterinary Science

TYPE Original Research
PUBLISHED 25 November 2024
DOI 10.3389/fvets.2024.1437352

OPEN ACCESS

EDITED BY
Miguel A. Gutiérrez Reinoso,
Universidad Técnica de Cotopaxi, Ecuador

REVIEWED BY
Vishal Suthar,
Gujarat Biotechnology University, India
Georgios Valergakis,
Aristotle University of Thessaloniki, Greece

*CORRESPONDENCE
Angela Costa
✉ angela.costa2@unibo.it

RECEIVED 23 May 2024
ACCEPTED 09 September 2024
PUBLISHED 25 November 2024

CITATION
Magro S, Costa A, Cavallini D, Chiarin E and De Marchi M (2024) Phenotypic variation of dairy cows' hematic metabolites and feasibility of non-invasive monitoring of the metabolic status in the transition period. *Front. Vet. Sci.* 11:1437352.
doi: 10.3389/fvets.2024.1437352

Phenotypic variation of dairy cows' hematic metabolites and feasibility of non-invasive monitoring of the metabolic status in the transition period

Silvia Magro[1], Angela Costa[2]*, Damiano Cavallini[2], Elena Chiarin[1] and Massimo De Marchi[1]

[1]Department of Agronomy, Food, Natural Resources, Animals and Environment, University of Padova, Legnaro, Italy, [2]Department of Veterinary Medical Sciences, Alma Mater Studiorum University of Bologna, Bologna, Italy

Introduction: The incidence of metabolic diseases tends to be highest during the transition period (±3 weeks around parturition) in dairy cows due to physiological changes and the onset of lactation. Although blood profile testing allows for the monitoring of nutritional and metabolic status, conducting extensive analyses in the herd is costly and stressful for cows due to invasive procedures. Therefore, mid-infrared spectroscopy (MIR) could be seen as a valid alternative.

Methods: In the present study, we used laboratory-determined reference blood data and milk spectra of 349 Holstein cows to (i) identify the non-genetic factors affecting the variability of major blood traits in healthy cows and, subsequently, (ii) test the predictive ability of milk MIR. Cows belonged to 14 Italian commercial farms and were sampled once between 5 and 38 days in milk. For β-hydroxybutyrate (BHB), non-esterified fatty acids (NEFA), cholesterol, glucose, urea, total protein, albumin, globulin, minerals, aspartate aminotransferase, gamma-glutamyl transferase, creatine kinase, total bilirubin, and cortisol, the effects of parity, days in milk, and season were investigated using a linear model.

Results and discussion: The results indicate that all fixed effects significantly affected the hematic concentration of most of the traits. Regarding MIR, the most predictable traits were BHB, NEFA, and urea, with coefficients of determination equal to 0.57, 0.62, and 0.89, respectively. These values suggest that MIR predictions of BHB and NEFA are not sufficiently accurate for precise and punctual determination of the hematic concentration, however, still the spectrum of the milk can be exploited to identify cows at risk of negative energy balance and subclinical ketosis. Finally, the predictions can be useful for herd screening, decision-making, and genetic evaluation.

KEYWORDS

metabolite, ketosis, negative energy balance, mid-infrared spectroscopy, reference interval

1 Introduction

The transition period conventionally refers to ±3 weeks around parturition and is known to be a challenging moment for dairy cows. In this phase the incidence of infections and metabolic diseases tends to be high due to nutritional, metabolic, hormonal, and immunological changes (1, 2) and all disorders/diseases that occur have severe implications

on the cow's productive performance and fertility during the lactation. This is because dairy cows commonly experience a negative energy balance (NEB), a condition caused by insufficient dry matter intake. Energy intake fails to meet the demands of both maintenance and milk production (3, 4).

To compensate for the lack of energy substrates, there is mobilization of body reserves that leads to an increase in the concentrations of NEB blood biomarkers such as non-esterified fatty acids (NEFA) and ketone bodies such as β-hydroxybutyrate (BHB) (2, 5).

Apart from the indicators of NEB, there are several blood traits important for dairy cow health monitoring, namely albumin, globulin, urea, hepatic aspartate aminotransferase (AST), gamma glutamyl transferase (GGT), creatine kinase (CK), and total bilirubin (BILT). Some of these parameters can vary simoultaneously, especially in some specific moments and/or in unhealthy animals. For instance, cows with metritis exhibit greater AST and BILT than healthy cows (6), and CK and AST concentrations jointly increase in uterine tissue in the presence of clinical endometritis (7).

Blood metabolic profile testing is time-consuming, invasive, and relatively expensive. Therefore, conducting extensive analyses on a large scale is not feasible in the field, also due to the absence of standardized and validated sampling protocols and analyses (8).

In this context, there is an evident interest in the Fourier-transform mid-infrared spectroscopy (FT-MIR), whose spectral data – already adopted to assess milk composition assessment (9, 10) – can be exploited to predict blood parameters (11, 12). Predicting mineral and hepato- and protein-profile indicators from milk spectra can represent a concrete and helpful opportunity for commercial farms. The present study aimed to (i) investigate the factors determining the variability of blood traits in healthy Holstein cows in early lactation, (ii) evaluate the association between blood and milk traits, and (iii) test the predictive ability of milk FT-MIR to predict hematic metabolic indicators.

2 Materials and methods

2.1 Sample collection

For this study, 14 commercial farms located in the Veneto region (Italy) were enrolled. The focus of this study was on Holstein cows under an intensive farming system. This means that the involved farms were characterized by a free stall barn, total mixed ration feeding, and no access to pasture. Between May and December 2020, each farm was visited once to sample cows in the first stage of lactation, i.e., between 3 and 38 days in milk (DIM). Animals with clinical signs of disease or those who received medical treatment at calving were excluded *a priori*, resulting in 349 clinically healthy cows, from calving up to the day of milk/blood sampling.

Individual blood (8 mL) and milk samples (50 mL) were collected as represented in Figure 1 during the morning milking, and information on DIM, parity, and milk yield (kg/d) was retrieved. Milk sampling was done in correspondence of the monthly official milk testing, and the tubes contained Bronopol (2-bromo 2-nitro 1,3-propandiol) for preservation in line with the guidelines of the International Committee for Animal Recording (ICAR). Milk samples were transported to the milk laboratory of the Breeders Association of Veneto Region (ARAV, Vicenza, Italy) for FT-MIR spectrum acquisition.

Blood sampling via venepuncture took place immediately after milking (within 1 h maximum, Figure 1), as performed in other studies (11, 13), and required immobilization of the animals in a containment trunk and preliminary cleaning of the venipuncture site (tail) with a disposable paper towel. Blood samples were stored into vacuum tubes containing lithium heparin (Greiner Bio-One GmbH, Kremsmünster, Austria) and were gently inverted 5 times, stored at 5°C and transported to the laboratory of the Experimental Zooprophylactic Institute of the Venezie (IZSVe, Padova, Italy).

2.2 Laboratory analysis

At the ARAV milk laboratory, samples (1 per cow) were scanned with a CombiFoss™ 7 machine (Foss Electric A/S, Hillerød, Denmark). For all cows, fat, protein, casein, and lactose content, and BHB and urea concentrations were determined via FT-MIR spectroscopy and somatic cell count (SCC, cells/mL) via flow cytometry. Infrared spectroscopy involves passing electromagnetic radiation through matter and measuring the energy absorbed at each wavelength ($n = 1{,}060$ in the case of CombiFoss™ 7). FT-MIR is commonly used in official milk laboratories to determine traditional milk quality traits for Dairy Herd Improvement as per ICAR guidelines (14). In this study, spectral information containing 1,060 infrared transmittance data points in the region between 5,000 and 900 cm^{-1} was stored using MilkoScan ™ 7 RM (Foss Electric A/S, Hillerød, Denmark).

At the IZSVe laboratory, blood samples (1 per cow) were centrifuged at 1,500 x g for 15 min at 4°C to separate the plasma. A set of parameters routinely used for blood profiling of lactating cows was considered: parameters related to both protein and energy metabolism (total protein, globulin, albumin, urea, glucose, NEFA, BHB, and cholesterol), enzymes and hepatic markers (AST, GGT, CK, and BILT), minerals (Ca, P, Mg, Na, K, and Cl) and cortisol. All plasma samples were analyzed with the COBAS C501 biochemical analyzer (Roche Diagnostics GmbH, Mannheim, Germany) using Roche BM commercial kits, except for the concentrations of NEFA and BHB, which were measured with an enzymatic colorimetric method (Randox Laboratories Ltd., Ardmore, United Kingdom). The analytical methods used for each blood parameter have been widely described by Cozzi et al. (15) who analyzed blood samples in the same laboratory. Intra-assay variation ranged from 0.31% for Cl to 4.17% for BILT. The inter-assay variation ranged from 0.47% for Na to 5.46% for BILT.

A database of blood parameters, milk spectral data, and individual cow information was created for subsequent statistical analyses.

2.3 Phenotypic variance

The software R v. 4.1.2 (16) was used for data handling and calculation of descriptive statistics and correlations. Traits were visually inspected to evaluate the Gaussian distribution, and whenever necessary, values underwent transformation to achieve normality. In particular, the values of BHB, NEFA, AST, GGT, CK, and cortisol were $\log_{10}$ transformed.

Values of plasma and milk traits deviating more than 3 SD from the respective mean were treated as missing deviating more

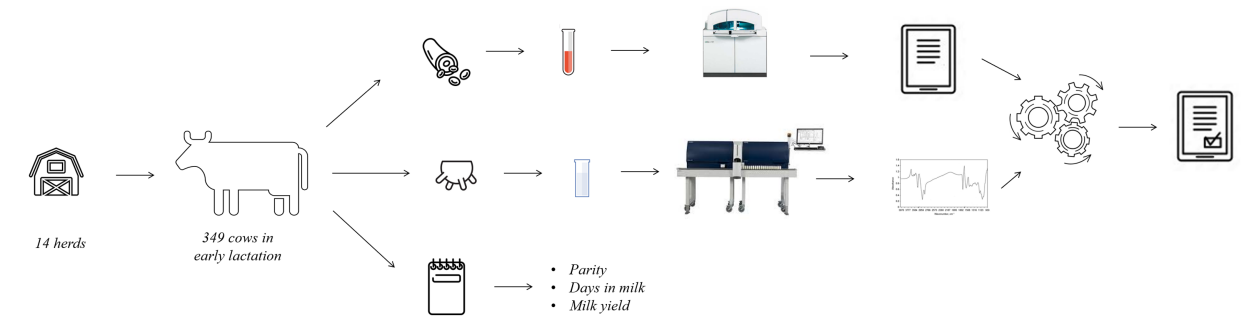

FIGURE 1
Experimental design and rationale of the study.

than 3 SD from the respective mean were treated as missing. Spearman's correlations were calculated between plasma traits and between plasma and milk traits.

To investigate the factors affecting plasma traits, analysis of variance was performed using the following generalized linear mixed model (Equation 1) with PROC GLIMMIX in SAS software v. 9.4 (SAS Institute Inc., Cary, NC, United States):

$$y_{ijklm} = \mu + P_i + D_j + \left(P\ x\ D\right)_{ij} + M_k + H_m + e_{ijklm} \quad (1)$$

where y_{ijklm} is the trait investigated; μ is the overall intercept of the model; P_i is the fixed effect of the ith parity ($i = 1, 2, \geq 3$, with the last class including cows up to parity 10); D_l is the fixed effect of the lth distance from calving ($l = 4$ classes, with the first being a class from 3 to 8 DIM, followed by 2 classes of 6 d each, and the last being a class from 21 to 38 DIM); ($P\ x\ D$) is the first order interaction between parity and DIM class; M_k is the fixed effect of the kth sampling season ($k = 3$ classes, May-Jun, Jul-Aug, Sep-Oct); H_m is the random effect of the mth herd ($m = 14$ levels) assumed to be distributed as $\sim N(0, \sigma^2_H)$, where σ^2_H is the herd variance; and e_{ijklm} is the random residual assumed to be distributed as $\sim N(0, \sigma^2_e)$, where σ^2_e is the residual variance. Multiple comparisons of least squares means (LSM) were performed using Bonferroni adjustment with significance at $p \leq 0.05$. The results for log-transformed variables were reported after back transformation.

Blood BILT was processed as a binary trait, with a value of '1' assigned if BILT was >4 μmol/L and '0' if it was ≤4 μmol/L. This was done because several samples presented BILT concentration below the laboratory limit of detection, i.e., < 2.5 μmol/L. A binary logistic regression analysis was performed using the model above described (Equation 1) in SAS v. 9.4. For each fixed effect, odds ratios were calculated and were considered as significant when the 95% confident interval did not include 1.

2.4 Mid-infrared prediction models

Each milk spectrum was paired with the relative blood sample values of BHB, NEFA, glucose, cholesterol, urea, Ca, P, Mg, Na, K, Cl, total protein, albumin, globulin, GGT, AST, CK, and cholesterol determined in the laboratory. For non-distributed traits, a logarithmic transformation was also applied. For each spectral wavelength, the value was transformed from transmittance to absorbance using the formula: Absorbance = $\log_{10}$(1/Transmittance).

Spectral regions where there is non-negligible noise due to water absorption were discarded (10, 17), leading to 338 wavelengths located/scattered in the following intervals within the spectrum: 945.5 to 1,585.6 cm^{-1}, 1,716.8 to 1,929.0 cm^{-1}, 2,507.7 to 2,970.7 cm^{-1}. Preliminary analysis of the spectral data was conducted using principal component analysis to identify anomalous samples in terms of the FT-MIR spectrum. This allowed for the elimination of nine spectral outliers. Before the development of the prediction model, spectra were independently subjected to standard normal variate (SNV) scatter correction with the aim of normalizing the spectral data to reduce baseline shifting or tilting due to nonspecific radiation scattering (18). The partial least squares (PLS) analysis was carried out using the 'trainControl' function available in the R package 'caret', whose details are described in Kuhn (19), following this process:

- The models were fine-tuned using leave-one-out cross-validation, and the number of components was set automatically but capped at a maximum of 20 to avoid overfitting;
- Spectral data points were centered and scaled;
- Predictions with residuals largely different from the observed values were removed;
- The complete data set was randomly split into a calibration set representing 70% of the total samples and a validation set (30%), both of which had similar mean and standard deviation of the target trait and were representative of all herds, parities, and DIM;
- The external validation was iterated 3 times, each time over a different portion of cows, and the reported fitting statistics were the average of the fitting statistics were the average of the fitting statistics of the 3 iterations.

The fitting statistics of the PLS consisted of: the standard error in leave-one-out cross-validation and external validation and the coefficient of determination (R^2) in leave-one-out cross-validation and external validation.

Using existing thresholds of BILT, BHB, and NEFA (20), partial least squares discriminant analysis (PLS-DA) was used through the same package to classify animals above or below the thresholds (e.g., 4 μmol/L for BILT), and therefore potentially at risk of certain metabolic disorders. PLS-DA performance included sensitivity, specificity, positively predictive values, negatively predictive values, and balanced accuracy in both calibration and validation. Balanced

accuracy is the mean of sensitivity and specificity, and positively and negatively predictive values are the proportions of positive and negative results that are true positive and true negative, respectively.

3 Results and discussion

3.1 Plasma traits

3.1.1 General overview

There is a metabolic priority toward the mammary gland in dairy breeds, so energy and nutrients primarily support milk synthesis. As reported by Bauman and Currie (21), in fact, "[…] the most pronounced example of homeorhesis would be in a dairy cow where initiation of lactation dramatically alters metabolism of many maternal organs in order that the mammary gland be supplied with nutrients necessary for synthesis of milk […]." The genetic pressure that dairy cattle breeds were exposed to in the past resulted in a progressive linear increase in milk productivity at the expense of fitness, fertility, resistance to disease, and overall health (22). This explains why conditions such as NEB, glucose drop and hyperketonemia are commonly considered normal and are observed in healthy animals with no clinical signs.

Descriptive statistics of the milk and plasma traits analyzed for early lactation cows before editing are presented in Tables 1, 2, respectively. The cows sampled had an average and SD of DIM and parity of 14.54 ± 7.62 and 2.40 ± 11.41, respectively. The average milk composition was in line with the average performance reported by the Italian Breeders Association (AIA) for Holsteins farmed in the Veneto region in 2020 (23).

Hematic traits are in the range of values commonly found in healthy high-producing cows (24). The minimum and the maximum values of BHB in this study were quite far from each other, 0.15 and 4.96 mmol/L, suggesting that the healthy cows involved differ widely in terms of mobilization.

In this study, the average NEFA was in line (0.52 mmol/L) with another study reporting the trend of this trait from 0 to 40 DIM (25). Blood urea, which is directly related to BUN, was within the conventional range (Table 2) in this study, except for a few cases presenting either a lower (< 1.70 mmol/L, 6 cows) or higher concentration (> 6.87 mmol/L, 11 cows).

Regarding the mineral profiles, the averages in Table 2 mirror those reported by Walter et al. (25). Due to osmotic equilibrium, Ca and P are expected to be scarcely variable in the blood of healthy cows. In the present study, it appeared that 6 cows out of 349 cows were in a state of hypocalcemia with a concentration of Ca below the threshold (2.10 mmol/L, 26). Total protein, albumin, and globulin were included in the protein profile (Table 2). Globulins are produced in response to inflammation of the chronic type and albumin is a protein that is synthesized in the liver and low levels reflect poor liver health or a poor supply of amino acids from the diet (27). The averages observed in the present study are in line with those of Cattaneo et al. (27), who evaluated the evolution of albumin and globulin concentrations before and after calving.

The average concentration of CK was 340.34 U/L (Table 2), while the median was 168 U/L. Walter et al. (25) indicated that the distribution of CK values is not normal; thus, the mean can be inflated by a limited number of samples (Figure 2). The average of both AST and GGT levels was in accordance with Fiore et al. (28), who evaluated how blood parameters were affected by different preventive treatments for hyperketonemia.

Cortisol is a valid indicator of chronic stress in livestock animals and, is detectable in a variety of matrices, e.g., saliva, milk, plasma, and hair (29). In this study, the minimum, average, and maximum values observed for this hormone were 1.94, 17.05, and 107.00 nmol/L.

3.1.2 Correlations

Spearman's correlations were calculated to evaluate if an association exists among blood parameters and between blood and milk traits (Figure 3). Such an investigation is useful for understanding how milk is capable of mirroring blood and, in addition, for determining whether some hematic traits change in parallel or not in the transition period.

Among the energy profile traits, the strongest positive and negative correlations were found between NEFA and urea (0.40) and between BHB and glucose (−0.39), respectively (Figure 3). A significant association between hypoglycemia, fat mobilization, and circulating nitrogen has been reported in previous studies that reported blood traits in cows within 35 DIM (11, 12). On average, these traits showed weak correlations with mineral and protein profiles. In particular, urea was positively correlated with albumin (0.40) and negatively with globulin (−0.24), as reported by Luke et al. (12). Among the mineral

TABLE 1 Descriptive statistics of milk traits before editing[1].

Milk trait[2]	Mean (SD)	Minimum	Maximum	N. missing values[3]	
				< Mean-3 SD	< Mean-3 SD
Yield, kg/d	39.04 (10.47)	10.00	62.80	0	1
Fat, %	4.39 (1.39)	0.67	13.08	0	2
Protein, %	3.34 (0.49)	2.36	6.59	0	4
Casein, %	2.57 (0.39)	1.72	5.22	0	4
Lactose, %	4.73 (0.26)	3.58	5.28	0	6
SCS	2.62 (2.09)	−1.64	9.38	0	0
Urea, mg/dL	27.39 (7.85)	10.8	65.6	0	2
Log_{10} BHB	−0.99 (0.24)	−3.00	−0.24	0	5

[1]Values of milk traits deviating more than 3 SD from the respective mean (if requested with log-transformed values) were treated as missing. [2]SCS, somatic cell score; calculated as SCS, 3 + log2 (SCC/100,000), where SCC is somatic cell count (cells/mL); BHB, β-hydroxybutyrate (mmol/L).

TABLE 2 Descriptive statistics of blood traits before editing[1].

Blood trait[2]	Mean (SD)	Minimum	Maximum	N. missing values[3]	
				<Mean-3 SD	> Mean + 3 SD
Energy profile					
Glucose, mmol/L	2.80 (0.53)	0.20	4.90	2	1
Cholesterol, mmol/L	2.66 (0.92)	0.60	6.00	0	2
NEFA, mmol/L	0.52 (0.34)	0.04	2.02	0	6
BHB, mmol/L	0.71 (0.54)	0.15	4.96	0	10
Urea, mmol/L	4.19 (1.31)	1.30	9.30	0	2
Mineral profile					
Na, mmol/L	138.88 (3.49)	129.00	150.00	0	1
K, mmol/L	4.39 (0.39)	2.61	5.94	1	3
Cl, mmol/L	98.54 (3.77)	71.00	111.00	1	2
Ca, mmol/L	2.45 (0.15)	1.98	3.21	1	2
P, mmol/L	1.60 (0.34)	0.63	3.11	0	3
Mg, mmol/L	0.96 (0.13)	0.56	1.40	2	1
Protein profile					
Total protein, g/L	74.37 (6.11)	59.00	98.00	0	1
Albumin, g/L	33.91 (4.34)	17.00	43.00	1	0
Globulin, g/L	40.46 (7.05)	26.00	66.00	0	6
Hepatic and muscular profile					
AST, U/L	98.14 (47.97)	53.00	629.00	0	3
GGT, U/L	16.30 (9.74)	4.00	152.00	0	2
CK, U/L	340.34 (694.34)	79.00	6,515.00	0	7
Stress profile					
Cortisol, nmol/L	17.05 (15.00)	1.94	107.00	0	4

[1]Values of blood traits deviating more than 3 SD from the respective mean were treated as missing. [2]NEFA, not esterified fatty acids (mmol/L); BHB, β-hydroxybutyrate (mmol/L); AST, aspartate aminotransferase (U/L); GGT, gamma glutamyl transferase (U/L); CK, creatin kinase (U/L). [3]Excluded for the analysis of variance. In the case of non-normally distributed traits, the missing values were identified using the log-transformed form (BHB, NEFA, AST, GGT, CK and cortisol).

profile traits, the strongest positive and negative correlations were found between Na and Cl (0.76) and between Cl and Ca (−0.29). The traits in the protein profile set were negatively correlated with Na and Cl. Moreover, in line with Luke et al. (12), a positive and moderate correlation was observed between albumin and Ca and Mg. Among the hepatic and muscular profile traits, the strongest correlation was found between CK and AST (0.49), and these traits showed weak correlations with NEFA and BHB (Figure 3). In addition, Sattler and Fürll (7) reported a positive correlation between CK and AST, both of which increased in the presence of uterine diseases.

According to the literature, blood NEFA, BHB, and urea are expected to go in parallel, especially in cows with severe NEB. However, their association could be nonlinear or weak (30). For instance, McCarthy et al. (31) found that the correlation between BHB and NEFA in the postpartum is moderate, despite positive (0.26).

Correlations were also calculated between plasma and milk traits (Figure 3). The strongest correlation was observed between urea in plasma and milk (0.89), followed by BHB (0.53). In agreement with Benedet et al. (11), milk BHB was positively correlated with NEFA and negatively correlated with glucose, while cholesterol was inversely associated with milk quality (i.e., fat, protein, and casein content). Blood BHB was positively correlated with fat content while negatively with protein, casein and lactose content. This association has also been reported by Benedet et al. (11). Regarding milk yield, the strongest positive and negative correlations were found with albumin (0.51) and P (−0.24), respectively, whereas, SCS was negatively correlated with Mg and cholesterol. On the other hand, Andjelić et al. (32) observed a negative correlation between milk fat and NEFA and BHB. Andjelić et al. (32) reported a positive correlation between blood and milk serum AST and GGT levels.

3.1.3 Variation across DIM

The transition from the dry-off to lactogenesis in the first days after calving is critical for dairy cow. After calving, especially if the diet is not properly balanced in the *pre-partum* period, nutritional status can play a dramatic role. For example, a significant reduction in hematic Ca and P is frequently observed around or immediately after calving, which can expose cows to hypocalcemia and other associated disorders (33). Furthermore, during this period, dairy cows undergo a natural state of immunosuppression, which is often considered the principal cause of their high vulnerability to infectious diseases such as mastitis or metritis (34). Monitoring changes in blood biomarkers can be informative, and the early identification of subclinical metabolic disorders in the first days after calving is advisable and

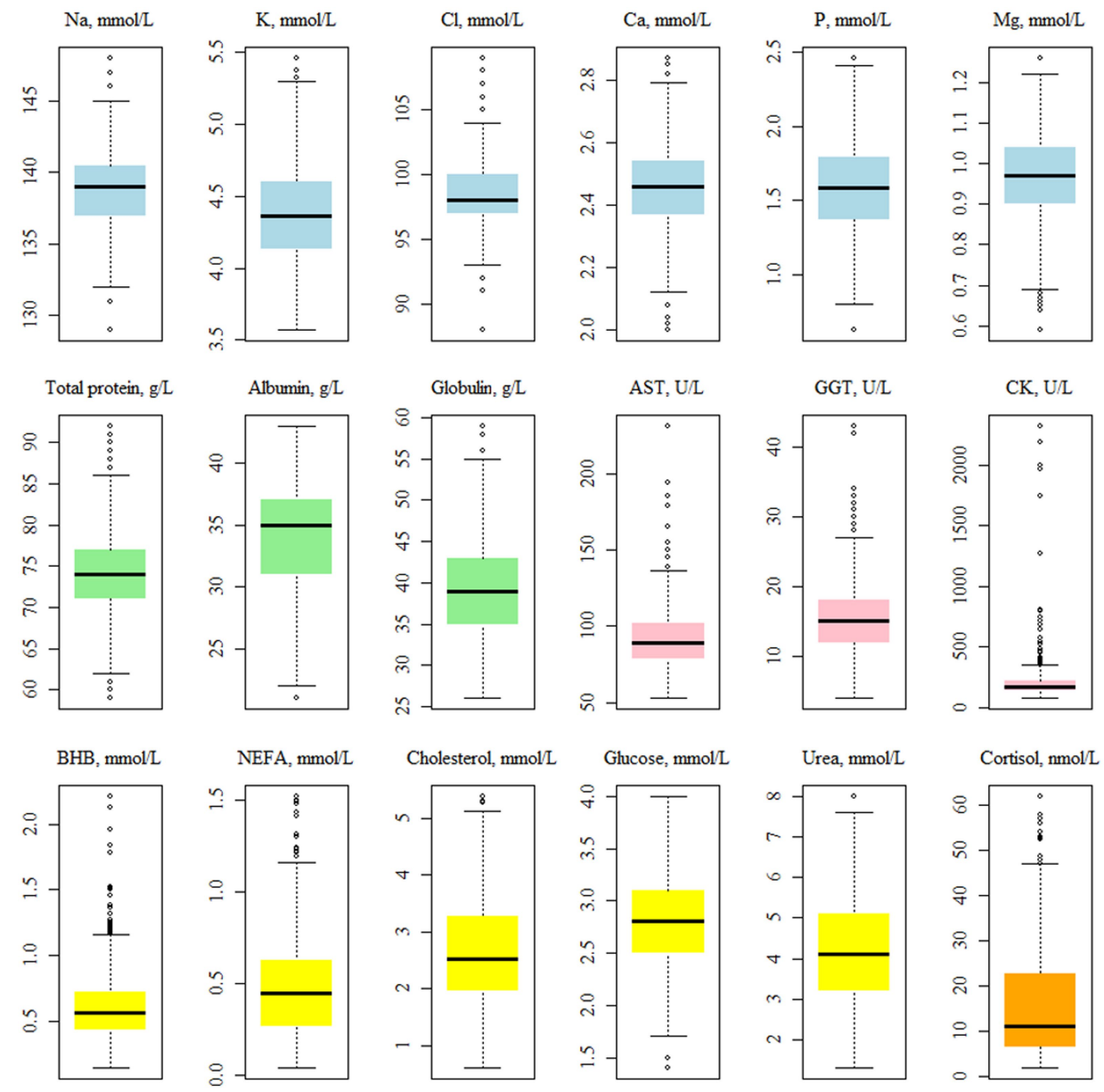

FIGURE 2
Boxplots showing the distribution[1] of the plasma traits[2] values. [1]Before the log-transformation of the non-normally distributed traits, i.e., AST, GGT, CK, BHB, NEFA and cortisol. [2]NEFA, not esterified fatty acids (mmol/L); BHB, β-hydroxybutyrate (mmol/L); AST, aspartate aminotransferase (U/L); GGT, gamma glutamyl transferase (U/L); CK, creatin kinase (U/L).

helpful, allowing for the detection of anomalies, animals at risk, proper decision-making, and timely management interventions (35).

The LSM of DIM classes are presented in Table 3 and revealed that NEFA concentration was lower in 21–38 DIM compared to the classes of DIM closest to calving (i.e., 3–8 DIM and 9–14 DIM), and that BHB concentration was numerically greater in the first two DIM classes (i.e., 3–8 DIM and 9–14 DIM) than the other two (i.e., 15–20 DIM and ≥21 DIM, Table 3). An increase in NEFA is expected in dairy cows in the first days after calving and is commonly observed in high-producing breeds, due to a massive mobilization of adipose reserves in dairy cows to overcome NEB (5). In contrast, the LSM of glucose concentration did not fluctuate dramatically in the first 38 DIM in the present study. Although there may be peaks or drops in glucose in correspondence of meals, the baseline level is subject to tight homeostatic regulation; therefore, glycemia is considered informative in animals suffering from specific disorders/pathologies (36). Cholesterol concentration increased with DIM, progressively raising from the first class onward (Table 3), likely due to its relationship with the dry matter intake of cows, which increases in the first week after calving (37). This finding was also observed by Walter et al. (25) in 362,586 serum samples obtained from clinically healthy German Holstein cows.

The P, Ca, and Mg concentrations were the lowest immediately after calving (3–8 DIM), followed by a gradual increase (Table 3). Luke et al. (12) observed a similar trend for Ca and Mg concentration in 773 spring-calving Holstein cows. Immediately after parturition, there is a

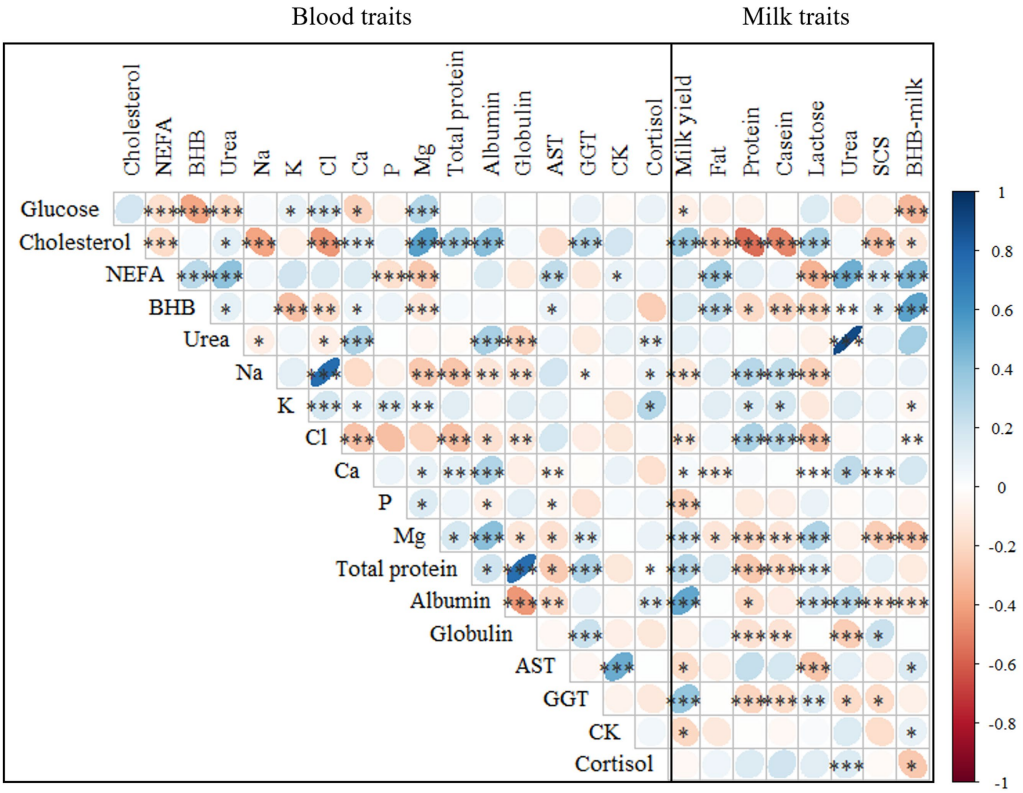

FIGURE 3
Spearman's correlations[1] between the investigated blood and milk traits[2]. [1]***$p \leq 0.001$; **$p \leq 0.01$; *$p \leq 0.05$. [2]NEFA, not esterified fatty acids (mmol/L); BHB, β-hydroxybutyrate (mmol/L); AST, aspartate aminotransferase (U/L); GGT, gamma glutamyl transferase (U/L); CK, creatin kinase (U/L); SCS, somatic cell score, calculated as SCS, $3 + \log_2(SCC/100{,}000)$, where SCC is somatic cell count (cells/mL).

significant and immediate demand for Ca for milk production (38). This, coupled with the typically low dry matter intake, results in substantially low Ca mobilization and Ca deficiency that requires several days to be adjusted (33, 38). In contrast, Mg and P play important roles in Ca homeostasis (33). Moreover, these minerals (i.e., Ca, Mg, and P) are present in high amounts in transition milk, and mature milk (39, 40). However, Na and Cl concentrations were the highest immediately after calving (3–8 DIM) and then gradually decreased (Table 3). The concentration of Cl was very high around calving, as it is common to increase the anionic quota (Cl and S) in prepartum diets to enhance feed intake and indirectly reduce the risk of hypocalcemia (41).

Total protein concentration was the lowest in the first class of DIM. Specifically, the lowest globulin concentration was observed in the period between 3 and 8 DIM, whereas the albumin concentration was relatively consistent across the 21 days and then reached the highest value in the last class, DIM ≥21 (35.58 g/L; Table 3). Similar patterns were observed by Luke et al. (12) who observed concentrations of about 34 g/L in 24–35 DIM.

With regard to the hepatic profile, a significant decrease in AST was observed from the first DIM class to the last (Class 1:102.82 vs. Class 4: 87.39 g/L). The GGT concentration showed an opposite trend, being the lowest immediately after calving (3–8 DIM, 9–14 DIM; Table 3). On the other hand, Moretti et al. (42) reported that the concentration of GGT was lower in the first days after calving (3 ± 1 DIM) due to the production of colostrum and milk and low feed intake. Hoffman and Solter (43) reported the highest concentration of GGT activity in the kidney, pancreas, intestines, and mammary glands. In contrast, CK and cortisol were not significantly affected by distance from calving, so the LSM of the DIM classes were not statistically different (Table 3).

Table 4 contains the odds ratio estimated for the BILT classes (> and ≤ 4 μmol/L). Overall, there were no differences related to distance from calving in the first 14 days, but LSM indicated that the probability to observe high BILT concentration (> 4 μmol/L) decreased as DIM progressed. It is likely that, higher LSM for AST were estimated near calving because they reflect tissue damage in the uterine tissue (25) and/or degradation of muscle cells caused by mobilization of body reserves (7). Authors of other studies (25, 44) observed that the highest levels of BILT are found in the first week postpartum as a consequence of the lipolysis.

3.1.4 Variation related to the effect of parity

The parity of cows played a crucial role in the variability of the plasma traits investigated, except for Na, Cl, K, albumin, AST, and cortisol (Table 5). Within the energy profile traits, glucose and cholesterol concentrations decreased with parity, whereas NEFA and BHB increased (Table 5). This is in line with the literature and supports that multiparous cows have a higher prevalence of hyperketonemia than primiparous due to greater milk production, mobilization of body reserves, and metabolic stress related to the previous lactation (5).

As regards the mineral profile, Ca, P and Mg concentrations were the greatest in the first two parity orders (Table 5). In older cows, low

TABLE 3 Least squares means (standard error) of blood traits[1] for the fixed effect of days in milk/ after calving (DIM) along with the *F*-value.

Blood trait	3–8 DIM	9–14 DIM	15–20 DIM	≥21 DIM	F-value
Energy profile					
Glucose, mmol/L	2.91 (0.10)	2.79 (0.10)	2.88 (0.10)	2.92 (0.10)	*ns*
Cholesterol, mmol/L	2.05^{d} (0.15)	2.45^{c} (0.15)	2.90^{b} (0.15)	3.49^{a} (0.15)	69.40 ***
NEFA, mmol/L	0.42^{a} (0.06)	0.41^{a} (0.06)	0.35^{ab} (0.05)	0.29^{b} (0.04)	7.15 ***
BHB, mmol/L	0.61 (0.03)	0.62 (0.03)	0.57 (0.03)	0.59 (0.03)	*ns*
Urea, mmol/L	3.60 (0.30)	3.62 (0.30)	3.52 (0.30)	3.77 (0.30)	*ns*
Mineral profile					
Na, mmol/L	140.23^{a} (0.64)	139.27^{ab} (0.63)	138.67^{b} (0.63)	138.27^{b} (0.64)	8.08 ***
K, mmol/L	4.35 (0.07)	4.40 (0.07)	4.42 (0.07)	4.38 (0.07)	*ns*
Cl, mmol/L	100.03^{a} (0.63)	98.88^{b} (0.62)	98.37^{b} (0.62)	97.72^{b} (0.62)	11.82 ***
Ca, mmol/L	2.41^{b} (0.02)	2.46 ^{ab} (0.02)	2.43^{ab} (0.02)	2.48^{a} (0.02)	5.70 **
P, mmol/L	1.50^{b} (0.06)	1.57^{ab} (0.06)	1.63^{ab} (0.06)	1.67^{a} (0.06)	5.12 **
Mg, mmol/L	0.90^{c} (0.01)	0.96^{b} (0.01)	0.99^{ab} (0.01)	1.02^{a} (0.01)	18.13 ***
Protein profile					
Total protein, g/L	70.53^{c} (0.77)	72.70^{b} (0.74)	75.58^{a} (0.76)	76.82^{a} (0.78)	21.79 ***
Albumin, g/L	32.87^{b} (0.60)	32.96^{b} (0.58)	33.42^{b} (0.59)	35.58^{a} (0.60)	8.66 ***
Globulin, g/L	37.31^{b} (0.90)	39.54^{a} (0.86)	41.61^{a} (0.88)	40.93^{a} (0.90)	8.66 ***
Urea, mmol/L	3.60 (0.30)	3.62 (0.30)	3.52 (0.30)	3.77 (0.30)	*ns*
Hepatic and muscular profile					
AST, U/L	102.82^{a} (4.22)	100.05^{a} (4.09)	92.34^{ab} (4.00)	87.39^{b} (3.44)	4.87 *
GGT, U/L	13.67^{b} (0.52)	14.51^{b} (0.53)	17.31^{a} (0.70)	17.11^{a} (0.71)	8.75 ***
CK, U/L	265.04 (26.28)	217.91 (22.23)	220.43 (22.08)	197.60 (20.20)	*ns*
Stress profile					
Cortisol, nmol/L	12.50 (1.60)	13.41 (1.66)	16.51 (2.09)	14.56 (1.85)	*ns*

[1]NEFA, not esterified fatty acids (mmol/L); BHB, β-hydroxybutyrate (mmol/L); AST, aspartate aminotransferase (U/L); GGT, gamma glutamyl transferase (U/L); CK, creatin kinase (U/L). Estimates with different superscript letters within row are statistically significantly different ($p \leq 0.05$).

minerals concentration can be associated with a decreased capacity to mobilize Ca from the bones, lower absorption at the intestinal level, and high requirement for Ca (33, 40).

In agreement with Cozzi et al. (15), total protein and globulin concentrations were greater in parity greater than 2 (Table 5) and GGT increased from parity 1 onwards (Table 5). On the other hand, the concentration of the CK was the greatest in parity 1 (Table 5). Cozzi et al. (15) and Walter et al. (25) hypothesized that the high CK level - a specific marker of skeletal muscle injury - in primiparous cows may be due to physical stress caused by hierarchical conflicts when they are grouped with multiparous cows.

Regarding the odds ratio of BILT classes (Table 5), there were no differences between parity 1 and 2, but the risk of having BILT above the threshold (> 4 μmol/L) in parity ≥3 was 3.85 times higher compared to party 1. This finding is in line with that of Walter et al. (25), who reported that the BILT baseline was higher in multiparous cows than in primiparous cows.

3.1.5 Interaction between parity and DIM

The first order interaction between parity and DIM class was not significant for the traits investigated, except for cholesterol, globulin, and total protein. In particular, total protein and globulin were significantly different – i.e. Seventy nine.00 and 45.70 g/L - in parity >3 between 15 and 20 DIM compared with the rest of the interaction levels. Ferreira et al. (45) observed that total protein and globulin concentrations increased during lactation and in their study were greater in multiparous than in primiparous cows. Cholesterol, on the other hand, was the greatest in the last DIM class regardless of parity. Walter et al. (25) reported a constant increasing trend of cholesterol after calving and was greater in multiparous than in primiparous cows.

3.1.6 Variation across seasons

Only few plasma traits were significantly affected by the effect of season, namely Na, Cl, K, albumin, globulin, urea, glucose and cholesterol. In this study, the sampling period spanned from May to October, excluding winter, late autumn, and early spring. In agreement with Cozzi et al. (15), the LSM estimated in this study for Na and Cl were the lowest in samples collected in July–August, while K concentration was the lowest in May–June (Table 6).

With regard to the protein profile, both albumin and urea concentrations slightly increased during the sampling period, with the highest LSM estimated for September–October. In contrast, globulin concentration decreased within the time window considered (Table 6). Regarding the energy profile, the lowest concentration of glucose was found in May–June and July–August (2.72 and 2.83 mmol/L; Table 3) and samples collected in July–August had the lowest LSM for cholesterol concentration (2.53 mmol/L; Table 6). During the core of summer, in presence of acute heat stress, cows decrease their feed

TABLE 4 Odds ratio and 95% confidence interval for total bilirubin (BILT) class[1] for each fixed effect.

Effect	Level	Prevalence [2], %	Odds ratio	95% confidence interval
Days in milk/after calving	3–8 DIM	41.57	Reference	
	9–14 DIM	37.62	0.82	0.43–1.54
	15–20 DIM	23.08	0.37 **	0.17–0.77
	≥21 DIM	19.23	0.20 ***	0.08–0.48
Parity	1	20.00	Reference	
	2	27.18	1.57	0.79–3.11
	≥3	43.61	3.85 ***	2.00–7.37
Season	May–June	31.01	Reference	
	July–August	31.16	2.88	0.98–8.50
	September–October	31.65	2.68	0.80–9.01

[1]"1" if BILT was > 4 μmol/L and "0" if ≤ 4 μmol/L. [2]of BILT class = 1.

TABLE 5 Least squares means (standard error) of blood traits[1] for the fixed effect of parity class along with the *F*-value.

Blood trait	Parity 1	Parity 2	Parity ≥3	*F*-value
Energy profile				
Glucose, mmol/L	3.05[a] (0.10)	2.75[b] (0.10)	2.83[b] (0.10)	19.86 ***
Cholesterol, mmol/L	2.80[a] (0.14)	2.81[a] (0.14)	2.56[b] (0.14)	6.27 **
NEFA, mmol/L	0.33[b] (0.05)	0.34[b] (0.05)	0.42[a] (0.06)	7.56 **
BHB, mmol/L	0.54[b] (0.02)	0.62[ab] (0.03)	0.64[a] (0.02)	5.77 **
Urea, mmol/L	3.57 (0.30)	3.80 (0.30)	3.51 (0.29)	3.28 *
Mineral profile				
Na, mmol/L	139.16 (0.62)	139.32 (0.62)	138.84 (0.61)	*ns*
K, mmol/L	4.40 (0.07)	4.43 (0.07)	4.33 (0.07)	*ns*
Cl, mmol/L	98.63 (0.61)	99.12 (0.61)	98.49 (0.60)	*ns*
Ca, mmol/L	2.45[ab] (0.02)	2.47[a] (0.02)	2.42[b] (0.02)	4.13 *
P, mmol/L	1.71[a] (0.04)	1.59[b] (0.04)	1.48[b] (0.04)	18.69 ***
Mg, mmol/L	0.99[a] (0.01)	0.97[a] (0.01)	0.94[b] (0.01)	7.29 ***
Protein profile				
Total protein, g/L	72.84[b] (0.72)	72.60[b] (0.72)	76.29[a] (0.67)	17.96 ***
Albumin, g/L	33.73 (0.57)	33.72 (0.56)	33.66 (0.53)	*ns*
Globulin, g/L	38.69[b] (0.84)	38.79[b] (0.84)	42.08[a] (0.79)	13.04 ***
Hepatic and muscular profile				
AST, U/L	93.29 (3.73)	96.99 (3.71)	96.12 (3.26)	*ns*
GGT, U/L	14.04[b] (0.50)	15.91[ab] (0.57)	16.89[a] (0.52)	7.87 **
CK, U/L	286.68[a] (27.03)	220.68[b] (21.17)	177.55[b] (15.73)	16.00 ***
Stress profile				
Cortisol, nmol/L	15.21 (1.87)	13.95 (1.69)	13.40 (1.55)	*ns*

[1]NEFA, not esterified fatty acids (mmol/L); BHB, β-hydroxybutyrate (mmol/L); AST, aspartate aminotransferase (U/L); GGT, gamma glutamyl transferase (U/L); CK, creatin kinase (U/L). Estimates with different superscript letters within row are statistically significantly different ($p \leq 0.05$).

intake, inevitably reducing the energy available (46, 47). Moreover, the forage quality may differ across seasons in Italy. Although these two factors can be a reasonable explanation for the low cholesterol and glucose in July–August, this study lacks of data on individual feed intake, ration composition and diet protein level to support this hypothesis.

3.2 Fourier-transform mid-infrared spectroscopy

3.2.1 Prediction ability of FT-MIR

The R^2 and RMSE of the prediction models for plasma trait concentrations are shown in Table 7. The percentage of samples

TABLE 6 Least squares means (standard error) of blood traits[1] for the fixed effect of sampling season along with the *F*-value.

Blood trait	May–June	July–August	September–October	*F*-value
Energy profile				
Glucose, mmol/L	2.72[b] (0.11)	2.83[b] (0.11)	3.08[a] (0.11)	8.02 ***
Cholesterol, mmol/L	2.83[a] (0.16)	2.53[b] (0.15)	2.80[ab] (0.15)	4.17 *
NEFA, mmol/L	0.23 (0.04)	0.47 (0.07)	0.44 (0.07)	*ns*
BHB, mmol/L	0.67 (0.03)	0.63 (0.03)	0.51 (0.02)	*ns*
Urea, mmol/L	3.12[c] (0.32)	3.61[b] (0.30)	4.16[a] (0.31)	10.45 ***
Mineral profile				
Na, mmol/L	140.02[a] (0.70)	137.62[b] (0.64)	139.68[a] (0.67)	14.06 ***
K, mmol/L	4.22[b] (0.08)	4.44[a] (0.07)	4.50[a] (0.07)	7.91 ***
Cl, mmol/L	98.93[a] (0.68)	97.43[b] (0.63)	99.88[a] (0.65)	12.83 ***
Ca, mmoL/L	2.44 (0.02)	2.47 (0.02)	2.42 (0.02)	*ns*
P, mmol/L	1.63 (0.06)	1.60 (0.06)	1.56 (0.06)	*ns*
Mg, mmol/L	0.95 (0.01)	0.98 (0.01)	0.98 (0.02)	*ns*
Protein profile				
Total protein, g/L	74.38 (0.83)	74.07 (0.74)	73.29 (0.83)	*ns*
Albumin, g/L	31.47[c] (0.66)	33.71[b] (0.59)	35.93[a] (0.64)	16.56 ***
Globulin, g/L	42.58[a] (0.98)	39.78[b] (0.87)	37.20[c] (0.96)	10.18 ***
Hepatic and muscular profile				
AST, U/L	94.12 (3.90)	93.35 (4.06)	98.97 (4.17)	*ns*
GGT, U/L	16.86 (0.55)	15.81 (0.48)	14.15 (0.59)	*ns*
CK, U/L	229.14 (25.89)	186.38 (18.07)	263.00 (29.08)	*ns*
Stress profile				
Cortisol, nmol/L	9.81 (1.38)	14.85 (1.88)	19.51 (2.65)	*ns*

[1]NEFA, not esterified fatty acids (mmol/L); BHB, β-hydroxybutyrate (mmol/L); AST, aspartate aminotransferase (U/L); GGT, gamma glutamyl transferase (U/L); CK, creatin kinase (U/L). Estimates with different superscript letters within row are statistically significantly different ($p \leq 0.05$).

identified as outliers and excluded ranged from 0.60 to 4.60%, and the number of LV used ranged from a minimum of 2 to a maximum of 17.

Regarding the quality of predicted phenotypes, Williams (48) and Grelet et al. (49) proposed classifications based on the R^2. In particular if the R^2 is (i) ≥ 0.91, the model can be used for punctual prediction, (ii) between 0.82 and 0.90 the model is suitable for good quantitative screening; (iii) between 0.66 and 0.81, the model is adequate for approximate screening; and (iv) between 0.50 and 0.65, the predicted trait should be used exclusively for detecting extreme values or comparing groups (48).

Overall, the prediction models developed for energy-related metabolites exhibited the best performance. In particular, the most outstanding model in terms of variance explained in the leave-one-out cross-validation was urea concentration ($R^2 = 0.89$; Table 7; Figure 4). When applied to an external set, the same model still showed a very good performance ($R^2 = 0.86$; Table 7; Figure 4). The prediction accuracy for blood urea in this study was higher than that reported in the literature (11, 50). In particular, Ho et al. (50), who used 3,027 samples of Holstein cows from 19 dairy herds in Australia to develop models, obtained R^2 of 0.87 in cross-validation and 0.69 in external validation (50). On the other hand, Luke et al. (12) reported an R^2 equal to 0.90 both in cross-validation and random validation on an independent external dataset. However, when validation was done using the herd-out approach (12), i.e., using an external independent farm, the performance reduced substantially ($R^2 = 0.35$).

Prediction models for BHB concentration and log-transformed BHB had the same R^2 in leave-one-out cross-validation ($R^2 = 0.62$; Table 7; Figure 4), whereas in external validation it was slightly greater for the log-transformed trait (0.52 vs. 0.45; Table 7; Figure 4). Conversely, the prediction model for the untransformed NEFA concentration fitted better than that for the log-transformed NEFA in both calibration and validation. The R^2 values in external validation were 0.57 and 0.46, respectively (Table 7; Figure 4).

Several studies have investigated the use of milk FT-MIR for predicting blood/serum metabolites, such as BHB and NEFA, to identify cows at risk of hyperketonemia, NEB, and excessive fat mobilization. The accuracy of NEFA and BHB predictions reported in this study are in line with those found previously by (11, 12, 50–52). Only Grelet et al. (52) found slightly greater R^2 for BHB concentration both in calibration and validation, i.e., equal to 0.77 and 0.70, respectively. All these studies used blood sampled from cows in early lactation within 40 DIM (11, 12, 50, 52), while Giannuzzi et al. (51) investigated prediction models for these metabolites throughout the whole lactation, obtaining slightly lower accuracy for BHB prediction.

It is important to highlight that time is a key factor for the data quality and representativeness, with potential consequences in the model performance. When predicting a certain blood element from

TABLE 7 Goodness of fit statistics[1] of the modified partial least squares regression models for blood traits[2] developed using milk mid-infrared spectra.

Blood trait	% Outliers	n. LV	R^2c	RMSEc	R^2v	RMSEv
Energy profile						
Glucose, mmol/L	1.8	15	0.43	0.36	0.29	0.40
Cholesterol, mmol/L	2.1	9	0.47	0.64	0.37	0.70
NEFA, mmol/L	2.9	10	0.57	0.20	0.46	0.22
Log-NEFA	2.4	8	0.50	0.20	0.42	0.21
BHB, mmol/L	2.1	15	0.62	0.25	0.45	0.30
Log-BHB	1.2	15	0.62	0.13	0.52	0.15
Urea, mmol/L	1.8	17	0.89	0.43	0.86	0.48
Mineral profile						
Na, mmol/L	2.4	13	0.30	2.70	0.21	2.89
K, mmol/L	3.2	13	0.16	0.29	0.02	0.33
Cl, mmol/L	0.9	13	0.41	2.62	0.11	3.43
Ca, mmo/L	2.6	13	0.44	0.10	0.23	0.12
P, mmol/L	2.1	8	0.26	0.26	0.14	0.29
Mg, mmol/L	2.6	7	0.39	0.09	0.23	0.10
Protein profile						
Total protein, g/L	1.5	14	0.23	5.06	0.03	6.20
Albumin, g/L	1.8	9	0.38	3.14	0.32	3.64
Globulin, g/L	2.4	9	0.24	5.55	0.05	6.03
Hepatic and muscular profile						
AST, U/L	1.5	8	0.27	20.90	0.18	22.11
Log-AST	2.5	7	0.25	0.08	0.19	0.09
GGT, U/L	0.9	2	0.06	5.39	0.01	5.8
Log-GGT	1.8	4	0.08	0.14	0.02	0.16
CK, U/L	3.5	10	0.17	226.45	0.08	192.39
Log-CK	4.6	12	0.26	0.18	0.02	0.21
Stress profile						
Cortisol, nmol/L	3.0	9	0.25	10.28	0.08	12.63
Log-Cortisol	0.6	9	0.21	0.32	0.11	0.36

[1]LV, latent variables; R^2_c, coefficient of determination in calibration; $RSME_C$, Root Mean Square Error in calibration; R^2_V, coefficient of determination in validation; $RSME_V$, Root Mean Square Error in validation. The percentage of outliers (%) here refers to samples whose prediction was far from the actual value, i.e., large residual. [2]NEFA, not esterified fatty acids (mmol/L); BHB, β-hydroxybutyrate (mmol/L); AST, aspartate aminotransferase (U/L); GGT, gamma glutamyl transferase (U/L); CK, creatin kinase (U/L).

the milk spectrum, in fact, the distance – in time - between the blood and the milk sampling plays a crucial role (53). In fact, it has been demonstrated that the morning plasma level of NEFA is predicted with significantly higher accuracy when using evening ($R^2 = 0.61$) than morning ($R^2 = 0.50$) milk spectra (53). This indicates that, although the milk is still expected to mirror the blood, there could be a "delay" in some traits. In addition to this, there is evidence that several traits show very high variability during the day in healthy cows, with either peaks and/or long or short plateaus (e.g., glucose and cortisol).

Cholesterol and glucose were predicted with less accuracy than the traits mentioned above, with an R^2 in leave-one-out cross-validation of 0.47 and 0.43, respectively (Table 7). These predictive abilities were generally similar to those reported by Benedet et al. (11), i.e., R^2 equal to 0.39 and 0.20, respectively. Using the PLS, Giannuzzi et al. (51) obtained similar accuracy for cholesterol concentration, but, on the other hand, a greater accuracy for glucose concentration. To justify this difference, it is worth stressing that the study of Giannuzzi et al. (51) dealt with blood samples collected during the whole lactation, up to >305 DIM. As previously discussed, even if glucose tends to be high around calving, it may still vary quite substantially within the same day due to the presence of non-negligible peaks corresponding to meal administration or acute episodes of stress (28).

Blood mineral concentrations were generally predicted with less accuracy compared to the other traits. In fact, the R^2 was below 0.50, regardless of the type of validation (Table 7) and the best model was the one developed for Ca concentration ($R^2 = 0.44$), followed by Mg concentration ($R^2 = 0.39$). When applied to an external set of samples, these two models showed lower R^2 values (both equal to 0.23). Despite this, the results can be considered more promising compared to those reported by Luke et al. (12), who observed R^2 in cross-validation of

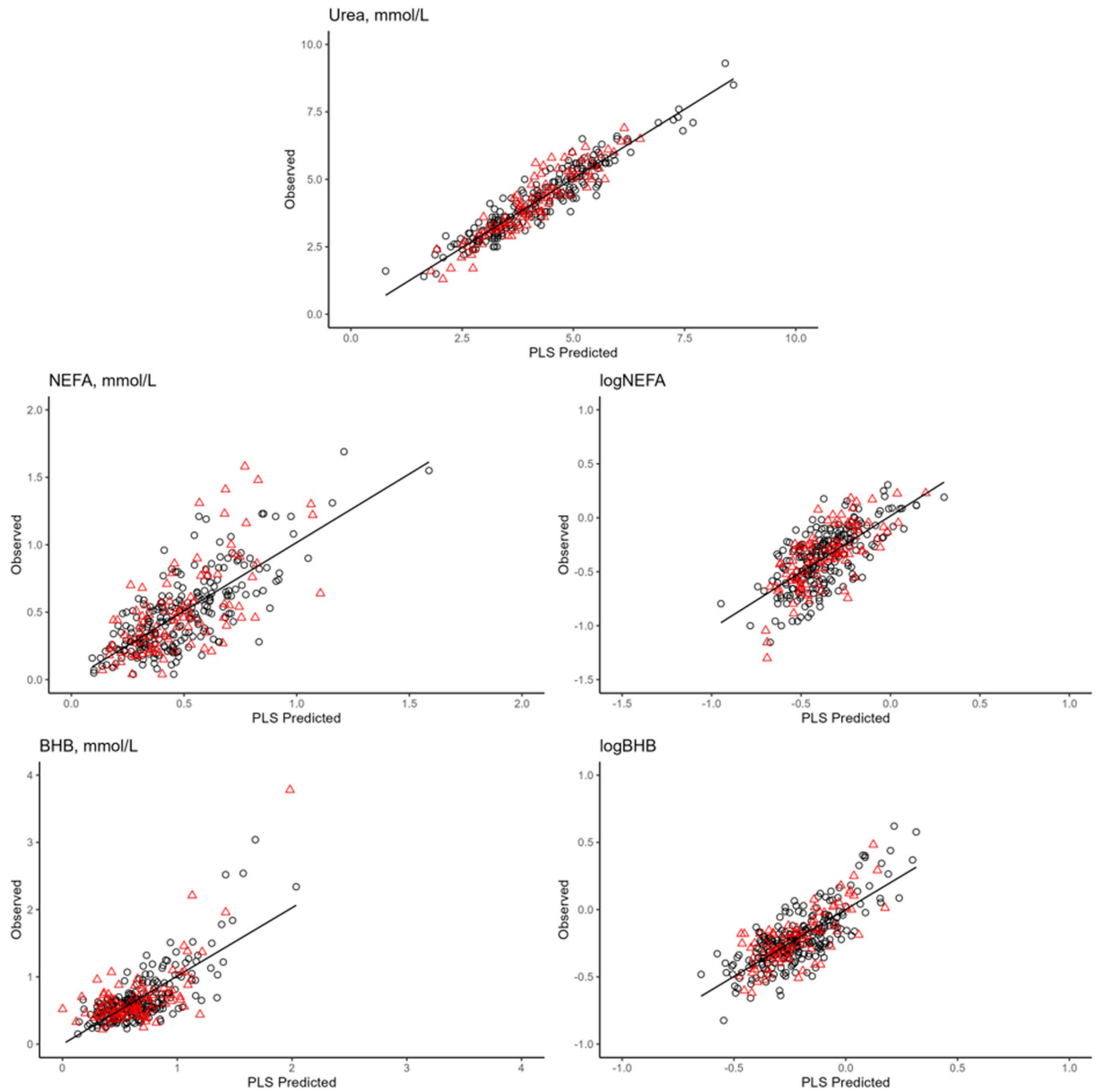

FIGURE 4
Plot of mid-infrared predictions (x-axis) and observed values (y-axis) for the blood traits[2]. Calibration set are reported in in red (▲), whereas validation set are black (●). [1]Only prediction models with coefficient of determination in validation >0.40 are presented, namely: blood urea, not esterified fatty acids (NEFA), logarithmic transformation of NEFA (logNEFA), β-hydroxybutyrate (BHB), and logarithmic transformation of BHB (logBHB).

0.08 and 0.06 for Ca and Mg, respectively. In their study (12), blood samples were taken immediately after or during milk sampling. Attempting to predict something present in the blood using the milk spectrum is challenging, as it is an indirect prediction, therefore low R^2 are inevitably expected.

For the others plasma traits, the R^2 in leave-one-out cross-validation was low, ranging from 0.08 (GGT) to 0.38 (albumin), as well as the one in external validation (0.01 to 0.32; Table 7). In general, whenever a trait was not normally distributed (e.g., BHB), prediction models were used for both the forms, log-transformed and untransformed. In general, the R^2 values in the external validation were slightly higher when the log-transformed trait was used. In line with Luke et al. (12), the prediction model for albumin fitted better than globulin (Table 7). It is widely known that components present in very low concentrations are more difficult to predict with FT-MIR because of the small signal(s) within the spectrum. Highly concentrated components have strong absorption peaks and are thereby easier to be predicted precisely and accurately.

Based on the classification of Williams (48), concentrations of BHB, NEFA, and urea predicted with the model in Table 7 can be considered as good enough for population screening and for carrying out selective breeding. Phenotypes predicted from the milk spectra may be scarcely or moderately correlated with the real trait (e.g., blood BHB), but still the predictions can be valuable for genetic investigations at the population level and for design of breeding programs (54, 55). For example, FT-MIR allows to identify cows within a given population with high BHB and/or NEFA and their sires, i.e., bulls with progeny at major risk of

TABLE 8 Performance[1] (%) of partial least squares discriminant analysis[2] based on milk mid-infrared spectra in calibration and validation.

Trait	Threshold[3]	Calibration set					Validation set				
		Sensitivity	Specificity	TP	TN	Balanced accuracy	Sensitivity	Specificity	TP	TN	Balanced accuracy
BILT, μmol/L	4 μmol/L	0.48	0.96	0.80	0.84	0.72	0.42	0.91	0.78	0.68	0.67
BHB, mmol/L	1.2 mmol/L	0.52	0.99	0.96	0.85	0.76	0.33	0.98	0.94	0.60	0.66
NEFA, mmol/L	0.7 mmol/L	0.56	0.97	0.88	0.83	0.76	0.36	0.96	0.84	0.73	0.66

[1]TP, true positives correctly classified; TN, true negatives correctly classified. [2]Binary classification (≤ vs. > threshold) for: NEFA, not esterified fatty acids (mmol/L); BHB, β-hydroxybutyrate (mmol/L); BILT, total bilirubin (μmol/L). [3]Values refer to cut-offs retrieved from the literature [Ospina et al. (20)].

metabolic diseases. The FT-MIR is a low-cost phenotyping tool since the analysis are regularly carried out for milk quality assessment in the framework of the official tests (14).

3.2.2 FT-MIR classification ability

The PLS-DA was performed for traits whose threshold found a consensus in the literature, i.e., BHB, NEFA and BILT, considering two levels: equal to or below the threshold (no risk) and above the threshold (at risk). In the dataset 22.30, 8.90, and 27.80% of the samples were above the thresholds for BHB, NEFA and BILT, respectively (Table 8).

Sensitivity, defined for each plasma traits class as the probability of correctly identifying cows at risk (above the threshold), ranged from 0.48 for BILT to 0.56 for NEFA in calibration. In validation, the maximum and minimum sensitivity were 0.42 and 0.33, respectively (Table 8). Specificity, complementary to sensitivity, represents the probability of correctly identifying the control cases, i.e., cows not at risk, below the threshold. This parameter was close to unity, being overall ≥0.96 in calibration and ≥0.91 in validation. The sensitivity calculated in this study for BHB was 0.33 in validation, and not far from the value (0.28) reported by Benedet et al. (11). This percentage indicated that approximately one third of the cows at risk in this study were correctly identified. In the case of NEFA and BILT, this percentage was slightly higher: 36 and 42%, respectively. The fact that specificity is close to unity does not necessarily mean that the model robustness of this study is sufficiently good for implementation. In fact, the real aim in the field is to precisely identify potentially sick cows rather than those that are not. This means that sensitivity instead of specificity should be ideally improved and maximized. Martín-Gómez et al. (56) recommended an optimization based on sensitivity and specificity to assess the quality of PLS-DA models that discriminate between two classes. The balanced accuracy in calibration was equal to 0.72 for BILT and 0.76 for both BHB and NEFA.

Considering that health data and clinical events of dairy cows are not routinely recorded in Italy due to the absence of validated standardized protocols, binary phenotypes obtained through the PLS-DA could be valid indicator traits to be used for various purposes. However, further efforts should be made to improve the scalability and sensitivity of the models.

4 Conclusion

In the present study, we investigated non-genetic factors affecting the variability of blood traits in healthy Holstein cows in the early lactation and we attempted to predict them using milk FT-MIR. Most of the plasma traits were significantly affected by the fixed effect of parity, distance from calving, and season. The performance of the FT-MIR models – especially in classification – indicated that the use of milk spectra for monitoring hematic traits is advisable, especially for BHB, NEFA, and urea. In regression, however, our prediction models were not sufficiently accurate for a punctual determination of the concentration of the parameters. Despite of the mid to low accuracy, the predictions represent nowadays a valid opportunity for farmers and breeders for both decision-making and genetic screening at the population level, to better identify sick animals or cows at risk. Further efforts should be made to understand if the FT-MIR spectra – coupled with additional data from other sources, such as sensors and genomic information – analysed via alternative machine learning algorithms will result into better scalability, sensitivity, and accuracy.

Data availability statement

The datasets presented in this article are not readily available because the raw used in the present study belong to the Breeders Association of Veneto Region (ARAV, Vicenza, Italy), and were shared after agreement with the University of Padova. The raw data supporting the conclusions of this article will be made available from the corresponding author upon request.

Ethics statement

The animal study was approved by Ethical Committee for the Care and Use of Experimental Animals of the University of Padova (Padova, Italy). Written informed consent was obtained from the owners for the participation of their animals in this study. The study was conducted in accordance with the local legislation and institutional requirements.

Author contributions

SM: Data curation, Formal analysis, Investigation, Methodology, Software, Visualization, Writing – original draft, Writing – review & editing. AC: Conceptualization, Investigation, Methodology, Project administration, Supervision, Visualization, Writing – original draft, Writing – review & editing. DC: Validation, Writing – review & editing. EC: Data curation, Writing – review & editing. MM: Conceptualization, Funding acquisition, Investigation, Project administration, Resources, Supervision, Writing – review & editing.

Funding

The authors declare that financial support was received for the research, authorship, and/or publication of this article. This study was carried out within the Agritech National Research Center and received funding from the European Union Next-GenerationEU (PIANO NAZIONALE DI RIPRESA E RESILIENZA (PNRR) – MISSIONE 4 COMPONENTE 2, INVESTIMENTO 1.4 – D.D. 1032 17/06/2022, CN00000022). This manuscript reflects only the authors' views and opinions, neither the European Union nor the European Commission can be considered responsible for them. For this research, MM was supported by the project "Ketogen" of the Breeders Association of Veneto Region (ARAV, Vicenza, Italy).

Acknowledgments

Authors would like to thank the farmers for joining the study, ARAV for providing milk samples data, and the Italian Holstein and Jersey Association (ANAFIBJ, Cremona, Italy) for the technical support. The software "Paperpal" by Editage (https://paperpal.com/) was adopted for proofreading the final version of the masnuscript.

Conflict of interest

The authors declare that the research was conducted in the absence of any commercial or financial relationships that could be construed as a potential conflict of interest.

Publisher's note

All claims expressed in this article are solely those of the authors and do not necessarily represent those of their affiliated organizations, or those of the publisher, the editors and the reviewers. Any product that may be evaluated in this article, or claim that may be made by its manufacturer, is not guaranteed or endorsed by the publisher.

References

1. Loiselle MC, Ster C, Talbot BG, Zhao X, Wagner GF, Boisclair YR, et al. Impact of postpartum milking frequency on the immune system and the blood metabolite concentration of dairy cows. *J Dairy Sci*. (2009) 92:1900–12. doi: 10.3168/jds.2008-1399

2. Gross JJ, Bruckmaier RM. Metabolic challenges in lactating dairy cows and their assessment via established and novel indicators in milk. *Animal*. (2019) 13:s75–81. doi: 10.1017/S175173111800349X

3. Grummer RR, Mashek DG, Hayirli A. Dry matter intake and energy balance in the transition period. *Vet Clin North Am Food Anim*. (2004) 20:447–70. doi: 10.1016/j.cvfa.2004.06.013

4. Rico JE, Barrientos-Blanco MA. INVITED REVIEW: ketone biology: the shifting paradigm of ketones and ketosis in the dairy cow. *J Dairy Sci*. (2024) 107:3367–88. doi: 10.3168/jds.2023-23904

5. Benedet A, Manuelian CL, Zidi A, Penasa M, De Marchi M. Invited review: β-hydroxybutyrate concentration in blood and milk and its associations with cow performance. *Animal*. (2019) 13:1676–89. doi: 10.1017/S175173111900034X

6. Mikulková K, Kadek R, Filípek J, Illek J. Evaluation of oxidant/antioxidant status, metabolic profile and milk production in cows with metritis. *Ir Vet J*. (2020) 73:8–11. doi: 10.1186/s13620-020-00161-3

7. Sattler T, Fürll M. Creatine kinase and aspartate aminotransferase in cows as indicators for endometritis. *J Vet Med*. (2004) 51:132–7. doi: 10.1111/j.1439-0442.2004.00612.x

8. Egger-Danner C, Fuerst-Waltl B, Obritzhauser W, Fuerst C, Schwarzenbacher H, Grassauer B, et al. Recording of direct health traits in Austria—experience report with emphasis on aspects of availability for breeding purposes. *J Dairy Sci*. (2012) 95:2765–77. doi: 10.3168/jds.2011-4876

9. ISO. Milk and liquid milk products. Guidelines for the application of mid-infrared spectrometry. ISO 9622. Geneva, Switzerland: International Organisation for Standardisation (2013).

10. De Marchi M, Toffanin V, Cassandro M, Penasa M. Invited review: mid-infrared spectroscopy as phenotyping tool for milk traits. *J Dairy Sci*. (2014) 97:1171–86. doi: 10.3168/jds.2013-6799

11. Benedet A, Franzoi M, Penasa M, Pellattiero E, De Marchi M. Prediction of blood metabolites from milk mid-infrared spectra in early-lactation cows. *J Dairy Sci*. (2019) 102:11298–307. doi: 10.3168/jds.2019-16937

12. Luke TDW, Rochfort S, Wales WJ, Bonfatti V, Marett L, Pryce JE. Metabolic profiling of early-lactation dairy cows using milk mid-infrared spectra. *J Dairy Sci*. (2019) 102:1747–60. doi: 10.3168/jds.2018-15103

13. Serrenho RC, Williamson M, Berkec O, LeBlanc SJ, DeVries TJ, McBride BW, et al. An investigation of blood, milk, and urine test patterns for the diagnosis of ketosis in dairy cows in early lactation. *J Dairy Sci*. (2022) 105:7719–27. doi: 10.3168/jds.2021-21590

14. ICAR, International Committee for Animal Recording. (2012). *International Strategies and New Developments in Milk Analysis*. Available at: https://www.icar.org/Documents/milk_laboratories_leray/Proc.%20RLN%20Meeting%202012,%20Cork%20IE.pdf.

15. Cozzi G, Ravarotto L, Gottardo F, Stefani AL, Contiero B, Moro L, et al. Reference values for blood parameters in Holstein dairy cows: effects of parity, stage of lactation, and season of production. *J Dairy Sci*. (2011) 94:3895–901. doi: 10.3168/jds.2010-3687

16. R Core Team. R: A language and environment for statistical computing. Vienna, Austria: R Foundation for Statistical Computing (2022).

17. Grelet C, Pierna JAF, Dardenne P, Baeten V, Dehareng F. Standardization of milk mid-infrared spectra from a European dairy network. *J Dairy Sci*. (2015) 98:2150–60. doi: 10.3168/jds.2014-8764

18. Manfredi M, Robotti E, Quasso F, Mazzucco E, Calabrese G, Marengo E. Fast classification of hazelnut cultivars through portable infrared spectroscopy and chemometrics. *Spectrochim Acta A Mol Biomol Spectrosc*. (2018) 189:427–35. doi: 10.1016/j.saa.2017.08.050

19. Kuhn M. Building predictive models in R using the caret package. *J Stat Softw*. (2008) 28:1–26. doi: 10.18637/jss.v028.i05

20. Ospina PA, Nydam DV, Stokol T, Overton TR. Evaluation of nonesterified fatty acids and β-hydroxybutyrate in transition dairy cattle in the northeastern United States: critical thresholds for prediction of clinical diseases. *J Dairy Sci*. (2010) 93:546–54. doi: 10.3168/jds.2009-2277

21. Bauman DE, Currie WB. Partitioning of nutrients during pregnancy and lactation: a review of mechanisms involving homeostasis and homeorhesis. *J Dairy Sci*. (1980) 63:1514–29. doi: 10.3168/jds.S0022-0302(80)83111-0

22. Miglior F, Fleming A, Malchiodi F, Brito LF, Martin P, Baes CF. A 100-year review: identification and genetic selection of economically important traits in dairy cattle. *J Dairy Sci*. (2017) 100:10251–71. doi: 10.3168/jds.2017-12968

23. Italian Breeders Association (AIA). (2023). Available at: http://bollettino.aia.it/Contenuti.aspx?CD_GruppoStampe=RS&CD_Specie=C4 (Accessed August 1, 2024).

24. Pawliński B, Gołębiewski M, Trela M, Witkowska-Piłaszewicz O. Comparison of blood gas parameters, ions, and glucose concentration in polish Holstein-Friesian dairy cows at different milk production levels. *Sci Rep*. (2023) 13:1414. doi: 10.1038/s41598-023-28644-7

25. Walter LL, Gärtner T, Gernand E, Wehrend A, Donat K. Effects of parity and stage of lactation on trend and variability of metabolic markers in dairy cows. *Animals*. (2022) 12:1008. doi: 10.3390/ani12081008

26. Venjakob PL, Borchardt S, Heuwieser W. Hypocalcemia—cow-level prevalence and preventive strategies in German dairy herds. *J Dairy Sci*. (2017) 100:9258–66. doi: 10.3168/jds.2016-12494

27. Cattaneo L, Lopreiato V, Piccioli-Cappelli F, Trevisi E, Minuti A. Plasma albumin-to-globulin ratio before dry-off as a possible index of inflammatory status and performance in the subsequent lactation in dairy cows. *J Dairy Sci*. (2021) 104:8228–42. doi: 10.3168/jds.2020-19944

28. Fiore E, Perillo L, Gianesella M, Giannetto C, Giudice E, Piccione G, et al. Comparison between two preventive treatments for hyperketonaemia carried out pre-partum: effects on non-esterified fatty acids, β-hydroxybutyrate and some biochemical parameters during peripartum and early lactation. *J Dairy Res*. (2021) 88:38–44. doi: 10.1017/S0022029921000108

29. Trevisi E, Bertoni G. Some physiological and biochemical methods for acute and chronic stress evaluationin dairy cows. *Ital J Anim Sci*. (2009) 8:265–86. doi: 10.4081/ijas.2009.s1.265

30. Imhasly S, Bieli C, Naegeli H, Nyström L, Ruetten M, Gerspach C. Blood plasma lipidome profile of dairy cows during the transition period. *BMC Vet Res*. (2015) 11:252–14. doi: 10.1186/s12917-015-0565-8

31. McCarthy MM, Mann S, Nydam DV, Overton TR, McArt JAA. Concentrations of nonesterified fatty acids and β-hydroxybutyrate in dairy cows are not well correlated during the transition period. *J Dairy Sci*. (2015) 98:6284–90. doi: 10.3168/jds.2015-9446

32. Andjelić B, Djoković R, Cincović M, Bogosavljević-Bošković S, Petrović M, Mladenović J, et al. Relationships between milk and blood biochemical parameters and metabolic status in dairy cows during lactation. *Meta*. (2022) 12:733. doi: 10.3390/metabo12080733

33. DeGaris PJ, Lean IJ. Milk fever in dairy cows: a review of pathophysiology and control principles. *Vet J*. (2008) 176:58–69. doi: 10.1016/j.tvjl.2007.12.029

34. Mulligan FJ, Doherty ML. Production diseases of the transition cow. *Vet J*. (2007) 176:3–9. doi: 10.1016/j.tvjl.2007.12.018v

35. Cavallini D, Mammi LME, Buonaiuto G, Palmonari A, Valle E, Formigoni A. Immune-metabolic-inflammatory markers in Holstein cows exposed to a nutritional and environmental stressing challenge. *J Anim Physiol Anim Nutr (Berl)*. (2007) 176:3–9. doi: 10.1111/jpn.13607

36. Whitaker DA. Use and interpretation of metabolic profiles In: AH Andrews, editor. The health if dairy cattle. Hoboken, NJ: Blackwell Science Ltd (2000). 89–107.

37. Janovick Guretzky NA, Carlson DB, Garrett JE, Drackley JK. Lipid metabolite profiles and milk production for Holstein and Jersey cows fed rumen-protected choline during the periparturient period. *J Dairy Sci*. (2021) 1:42–55. doi: 10.3168/jds.S0022-0302(06)72083-5

38. Goff JP. The monitoring, prevention, and treatment of milk fever and subclinical hypocalcemia in dairy cows. *Vet J*. (2008) 176:50–7. doi: 10.1016/j.tvjl.2007.12.020

39. Tsioulpas A, Grandison AS, Lewis MJ. Changes in physical properties of bovine milk from the colostrum period to early lactation. *J Dairy Sci*. (2007) 90:5012–7. doi: 10.3168/jds.2007-0192

40. Goi A, De Marchi M, Costa A. Minerals and essential amino acids of bovine colostrum: phenotypic variability and predictive ability of mid-and near-infrared spectroscopy. *J Dairy Sci*. (2023) 106:8341–56. doi: 10.3168/jds.2023-23459

41. DeGroot MA, Block E, French PD. Effect of prepartum anionic supplementation on periparturient feed intake, health, and milk production. *J Dairy Sci*. (2010) 93:5268–79. doi: 10.3168/jds.2010-3092

42. Moretti P, Paltrinieri S, Trevisi E, Probo M, Ferrari A, Minuti A, et al. Reference intervals for hematological and biochemical parameters, acute phase proteins and markers of oxidation in Holstein dairy cows around 3 and 30 days after calving. *Res Vet Sci*. (2017) 114:322–31. doi: 10.1016/j.rvsc.2017.06.012

43. Hoffmann WE, Solter PF. Diagnostic enzymology of domestic animals. *Clin Biochem Domest Anim*. (2008) 6:351–78. doi: 10.1016/B978-0-12-370491-7.00012-X

44. Bionaz M, Trevisi E, Calamari L, Librandi F, Ferrari A, Bertoni G. Plasma paraoxonase, health, inflammatory conditions, and liver function in transition dairy cows. *J Dairy Sci*. (2007) 90:1740–50. doi: 10.3168/jds.2006-445

45. Ferreira MFDL, Rennó LN, Rodrigues II, Detmann E, Paulino MF, de Campos Valadares Filho S, et al. Effects of parity order on performance, metabolic, and hormonal parameters of grazing beef cows during pre-calving and lactation periods. *BMC Vet Res*. (2021) 17:311–5. doi: 10.1186/s12917-021-03019-0

46. Felini R, Cavallini D, Buonaiuto G, Bordin T. Assessing the impact of thermoregulatory mineral supplementation on thermal comfort in lactating Holstein cows. *Vet Anim Sci*. (2024) 24:100363. doi: 10.1016/j.vas.2024.100363

47. Abeni F, Calamari L, Stefanini L. Metabolic conditions of lactating Friesian cows during the hot season in the Po valley. 1. Blood indicators of heat stress. *Int J Biometeorol*. (2007) 52:87–96. doi: 10.1007/s00484-007-0098-3

48. Williams P. *Near-infrared technology: Getting the best out of light: A short course in the practical implementation of near-infrared spectroscopy for the user*. PDK Projects, Incorporated (2004).

49. Grelet C, Dardenne P, Soyeurt H, Fernandez JA, Vanlierde A, Stevens F, et al. Large-scale phenotyping in dairy sector using milk MIR spectra: key factors affecting the quality of predictions. *Methods*. (2021) 186:97–111. doi: 10.1016/j.ymeth.2020.07.012

50. Ho PN, Luke TDW, Pryce JE. Validation of milk mid-infrared spectroscopy for predicting the metabolic status of lactating dairy cows in Australia. *J Dairy Sci*. (2021) 104:4467–77. doi: 10.3168/jds.2020-19603

51. Giannuzzi D, Mota LFM, Pegolo S, Tagliapietra F, Schiavon S, Gallo L, et al. Prediction of detailed blood metabolic profile using milk infrared spectra and machine learning methods in dairy cattle. *J Dairy Sci*. (2023) 106:3321–44. doi: 10.3168/jds.2022-22454

52. Grelet C, Vanlierde A, Hostens M, Foldager L, Salavati M, Ingvartsen KL, et al. Potential of milk mid-IR spectra to predict metabolic status of cows through blood components and an innovative clustering approach. *Animal*. (2019) 13:649–58. doi: 10.1017/S1751731118001751

53. Aernouts B, Adriaens I, Diaz-Olivares J, Saeys W, Mäntysaari P, Kokkonen T, et al. Mid-infrared spectroscopic analysis of raw milk to predict the blood nonesterified fatty acid concentrations in dairy cows. *J Dairy Sci*. (2020) 103:6422–38. doi: 10.3168/jds.2019-17952

54. Bovenhuis H, Jibrila I, Dijkstra J. *Predicting milk phosphorus content based on genotypic and milk infrared data*. Proceedings of the 11th world congress on genetics applied to livestock production, Auckland (New Zealand). (2018).

55. Zaalberg RM, Poulsen NA, Bovenhuis H, Sehested J, Larsen LB, Buitenhuis AJ. Genetic analysis on infrared-predicted milk minerals for Danish dairy cattle. *J Dairy Sci*. (2021) 104:8947–58. doi: 10.3168/jds.2020-19638

56. Martín-Gómez A, Rodríguez-Hernández P, Cardador MJ, Vega-Márquez B, Rodríguez-Estévez V, Arce L. Guidelines to build PLS-DA chemometric classification models using a GC-IMS method: dry-cured ham as a case of study. *Talanta Open*. (2023) 7:100175. doi: 10.1016/j.talo.2022.100175

frontiers | Frontiers in Veterinary Science

TYPE Original Research
PUBLISHED 06 January 2025
DOI 10.3389/fvets.2024.1514362

OPEN ACCESS

EDITED BY
Manuel Garcia-Herreros,
National Institute for Agricultural and Veterinary Research (INIAV), Portugal

REVIEWED BY
Li Xin Hong,
Shanghai Jiao Tong University, China
Elsayed Metwally,
Suez Canal University, Egypt

*CORRESPONDENCE
Tianzeng Song
✉ songtianzeng123@sina.com
Guangbin Zhou
✉ zguangbin@sicau.edu.cn

†These authors have contributed equally to this work

RECEIVED 20 October 2024
ACCEPTED 13 December 2024
PUBLISHED 06 January 2025

CITATION
Zang S, Zou S, Chen X, Pan B, Ning A, Qin J, Wei Y, Du K, Ye J, Liang Q, Fang Y, Qiongla, Cirenlamu, Song T and Zhou G (2025) Abnormalities in mitochondrial energy metabolism induced by cryopreservation negatively affect goat sperm motility. *Front. Vet. Sci.* 11:1514362. doi: 10.3389/fvets.2024.1514362

Abnormalities in mitochondrial energy metabolism induced by cryopreservation negatively affect goat sperm motility

Shengqin Zang[1†], Shuqi Zou[1†], Xiangyi Chen[1], Bo Pan[1], Ao Ning[1], Jianpeng Qin[1], Yaozong Wei[1], Kunlin Du[1], Jiangfeng Ye[1], Qiuxia Liang[2], Yi Fang[3], Qiongla[4], Cirenlamu[4], Tianzeng Song[5,6]* and Guangbin Zhou[1]*

[1]Farm Animal Genetic Resources Exploration and Innovation Key Laboratory of Sichuan Province, College of Animal Science and Technology, Sichuan Agricultural University, Chengdu, China, [2]College of Life Science, Sichuan Agricultural University, Ya'an, Sichuan, China, [3]Key Laboratory of Animal Production, Product Quality and Security, Ministry of Education, College of Animal Science and Technology, Jilin Agricultural University, Changchun, China, [4]The Service Station of Agricultural and Animal, Husbandry Technical of Nyalam County, Shigatse, China, [5]Institute of Animal Science, Xizang Academy of Agricultural and Animal Husbandry Science, Lhasa, China, [6]Key Laboratory of Animal Genetics and Breeding on Xizang Plateau, Ministry of Agriculture and Rural Affairs, Lhasa, China

The motility of sperm decreases following cryopreservation, which is closely associated with mitochondrial function. However, the alterations in mitochondrial metabolism after sperm freezing in goats remain unclear. This experiment aimed to investigate the impact of ultra-low temperature freezing on goat sperm's mitochondrial energy metabolism and its potential correlation with sperm motility. The results revealed that goat sperm exhibited mitochondrial vacuolization, reduced matrix density, and significantly decreased levels of high-membrane potential mitochondria and adenosine triphosphate content, accompanied by a substantial increase in reactive oxygen species levels, ultimately leading to a significant decline in sperm viability. Further investigations unveiled that energy-related differential metabolites (capric acid, creatine, and D-glucosamine-6-phosphate) and differential metabolites with antioxidant effects (saikosaponin A, probucol, and cholesterol sulfate) were significantly downregulated. In addition, the activity of key rate-limiting enzymes involved in very long-chain fatty acid biosynthesis and β-oxidation—specifically acetyl-CoA carboxylase, fatty acid synthase, and carnitine palmitoyltransferase I related to capric acid metabolism—was considerably reduced. Furthermore, supplementation of differential metabolite capric acid (500 μM) significantly enhanced the motility of frozen–thawed goat sperm. These findings indicated that the mitochondrial ultrastructure of goat sperm is damaged and energy metabolism becomes abnormal after cryopreservation, potentially affecting sperm viability. The addition of different metabolites such as capric acid to the freezing extender can alleviate the decrease in sperm motility induced by cryopreservation.

KEYWORDS

goat sperm, cryopreservation, sperm motility, energy metabolism, metabolomics

1 Introduction

Semen cryopreservation technology has the potential to overcome the limitations of time and space, facilitating long-distance transportation of animal semen and accelerating the global adoption and application of modern biotechnology such as artificial insemination and *in vitro* fertilization (1). However, it is worth noting that post-thaw sperm motility is significantly lower compared to fresh sperm: 39.47% vs. 87.33% in pigs (2, 3), 36.0% vs. 83.4% in horses (4, 5), 37.12% vs. 90.30% in cattle (6, 7), 37.60% vs. 82.18% in sheep (8, 9), and 23.3% vs. 80.0% in goats (10, 11). Previous studies have indicated that decreased sperm motility after freezing is associated with mitochondrial damage (12–14). Given that mitochondria play a key role in energy metabolism, which is closely related to sperm motility (15). Thus, sperm mitochondria damage could be tightly linked to decline of sperm motility (16, 17). It has been reported that the mitochondrial permeability transition pore, a transmembrane protein on the inner mitochondrial membrane (IMM), usually remains closed (18). However, sperm cryopreservation tends to cause the formation and prolonged opening of the mitochondrial permeability transition pore, which leads to the disruption of the energy supply and causes mitochondrial damage (19, 20). Apparently, there is an inevitable connection between the energy metabolism disruption induced by mitochondrial dysfunction and the decline in sperm motility; however, the exact mechanism is still unclear. Therefore, investigating the characteristics of mitochondrial energy metabolism following sperm cryopreservation can provide valuable insights into understanding the mechanisms underlying reduced sperm motility and exploring potential mitigation strategies.

After sperm cryopreservation, the mitochondria primarily exhibit ultrastructural damage, a reduction in adenosine triphosphate (ATP) content, decreased mitochondrial membrane potential (MMP), and abnormal opening of the mitochondrial membrane permeability transition pore. This is also accompanied by the production of a large amount of reactive oxygen species (ROS), especially in complexes I and III of the mitochondrial electron transport chain (ETC) (21, 22). Excessive accumulation of ROS leads to oxidative stress, which damages the mitochondrial membrane and its function, leading to a self-perpetuating cycle of ROS generation (15, 23). Previous studies have demonstrated that freezing results in mitochondrial ultrastructural damage in human sperm and significant alterations in the citrate cycle (TCA cycle) in mitochondria (24). However, further investigation is needed to explore how mitochondrial metabolism changes after sperm cryopreservation in goats and its impact on sperm viability.

As metabolomic technology continues to advance, there has been a notable increase in studies targeting metabolites in the frozen–thawed sperm of domestic animals. An analysis of the results of these existing studies revealed that there are differences in the sperm metabolomic profiles of different species (such as Dorper sheep and bull) (25, 26) or breeds (such as Yunshang black goat and Guanzhong dairy goat) (27, 28). This suggests that exploring the key differential metabolites specific to different breeds may enhance the effectiveness of sperm cryopreservation. However, the changes in energy metabolism in semen from the Chengdu brown goat (CBG), a breed recognized under China's National Product of Geographical Indication, after freezing, remains unclear. Therefore, this study aims to investigate (1) the impact of cryopreservation on mitochondrial ultrastructure, function, and sperm motility in CBG, (2) the effects of ultra-low temperature freezing on energy metabolism in CBG sperm and identification of differential metabolites, and (3) the influence of these differential metabolites on the motility of frozen–thawed CBG sperm.

2 Materials and methods

Unless otherwise noted, all chemicals were purchased from Sigma-Aldrich (St. Louis, MO, USA). All experimental procedures were conducted in strict accordance with the regulations of the Animal Ethics and Welfare Committee (AEWC) of Sichuan Agricultural University, China (Approval code: AEWC2016, 6 January 2016).

2.1 Animal semen collection and quality assessment

We collected semen at Xilingxue Agricultural Development Co., Ltd. (103°17′E, 30°35'N) in Chengdu, Sichuan Province, China, during the breeding season (August–November) in 2023. A total of 10 healthy goats of normal breeding age (2–4 years old) were selected, and each male goat was individually housed and managed. All male goats had free access to water and feed. Semen was collected from the male goats using an artificial vagina method (with water temperature controlled between 40 and 42°C). Collections were performed once a week for 12 weeks, with semen samples taken from five male goats each time. The semen was collected using disposable centrifuge tubes, and the volume was recorded each time. First, the color and viscosity of the semen were observed visually. Then, the collected semen was diluted with a base extender, wrapped in a cotton gauze, and transported in a foam box (18–20°C) to the laboratory within 1 h.

A 3 μL aliquot of diluted semen was transferred into a pre-heated (37°C) disposable sperm test plate. Computer-assisted semen analysis (CASA) (AndroVision®, Minitube, Germany) was used to select the goat species in the software, and the relevant parameters were analyzed and recorded at 200x magnification. For each sample, five fields were counted, and at least 2,500 sperm were analyzed. The CASA system parameters were set as described in published article (8), including curvilinear velocity (VCL; μm/s), velocity of straight line (VSL; μm/s), velocity of average path (VAP; μm/s), beat cross-frequency (BCF; HZ); radius: sperm path radioactivity coefficient. Briefly, sperm trajectory motion were continuously captured within 0.5 s using the following parameters, in situ motility (VSL < 24.0000, VCL < 48.0000), circular motion (radius > 9.00 and radius < 90.00 and rotation >0.70) and slow motion (VCL < 120.0000), respectively. The semen samples used in this study had to meet the following criteria: volume ranging from 0.7 mL to 2 mL, a minimum sperm density of 2.5×10^9 sperm/mL, and total motility of at least 70%.

2.2 Semen dilution, freezing, and thawing

The semen from each goat after passing the quality test was equally divided into four groups: fresh and frozen groups treated with commercial diluent (CD) and fresh and frozen groups treated with

homemade diluent. The CD for the goat was divided into liquid I and liquid II (Beijing Tianyuan Aorui Biotechnology Co., Ltd., China). The commercial fresh group was diluted with liquid I (1:19). When the CD is used as the cryopreservation diluent, 25% (v:v) fresh yolk solution should be added to both liquid I and liquid II before use. In brief, the homemade base extender composition included 19.98 mM Tris (T8060, Solarbio, China), 4.67 mM glucose, 7.18 mM citric acid (C8610, Solarbio, China), 5.84 mM sucrose, and 100,000 IU each of penicillin and streptomycin. This solution was used to dilute fresh sperm at a ratio of 1:19, with 100 mL of dilution solution. Liquid I was prepared by adding 20% egg yolk (v:v) to the homemade base extender. Liquid II was then prepared by adding 6% glycerol (v:v) and 0.6% Equex STM paste (v:v) to liquid I (13,560/0008, Minitube, Germany).

Semen freezing was performed using a two-step dilution method. The specific procedure was as follows: Cryopreservation dilution liquids I and II containing sperm were mixed homogeneously (1:9:10) at isothermal and equal volumes; then, the semen samples were packed in 0.25 mL plastic straws (1.25×10^8 sperm/mL), which was sealed with polyvinyl alcohol powder, wrapped in 8 layers of cotton gauze, and placed in a refrigerator at 4°C for cooling and equilibration for 1.5 to 2 h. The plastic straws were placed 4 cm above liquid nitrogen for 10 min, and the temperature was kept at −130°C, then plunged into liquid nitrogen (− 196°C), and kept for 7 days. The straws were thawed in a water bath at 37°C for 30 s before use. The qualified semen, with sperm motility above 0.35, was first centrifuged at 4,000 rpm and 4°C for 5 min to remove the supernatant. Then, it was resuspended in phosphate buffer saline (PBS) without calcium and magnesium, washed three times, and diluted to a concentration of 1.25×10^8 sperm/mL, The diluted semen was incubated at 37°C for 1 h, followed by centrifugation again (4,000 rpm, 4°C, 5 min) in preparation for the next step of metabolomics analysis. The flowchart of the experimental design is shown in Figure 1.

2.3 Sperm ATP content, ROS levels, and MMP assays

The Enhanced ATP Assay Kit (S0027, Beyotime, China) was used for the analysis. Before the analysis, the thawed semen was diluted to 1.6×10^6 sperm/mL, washed three times with calcium and magnesium-free PBS, and centrifuged at 4000 rpm for 5 min at 4°C each time; after discarding the supernatant, the precipitate was left. After each group was added with 200 μL lysate, repeated blowing was performed to lyse the cells (placed on ice). After lysis, the cells were centrifuged at 4°C 12000 *g*, and the supernatant was taken and used for the determination of subsequent tests. The ATP standard solution was diluted to concentrations of 0.01, 0.03, 0.1, 0.3, 1, and 3 μM using ATP assay solution. The ATP assay reagent was then diluted with the ATP assay reagent diluent at a ratio of 1:4. Next, 100 μL of ATP assay working solution was added to the assay wells and left at room temperature for 3–5 min to allow for the consumption of any background ATP. The

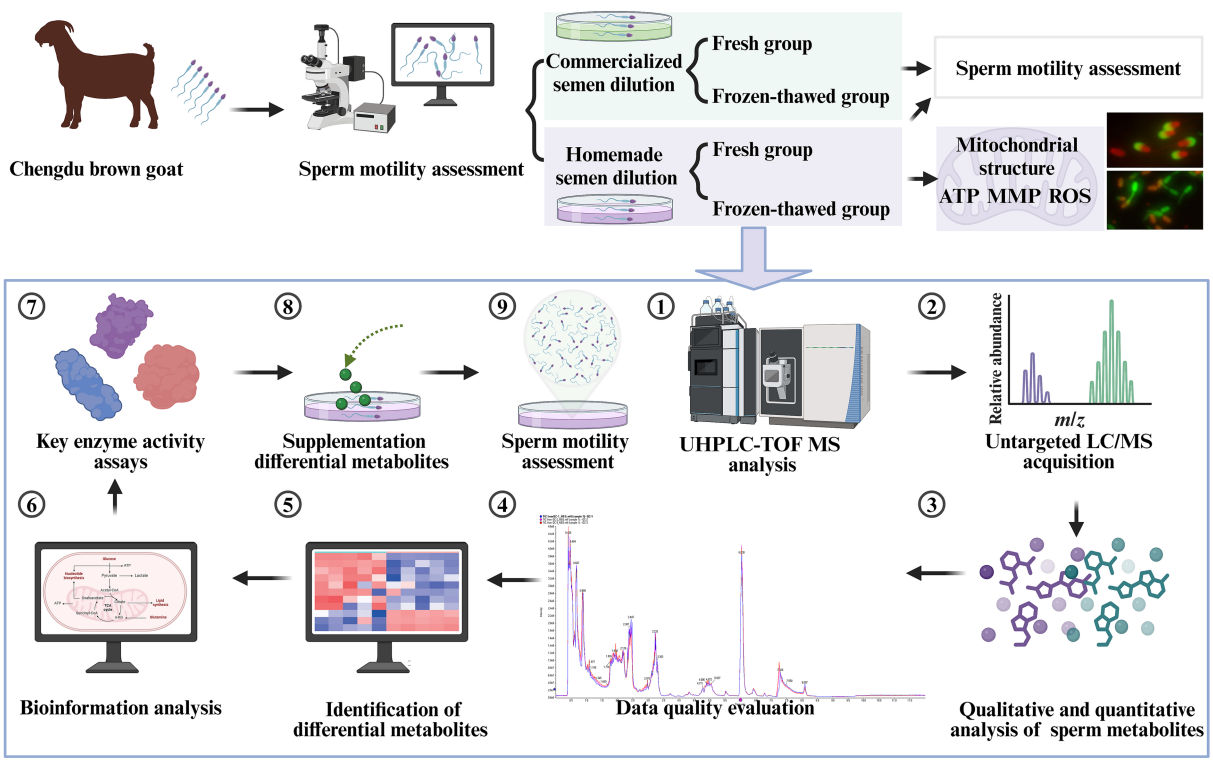

FIGURE 1
Schematic diagram of the experimental design. UHPLC-Q-TOF-MS is an ultra-high performance liquid chromatography quadrupole time-of-flight mass spectrometer (created in BioRender.com).

RLU values were determined using a luminometer (Varioskan LUX, Thermo, USA), and ATP content was calculated.

A volume of 900 μL of fresh semen was injected into a clean EP tube. A volume of 100 μL of Rosup reagent from the reactive oxygen detection kit (CA1410, Solarbio, China) was added to the test tube and then incubated for 20 min at 37°C in an incubator as a positive control sample to be tested. The volume of 2′,7'-Dichlorodihydrofluorescein diacetate (DCFH-DA) working solution (200 μL/tube) was calculated according to the number of samples to be tested, and the DCFH-DA probe was diluted with sterile PBS buffer at a ratio of 1:3000. After that, 200 μL of each semen to be tested was mixed with an equal volume of working solution and then incubated at 37°C for 20 min, during which the samples were inverted several times every 5 min to make full contact between the semen and the probe. Another sample without a probe was set as a blank control. After incubation, the samples were centrifuged (4,000 rpm, 37°C, 5 min), the supernatant was discarded and washed twice with PBS, and 500 μL of PBS was added to the precipitate to be detected by flow cytometry.

Next, 1 mg of JC-1 dry powder (J8030, Solarbio, China) was added to 1 mL of dimethyl sulfoxide (DMSO) and mixed well to form a storage solution. PBS was used for the dilution of JC-1 stock solution to create a final concentration of 250 μg/mL (working solution). An equal volume of semen and working solution was taken and mixed well by gently blowing followed by incubation at 37°C for 20 min and centrifugation (4,000 rpm, 4°C, 5 min). After that, the supernatant was discarded and precipitation was washed twice with PBS (4,000 rpm, 4°C, 5 min), and finally, 600 μL of PBS was added. For the blank control, a sample without JC-1 treatment was used. A Canto II flow cytometer (Becton Dickinson, Franklin Lakes, NJ, USA) was used for the evaluation of samples by setting a total of 10,000 events per sample, and then, data were processed using FlowJo software (Becton Dickinson).

2.4 The ultrastructure analyses of sperm mitochondria, acrosome, and plasma membrane by transmission electron microscopy

Fresh group sperm were centrifuged directly (1,000 rpm, 4°C, 5 min), and the supernatant was discarded. The spermatozoa of the frozen group were thawed and washed three times with calcium and magnesium-free PBS (1,000 rpm, 4°C, 5 min), and the supernatant was discarded after the final time to leave the precipitate. The cells were resuspended by slowly adding 1:5 (3% glutaraldehyde: 0.1 mol/L PBS buffer) diluted fixative along the wall of the tubes with a pipette and left to stand for 5 min at 4°C. High-speed centrifugation (12,000 rpm, 4°C, 10 min) was performed, the supernatant was discarded, and the precipitate was retained. Then, 3% glutaraldehyde fixative (3%, Sinopharm Chemical Reagent Co., Ltd., China) was again added along the wall of the tube (not to be blown out of the cells) and stored at 4°C. The collected samples were fixed, dehydrated, permeabilized, embedded, sectioned, and stained, and then, the mitochondrial ultrastructure of spermatozoa was observed using transmission electron microscopy (JEM-1400FLASH, JEOL, Japan).

2.5 Acrosome integrity and membrane integrity assays

Fluorescein isothiocyanate conjugated peanut agglutinin (FITC-PNA; Sigma, L7381) and propidium iodide (PI) were used to detect sperm acrosome integrity according to the manufacturer's instruction. In brief, after washing three times with PBS, 980 μL of sperm suspension was stained with 20 μL of FITC-PNA stock solution (20 μg/mL) and 5 μL of propidium iodide (PI) stock solution (20 μg/mL) for 25 min in the dark. Aliquots of the stained suspensions were analyzed using the fluorescence microscope.

Membrane integrity was measured using the LIVE/DEAD™ Sperm Viability Kit (L-7011; Thermo Fisher Scientific) according to the manufacturer's instructions. In brief, the goat sperm samples were stained with SYBR-14/PI. The staining was analyzed using fluorescence microscopy with excitation/emission = 485/517 nm for SYBR-14 fluorescence and excitation/emission = 586/617 nm for PI fluorescence. A total of 2,896 sperm were analyzed.

2.6 Metabolomics analysis of goat sperm

The sperm precipitation was followed by thawing at 4°C, and then 800 μL of cold methanol/acetonitrile (1:1) was used to remove proteins and extract metabolites. The mixture was collected into a new centrifuge tube and centrifuged at 14000 *g* for 20 min to collect the supernatant, and then the supernatant was dried in a vacuum. For liquid chromatography–tandem mass spectrometry (LC–MS) analysis, the samples were re-dissolved in 100 μL acetonitrile/water (1:1, v/v) solvent and centrifuged at 14000 *g* at 4°C for 15 min; then the supernatant was injected.

Analysis was performed using ultra-high-performance liquid chromatography (UHPLC) (1,290 Infinity LC, Agilent Technologies; Shanghai Applied Protein Technology Co., Ltd.; Shanghai, China). For hydrophilic interaction liquid chromatography (HILIC) separation, the samples were analyzed using a 2.1 mm × 100 mm ACQUIY UPLC BEH Amide 1.7 μm column (waters, Ireland). In both positive and negative modes of electrospray ionization (ESI), the mobile phase contained 25 mM ammonium acetate +25 mM ammonium hydroxide in water (labeled A) and acetonitrile (labeled B). The gradient was 95% B for 0.5 min, linearly reduced to 65% in 6.5 min, reduced to 40% in 1 min and kept for 1 min, and then increased to 95% in 0.1 min, with a 3-min re-equilibration period employed. Gradients were at a flow rate of 0.5 mL/min, and column temperatures were kept constant at 25°C. A 2 μL aliquot of each sample was injected.

The mass spectrometry analysis was performed using a quadrupole time-of-flight mass spectrometer (Q-TOF) (AB SCIEX TripleTOF 6,600; Shanghai Applied Protein Technology Co., Ltd.; Shanghai, China). The conditions for the ESI source were set as follows: Ion Source Gas 1 and 2 were both set at 60, the curtain gas was set to 30, the source temperature was set to 600°C, and the ion spray voltage floating (ISVF) was set to ±5,500 V. During MS-only acquisition, the instrument was programmed to acquire data over the m/z range of 60–1,000 Da, with an accumulation time of 0.20s/spectrum for TOF MS scans. For auto MS/MS acquisition, the instrument was set to acquire data over the m/z range of

25–1,000 Da, with an accumulation time of 0.05 s/spectrum for production scans. The production scan was obtained using information-dependent acquisition (IDA) with a high-sensitivity mode selected. The parameters for IDA were as follows: The collision energy (CE) was fixed at 35 V with a ± 15 eV range, the declustering potential (DP) was set to 60 V (+) and − 60 V (−), and isotopes within 4 Da were excluded. In addition, 10 candidate ions were monitored per cycle.

2.7 Metabolomics data processing and analysis

Raw MS data were converted to MzXML files using ProteoWizard MSConvert before free import was available in the XCMS software. For peak pickup, the following parameters were used: centWave m/z = 10 ppm; peak width = c (10, 60), and prefilter = c (10, 100). Peak grouping was performed with the following parameters: bw = 5, mzwid = 0.025, and minfrac = 0.5. The Collection of Algorithms of Metabolite Profile Annotation (CAMERA) was used for isotopes and adducts. Only variables with more than 50% non-zero measurements had at least one set of values that remained constant in the extracted ion features. Compound identification accuracy was assessed by comparing the m/z values (<10 ppm) of metabolites and MS/MS spectra with an in-house database (Shanghai Applied Protein Technology), which includes authentic standards for reliable identification.

Statistical analyses were performed, and data normality was assessed using SPSS (v.27.0, IBM, Chicago, IL, USA) with the Shapiro–Wilk test. After normalization, the processed data were analyzed using the R package (ropls), in which processed multivariate data analyses were carried out using overall sample principal component analysis (PCA) and orthogonal partial least squares-discriminant analysis (OPLS-DA) to differentiate the overall differences in metabolic profiles between the groups and to identify the metabolites that differed between the before and after semen freezing in CBG. To prevent model overfitting, we used a 7-fold cross-validation and response alignment test to assess the robustness of the model. Variable importance in the projection (VIP) obtained from the OPLS-DA model can be used to measure the strength and explanatory power of the influence of the expression pattern of each metabolite on the classification and discrimination of each group of samples and to mine biologically significant differential metabolites. Fold multiplicity of variation and VIP > 1, with $p < 0.05$, were used to screen for significantly varying metabolites. Student's *t*-test was applied to determine the significance of differences between fresh and frozen groups. All metabolite identifications were performed using the in-house database (Shanghai Applied Protein Technology).

2.8 Acetyl coenzyme a carboxylase (ACACA), fatty acid synthase (FASN), and carnitine palmitoyltransferase I (CPT-1) activity assays

ACACA activity was measured according to the instructions of the assay kit (KTB1261, Abbkine, China). Briefly, fresh sperm and frozen–thawed goat sperm were washed with pre-cooled PBS. Briefly, frozen–thawed goat sperm were washed three times with pre-cooled PBS to remove extra homemade extender and then centrifuged to discard the supernatant (4,000 rpm, 4°C, 5 min). One milliliter of extraction buffer from the kit was added, and the sperm were broken by ultrasonic waves in an ice bath, with 30 cycles (200 W, ultrasonic waves for 3 s at 7 s intervals for a total time of 5 min). The mixture was then centrifuged (8,000 *g*, 4°C, 10 min), and the supernatant was collected and placed on ice to be measured. Then, the protein concentration of the samples was determined using a BCA protein assay kit (PC0020, Solarbio, China). Detection was carried out via a microplate reader with the wavelength parameter set to 660 nm. The ACACA activity was calculated from the sample protein concentration.

FASN activity was carried out according to the manufacturer's instructions for the assay kit (BC0555, Solarbio, China). In short, 1 mL of the extract from the kit was added to the prepared sperm precipitate, broken by ultrasonic waves in an ice bath, with 30 cycles (power 300 W, ultrasonic waves for 3 s, intervals of 9 s, total time 5 min). The mixture was then centrifuged (12,000 *g*, 4°C, 20 min), and the protein concentration was detected after the supernatant was taken. Detection was performed via a microplate reader with the wavelength parameter set to 340 nm. The FASN activity was calculated according to the sample protein concentration.

CPT-1 activity was assayed according to the kit instructions (ml076617, Shanghai Enzyme-linked Biotechnology Co., Ltd., China). The wavelength setting parameter of the microplate reader was 412 nm. The CPT-1 activity was calculated by sample protein concentration.

2.9 Treatment of goat semen diluent with varying concentrations of capric acid

Different concentrations of capric acid were added to homemade semen diluents I and II, respectively, and divided into the following groups: fresh group and capric acid frozen–thawed group treated with different concentrations (0 μM, 125 μM, 250 μM, 500 μM, and 1,000 μM groups), incubated together at room temperature for 1 h, and then frozen by liquid nitrogen fumigation. Fresh and frozen–thawed groups (0 μM) were used as control groups, after at least 2 weeks of preservation in liquid nitrogen. Then, the motility of thawed sperm was evaluated according to the steps described in Section 2.3 of the Materials and Methods section.

2.10 Statistical analysis

All experiments were repeated at least three times, all raw data were counted and organized using Excel 2019 (Microsoft, USA). Statistical analysis was performed using SPSS (v.27.0, IBM, Chicago, IL, USA). Student's *t*-test was performed to compare the two groups. A one-way analysis of variance (ANOVA) followed by *post-hoc* Fisher's least significant difference (LSD) test was used to compare more than two groups. All data were expressed as mean ± standard error (mean ± SEM). Graphs were made jointly using GraphPad Prism (v.5.0, GraphPad Software LLC, USA) and Adobe Illustrator 2020 (Adobe Inc., USA). A *p*-value of < 0.05 indicates a statistical difference.

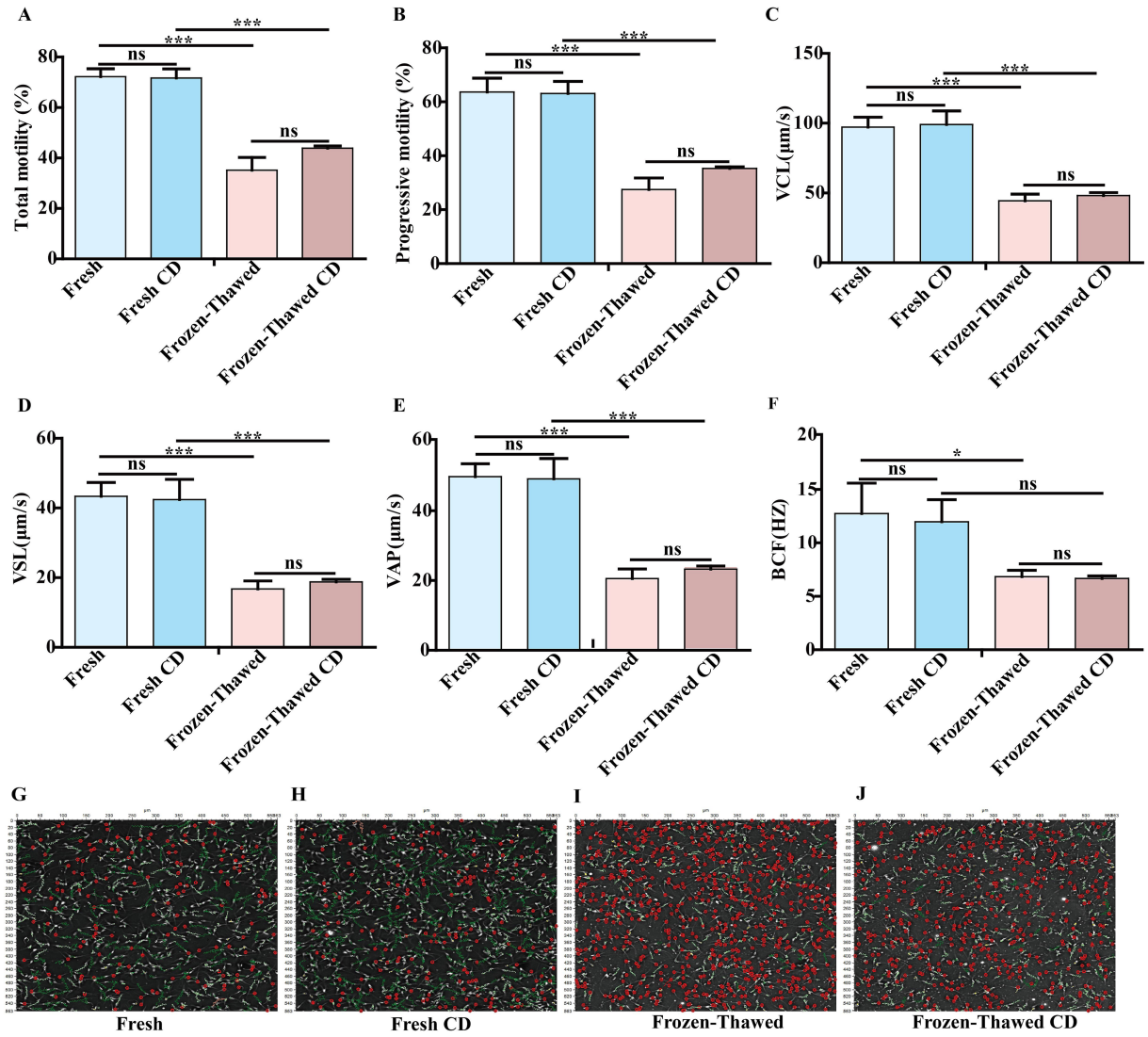

FIGURE 2
Comparison of the effect of homemade dilutions and commercial dilutions (CD) on goat semen freezing. **(A)** Total motility. **(B)** Progressive motility. **(C)** Velocity of trajectory curve (VCL; μm/s). **(D)** Velocity of straight line (VSL; μm/s). **(E)** Velocity of average path (VAP; μm/s) **(F)** Beat cross-frequency (BCF; HZ). Sperm movement trajectories of the fresh group: **(G)** The fresh group of homemade diluents is indicated by Fresh. **(H)** The fresh group of CD is indicated by Fresh CD. Movement trajectories of frozen–thawed spermatozoa: **(I)** The frozen group with homemade diluents is indicated by Frozen–thawed. **(J)** The frozen group with CD is indicated by Frozen–thawed CD. Orange trajectory: circular motion; dark green trajectory: fast motion; bright green motion trajectory: slow motion; yellow motion trajectory: *in situ* motion; red circle: inactive. Asterisks indicate $p < 0.05$ (*) and $p < 0.001$ (***), and "ns" indicates a non-significant difference.

3 Results

3.1 Reduced motility of goat sperm following cryopreservation

After ultra-low temperature freezing, the total motility (72.21 ± 3.14% vs. 35.15 ± 5.05%, Figure 2A), progressive motility (63.65 ± 5.13% vs. 27.49 ± 4.31%, Figure 2B), VCL (97.16 ± 7.21 vs. 44.45 ± 4.77%, Figure 2C), VSL (43.36 ± 3.99 vs. 16.77 ± 2.30, Figure 2D), VAP (49.75 ± 3.73 vs. 20.57 ± 2.74, Figure 2E), and BCF (12.74 ± 2.86 vs. 6.85 ± 0.60, Figure 2F) of goat sperm were significantly reduced compared to the fresh group when using homemade dilutions ($p < 0.05$). Similarly, when a commercial diluent was used, the total motility (71.73 ± 3.59% vs. 43.91 ± 0.87%, Figure 2A), progressive motility (63.12 ± 4.48% vs. 35.30 ± 0.58%, Figure 2B), VCL (99.11 ± 9.73 vs. 48.13 ± 2.18, Figure 2C), VSL (42.44 ± 5.78 vs. 18.77 ± 0.76, Figure 2D), and VAP (49.14 ± 5.81 vs. 23.29 ± 0.91, Figure 2E) of goat sperm showed significant decrease after ultra-low temperature freezing compared to the fresh group ($p < 0.05$). However, there was no significant difference in BCF (11.97 ± 2.07 vs. 6.67 ± 0.35, Figure 2F) ($p > 0.05$). Furthermore, an analysis of the movement trajectories of fresh sperm diluted with homemade and commercial diluent showed no significant differences (Fresh vs. Fresh CD) (Figures 2G,H). Similarly, when sperm was diluted with homemade and commercial diluent before cryopreservation, there were also no significant differences in the movement trajectories for frozen-thawed sperm (Frozen-thawed vs. Frozen-thawed CD) (Figures 2I,J). These findings suggest both our homemade diluent and the commercial diluent can be used interchangeably for treating and freezing CBG semen without affecting sperm motility or other parameters in either

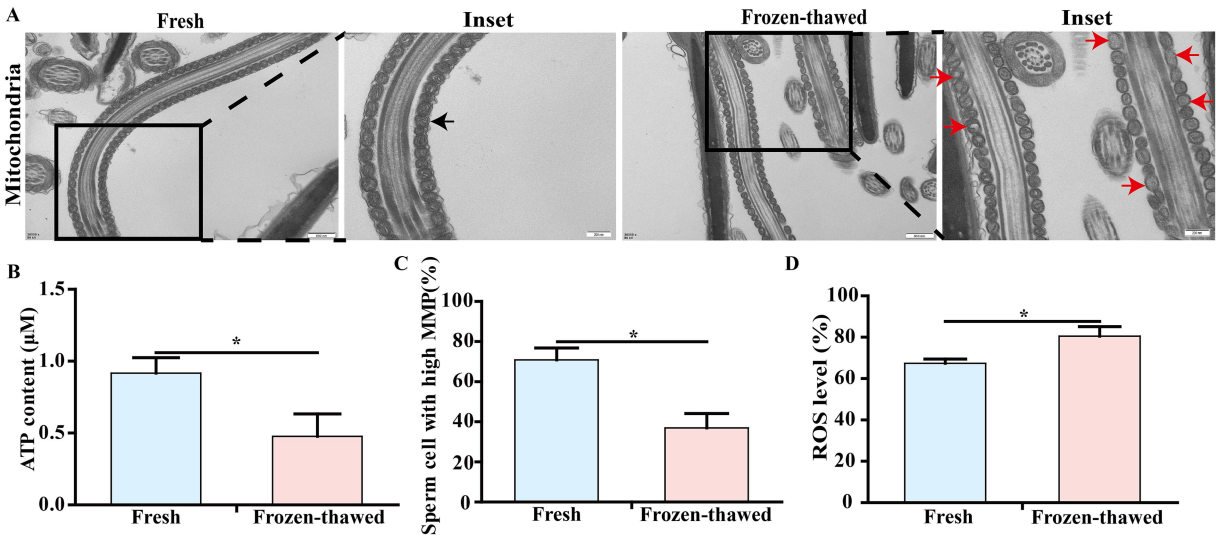

FIGURE 3
Effects of cryopreservation on the ultrastructure and ATP content of mitochondria, mitochondrial membrane potential (MMP), and ROS level in sperm of goat. **(A)** Transmission electron microscopy of sperm mitochondria, scale bar = 500 nm; local magnification scale bar = 200 nm; black arrows represent normal mitochondrial structure; red arrows represent mitochondrial structural vesicles destroyed, vacuoles, or mitochondrial matrix density reduced. **(B)** ATP content assay. **(C)** MMP assay. **(D)** ROS level assay. '*' indicates statistical differences, $p < 0.05$.

the fresh or frozen–thawed groups (Figures 2A,B) ($p > 0.05$). Considering factors such as timeliness and cost, we chose to use our homemade diluent for subsequent experiments.

3.2 The cryogenic freezing process induces structural and functional impairments in the mitochondrial of goat sperm

Since mitochondria are closely associated with sperm viability, we subsequently investigated the mitochondrial ultrastructure and function of sperm. Our findings revealed that frozen CBG sperm exhibited vacuolization in the mitochondrial vesicles, as well as a reduction in the density of the mitochondrial matrix (Figure 3A), indicating impaired mitochondrial ultrastructure. Following ultra-low temperature freezing, there was a significant decrease in ATP content (0.92 ± 0.11 vs. 0.40 ± 0.17, Figure 3B), high-MMP ratio (70.83 ± 5.97% vs. 36.97 ± 7.13%, Figure 3C), and ROS level (67.37 ± 1.22% vs. 80.57 ± 2.64%, Figure 3D) of sperm compared to the fresh group ($p < 0.05$).

3.3 Cryopreservation compromises acrosome integrity and membrane integrity of goat sperm

To elucidate the effect of cryopreservation on the integrity of the acrosome and plasma membrane of goat sperm, we observed the ultrastructure of the sperm acrosome and plasma membrane using transmission electron microscopy, respectively. The results showed that sperm exhibited acrosomal detachment and plasma membrane damage after freezing (Figure 4A). In addition, we reassessed the sperm acrosome and plasma membrane integrity by fluorescence staining that showed a significant decrease in acrosomal integrity of sperm (40.27 ± 0.99% vs. 52.41 ± 1.11%, $p < 0.01$) (Figures 4B,D) and the integrity of sperm plasma membrane (50.62 ± 4.56% vs. 69.04 ± 2.71%, $p < 0.05$) (Figures 4C,E), respectively, in frozen–thawed group compared to the fresh group.

3.4 Metabolomic analysis of goat sperm pre- and post-cryopreservation

To further evaluate the impact of cryopreservation-induced mitochondrial damage on mitochondrial metabolism, we performed untargeted metabolomics analysis on pre- and post-freezing sperm samples. Our findings demonstrated a clear distinction in metabolite profiles between the fresh and frozen groups (Figures 5A–D), with validation provided by PLS-DA and OPLS-DA analysis models (Tables 1, 2). In total, we identified a total of 1,384 metabolites in goat sperm samples before and after freezing (772 in positive ion mode and 612 in negative ion mode). These metabolites were categorized based on their chemical composition into lipids and lipid-like molecules (30.708%), organic acids and derivatives (20.014%), undefined metabolites (12.283%), organoheterocyclic compounds (9.682%), and organic oxygen compounds (9.538%) (Figure 5E).

Based on the univariate analysis of the variance method, significant differences were observed in the metabolites of frozen and thawed goat sperm (FC > 1.5 or FC < 0.67, $p < 0.05$). The predominant differential metabolites were identified as lipids and lipid-like molecules (Figures 6A,B). Out of the 342 differential metabolites identified (OPLS-DA VIP > 1, $p < 0.05$), 246 were upregulated and 96 were downregulated (Figure 6C). The Kyoto Encyclopedia of Genes and Genomes (KEGG) pathway analysis revealed that these differential metabolites were mainly enriched in nine metabolic pathways: β-oxidation of very long-chain fatty acids, fatty acid biosynthesis, glutamate metabolism, steroidogenesis, arginine and proline metabolism, ketone body metabolism, spermidine and spermine biosynthesis, mitochondrial electron transport chain, and butyrate metabolism (Figure 6D). These nine KEGG metabolic pathways can

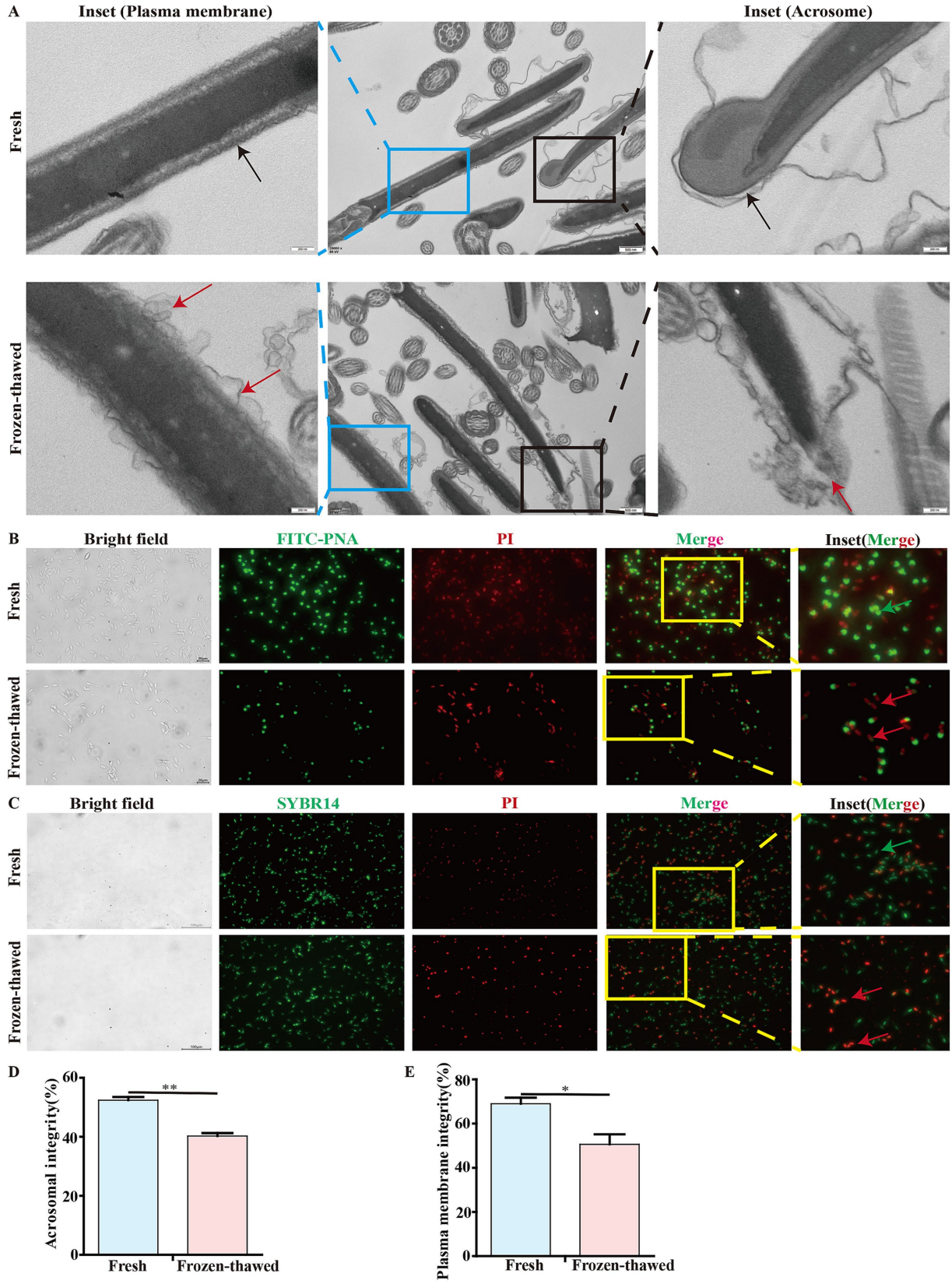

FIGURE 4
Effect of cryopreservation on the acrosome integrity and membrane integrity of goat sperm. **(A)** Detection of the ultrastructure of sperm plasma membrane and acrosome by transmission electron microscopy. The black box indicates the acrosome, and the blue box indicates the plasma membrane. In these two enlarged images, the black arrows represent the integrity of the acrosome and the integrity of the plasma membrane,

(Continued)

FIGURE 4 (Continued)
respectively; the red arrows indicate the detachment of the acrosome and the damage to the plasma membrane, respectively. Scale bar = 500 nm; local magnification scale bar = 200 nm. **(B,C)** Detection of acrosome integrity and plasma membrane integrity of goat sperm using FITC-PNA/PI and SBYR14/PI fluorescent staining methods. The yellow box indicates the area selected for enlargement. In the detection of acrosome integrity, scale bar = 20 μm. In the detection of the plasma membrane, scale bar = 100 μm. In these two enlarged images, the green arrows represent sperm with intact acrosomes and plasma membranes, respectively, while the red arrows represent sperm with acrosome loss or damage and plasma membrane injury, respectively. **(D,E)** The bar chart represents the statistical analysis of the percentage of fluorescent staining results for sperm acrosome integrity and membrane integrity. Asterisks indicate $p < 0.05$ (*) and $p < 0.01$ (**).

be classified into two categories based on their relevance to freeze-thawed sperm quality (Figure 6E): energy-related metabolites such as capric acid (Figure 7A), glucosamine-6-phosphate (Figure 7B), malonyl-L-carnitine (Figure 7C), creatine (Figure 7J), creatinine (Figure 7K), and antioxidant-related metabolites such as cholesterol sulfate (Figure 6D), probucol (Figure 7E), and saikosaponin A (Figure 7F) showed a significant decrease, while succinate (Figure 7G), cholesterol (Figure 7H), and phytosphingosine (Figure 7I) exhibited a significant upregulation pattern within other categories. Furthermore, our literature review indicated that creatine is highly expressed in sperm cells, with its synthesis and degradation primarily occurring through spontaneous, non-enzymatic processes (29). Within the cell, ATP, adenosine diphosphate (ADP), creatine, and phosphocreatine must diffuse or be transported through the cell membrane for high-energy phosphate transfer between mitochondria and ATP utilization sites (30). Therefore, the downregulated expression of creatinine and creatine in frozen spermatozoa has negative effects on creatine metabolism (Figure 7L).

3.5 Abnormal fluctuations of key rate-limiting enzyme activities in fatty acid biosynthesis and β-oxidation metabolism pathways after sperm cryopreservation

Among the nine metabolic pathways observed in metabolomic analysis, fatty acid biosynthesis and β-oxidation metabolism play crucial roles in sperm energy production (31, 32). Consequently, we conducted further analysis of the activities of the key rate-limiting enzymes ACACA, FASN, and CPT-1 in these metabolic pathways. The activities of ACACA (0.68 ± 0.07 vs. 0.41 ± 0.05, $p < 0.01$) (Figure 8A), FASN (20.57 ± 1.12 vs. 8.46 ± 0.66, $p < 0.01$) (Figure 8B), and CPT-1 (13.32 ± 2.77 vs. 0.81 ± 0.37, $p < 0.05$) (Figure 8C) were significantly lower compared to those of fresh controls.

3.6 Capric acid can improve the motility of goat frozen–thawed sperm

Considering that the differentially expressed metabolite capric acid significantly decreased in frozen–thawed sperm and was enriched in the fatty acid synthesis metabolic pathway (Figure 7A), we investigated the effects of various concentrations of capric acid on the motility of frozen–thawed sperm. The results showed that compared to the fresh group, the total motility (85.80 ± 2.51 vs. 34.80 ± 2.29, $p < 0.001$) (Figure 8D) and progressive motility (76.23 ± 0.91 vs. 26.77 ± 3.12, $p < 0.001$) (Figure 8E) of sperm significantly decreased after freezing–thawing, while the addition of 500 μM capric acid significantly improved the total motility (63.40 ± 2.67 vs. 34.80 ± 2.29, $p < 0.001$) (Figure 8D) and progressive motility (52.47 ± 2.62 vs. 26.77 ± 3.12, $p < 0.001$) (Figure 8E) of goat sperm after cryopreservation.

4 Discussion

In this study, we initially found that the freezing process resulted in an extremely significant decrease in sperm motility (Figures 2A,B). Furthermore, it was observed that the mitochondrial ultrastructure was impaired following sperm freezing in CBG (Figure 3A). In addition, there was a reduction in ATP content and MMP, accompanied by a significant increase in ROS levels (Figures 3B–D). These findings are consistent with previous studies on mammalian species such as humans (24), pigs (33), horses (34), bulls (35, 36), and sheep (8). This suggests that the detrimental effects of ultra-low temperature freezing on sperm viability are universal across different animal species. Furthermore, it is widely accepted that excessive production of ROS during the freezing process induces oxidative stress (21, 37), which subsequently leads to decreased sperm viability (38). Recent studies have demonstrated that there were two principal sources of intracellular ROS in sperm: one originating from the mitochondria and the other from the plasma membrane (39, 40). ADPH oxidase presented in sperm plasma membrane could be responsible for ROS generation during sperm capacitation (41). The results of our study demonstrated that following the freezing and thawing of the sperm, plasma membrane damage and capacitation-like (cryo-capacitation) changes were observed (Figures 4A–C), as evidenced by complete acrosome detachment or leakage of acrosomal enzymes, similar to natural capacitation, which affect the fertility potential of frozen–thawed sperm.

Given the critical role of sperm mitochondria in energy production and metabolic regulation, we hypothesized that mitochondrial dysfunction may result in disturbances in mitochondrial energy metabolism, which in turn affects the motility of frozen–thawed sperm. To test this hypothesis, we employed metabolomics to explore metabolic profiles of goat freeze-thawed sperm. Previous studies have demonstrated that the differential metabolites between fresh and frozen–thawed semen groups in Dorper sheep include linoleic acid, docosahexaenoic acid, and arachidonic acid, which primarily affect the metabolic pathway of unsaturated fatty acid biosynthesis (25). In Yunshang black goat sperm before and after freezing, the differential metabolites include mannitol, capric acid, and gamma-linolenic acid, which significantly impact the linoleic acid metabolic pathway (27). In Guanzhong dairy goat sperm before and after freezing, sphingolipids, betaine, and choline have been identified as differential metabolites that affect the metabolic pathways of the TCA cycle, unsaturated fatty acids biosynthesis, and

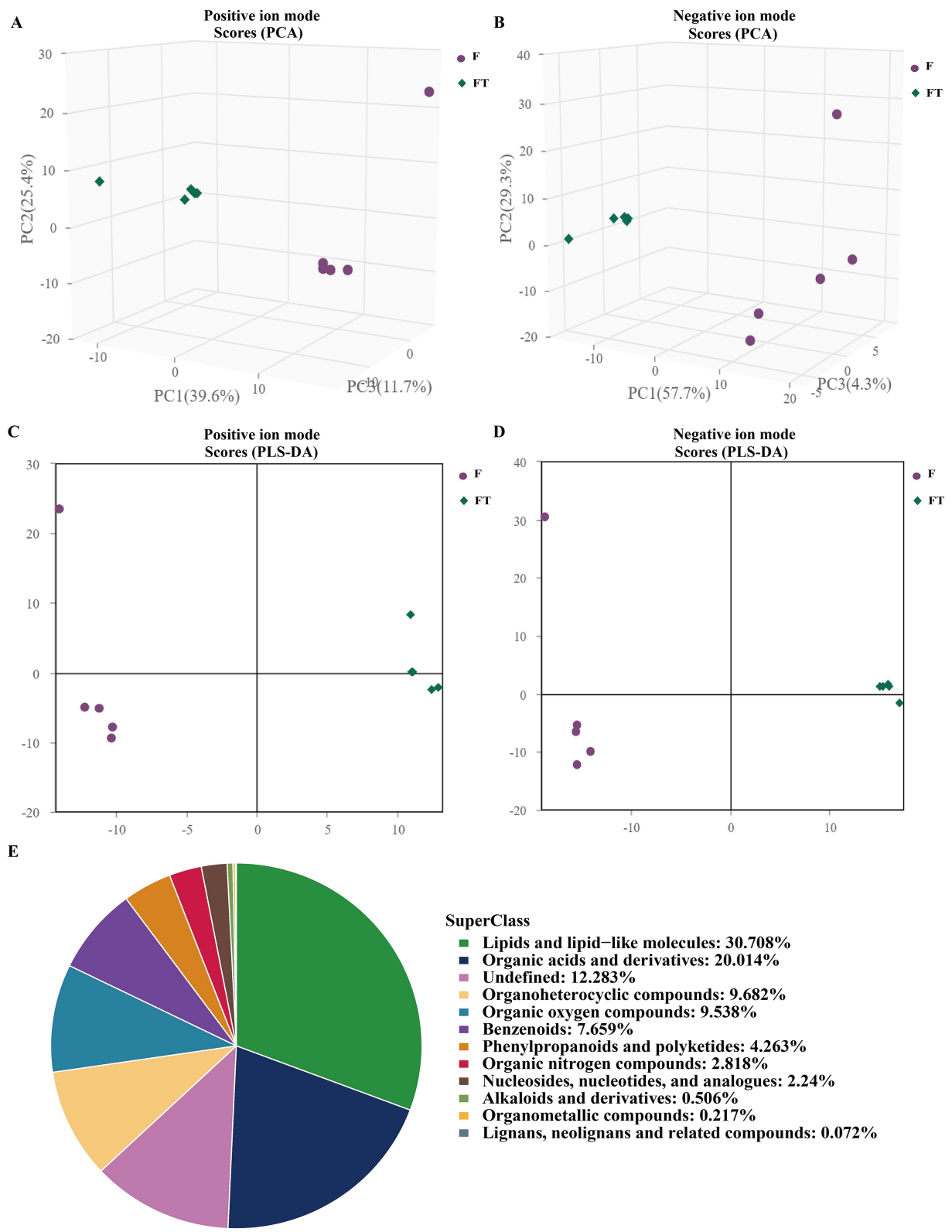

FIGURE 5
Graphs of multivariate statistical analyses and chemical classification of metabolites identified in goat sperm. **(A,B)** Graphs of PCA scores in positive and negative ion modes. **(C,D)** Graphs of PLS-DA scores in positive and negative ion modes. **(E)** Chemical classification of identified metabolites. (1) The horizontal coordinate t[1] in the graph represents principal component 1, and the vertical coordinate t[2] represents principal component. (2) The dots of the same color indicate the individual biological replicates within the group, and the distribution status of the dots reflects the degree of inter- and intra-group variability.

TABLE 1 PLS-DA validity.

Sample groups	Ion mode	A	R^2X(cum)	R^2Y(cum)	Q^2(cum)
FT vs. F	Positive	1	0.646	0.997	0.971
	Negative	1	0.87	0.999	0.994

A: denotes the main score.
R^2X: denotes the explanation rate of the model to the X variable.
R^2Y: denotes the explanation rate of the model to the Y variable.
Q^2: denotes the predictive ability of the model.

TABLE 2 OPLS-DA validity.

Sample groups	Ion mode	A	R^2X(cum)	R^2Y(cum)	Q^2(cum)
FT vs. F	Positive	1	0.646	0.997	0.996
	Negative	1	0.87	0.999	0.997

A: denotes the main score.
R^2X: denotes the explanation rate of the model to the X variable.
R^2Y: denotes the explanation rate of the model to the Y variable.
Q^2: denotes the predictive ability of the model.

sphingolipid metabolism (28). Bull sperm before and after freezing exhibit glycine betaine and pyro-l-glutaminyl-l-glutamine as differential metabolites (26). Our study reveals that the differential metabolites of CBG sperm before and after freezing can be categorized into two main groups: one associated with energy metabolism (capric acid, creatine, and D-glucosamine-6-phosphate), and the other related to the antioxidant activity (saikosaponin A, probucol, and cholesterol sulfate) (Figure 6E). These metabolites predominantly influence fatty acid oxidation and biosynthesis (Figure 6D). It is evident that the changes in differential metabolites along with affected pathways due to ultra-low-temperature freezing negatively impact normal energy metabolism of sperm across different species.

In this study, freezing significantly decreased the activity of ACACA, FASN, and CPT-1 in goat sperm (Figures 8A–C). ACACA catalyzes the conversion of acetyl-CoA to malonyl-CoA (42); FASN is a pivotal enzyme in the endogenous lipogenesis pathway primarily responsible for synthesizing long-chain saturated FA palmitate from acetyl-CoA and malonyl-CoA (43–45), while CPT1 acts as a crucial enzyme initiating the transport of free fatty acids to the mitochondria (31). These three key enzymes play essential roles in fatty acid metabolism (31, 46–48), which generates ATP within the mitochondria to facilitate linear sperm movement (32, 49). Consequently, reduced activity of these three enzymes due to ultra-low temperature freezing undoubtedly impairs sperm motility.

In this study, the expression of antioxidant-related differential metabolites such as saikosaponin A, probucol, and cholesterol sulfate in frozen–thawed sperm was significantly downregulated (Figures 7D–F). Saikosaponin A not only inhibits the overaccumulation of ROS by increasing the activity of antioxidant enzymes but also suppresses inflammation and iron-induced cell death through the PI3K/Akt/Nrf2 pathway (50) or activates the SIRT1/Nrf2 pathway to mitigate oxidative stress in cells (51). Furthermore, it has been demonstrated that saikosaponin A has the capacity to alleviate lipid metabolism disorders in rat liver by stimulating the expression of intracellular lipid and cholesterol catabolism-related genes, including peroxisome proliferator-activated receptor α (PPARα), and cholesterol 7α-hydroxylase-1 (CYP7a1) (52, 53). On the other hand, probucol protects cells from peroxide-induced damage directly by activating glutathione peroxidase-1 (54), while cholesterol sulfate enhances resistance against oxidative stress by increasing ATP, lipid, and glycogen content (55). Cholesterol sulfate is a component of cell membranes and has been demonstrated to exert a stabilizing effect, as well as to regulate sperm capacitation (56). Furthermore, it has been demonstrated that it regulates brain energy metabolism through the activation of the Akt/Bcl2 pathway, which reduces the production of ROS, thereby providing neuroprotection (55). Therefore, the decrease in these differential antioxidant-related metabolites after semen freezing in CBG leads to an imbalance in the sperm's antioxidant system through their respective pathways mentioned above. Consequently, this exacerbates oxidative stress and affects sperm viability (23, 57).

In this study, D-glucosamine-6-phosphate, creatine, and capric acid metabolites associated with energy metabolism exhibited significant downregulation following sperm freezing in goats (Figures 7A,B,J). The diminished metabolites may exert an influence on the synthesis of ATP, which in turn affects the viability of sperm. It has been demonstrated that D-glucosamine-6-phosphate serves as an energy source in the form of phosphosugars (58), while creatine can efficiently generate ATP by connecting ATP-producing sites to subcellular sites of ATP utilization through the creatine/phosphocreatine shuttle system (30). It was reported that SH-SY5Y cells exposed to capric acid for a period of 6 days were demonstrated to have increased activities in several mitochondrial markers, including the activities of citrate synthase and mitochondrial respiratory chain complex I (59). It is also noteworthy that capric acid exposure not only elevates acyl-CoA oxidase 1 activity but also enhances peroxisomal β-oxidation of docosanoic acid (60). Furthermore, it has been demonstrated that capric acid can mitigate the oxidative stress induced by cyclophosphamide in IPEC-J2 cells (61). Numerous studies have indicated that capric acid is a potent antioxidant that elicits antioxidant responses through the activation of the Nrf2/ERK1/2 pathway (62–64). Concurrently, capric acid serves as an energy source for brain cells by stimulating glycolysis, which results in the production of lactic acid (65). In this study, we found that the differential metabolite capric acid enriched in goat sperm is involved in the fatty acid synthesis pathway. When 500 μM capric acid was added to the homemade freezing diluent, the motility of cryopreserved goat sperm increased (Figures 8D,E), suggesting that supplemented capric acid may promote ATP production through the above pathway (60), thereby alleviating the decrease in sperm viability induced by freezing.

5 Conclusion

Following ultra-low temperature freezing, goat sperm exhibited compromised ultrastructure, disturbed energy metabolism (downregulation of capric acid, D-glucosamine-6-phosphate, and creatine), and antioxidant imbalance (downregulation of

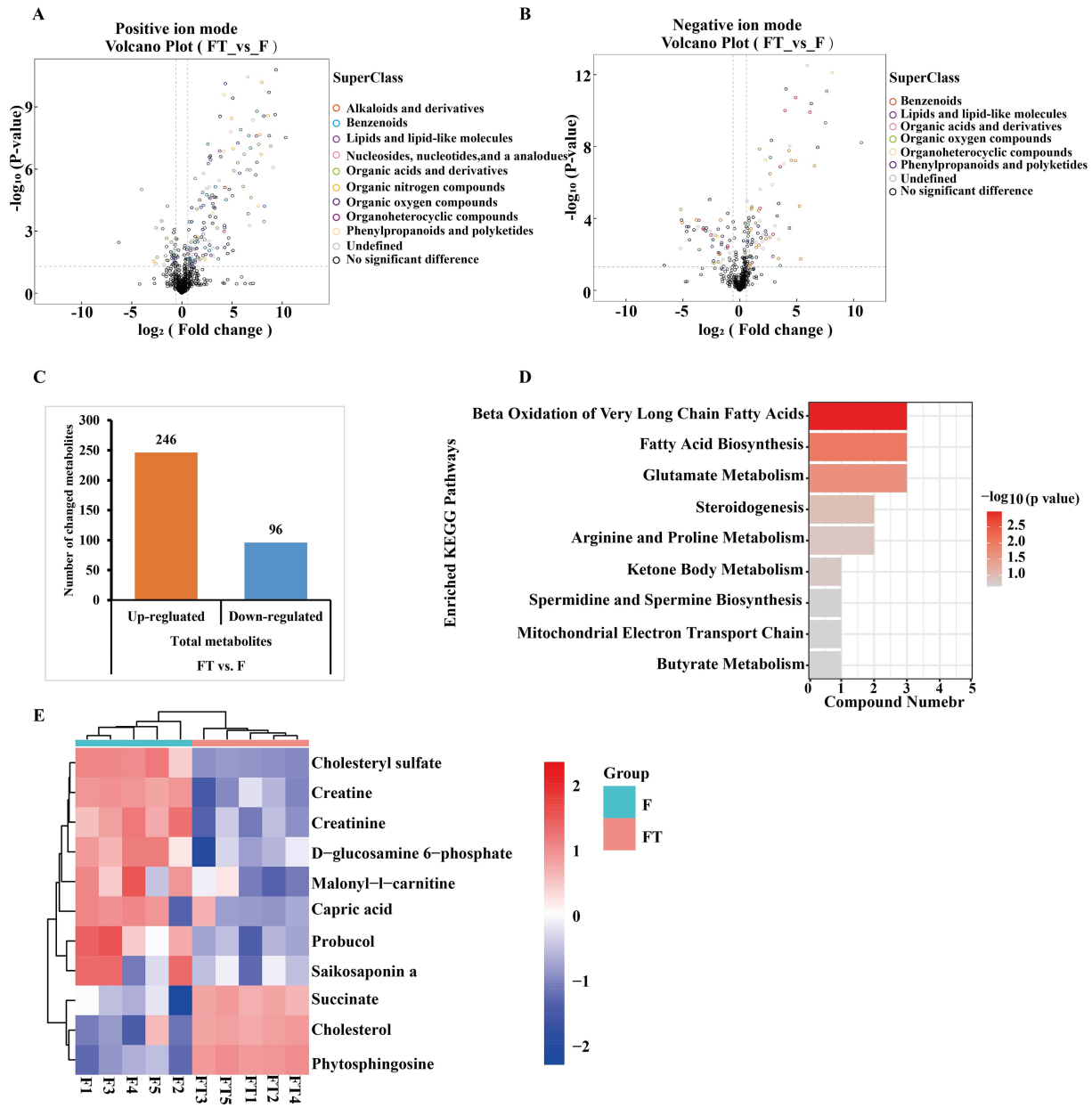

FIGURE 6
Differential metabolite identification and KEGG pathway enrichment analysis before and after goat sperm freezing. **(A,B)** Positive and negative ion pattern differential metabolite volcano plots. Different colors represent different chemical classifications. **(C)** Total number of differential metabolites identified. Each bar line represents the total number of significant differential metabolites, with orange representing upregulated metabolites and blue representing downregulated metabolites. **(D)** KEGG enrichment pathway map. The vertical axis in the bar graph represents each KEGG metabolic pathway, and the horizontal axis indicates the number of differentially expressed metabolites contained in each KEGG metabolic pathway. The color indicates the *p*-value of enrichment analysis, the darker the color, the smaller the *p*-value and the more significant the enrichment. **(E)** Heatmap of KEGG pathway differential metabolite clustering. FT represents frozen–thawed sperm, and F represents fresh sperm. Each row of the graph represents a differential metabolite (i.e., the vertical coordinate is the significantly differentially expressed metabolite), and each column represents a set of samples (i.e., the horizontal coordinate is the sample information). The color blocks at different positions represent the relative expression of the metabolites at the corresponding positions, red represents relatively high expression, blue represents relatively low expression, and metabolites with close expression patterns are clustered under the same cluster on the left.

saikosaponin A, probucol, and cholesterol sulfate). Moreover, key enzymes involved in the synthesis of long-chain fatty acids and β-oxidation metabolism pathways in the sperm (FASN, ACACA, and CPT-1) demonstrated reduced activity, resulting in abnormal mitochondrial function and decreased sperm motility. Exogenous supplementation of the metabolic intermediate capric acid (500 μM) significantly enhanced the motility of frozen–thawed goat sperm (Figure 9).

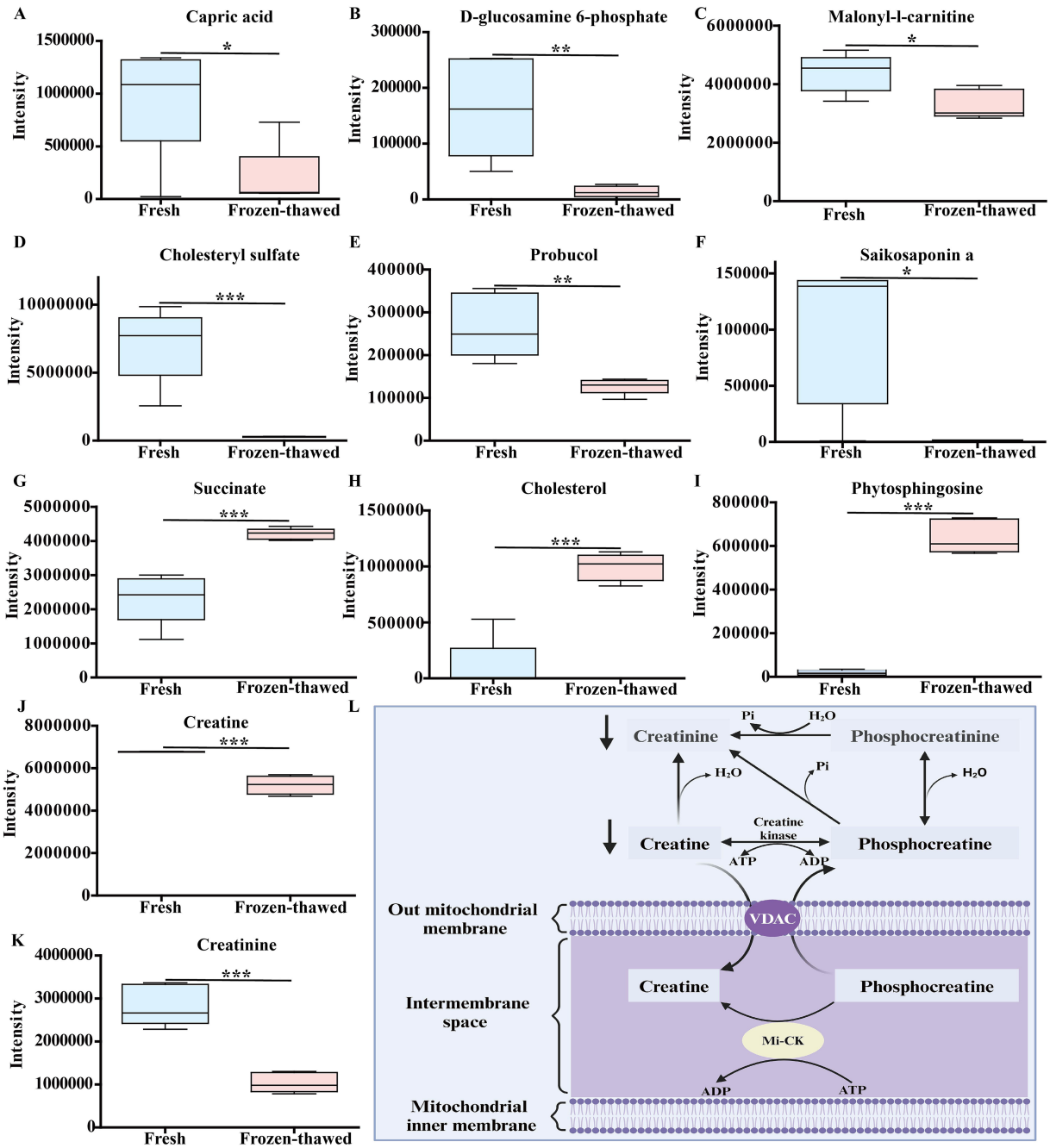

FIGURE 7
Differences in metabolic profiles between fresh and frozen–thawed sperm. **(A–K)** Metabolomics-based comparative analysis of changes in sperm differential metabolites before and after freezing. The fresh group is labeled in blue and the frozen group in pink, and asterisks indicate $p < 0.05$ (*), $p < 0.01$ (**), and $p < 0.001$ (***). **(L)** Schematic diagram of the relationship between creatinine, creatine, and mitochondrial energy metabolism, where creatinine and water reversibly produce creatine, which dissipates that energy ATP turnover by stimulating the cycling of energy stored in the inner membrane of the mitochondria, mediated by mitochondrial creatine kinase and coupled with the turnover of phosphocreatine (created in Biorender.com). Mitochondrial creatine kinase (Mi-CK); voltage-dependent anion channel (VDAC).

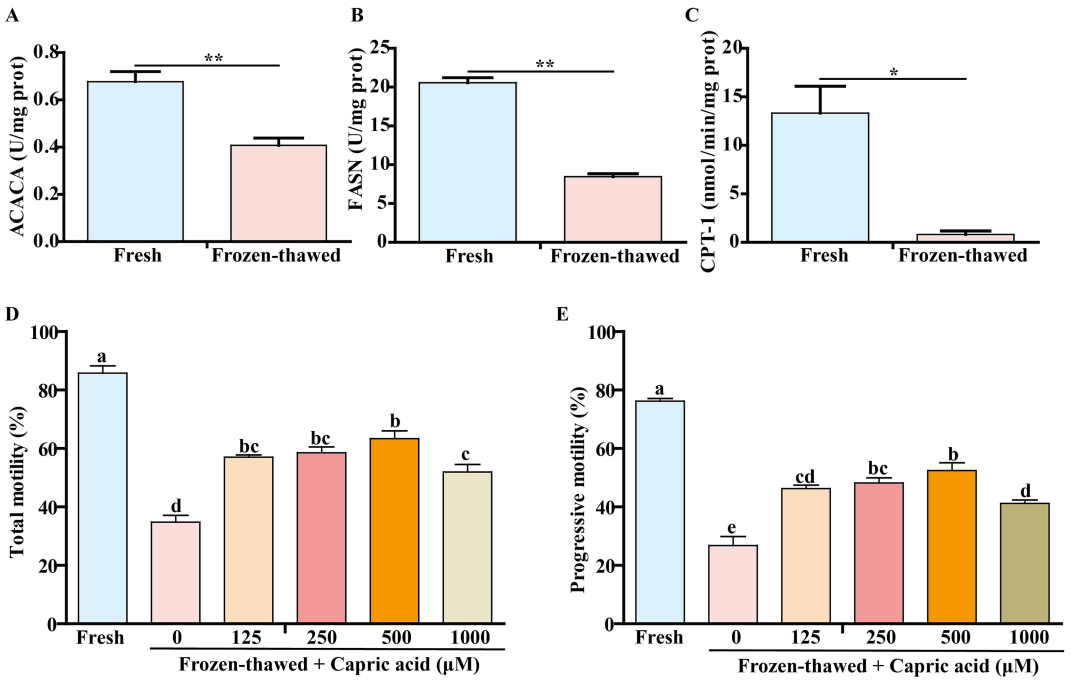

FIGURE 8
Changes in the activities of key rate-limiting enzymes of metabolic pathways in frozen–thawed sperm and the effect of capric acid on the motility of frozen–thawed sperm. **(A–C)** Changes in ACACA, FASN, and CPT-1 activity before and after sperm freezing. $p < 0.05$ (*) and $p < 0.01$ (**). Effect of adding different concentrations of capric acid to the homemade freezing diluent on the motility of frozen–thawed sperm. **(D)** Total motility. **(E)** Progressive motility. [a–e] Within a panel, means without a common superscript differed ($p < 0.05$).

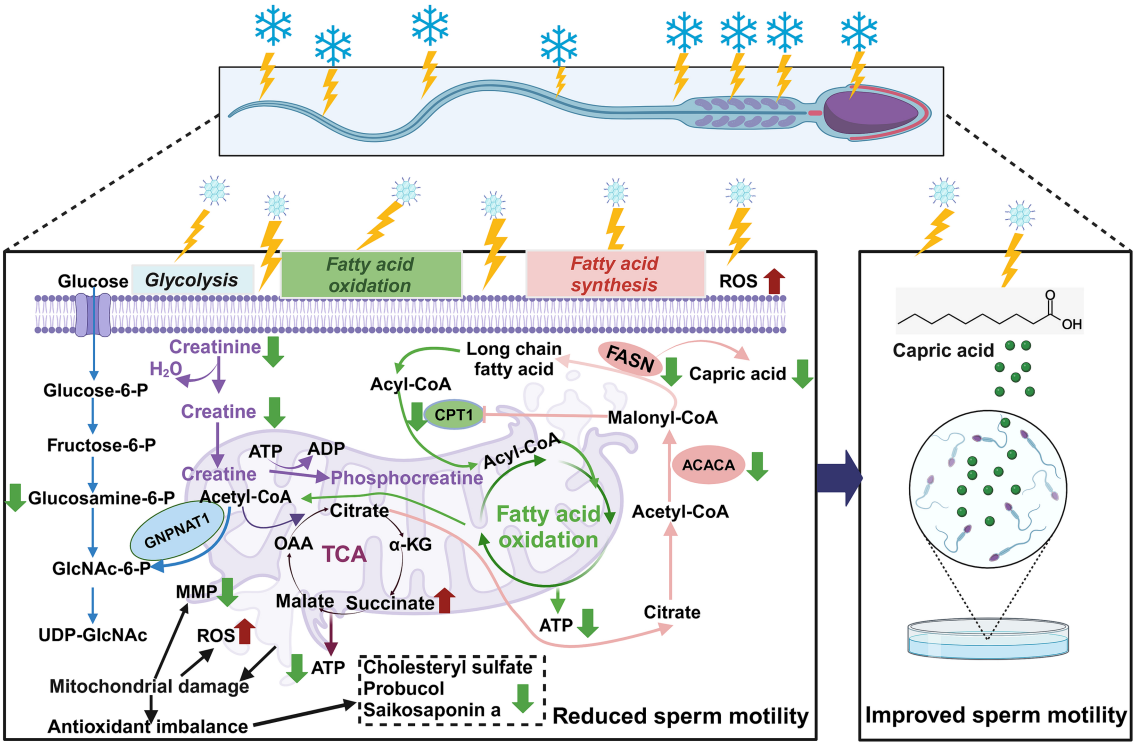

FIGURE 9
Metabolomics-based analysis of the effects of ultra-low temperature freezing on mitochondrial energy metabolism in goat sperm. Red arrows indicate increases; green arrows indicate decreases. Reactive oxygen species (ROS); mitochondrial membrane potential (MMP); tricarboxylic acid cycle (TCA); adenosine triphosphate (ATP); α-ketoglutarate (α-KG); oxaloacetate (OAA); carnitine palmitoyltransferase I (CPT-1); acetyl coenzyme A carboxylase (ACACA); fatty acid synthase (FASN); CPT-1 can be directly inhibited by ACACA direct inhibition by ACACA-produced malonyl coenzyme A. Malonyl coenzyme A is a key intermediate in fatty acid synthesis (FAS) that prevents simultaneous activation of FAS and fatty acid oxidation (FAO) (created in BioRender.com).

Data availability statement

The raw data supporting the conclusions of this article will be made available by the authors, without undue reservation.

Ethics statement

The animal study was approved by the Animal Ethics and Welfare Committee (AEWC) of Sichuan Agricultural University, China (Approval code: AEWC2016, January 6, 2016). The study was conducted in accordance with the local legislation and institutional requirements.

Author contributions

SZa: Data curation, Formal analysis, Investigation, Methodology, Validation, Visualization, Writing – original draft, Writing – review & editing. SZo: Data curation, Formal analysis, Investigation, Validation, Writing – original draft. XC: Investigation, Writing – original draft, Validation. BP: Writing – review & editing. AN: Investigation, Validation, Writing – original draft. JQ: Formal analysis, Methodology, Writing – original draft. YW: Investigation, Validation, Writing – original draft. KD: Investigation, Validation, Writing – original draft. JY: Project administration, Writing – original draft. QL: Writing – review & editing. YF: Formal analysis, Writing – review & editing. Qiongla: Investigation, Validation, Writing – original draft. Cirenlamu: Investigation, Validation, Writing – original draft. TS: Conceptualization, Funding acquisition, Resources, Supervision, Writing – review & editing. GZ: Conceptualization, Funding acquisition, Investigation, Methodology, Project administration, Resources, Supervision, Writing – original draft, Writing – review & editing.

Funding

The author(s) declare that financial support was received for the research, authorship, and/or publication of this article. This study was supported by the (Shigatse) Regional Science and Technology Collaborative Innovation Special Project (QYXTZX-RKZ2023-06).

Acknowledgments

The authors express their gratitude for the support and collaboration of the technical and farm staff at Xilingxue Agricultural Development Co., Ltd. in Chengdu, Sichuan Province, China.

Conflict of interest

The authors declare that the research was conducted in the absence of any commercial or financial relationships that could be construed as a potential conflict of interest.

Generative AI statement

The authors declare that no Gen AI was used in the creation of this manuscript.

Publisher's note

All claims expressed in this article are solely those of the authors and do not necessarily represent those of their affiliated organizations, or those of the publisher, the editors and the reviewers. Any product that may be evaluated in this article, or claim that may be made by its manufacturer, is not guaranteed or endorsed by the publisher.

References

1. Peris-Frau P, Soler AJ, Iniesta-Cuerda M, Martín-Maestro A, Sánchez-Ajofrín I, Medina-Chávez D, et al. Sperm cryodamage in ruminants: understanding the molecular changes induced by the cryopreservation process to optimize sperm quality. *Int J Mol Sci*. (2020) 21:2781. doi: 10.3390/ijms21082781

2. Guo H-T, Wang J-R, Sun L-Z, Jin X-H, Shi X-Y, Lin J-Y, et al. Effects of astaxanthin on plasma membrane function and fertility of boar sperm during cryopreservation. *Theriogenology*. (2021) 164:58–64. doi: 10.1016/j.theriogenology.2021.01.007

3. Yang D, Wang C, Lu W, Tian X, Sun Y, Peng H. Beneficial effects of melatonin on boar sperm motility and kinematics are mediated by MT1 receptor. *Theriogenology*. (2024) 226:95–103. doi: 10.1016/j.theriogenology.2024.06.003

4. Segabinazzi LGTM, Dell'Aqua CPF, Cavalero T, Frasson M, Lisboa FP, Papa FO, et al. Post-cooling sperm processing can rescue sperm quality of cooled-stored stallion semen. *Theriogenology*. (2024) 227:21–30. doi: 10.1016/j.theriogenology.2024.07.004

5. Hernández-Avilés C, Ramírez-Agámez L, Varner DD, Love CC. Factors affecting the analysis and interpretation of sperm quality in frozen/thawed stallion semen. *Theriogenology*. (2024) 218:35–44. doi: 10.1016/j.theriogenology.2024.01.039

6. Galarza DA, Jaramillo J, Amón N, Campoverde B, Aguirre B, Taboada J, et al. Effect of resveratrol supplementation in conventional slow and ultra-rapid freezing media on the quality and fertility of bull sperm. *Anim Reprod Sci*. (2024) 266:107495. doi: 10.1016/j.anireprosci.2024.107495

7. Qin W, Chu M, Ma X, Pei J, Xiong L, Bao P, et al. Comparative iTRAQ proteomics identified proteins in fresh and frozen thawed yak spermatozoa. *Int J Biol Macromol*. (2023) 246:125728. doi: 10.1016/j.ijbiomac.2023.125728

8. Zang S, Yang X, Ye J, Mo X, Zhou G, Fang Y. Quantitative phosphoproteomics explain cryopreservation-induced reductions in ram sperm motility. *J Proteome*. (2024) 298:105153. doi: 10.1016/j.jprot.2024.105153

9. Zhu Z, Zhao H, Cui H, Adetunji AO, Min L. Resveratrol improves the frozen-thawed ram sperm quality. *Animals*. (2023) 13:3887. doi: 10.3390/ani13243887

10. Hatami M, Masoudi R, Hatefi A, Alipour-Jenaghard P, Esmaeili V. The effects of MitoQ as a mitochondrial-targeted antioxidant in a plant-based extender on buck sperm quality parameters during cryopreservation. *Anim Reprod Sci*. (2024) 266:107517. doi: 10.1016/j.anireprosci.2024.107517

11. Kamel AM, Abd El-Hamid IS, Khalifa M, Shaker YM, Rateb SA. Influence of incorporating L-carnitine or Moringa oleifera leaves extract into semen diluent on cryosurvival and in vitro fertilization competence of buck sperm. *Anim Reprod Sci*. (2024) 268:107562. doi: 10.1016/j.anireprosci.2024.107562

12. Gonzalez M, Prashar T, Connaughton H, Barry M, Robker R, Rose R. Restoring sperm quality post-cryopreservation using mitochondrial-targeted compounds. *Antioxidants*. (2022) 11:1808. doi: 10.3390/antiox11091808

13. Madeja ZE, Podralska M, Nadel A, Pszczola M, Pawlak P, Rozwadowska N. Mitochondria content and activity are crucial parameters for bull sperm quality evaluation. *Antioxidants*. (2021) 10:1204. doi: 10.3390/antiox10081204

14. Rezaei A, Bahmani HR, Mafakheri S, Farshad A, Nazari P, Masoudi R. Protective effects of different doses of MitoQ separately and combined with trehalose on oxidative stress and sperm function of cryopreserved Markhoz goat semen. *Cryobiology*. (2023) 110:36–43. doi: 10.1016/j.cryobiol.2022.12.019

15. Boguenet M, Bouet P-E, Spiers A, Reynier P, May-Panloup P. Mitochondria: their role in spermatozoa and in male infertility. *Hum Reprod Update*. (2021) 27:697–719. doi: 10.1093/humupd/dmab001

16. Popova D, Bhide P, D'Antonio F, Basnet P, Acharya G. Sperm mitochondrial DNA copy numbers in normal and abnormal semen analysis: a systematic review and meta-analysis. *BJOG*. (2022) 129:1434–46. doi: 10.1111/1471-0528.17078

17. Guo H, Gong Y, He B, Zhao R. Relationships between mitochondrial DNA content, mitochondrial activity, and boar sperm motility. *Theriogenology*. (2017) 87:276–83. doi: 10.1016/j.theriogenology.2016.09.005

18. Briston T, Roberts M, Lewis S, Powney B, Staddon J, Szabadkai G, et al. Mitochondrial permeability transition pore: sensitivity to opening and mechanistic dependence on substrate availability. *Sci Rep*. (2017) 7:10492. doi: 10.1038/s41598-017-10673-8

19. Fang Y, Zhao C, Xiang H, Zhao X, Zhong R. Melatonin inhibits formation of mitochondrial permeability transition pores and improves oxidative phosphorylation of frozen-thawed ram sperm. *Front Endocrinol*. (2019) 10:896. doi: 10.3389/fendo.2019.00896

20. Fang Y, Zhao C, Xiang H, Jia G, Zhong R. Melatonin improves cryopreservation of ram sperm by inhibiting mitochondrial permeability transition pore opening. *Reprod Domest Anim*. (2020) 55:1240–9. doi: 10.1111/rda.13771

21. Gualtieri R, Kalthur G, Barbato V, Di Nardo M, Adiga SK, Talevi R. Mitochondrial dysfunction and oxidative stress caused by cryopreservation in reproductive cells. *Antioxidants*. (2021) 10:337. doi: 10.3390/antiox10030337

22. Brand MD. Mitochondrial generation of superoxide and hydrogen peroxide as the source of mitochondrial redox signaling. *Free Radic Biol Med*. (2016) 100:14–31. doi: 10.1016/j.freeradbiomed.2016.04.001

23. Tiwari S, Dewry RK, Srivastava R, Nath S, Mohanty TK. Targeted antioxidant delivery modulates mitochondrial functions, ameliorates oxidative stress and preserve sperm quality during cryopreservation. *Theriogenology*. (2022) 179:22–31. doi: 10.1016/j.theriogenology.2021.11.013

24. Fu L, Fang F, Guo Y, Ma J, Wang S, Gu Y, et al. Combined analysis of the transcriptome, proteome and metabolome in human cryopreserved sperm. *World J Mens Health*. (2024) 42:610–9. doi: 10.5534/wjmh.230091

25. Ofosu J, Nartey MA, Mo XH, Ye JF, Zhang Y, Zeng CJ, et al. Ram sperm cryopreservation disrupts metabolism of unsaturated fatty acids. *Theriogenology*. (2023) 204:8–17. doi: 10.1016/j.theriogenology.2023.03.023

26. Longobardi V, Kosior MA, Pagano N, Fatone G, Staropoli A, Vassetti A, et al. Changes in bull semen metabolome in relation to cryopreservation and fertility. *Animals*. (2020) 10:1065. doi: 10.3390/ani10061065

27. Yuan YX, Wang G, Zou JH, Zhang YT, Li DX, Yu MQ, et al. Study on comparative analysis of differential metabolites in Guanzhong dairy goat semen before and after freezing. *Theriogenology*. (2023) 197:232–9. doi: 10.1016/j.theriogenology.2022.12.009

28. Li C, Lv C, Larbi A, Liang J, Yang Q, Wu G, et al. Revisiting the injury mechanism of goat sperm caused by the cryopreservation process from a perspective of sperm metabolite profiles. *Int J Mol Sci*. (2024) 25:9112. doi: 10.3390/ijms25169112

29. Wyss M, Kaddurah-Daouk R. Creatine and creatinine metabolism. *Physiol Rev*. (2000) 80:1107–213. doi: 10.1152/physrev.2000.80.3.1107

30. Kazak L, Cohen P. Creatine metabolism: energy homeostasis, immunity and cancer biology. *Nat Rev Endocrinol*. (2020) 16:421–36. doi: 10.1038/s41574-020-0365-5

31. Li Y, Hu Y, Wang Z, Lu T, Yang Y, Diao H, et al. IKBA phosphorylation governs human sperm motility through ACC-mediated fatty acid beta-oxidation. *Commun Biol*. (2023) 6:323. doi: 10.1038/s42003-023-04693-6

32. Zhu Z, Li R, Feng C, Liu R, Zheng Y, Hoque SAM, et al. Exogenous oleic acid and palmitic acid improve boar sperm motility via enhancing mitochondrial B-oxidation for ATP generation. *Animals*. (2020) 10:591. doi: 10.3390/ani10040591

33. Grötter LG, Cattaneo L, Marini PE, Kjelland ME, Ferré LB. Recent advances in bovine sperm cryopreservation techniques with a focus on sperm post-thaw quality optimization. *Reprod Domest Anim*. (2019) 54:655–65. doi: 10.1111/rda.13409

34. Contreras MJ, Arias ME, Fuentes F, Muñoz E, Bernecic N, Fair S, et al. Cellular and molecular consequences of stallion sperm cryopreservation: recent approaches to improve sperm survival. *J Equine Vet*. (2023) 126:104499. doi: 10.1016/j.jevs.2023.104499

35. Bucak MN, Ataman MB, Başpınar N, Uysal O, Taşpınar M, Bilgili A, et al. Lycopene and resveratrol improve post-thaw bull sperm parameters: sperm motility, mitochondrial activity and DNA integrity. *Andrologia*. (2015) 47:545–52. doi: 10.1111/and.12301

36. Li CY, Hao HS, Zhao YH, Zhang PP, Wang HY, Pang YW, et al. Melatonin improves the fertilization capacity of sex-sorted bull sperm by inhibiting apoptosis and increasing fertilization capacitation via MT1. *Int J Mol Sci*. (2019) 20:3921. doi: 10.3390/ijms20163921

37. Shi H, Li QY, Li H, Wang HY, Fan CX, Dong QY, et al. ROS-induced oxidative stress is a major contributor to sperm cryoinjury. *Hum Reprod*. (2024) 39:310–25. doi: 10.1093/humrep/dead250

38. Amaral A, Lourenço B, Marques M, Ramalho-Santos J. Mitochondria functionality and sperm quality. *Reproduction*. (2013) 146:R163–74. doi: 10.1530/REP-13-0178

39. Mateo-Otero Y, Llavanera M, Torres-Garrido M, Yeste M. Embryo development is impaired by sperm mitochondrial-derived ROS. *Biol Res*. (2024) 57:5. doi: 10.1186/s40659-024-00483-4

40. Aitken RJ, Drevet JR, Moazamian A, Gharagozloo P. Male infertility and oxidative stress: a focus on the underlying mechanisms. *Antioxidants*. (2022) 11:306. doi: 10.3390/antiox11020306

41. O'Flaherty C. Redox regulation of mammalian sperm capacitation. *Asian J Androl*. (2015) 17:583–90. doi: 10.4103/1008-682X.153303

42. Jeon YG, Kim YY, Lee G, Kim JB. Physiological and pathological roles of lipogenesis. *Nat Metab*. (2023) 5:735–59. doi: 10.1038/s42255-023-00786-y

43. Menendez JA, Lupu R. Fatty acid synthase and the lipogenic phenotype in cancer pathogenesis. *Nat Rev Cancer*. (2007) 7:763–77. doi: 10.1038/nrc2222

44. Jones SF, Infante JR. Molecular pathways: fatty acid synthase. *Clin Cancer Res*. (2015) 21:5434–8. doi: 10.1158/1078-0432.Ccr-15-0126

45. Schroeder B, Vander Steen T, Espinoza I, Venkatapoorna CMK, Hu Z, Silva FM, et al. Fatty acid synthase (FASN) regulates the mitochondrial priming of cancer cells. *Cell Death Dis*. (2021) 12:977. doi: 10.1038/s41419-021-04262-x

46. Kuang W, Zhang J, Lan Z, Deepak RNVK, Liu C, Ma Z, et al. SLC22A14 is a mitochondrial riboflavin transporter required for sperm oxidative phosphorylation and male fertility. *Cell Rep*. (2021) 35:109025. doi: 10.1016/j.celrep.2021.109025

47. Xue D, Zhang Y, Wang Y, Wang J, An F, Sun X, et al. Quantitative proteomic analysis of sperm in unexplained recurrent pregnancy loss. *Reprod Biol Endocrinol*. (2019) 17:52. doi: 10.1186/s12958-019-0496-5

48. Tang M, Dong X, Xiao LB, Tan ZQ, Luo XJ, Yang LF, et al. CPT1A-mediated fatty acid oxidation promotes cell proliferation via nucleoside metabolism in nasopharyngeal carcinoma. *Cell Death Dis*. (2022) 13:331. doi: 10.1038/s41419-022-04730-y

49. Islam MM, Umehara T, Tsujita N, Shimada M. Saturated fatty acids accelerate linear motility through mitochondrial ATP production in bull sperm. *Reprod Med Biol*. (2021) 20:289–98. doi: 10.1002/rmb2.12381

50. Huang M, Yan Y, Deng Z, Zhou L, She M, Yang Y, et al. Saikosaponin a and D attenuate skeletal muscle atrophy in chronic kidney disease by reducing oxidative stress through activation of PI3K/AKT/Nrf2 pathway. *Phytomedicine*. (2023) 114:154766. doi: 10.1016/j.phymed.2023.154766

51. Zhao L, Jin L, Yang B. Saikosaponin a alleviates Staphylococcus aureus-induced mastitis in mice by inhibiting ferroptosis via SIRT1/Nrf2 pathway. *J Cell Mol Med*. (2023) 27:3443–50. doi: 10.1111/jcmm.17914

52. Li X, Ge J, Li Y, Cai Y, Zheng Q, Huang N, et al. Integrative lipidomic and transcriptomic study unravels the therapeutic effects of saikosaponins a and D on non-alcoholic fatty liver disease. *Acta Pharm Sin B*. (2021) 11:3527–41. doi: 10.1016/j.apsb.2021.03.018

53. Zheng Q, Li X, Huang N, Li F, Ge J, Wang D, et al. Saikosaponins ameliorate hyperlipidemia in rats by enhancing hepatic lipid and cholesterol metabolism. *J Ethnopharmacol*. (2023) 305:116110. doi: 10.1016/j.jep.2022.116110

54. Santos DB, Colle D, Moreira ELG, Santos AA, Hort MA, Santos K, et al. Probucol protects neuronal cells against peroxide-induced damage and directly activates glutathione peroxidase-1. *Mol Neurobiol*. (2020) 57:3245–57. doi: 10.1007/s12035-020-01963-w

55. Prah J, Winters A, Chaudhari K, Hersh J, Liu R, Yang S-H. Cholesterol sulfate alters astrocyte metabolism and provides protection against oxidative stress. *Brain Res*. (2019) 1723:146378. doi: 10.1016/j.brainres.2019.146378

56. Strott CA, Higashi Y. Cholesterol sulfate in human physiology: what's it all about? *J Lipid Res*. (2003) 44:1268–78. doi: 10.1194/jlr.R300005-JLR200

57. Bisht S, Faiq M, Tolahunase M, Dada R. Oxidative stress and male infertility. *Nat Rev Urol*. (2017) 14:470–85. doi: 10.1038/nrurol.2017.69

58. Wolosker H, Kline D, Bian Y, Blackshaw S, Cameron AM, Fralich TJ, et al. Molecularly cloned mammalian glucosamine-6-phosphate deaminase localizes to transporting epithelium and lacks oscillin activity. *FASEB J*. (1998) 12:91–9. doi: 10.1096/fasebj.12.1.91

59. Hughes SD, Kanabus M, Anderson G, Hargreaves IP, Rutherford T, O'Donnell M, et al. The ketogenic diet component decanoic acid increases mitochondrial citrate synthase and complex I activity in neuronal cells. *J Neurochem*. (2014) 129:426–33. doi: 10.1111/jnc.12646

60. Baldwin T, Clayton P, Rutherford T, Heales S, Eaton S. SH-SY5Y cells undergo changes in peroxisomal metabolism when exposed to decanoic acid. *J Neurochem*. (2024) 168:3108–15. doi: 10.1111/jnc.16185

61. Lee SI, Kang KS. Function of capric acid in cyclophosphamide-induced intestinal inflammation, oxidative stress, and barrier function in pigs. *Sci Rep*. (2017) 7:16530. doi: 10.1038/s41598-017-16561-5

62. Mett J, Muller U. The medium-chain fatty acid decanoic acid reduces oxidative stress levels in neuroblastoma cells. *Sci Rep*. (2021) 11:6135. doi: 10.1038/s41598-021-85523-9

63. Wang D, Chen J, Sun H, Chen W, Yang X. MCFA alleviate H(2) O(2) -induced oxidative stress in AML12 cells via the ERK1/2/Nrf2 pathway. *Lipids*. (2022) 57:153–62. doi: 10.1002/lipd.12339

64. Shekhar N, Tyagi S, Rani S, Thakur AK. Potential of Capric acid in neurological disorders: An overview. *Neurochem Res*. (2023) 48:697–712. doi: 10.1007/s11064-022-03809-4

65. Thevenet J, De Marchi U, Domingo JS, Christinat N, Bultot L, Lefebvre G, et al. Medium-chain fatty acids inhibit mitochondrial metabolism in astrocytes promoting astrocyte-neuron lactate and ketone body shuttle systems. *FASEB J*. (2016) 30:1913–26. doi: 10.1096/fj.201500182

frontiers | Frontiers in Veterinary Science

TYPE Original Research
PUBLISHED 31 March 2025
DOI 10.3389/fvets.2025.1544718

OPEN ACCESS

EDITED BY
Manuel Garcia-Herreros,
National Institute for Agricultural and Veterinary Research (INIAV), Portugal

REVIEWED BY
Penelope Banchi,
Ghent University, Belgium
Svetlana Uzbekova,
Institut National de recherche pour l'agriculture, l'alimentation et l'environnement (INRAE), France

*CORRESPONDENCE
Jiwen Wang
wjw2886166@163.com

†These authors have contributed equally to this work

RECEIVED 13 December 2024
ACCEPTED 12 March 2025
PUBLISHED 31 March 2025

CITATION
Yuan X, Zhang X, Lin Y, Xie H, Wang Z, Hu X, Hu S, Li L, Liu H, He H, Han C, Gan X, Liao L, Xia L, Hu J and Wang J (2025) Proteome of granulosa cells lipid droplets reveals mechanisms regulating lipid metabolism at hierarchical and pre-hierarchical follicle in goose.
Front. Vet. Sci. 12:1544718.
doi: 10.3389/fvets.2025.1544718

Proteome of granulosa cells lipid droplets reveals mechanisms regulating lipid metabolism at hierarchical and pre-hierarchical follicle in goose

Xin Yuan[1†], Xi Zhang[1†], Yueyue Lin[1], Hengli Xie[1], Zhujun Wang[1], Xinyue Hu[1], Shenqiang Hu[1], Liang Li[1], Hehe Liu[1], Hua He[1], Chunchun Han[1], Xiang Gan[2], Ling Liao[3], Lu Xia[1], Jiwei Hu[1] and Jiwen Wang[1]*

[1]College of Animal Science and Technology, Sichuan Agricultural University, Chengdu, China, [2]Scientific Research Center, Guilin Medical University, Guilin, Guangxi, China, [3]College of Horticulture, Sichuan Agricultural University, Chengdu, China

Avian hierarchical follicles are formed by selection and dominance of pre-hierarchical follicles, and lipid metabolism plays a pivotal role in this process. The amount of lipid in goose follicular granulosa cells increases with the increase of culture time, and the neutral lipid in the cells is stored in the form of lipid droplets (LDs). LD-associated proteins (LDAPs) collaborate with LDs to regulate intracellular lipid homeostasis, which subsequently influences avian follicle development. The mechanism by which LDAPs regulate lipid metabolism in goose granulosa cells at different developmental stages is unclear. Therefore, using BODIPY staining, we found that at five time points during *in vitro* culture, the LD content in hierarchical granulosa cells was significantly higher than that in pre-hierarchical granulosa cells in this study ($p < 0.001$). Next, we identified LDAPs in both hierarchical and pre-hierarchical granulosa cells, and screened out 1,180, 922, 907, 663, and 1,313 differentially expressed proteins (DEPs) at the respective time points. Subsequently, by performing Clusters of Orthologous Groups (COGs) classification on the DEPs, we identified a large number of proteins related to lipid transport and metabolism. Following this, the potential functions of these DEPs were investigated through Gene Ontology (GO) and Kyoto Encyclopedia of Genes and Genomes (KEGG) functional enrichment analysis. Finally, the important pathway of fatty acid degradation and the key protein ACSL3 were screened out using Short Time-series Expression Miner (STEM) and Protein–Protein Interaction (PPI) analysis methods. It is hypothesized that ACSL3 may potentially modulate lipid metabolism through the fatty acid degradation pathway, thereby contributing to the difference in lipid content between hierarchical and pre-hierarchical granulosa cells. These findings will provide a theoretical foundation for further studies on the role of LDs and LDAPs in avian follicle development.

KEYWORDS

goose, granulosa cell, lipid metabolism, lipid droplet, lipid droplet-associated proteins

1 Introduction

Lipids not only provide energy for follicle development but also serve as important regulatory factors in this process (1). A mature follicle usually consists of oocyte, granulosa, theca and connective tissue layer (2). The granulosa cell is the main component of the follicular wall and is one of the most important structures of the follicle (3, 4). Recently, lipid metabolism in granulosa cells has attracted attention. Studies on mice have shown that treating granulosa cells with palmitic acid (PA) or lysophosphatidylcholine (LPC) reduces cell viability and induces apoptosis (5, 6). Oleic acid (OA) alters lipid storage in porcine ovarian granulosa cells and reduces steroidogenesis (7). Furthermore, arachidonic acid (AA), a polyunsaturated fatty acid, has a significant impact on granulosa cell function and follicle development. Research has found that low doses of AA can induce the accumulation of low-density lipoprotein in bovine granulosa cells and enhance granulosa cell survival (8). Granulosa cells also play a pivotal role in follicle development and maturation. During follicle growth, maturation, and ovulation, granulosa cells transport nutrients to the follicle, provide mechanical support, and synthesize steroids (9, 10). Undeniably, lipid metabolism in granulosa cells is crucial for the development of mammalian follicles.

Unlike mammalian follicular development, avian follicular development exhibits a unique hierarchical system, including hierarchical follicles and pre-hierarchical follicles. During follicular development, only a very small number of pre-hierarchical follicles can develop into hierarchical follicles (11). There are significant differences in tissue morphology and steroid secretion between hierarchical and pre-hierarchical follicles (12, 13). Recent studies have found that there are also differences in lipid metabolism between hierarchical and pre-hierarchical granulosa cells, with the ability of hierarchical granulosa cells to accumulate lipids being stronger (14). Research using mass spectrometry on the lipid profile of granulosa cells also suggests that granulosa cell lipids are important for follicular development (15). Neutral lipids in granulosa cells are stored in the form of lipid droplets (LDs). LDs, ubiquitous lipid-storing organelles (16, 17), participate in diverse cellular processes like energy metabolism (18), lipid storage, transport, and metabolism (19, 20), as well as protein storage and degradation (21, 22). The functionality of LDs is heavily reliant on the associated proteins, which are collectively referred to as lipid droplet-associated proteins (LDAPs). LDs have been isolated from human (23), mouse (24, 25), pig, fish (26, 27), and hundreds of proteins associated with LDs have been reliably detected by means of proteomic (28). LDAPs are involved in the regulation of cellular lipid metabolism in concert with LDs. It has been found that LDs contain a large number of LDAPs related to lipid metabolism, such as Perilipins (PLIN) (29), Acyl-CoA synthetase proteins (ACSL) (30), Adipose triglyceride lipase (ATGL) (31), and these proteins further regulate the process of lipid metabolism through the way of promoting the synthesis and degradation of LDs.

Lipid metabolism in granulosa cells is crucial for follicular development (13), yet the regulation of LDAPs in avian granulosa cells remains understudied, and there is currently no report on the proteome of LDs in geese. Therefore, this study first examined the differences in LD content in granulosa cells at various developmental stages through LD staining. Subsequently, LDs were isolated, and their associated proteins were identified using proteomics. Lastly, proteomic analysis was employed to delve into the molecular mechanisms underlying the regulation of lipid metabolism in granulosa cells by LDAPs.

2 Materials and methods

2.1 Animals

Healthy female lines of Tianfu geese (*Anser cygnoides*) were selected. Food and water were provided to the geese under natural light and temperature conditions at the Waterfowl Breeding Experimental Farm of Sichuan Agricultural University (Ya'an, China). The spawning cycle of each goose was recorded, and ovarian follicles were collected from all geese during the same spawning cycle. All selected geese were euthanized by carbon dioxide inhalation and cervical dislocation performed by competent, experienced personnel who applied the techniques correctly. Efforts were made to minimize animal suffering in accordance with the requirements of the Beijing Animal Welfare Committee. All experimental procedures involving animal manipulation were approved by the Committee of the School of Farm Animal Genetic Resources Exploration and Innovation Key Laboratory, College of Animal Science and Technology, Sichuan Agricultural University, under permit no. DKY20170913, and were conducted in accordance with the Regulations of the Administration of Affairs Concerning Experimental Animals (China 1988).

2.2 Cells culture and incubation conditions

For granulosa cell culture, after euthanasia of 18 randomly selected geese with regular egg production, follicles were collected from the coelomic cavity of goose, placed in sterile saline, and divided into hierarchical (F2-F4 large yellow follicles) and pre-hierarchical follicles (small follicles between 8 and 10 mm in diameter) according to previously reported nomenclature (32). The outer connective tissue was removed from the follicles, and follicles were bisected to allow the yolk and adherent granulosa layer to flow out (33). Collecting the granulosa layer, incubated with 0.05% type II collagenase (Sigma, USA) for 10 min in a 37°C water bath, dispersed, resuspended in 3 mL of fresh collagenase-free basal medium, and centrifuged. Cells were then dispersed in Dulbecco's modified Eagle medium (DMEM) supplemented with 1% antibiotic/antimycotic solution (Solarbio, Beijing, China) and 5% fetal bovine serum (Gibco, Waltham, MA, USA). Then, cells were incubated in a water-saturated atmosphere of 95% air and 5% CO2 at 37°C in an incubator (Thermo, Waltham, MA, USA), as previously described (34).

2.3 BODIPY staining of lipids in granulosa cells

The cell samples were rinsed 2–3 times with phosphate-buffered saline (PBS) to remove the medium. 4% paraformaldehyde solution was added to cover the cell samples, and fixation was carried out for 30 min at room temperature. After fixation, the cell samples were rinsed 2–3 times with PBS. The BODIPY staining solution was then added, and the samples were incubated for 15 min. The cell samples were washed 2–3 times with PBS to remove unbound staining

solution. The DAPI staining solution was added, and the samples were incubated for 15 min at room temperature, followed by rinsing 2–3 times with PBS. Finally, the cell samples were observed under a fluorescence microscope using appropriate fluorescent filters. The images were further analyzed and processed using the ImageJ software package. The area of the LDs (green) and the area of the nucleus (blue) were measured using the software, and the LDs area/nucleus area was calculated as the relative fluorescence ratio. Three biological replicates, each with three technical replicates ($n = 9$).

2.4 LDs isolation from granulosa cells

LDs were isolated from granulosa cells according to the manufacturer's instructions (Cell Biolabs, INC. cat#MET-5011). Briefly, 1.5×10^7 granulosa cells were digested, and the medium was removed by first washing the cells with PBS. After washing, the cells were resuspended in 200 μL of Reagent A, incubated on ice for 10 min, and then 800 μL of Reagent B was added. The cells were homogenized by passing them through a 27-gauge needle five times. 600 μL of Reagent B are cautiously added to the homogenate and centrifuged at 18,000 g at 4°C for 3 h. Subsequently, the uppermost 270 μL of the stratified solution were aspirated to yield the LDs.

2.5 DEPs sample preparation for LC-MS/MS analysis

LDs were isolated from hierarchical and pre-hierarchical granulosa cells after 2 d, 3 d, 4 d, 5 d, and 6 d of culture, respectively. Three technical replicates were performed for each time point ($n = 15$). LDs isolated from hierarchical granulosa cells after 2 d of culture were referred to as the H2 group, while LDs from pre-hierarchical granulosa cells after 2 d of culture were referred to as the P2 group. The remaining samples were named sequentially. Total protein amount for each sample was at least 30 μg, proteomic analysis of LD proteins from each sample was performed by mixing a specific concentration of formic acid with the digested sample, adjusting the pH below 3, and centrifuging at 12,000 g for 5 min at room temperature. The samples were then desalted using a C18 desalting column, and the eluate was collected and lyophilized.

The spectra library for data-independent acquisition (DIA) was constructed using UHPLC–MS/MS in Novogene Bioinformatics Technology Co., Ltd. (Beijing, China). To build the library, LD proteomics analysis was performed using a Vanquish Neo upgraded UHPLC system (Thermo Fisher, America), and the separated peptides were analyzed using a Thermo Orbitrap Fusion Lumos mass spectrometer (Thermo Fisher, America). To improve the quality of the analytical results, the DIA-NN software further filtered the search results by retaining only credible Peptide Spectrum Matches (PSMs) with a confidence level of 99% or higher.

2.6 Protein identification and quantification

The raw files were searched and analyzed using the DIA-NN library search software, based on the UniProt database specific to the *Anser cygnoides* proteome. Only credible spectral peptides and proteins were retained, and FDR validation was performed to remove peptides and proteins with an FDR greater than 1%. Proteins were quantified in all three replicate samples. Proteins with a peptide number greater than 2 were selected for further analysis. Significantly differentially expressed proteins (DEPs) were screened according to the criteria with fold change >1.5 (up-regulation) or < 0.67 (down-regulation) and $p < 0.05$.

2.7 Bioinformatic analysis

The original functions of the proteins were clustered using Clusters of Orthologous Groups (COGs) analysis.[1] Gene Ontology (GO) functional annotation was performed using InterProScan software, with reference to the chicken (*Gallus gallus*) database. The functions of different proteins were categorized using GO assignment[2] to classify the identified proteins into three main categories: biological processes, cellular components, and molecular functions. The most important biochemical metabolic pathways and signal transduction pathways of the proteins were identified using the Kyoto Encyclopedia of Genes and Genomes (KEGG) pathway.[3] Short Time-Series Expression Miner (STEM) clustering algorithm was used to identify temporal expression profiles of LD proteins. Representative temporal expression profiles were defined as model profiles, and protein expression values were transformed into logarithmic ratios of expression relative to Day 2. Each protein was then assigned to a model profile based on the screening criteria, and the correlation coefficients between the protein's expression profile and the model profile were determined. If the correlation coefficients indicate statistical significance, the corresponding data points or boxes in the plot are colored. Interactions between proteins were analyzed by constructing PPI networks. The interaction information of all proteins was collected using the online database STRING,[4] and the results were imported into Cytoscape for visualization.

2.8 Statistical analysis

For each experimental procedure, data were collected simultaneously from at least three geese per group, with at least three technical repetitions set up. The data were expressed as mean ± standard error of the mean (SEM), significant differences between the proteins in the two phases of LDs were determined using independent t-tests and one-way ANOVA (GraphPad Prism 5), the obtained data were initially analyzed for normal distribution using descriptive statistics in SPSS, followed by significance analysis using t-tests and one-way ANOVA (SPSS version 20.0, IBM, Armonk, IL, USA). Differences with $p < 0.05$ were considered statistically significant, images drawn using Prism 5, Graphpad software. Metabolic pathway plots were drawn using Adobe Photoshop.

1 https://www.ncbi.nlm.nih.gov/research/cog
2 https://www.geneontology.org
3 https://www.genome.jp/kegg
4 https://string-db.org/

3 Results

3.1 Differences of LDs content *in vitro* cultured granulosa cells from geese follicles at different developmental stages

Using BODIPY staining, we investigated the LD content in two distinct groups of granulosa cells, isolated from follicles at different developmental stages. As shown in Figure 1, the results indicated that LDs of granulosa cells were spherical in shape, and with increasing incubation time, the hierarchical granulosa cells tended to accumulate larger LDs, in contrast to the smaller droplets formed by pre-hierarchical granulosa cells. The staining results indicate significant differences in LD content between granulosa cells at different developmental stages. Specifically, the LD content in hierarchical granulosa cells is significantly higher than that in pre-hierarchical granulosa cells ($p < 0.001$). To gain further insights into the underlying mechanisms, we subsequently purified high-quality LDs from granulosa cells for comprehensive proteomic analysis.

3.2 Identification and classification of LDAPs

Proteomic studies were conducted to gain insights into the LDAPs in granulosa cells from hierarchical and pre-hierarchical follicles, a schematic workflow is shown in Figure 2A. The application of Principal Component Analysis (PCA) to the amassed proteomic dataset reveals distinct separation between hierarchical granulosa cells hierarchical granulosa cells (H group) and pre- hierarchical granulosa cells (P group), as shown in Figure 2B. Comparison with the UniProt database identified and quantified a total of 4,365 LDAPs. Of these, 3,959 LDAPs were identified from the H group and 4,118 from the P group, with 3,712 proteins co-identified in both groups (Figure 2C). To further analyze these proteins, we performed a Cluster of Orthologous Groups (COGs) analysis, which categorized the 4,365 proteins into 10 groups based on their cellular functions using the COGs database. As shown in Figure 2D and Supplementary Table S1, we found that many proteins were enriched in the COGs category 'lipid transport and metabolism', including numerous enzymes related to lipid synthesis and degradation, such as Fatty acid synthase (FASN), Fatty acid-binding proteins (FABP1, FABP4, FABP7), long-chain acyl-coenzyme A synthases (ACSL1, ACSL3, ACSL4), Acyl-CoA synthetase family members (ACSF2, ACSF3), Methylsterol monooxygenase 1 (MSMO1), Diacylglycerol kinases (DGKD, DGKQ), and Monoglyceride lipase (MGLL).

3.3 DEPs between hierarchical and pre-hierarchical granulosa cells

We further analyzed the DEPs in the H and P groups across five time points. At 2 d of cell culture (H2 vs. P2), a total of 1,180 DEPs were identified, with 856 DEPs up-regulated and 324 DEPs down-regulated. At 3 d (H3 vs. P3), 922 DEPs were identified, comprising 640 up-regulated and 282 down-regulated proteins. Similarly, at 4 d (H4 vs. P4), 907 DEPs were identified, including 468 up-regulated and 439

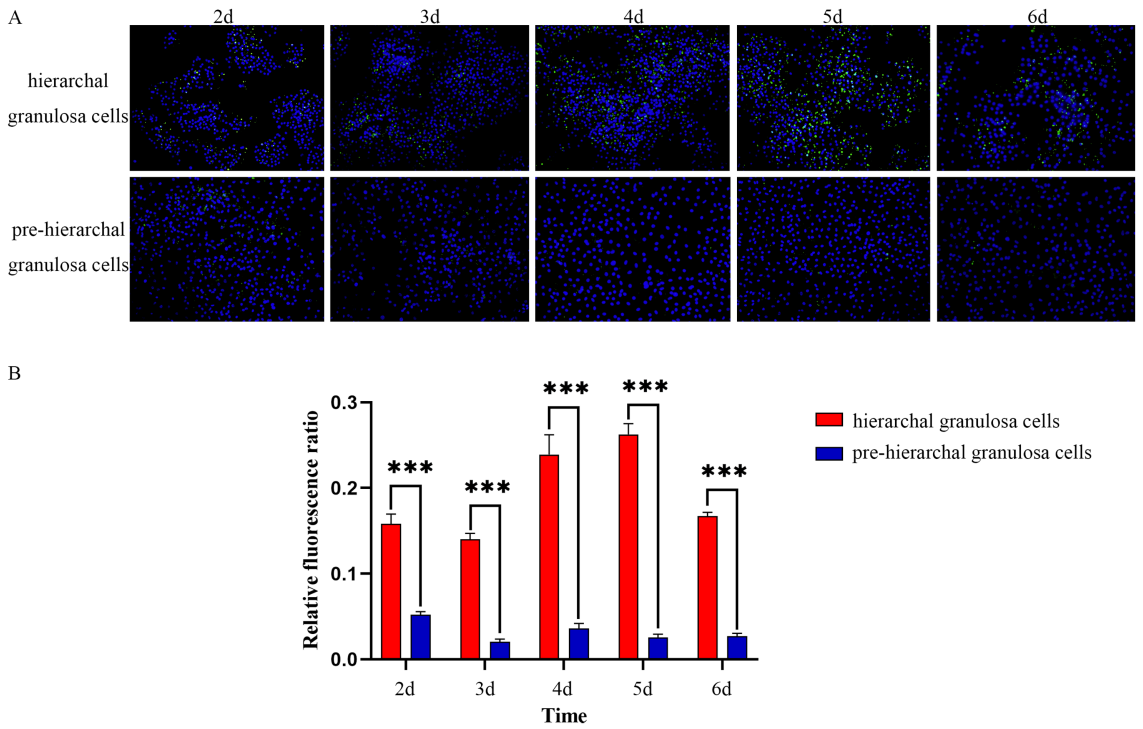

FIGURE 1
BODIPY staining of LDs. **(A)** Morphological characteristics of LDs in granulosa cells detection by BODIPY (green) and DAPI (blue) staining. **(B)** With increasing incubation time, the LDs content in hierarchical granulosa cells and pre-hierarchical granulosa cells showed dynamic changes, and the LDs content in hierarchical granulosa cells was significantly higher than that in pre-hierarchical granulosa cells. ***$p < 0.001$.

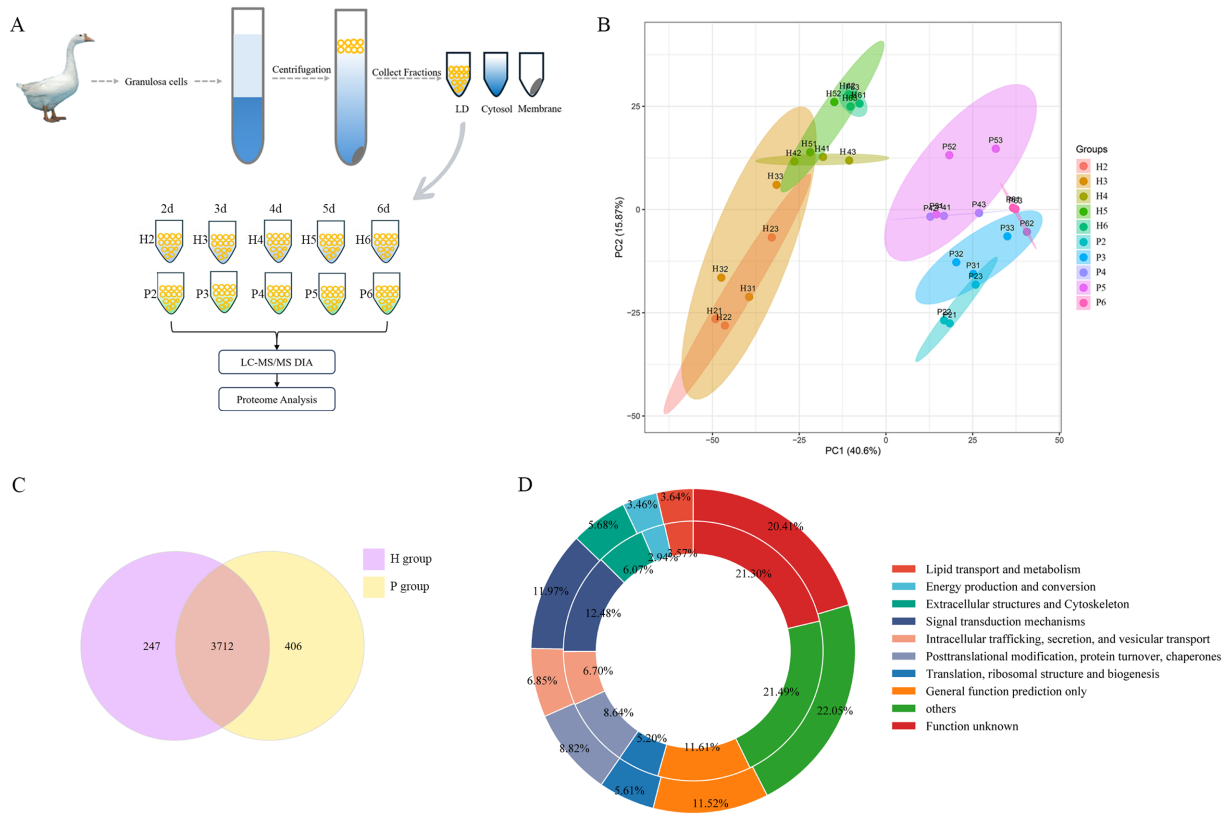

FIGURE 2
Identification and classification of LDAPs. **(A)** Schematic of protein sample collection. **(B)** PCA analysis of all proteins. **(C)** The Venn diagram showed overlapping proteins between the H and P groups proteomes.**(D)** The 4,365 proteins of LDs identified in two groups samples were categorized into 10 groups: Lipid transport and metabolism; Energy production and conversion; Extracellular structures and Cytoskeleton; Signal transduction mechanisms; Intracellular trafficking, secretion, and vesicular transport; Posttranslational modification, protein turnover, chaperones; Translation, ribosomal structure and biogenesis; General function prediction only; others and Function unknown protein. Circles from outer to inner represent H and P groups.

down-regulated. At 5 d (H5 vs. P5), 663 DEPs were screened, with 356 up-regulated and 307 down-regulated. Lastly, at 6 d (H6 vs. P6), 1,313 DEPs were screened, of which 1,072 were up-regulated and 241 were down-regulated (Figure 3A). Notably, NPC intracellular cholesterol transporter 2 (NPC2) was consistently among the top 20 up-regulated DEPs across all five time points. Monoglyceride lipase (MGLL), Retinol dehydrogenase 10 (RDH10), and Interleukin-1 receptor-associated kinase 4 (IRAK4) were also among the top 20 up-regulated DEPs in four of the time points. Conversely, five DEPs, including Carboxylic ester hydrolase (TGH), Neurofilament light (NEFL), Filamin C (FLNC), Peptidyl-cysteine S-nitrosylase GAPDH (GAPDHS), and CD2 associated protein (CD2AP) were consistently among the top 20 down-regulated DEPs across all five time points. Lymphocyte-specific protein 1 (LSP1), Phosphoglucomutase 5 (PGM5), cGMP-dependent protein kinase (PRKG1), Creatine kinase B (CKB), and Transglutaminase 2 (TGM2) were also among the top 20 down-regulated DEPs in four of these time points (Figure 3B; Supplementary Table S2).

3.4 Pathway enrichment analysis of DEPs

To elucidate the potential functions of these proteins, we performed GO and KEGG pathway enrichment analysis (Supplementary Table S3). In the five time points, BP was enriched for a large number of biological processes related to fatty acid metabolism, such as fatty acid metabolism, fatty acid biosynthesis, and fatty acid β-oxidation. CC was enriched for cellular components such as LDs, mitochondria, endoplasmic reticulum, and MF was enriched for molecular functions such as lipid-binding, calcium-dependent phospholipid-binding, and phospholipid-binding. The five groups of KEGG pathways were enriched in 114 metabolic pathways, of which 23 were all related to lipid metabolism (Table 1). Five of these pathways were significant in each group, namely fatty acid metabolism, fatty acid degradation, fatty acid biosynthesis, glycerophospholipid metabolism, and PPAR signaling pathway. The top 20 most significantly enriched GO terms and KEGG pathways in the five time points, according to the smallest to largest *P*, are shown in Supplementary Figure S1.

3.5 DEGs short time-series expression miner (STEM) analysis

There were 173 DEPs in 23 pathways related to lipid metabolism, and further analysis for STEM analysis of these 173 DEPs showed that a total of 119 DEPs were significantly expressed

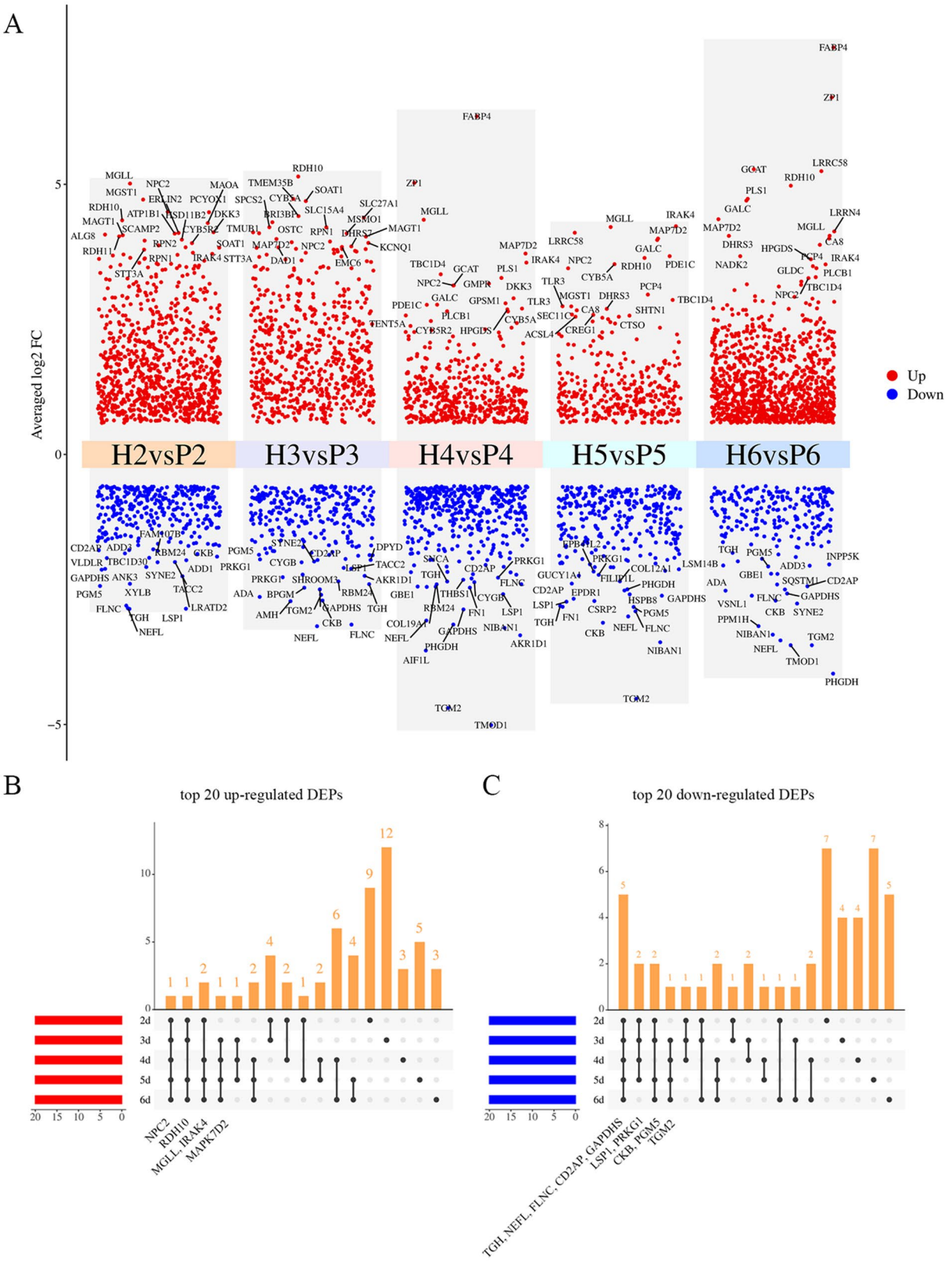

FIGURE 3
Significantly changed proteins at five times points. **(A)** Volcano plot of DEPs at five time points, top 20 up- and down-regulated DEPs are labeled in the figure, red and blue show up- and down-regulated proteins. **(B)** Upset plot of top 20 up-regulated DEPs at five time points, the annotated proteins were those significantly up-regulated and ranked within the top 20 at all 4 or 5 time points. **(C)** Upset plot of top 20 down-regulated DEPs at five time points, the annotated proteins were those significantly down-regulated and ranked within the top 20 at all 4 or 5 time points.

TABLE 1 23 pathways related to lipid transport and metabolism in KEGG.

KEGG pathway	H2vsP2		H3vsP3		H4vsP4		H5vsP5		H6vsP6	
	P	Protein number	P	Protein number	P	Protein number	P	Protein number	P	Protein number
Adipocytokine signaling pathway	0.081903718	6	0.399736772	3	0.894016652	1	0.496527864	2	0.238992617	5
Arachidonic acid metabolism	0.391842125	3	0.259843213	3	0.104576542	4	0.720128934	1	0.11790552	5
Biosynthesis of unsaturated fatty acids	0.004129396	6	0.006264012	5	0.100075282	3	0.545797932	1	0.079336257	4
Ether lipid metabolism	0.059640273	5	0.024985137	5	0.212907204	3	0.322021909	2	0.086035527	5
Fatty acid metabolism	8.61185E-10	18	6.88941E-09	15	4.37861E-08	14	0.000743567	7	1.47597E-10	20
Fatty acid degradation	4.63435E-08	13	1.36009E-06	10	1.31832E-06	10	0.000395103	6	7.99851E-11	17
Fatty acid elongation	0.001875318	6	0.016049957	4	0.015866054	4	0.484105001	1	0.000693086	7
Fatty acid biosynthesis	0.011553426	4	0.000731424	5	0.004949534	4	0.013081478	3	0.00061686	6
FoxO signaling pathway	0.063064124	10	0.929063184	2	0.01525887	10	0.219977859	5	0.187334174	9
Glycerophospholipid metabolism	7.08801E-05	15	7.06706E-05	13	0.022661473	8	0.004206846	8	0.028526744	10
Glycerolipid metabolism	0.008863215	8	0.173087583	4	0.02420311	6	0.006225667	6	0.042033529	7
Inositol phosphate metabolism	0.051616502	7	0.251519932	4	0.005276411	8	0.003455361	7	0.000184138	13
mTOR signaling pathway	0.007077796	14	0.725976268	4	0.067441344	9	0.077998002	7	0.034069214	13
PPAR signaling pathway	0.000364143	11	0.000197038	10	0.010179646	7	0.008263097	6	1.93212E-05	14
Pyruvate metabolism	0.191688717	3	0.115259819	3	0.032706427	4	0.012291826	4	7.50742E-07	12
p53 signaling pathway	0.090967725	6	0.677731516	2	0.213122638	4	0.099369061	4	0.65280141	3
Phosphatidylinositol signaling system	0.012063792	10	0.113077519	6	0.002263618	10	0.000939587	9	0.000170706	15
Sphingolipid metabolism	0.000108941	10	0.027010105	5	0.08386048	4	0.008219112	5	0.2099859	4
Steroid biosynthesis	0.053126518	3	0.000731424	5	0.028781386	3	0.000181817	5	0.00061686	6
Steroid hormone biosynthesis	0.099921091	4	0.384618981	2	0.730563293	1	0.619992007	1	0.56707676	2
TGF-beta signaling pathway	0.584061319	4	0.824900947	2	0.220264115	5	0.41485102	3	0.988947716	1
VEGF signaling pathway	0.021856082	7	0.870519274	1	0.158462864	4	0.070380945	4	0.350247013	4
Wnt signaling pathway	0.951386512	3	0.239879709	7	0.380932336	6	0.165932671	6	0.03563754	13

(Figure 4A). 55 DEPs were significantly expressed in the H group, 95 DEPs were significantly expressed in the P group, and 31 DEPs were significantly expressed in both groups (Table 2). A heat map of the 119 DEPs is shown in Figure 4B. Among them, the expression of Arylsulfatase A (ARSA), Calcium/calmodulin-dependent protein kinase (CAMK2G), Beta-galactosidase (GLB1), Phospholipase A2 group XV (PLA2G15), Phospholipase D family member 3 (PLD3), Inositol hexakisphosphate and Diphosphoinositol-pentakisphosphate kinase (PPIP5K2), Palmitoyl-protein thioesterase 1 (PPT1), Ras-related GTP-binding

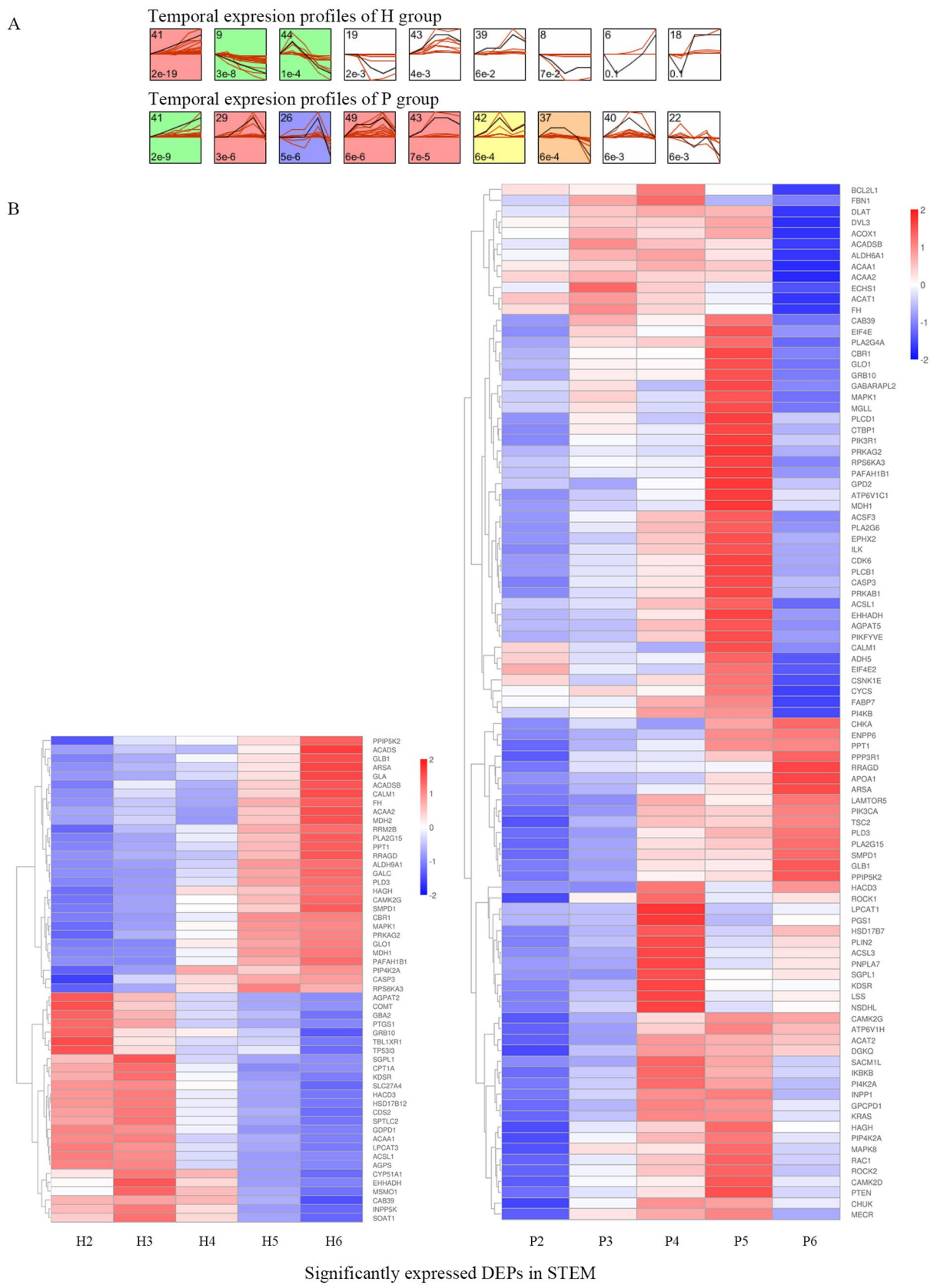

FIGURE 4
STEM analysis of DEPs. **(A)** The temporal expression profiles of proteins in H and P groups are shown, with the colored backgrounds of the clusters indicating significant changes in the expression trends of proteins within these clusters. A total of 119 proteins exhibited significant expression trends, among which 55 DEPs were identified in the colored clusters of H group, while 95 DEPs were identified in the colored clusters of P group. **(B)** The heatmap of 119 DEPs in the colored clusters is shown, with the left side displaying the heatmap of 55 DEPs from H group and the right side displaying the heatmap of 95 DEPs from P group.

TABLE 2 119 proteins with significance in STEM.

Group	Profile	Protein description (Gene name)	Number
H	9	Acetyl-CoA acyltransferase 1 (ACAA1), Long-chain-fatty-acid--CoA ligase (ACSL1), 1-acyl-sn-glycerol-3-phosphate acyltransferase (AGPAT2), Alkylglycerone-phosphate synthase (AGPS), Phosphatidate cytidylyltransferase (CDS2), Catechol O-methyltransferase (COMT), Glucosylceramidase beta 2 (GBA2), Glycerophosphodiester phosphodiesterase domain containing 1 (GDPD1), Growth factor receptor bound protein 10 (GRB10), Very-long-chain (3R)-3-hydroxyacyl-CoA dehydratase (HACD3), Hydroxysteroid 17-beta dehydrogenase 12 (HSD17B12), Lysophosphatidylcholine acyltransferase 3 (LPCAT3), Prostaglandin-endoperoxide synthase 1 (PTGS1)M, Solute carrier family 27 member 4 (SLC27A4), Transducin beta like 1 X-linked receptor 1 (TBL1XR1), Tumor protein p53 inducible protein 3 (TP53I3)	16
	41	Acetyl-CoA acyltransferase 2 (ACAA2), Acyl-CoA dehydrogenase short chain (ACADS), Acyl-CoA dehydrogenase short/branched chain (ACADSB), Aldehyde dehydrogenase 9 family member A1 (ALDH9A1), Arylsulfatase A (ARSA), Calmodulin 1 (CALM), calcium/calmodulin-dependent protein kinase (CAMK2G), Caspase 3 (CASP3), carbonyl reductase (NADPH)(CBR1), Fumarate hydratase, mitochondrial (FH), Galactocerebrosidase (GALC), Alpha-galactosidase (GLA), Beta-galactosidase (GLB1), Lactoylglutathione lyase (GLO1), Hydroxyacylglutathione hydrolase (HAGH), mitogen-activated protein kinase (MAPK1), Malate dehydrogenase (MDH1), Malate dehydrogenase (MADH2), Lissencephaly-1 homolog (PAFAH1B1), Phosphatidylinositol-5-phosphate 4-kinase type 2 alpha (PIP4K2A), Phospholipase A2 group XV (PLA2G15), Phospholipase D family member 3 (PLD3), Inositol hexakisphosphate and diphosphoinositol-pentakisphosphate kinase (PPIP5K2), Palmitoyl-protein thioesterase 1 (PPT1), Protein kinase AMP-activated non-catalytic subunit gamma 2 (PRKAG2), Ribosomal protein S6 kinase (RPS6KA3), Ras-related GTP-binding protein (RRAGD), Ribonucleotide reductase regulatory TP53 inducible subunit M2B (RRM2B), Sphingomyelin phosphodiesterase 1 (SMPD1)	29
	44	Calcium binding protein 39 (CAB39), carnitine O-palmitoyltransferase (CPT1A), Cytochrome P450 family 51 subfamily A member 1 (CYP51A1), enoyl-CoA hydratase (EHHADH), Inositol polyphosphate-5-phosphatase K (INPP5K),3-dehydrosphinganine reductase (KDSR), Methylsterol monooxygenase 1 (MSMO1), Sphingosine-1-phosphate lyase 1 (SGPL1), O-acyltransferase (SOAT1), Serine palmitoyltransferase long chain base subunit 2 (SPTLC2)	10
P	26	S-(hydroxymethyl)glutathione dehydrogenase (ADH5), Calmodulin 1 (CALM1), carbonyl reductase (CBR1), Casein kinase 1 epsilon (CSNK1E), Cytochrome c (CYCS), Disheveled segment polarity protein 3 (DVL3), Eukaryotic translation initiation factor 4E family member 2 (EIF4E2), Fatty acid binding protein 7 (FABP7), GABA type A receptor associated protein like 2 (GABARAPL2), Lactoylglutathione lyase (GLO1), Growth factor receptor bound protein 10 (GRB10), mitogen-activated protein kinase (MAPK1), Monoglyceride lipase (MGLL), Phosphatidylinositol 4-kinase beta (PI4KB), Phospholipase A2 (PLA2G4A), Ribosomal protein S6 kinase (RPS6KA3)	16
	29	Acyl-CoA synthetase family member 3 (ACSF3), Long-chain-fatty-acid--CoA ligase (ACSL1), 1-acylglycerol-3-phosphate O-acyltransferase 5 (AGPAT5), V-type proton ATPase subunit C (ATP6V1C1), Caspase 3 (CASP3), Cyclin dependent kinase 6 (CDK6), enoyl-CoA hydratase (EHHADH), Epoxide hydrolase 2 (EPHX2), Glycerol-3-phosphate dehydrogenase (GPD2), Integrin-linked protein kinase (ILK), Malate dehydrogenase (MDH1), Lissencephaly-1 homolog (PAFAH1B1), 1-phosphatidylinositol-3-phosphate 5-kinase (PIKFYVE), phospholipase A2 (PLA2G6), 1-phosphatidylinositol 4, 5-bisphosphate phosphodiesterase (PLCB1), Protein kinase AMP-activated non-catalytic subunit beta 1 (PRKAB1), Protein kinase AMP-activated non-catalytic subunit gamma 2 (PRKAG2)	17
	37	Acetyl-CoA acyltransferase 1 (ACAA1), Acetyl-CoA acyltransferase 2 (ACAA2), Acyl-CoA dehydrogenase short/branched chain (ACADSB), Acetyl-CoA acetyltransferase 1 (ACAT1), Acyl-coenzyme A oxidase (ACOX1), Aldehyde dehydrogenase 6 family member A1 (ALDH6A1), Bcl-2-like protein 1 (BCL2L1), Acetyltransferase component of pyruvate dehydrogenase complex (DLAT), Enoyl-CoA hydratase, short chain 1 (ECHS1), Fibrillin 1 (FBN1), Fumarate hydratase, mitochondrial (FH)	11
	41	Apolipoprotein A1 (APOA1), Arylsulfatase A (ARSA), calcium/calmodulin-dependent protein kinase (CAMK2G), Choline kinase alpha (CHKA), Ectonucleotide pyrophosphatase/phosphodiesterase 6 (ENPP6), Beta-galactosidase (GLB1), Ragulator complex protein LAMTOR5 (LAMTOR5), phosphatidylinositol-4, 5-bisphosphate 3-kinase (PIK3CA), Phospholipase A2 group XV (PLA2G15), Phospholipase D family member 3 (PLD3), Inositol hexakisphosphate and diphosphoinositol-pentakisphosphate kinase (PPIP5K2), Protein phosphatase 3 regulatory subunit B, alpha (PPP3R1), Palmitoyl-protein thioesterase 1 (PPT1), Ras-related GTP-binding protein (RRAGD), Sphingomyelin phosphodiesterase 1 (SMPD1), TSC complex subunit 2 (TSC2)	16
	42	Acyl-CoA synthetase long chain family member 3 (ACSL3), Very-long-chain (3R)-3-hydroxyacyl-CoA dehydratase (HACD3), Hydroxysteroid 17-beta dehydrogenase 7 (HSD17B7), 3-dehydrosphinganine reductase (KDSR), Lysophosphatidylcholine acyltransferase 1 (LPCAT1), Terpene cyclase/mutase family member (LSS), NAD (P) dependent steroid dehydrogenase-like (NSDHL), CDP-diacylglycerol--glycerol-3-phosphate 3-phosphatidyltransferase (PGS1), Perilipin (PLIN2), Patatin like phospholipase domain containing 7 (PNPLA7), non-specific serine/threonine protein kinase (ROCK1), Sphingosine-1-phosphate lyase 1 (SGPL1)	12
	43	Acetyl-CoA acetyltransferase 2 (ACAT2), V-type proton ATPase subunit H (ATP6V1H), Inhibitor of nuclear factor kappa-B kinase subunit alpha (CHUK), Diacylglycerol kinase (DGKQ), Glycerophosphocholine phosphodiesterase 1 (GPCPD1), IkappaB kinase (IKBKB), Inositol polyphosphate-1-phosphatase (INPP1), KRAS proto-oncogene, GTPase (KRAS), Phosphatidylinositol 4-kinase type 2 (PI4K2A), SAC1 like phosphatidylinositide phosphatase (SACM1L)	10
	49	Calcium binding protein 39 (CAB39), calcium/calmodulin-dependent protein kinase (CAMK2D), C-terminal binding protein 1 (CTBP1), Eukaryotic translation initiation factor 4E (EIF4E), Hydroxyacylglutathione hydrolase (HAGH), Stress-activated protein kinase JNK (MAPK8), Mitochondrial trans-2-enoyl-CoA reductase (MECR), Phosphatidylinositol 3-kinase regulatory subunit alpha (PIK3R1), Phosphatidylinositol-5-phosphate 4-kinase type 2 alpha (PIP4K2A), Phosphoinositide phospholipase C (PLCD1), Phosphatidylinositol 3,4,5-trisphosphate 3-phosphatase and dual-specificity protein phosphatase PTEN (PTEN), Rac family small GTPase 1 (RAC1), Rho-associated protein kinase (ROCK2)	13

10.3389/fvets.2025.1544718

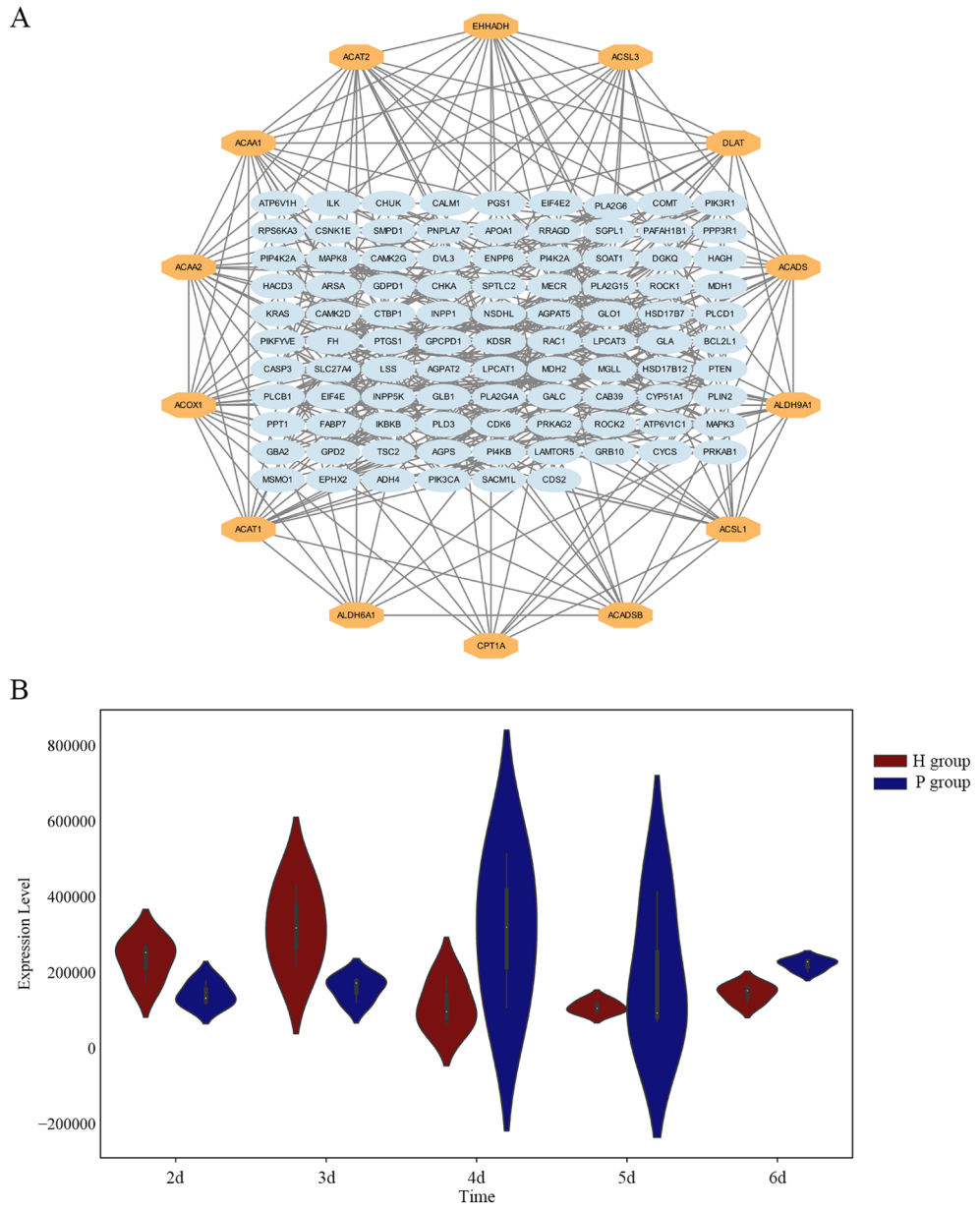

FIGURE 5
Screening of key proteins. **(A)** Protein–protein interaction (PPI) network analysis for DEPs, the 14 proteins in the outer circle are the hub proteins. **(B)** The violin plot illustrates the distribution of ACSL3 protein expression levels. Across the five time points, ACSL3 protein expression levels show significant differences between H and P groups.

protein (RRAGD), and Sphingomyelin phosphodiesterase 1 (SMPD1), a total of nine DEPs showed an upward trend in both the H and P groups.

3.6 Protein–protein interaction (PPI) network analysis

A protein–protein interaction (PPI) network was constructed using the network visualization resource STRING for 119 DEPs, as shown in Figure 5A. Fourteen key proteins were screened, including Long-chain acyl-CoA synthetases family members (ACSL1, ACSL3), Acetyl-CoA acetyltransferase (ACAT1, ACAT2), Acetyl-CoA acyltransferase (ACAA1, ACAA2), Carnitine O-acyltransferase CPT1 (CPT1A), Acyl-CoA oxidase (ACOX1), Short-chain acyl-CoA dehydrogenase (ACADS, ACADSB), Aldehyde dehydrogenase family members (ALDH6A1, ALDH9A1), Enoyl-CoA hydratase (EHHADH), and Dihydrolipoamide acetyltransferase (DLAT). 12 of these proteins were involved in the fatty acid degradation process, suggesting that fatty acid degradation plays a key role in lipid metabolism in hierarchical follicles and pre-hierarchical follicles. ACSL3 is a key rate-limiting protein in fatty acid degradation and is a repeatedly identified LD protein. In this study, ACSL3 was differentially expressed in both phases (Figure 5B), and there was a highly significant difference in ACSL3 expression at 6 d of cell culture.

4 Discussion

The development of avian follicles follows a strict hierarchy. During the progression from pre-hierarchical follicles to hierarchical follicles, there is a gradual deposition of yolk precursors (primarily lipids) within the follicles. Cellular neutral lipids are stored in the form of LDs, which may play a more significant role in the development of goose follicles. LDs have been reported to be associated with follicular development, with the size and number of LDs changing as the follicle grows, total intracellular lipid content also increases gradually with follicular growth (35–37). In geese, differences in the morphology and lipid content of LDs have been reported in hierarchical and pre-hierarchical granulosa cells (13). In the present study, we found highly significant differences in LDs in granulosa cells of goose follicles at different stages of development. The content of LDs was significantly higher in hierarchical granulosa cells than in pre-hierarchical granulosa cells, and hierarchical granulosa cells tended to synthesize large LDs, whereas pre-hierarchical granulosa cells tended to form smaller LDs. The content of LDs in hierarchical granulosa cells gradually increased with increasing culture time, reaching a maximum after 5 d of cell culture and then decreasing. These findings are consistent with previous reports.

The functions of LDs are primarily carried out by LDAPs, and previous studies have identified hundreds of these proteins within LDs. In this study, we found a large number of enzymes involved in lipid synthesis processes, such as FASN, ACSFs, ACSLs, DGKs, and MSMO1, these enzymes are found in both hierarchical granulosa cells and pre-hierarchical granulosa cells. This also suggests an important role for LD lipid metabolism in granulosa cells. FASN is a key enzyme in fatty acid synthesis in mammals, with mRNA and protein expression observed in rat, bovine, and human granulosa cells (38). Previous studies have identified FASN in the granulosa layer of the goose small white follicle and small yellow follicle by using transcriptome sequencing (39). ACSF, an isoenzyme of ACS, has been shown to be involved in fatty acid and cholesterol synthesis (40) and is associated with egg production in poultry (41, 42). Long-chain acyl-coenzyme A synthases (ACSLs) are key enzymes in the regulation of lipid metabolism, including fatty acid elongation, oxidative decomposition, and phospholipid generation (43). ACSL3 localizes to LDs and promotes their biogenesis (44). We also previously identified ACSL3 mRNA expression in the granulosa cells of goose hierarchical follicles (45). Diacylglycerol kinase (DGK) is a lipid kinase converting diacylglycerol (DAG) to phosphatidic acid (PA) and can be involved in various cellular responses by regulating balance of the two lipid messengers (46). Expression of DGK protein has been found in both the ovary and uterus of mice, suggesting a role for DGK in the maturation of mouse oocytes (47). MSMO1 gene encodes an enzyme involved in cholesterol biosynthesis. Cholesterol and intermediates in its biosynthetic pathway are required for many developmental processes including membrane biosynthesis, steroid biosynthesis, and adipogenesis (48). DEPs mentioned above were involved in the fatty acid synthesis process, confirming that both goose hierarchical follicles and pre-hierarchical follicles have fatty acid synthesis function (14), and that there are some differences in the lipid synthesis process between hierarchical follicles and pre-hierarchical follicles. These DEPs may influence goose follicle development by regulating lipid synthesis in LDs, which in turn modulates cellular lipid metabolism.

In addition to enzymes involved in lipid metabolism, LDs are also enriched with various other proteins that participate in multiple cellular life activities. This study identified differential proteins associated with steroid hormone secretion and cell proliferation and apoptosis in both hierarchical and pre-hierarchical granulosa cells. These differential proteins may influence follicular development by regulating steroid hormone secretion, cell proliferation, and apoptosis.

Avian follicles exhibit a unique hierarchical development, where small pre-hierarchical follicles are unable to synthesize active steroid hormones using steroids as substrate, and steroid hormone secretion occurs only in the hierarchical granulosa cells. Among the top 20 up-regulated DEPs in this study, NPC2 is an intracellular cholesterol transporter protein, which has the intracellular activity of extracting cholesterol from low-density lipoproteins (LDL) and delivering it to membrane-bound NPC1, which cooperates with downstream proteins to transport cholesterol throughout the cell to fulfill its biological function (49). Previous research on chicken small yellow and large yellow follicles revealed a six-fold upregulation of NPC2 mRNA expression (50). Similarly, our study found significant upregulation of NPC2 protein at all five time points in both H and P groups. MGLL, a member of the serine hydrolase superfamily, is localized to LDs and plays a key role in breaking down monoacylglycerol into free fatty acids and glycerol (47). It also hydrolyzes 2-arachidonoylglycerol (2-AG) to arachidonic acid (AA). Additionally, RDH10 is also localized in LDs and binds to their surface during acyl ester biosynthesis (49). We hypothesized that lipids in the LDs of hierarchical follicles are degraded by hydrolytic enzymes, such as MGLL. The degradation product, cholesterol, is then transported by transporter enzymes, which are involved in the process of steroid hormone secretion. This hypothesis confirms the differences in steroid hormone secretion between avian hierarchical follicles and pre-hierarchical follicles. Granulosa cells promote cholesterol biosynthesis and hydrolysis through different enzymes, ensuring a steady supply of cholesterol for steroidogenesis, reflecting their ability to respond to hormonal signals and provide energy for follicular development. Among the down-regulated top 20 DEPs, we identified several proteins related to the cytoskeleton and structure, such as NEFL, FLNC, LSP1, PGM5. The movement of LDs is primarily driven by associated proteins such as the cytoskeleton, suggesting that in hierarchical follicles, the reduced expression of these proteins may lead to decreased movement of LDs and reduced contact with other organelles. Our findings align with the observed differences in lipid metabolism and steroid hormone secretion between hierarchical and pre-hierarchical follicles.

With increasing incubation time, we found that the expression of certain proteins showed a continuous upward trend, among which CAMK2G, RRAGD, SMPD1 and PPIP5K2 were closely related to cell proliferation and apoptosis, potentially playing essential roles in the development of goose follicles. Intracellular calcium ions regulate steroidogenesis in both the testis and the

ovary, whereas CAMK2G, which is involved in the calcium signaling pathway, regulates apoptosis and also acts as a regulator of cell adhesion, proliferation, and survival (51). Its expression has been detected in the ovaries of mice, goats, and pigs (52, 53). CAMK2G is known to control oocyte activation by restoring the cell cycle in mouse oocytes (54, 55). RRAGD mediates amino acid stimulation of the mTOR signaling pathway, a crucial pathway for cell growth and proliferation (56). SMPD1 protects human luteinizing granulosa cells from apoptosis and plays a vital role in initiating female germ cell death signaling (57). PPIP5K2 is highly expressed in colorectal cancer (CRC) and enhances the proliferation and migration abilities of CRC cells (58). These DEPs showed a progressive increase in protein expression with time in H and P groups and were significant findings in STEM analysis, which may be important for follicular development. We propose that these DEPs may play similar roles in avian species, further affecting goose follicle development by controlling a range of life activities such as granulosa cells proliferation and apoptosis.

Finally, we performed PPI network analysis and identified 14 candidate key proteins that may regulate lipid metabolism in granulosa cells. After pathway analysis, we found that 12 of these proteins were involved in the fatty acid degradation process, and therefore hypothesized that the fatty acid degradation pathway might be an important contributor to the differences in LDs of granulosa cells at different developmental stages. Fatty acid oxidation (FAO) is the main pathway for fatty acid degradation, and CPT1A is the key rate-limiting enzyme in FAO. It has been reported that knockdown of CPT1A induces lipid differentiation in chicken adipocytes, inhibits the β-oxidation process, and promotes the formation of LDs (59). The ACAA gene encodes an enzyme of the thiolase family, and in sheep preadipocytes, overexpression of ACAA1 reduced cellular lipid accumulation and triglyceride content (60), while lack of ACAA2 expression may also lead to reduced LD formation (61). ACAA1 and ACAA2 can be involved in fatty acid elongation and degradation by catalyzing the final step of the β-oxidation pathway and are therefore essential for energy production and lipid metabolism (62). In addition, ACOX1, EHHADH, and ACAD are enzymes involved in the fatty acid β-oxidation pathway. One of the main functions of LDs is to produce energy through the fatty acid β-oxidation pathway by oxidizing free fatty acids. Mitosis is prevalent in pre-hierarchical granulosa cells and requires large amounts of energy to supply the metabolism of these cells. It can be speculated that in pre-hierarchical granulosa cells, fatty acids are oxidized and used primarily to generate energy for autotrophic requirements rather than synthesizing LDs.

ACSLs are a group of rate-limiting enzymes in fatty acid metabolism. They are essential for the activation of long chain fatty acids (LCFA). Once esterified by ACSL, LCFAs can enter various metabolic pathways, including cellular fatty acid catabolism, phospholipid synthesis, TG synthesis and CE synthesis. The mammalian ACSLs family contains five members, including ACSL1, ACSL3, ACSL4, ACSL5, and ACSL6. ACSL1 promotes fatty acids uptake and free fatty acids deposition, also affecting TG levels through the PPARγ pathway (63). ACSL3, frequently identified as an abundant LDAP (64). Intracellularly, ACSL3 is predominantly distributed in the periphery of LDs and on the cytoplasmic surface of the endoplasmic reticulum (44). ACSL3 is a key enzyme for LD biogenesis that redistributes from the endoplasmic reticulum to LDs during LD formation, and this localization mechanism of ACSL3 is associated with Rab18 and PLIN2. Rab18 interacts with PLIN2 and forms a complex with ACSL3, promotes the localization of ACSL3 on the surface of nascent LDs, thereby increasing the content of intracellular LDs (65). Addition of oleic acid (OA) to human hepatocyte medium enhances intracellular LD accumulation, accompanied by increased ACSL3 expression, while ACSL inhibitors Triacsin C reduce LD content, indicating that ACSL is involved in neutral lipid synthesis and LD formation (66). Recently, it was found that ACSL3 not only regulates the biogenesis of LDs in cells, but also decreases the susceptibility of cells to ferroptosis (67). In conclusion, ACSL3 is involved in intracellular lipid metabolism by promoting the formation and maturation of LDs. Expression of ACSL3mRNA is currently detected in granulosa cells from humans (1), bovine (68), goose (45). Recent evidence suggests that ACSL3 is important in maintaining the channeling of extracellularly-derived lipids to FAO (69). In our study, ACSL3 protein was expressed in both hierarchical follicles and pre-hierarchical follicles, and protein expression changed with time. In pre-hierarchical follicles, lipid metabolism in granulosa cells primarily focuses on maintaining cellular structure and basal metabolism. During this phase, granulosa cells exhibit weak lipid synthesis capacity, limited lipid accumulation, and low activity of lipid metabolism-related enzymes. The main functions of lipids are to construct cell membranes and provide energy. In contrast, lipid metabolism in granulosa cells of hierarchical follicles is significantly enhanced, particularly in the synthesis and accumulation of yolk precursor substances, to meet the demands of yolk formation and rapid follicular development. During this phase, the activity of lipid synthesis-related enzymes is markedly increased, and lipids accumulate extensively in the form of TG and CE. Therefore, we hypothesize that in goose hierarchical follicular granulosa cells, most of the fatty acids activated by ACSL3 are utilized for the synthesis of TG and CE, which further contribute to the formation of LDs, ultimately leading to differences in lipid deposition.

5 Conclusion

In conclusion, we observed significantly higher levels of LDs in hierarchical granulosa cells than in pre-hierarchical granulosa cells. Moreover, the content of LDs in granulosa cells at different developmental stages underwent dynamic changes with the extension of cell culture time. Importantly, this study marks the first proteomic analysis of LDs in goose follicle granulosa cells, offering detailed insights into the primary components of LDAPs. These foundational data serve as a valuable reference for future investigations into LDs in geese. Furthermore, we identified ACSL3, a crucial regulator of lipid metabolism in granulosa cells, and hypothesize that ACSL3 acts as a pivotal modulator of lipid variations in granulosa cells across different developmental stages. Specifically, in pre-hierarchical granulosa cells, fatty acids activated by ACSL3 are primarily oxidized and enter the TCA cycle to meet the energy demands of the cells. In contrast, in hierarchical granulosa cells, fatty acids activated by ACSL3 are utilized for the synthesis of TG and CE, further promoting the formation of LDs. This process leads to a significant increase in lipid deposition within hierarchical granulosa cells (Figure 6). However, the precise regulatory mechanisms underlying these processes remain to be elucidated (70).

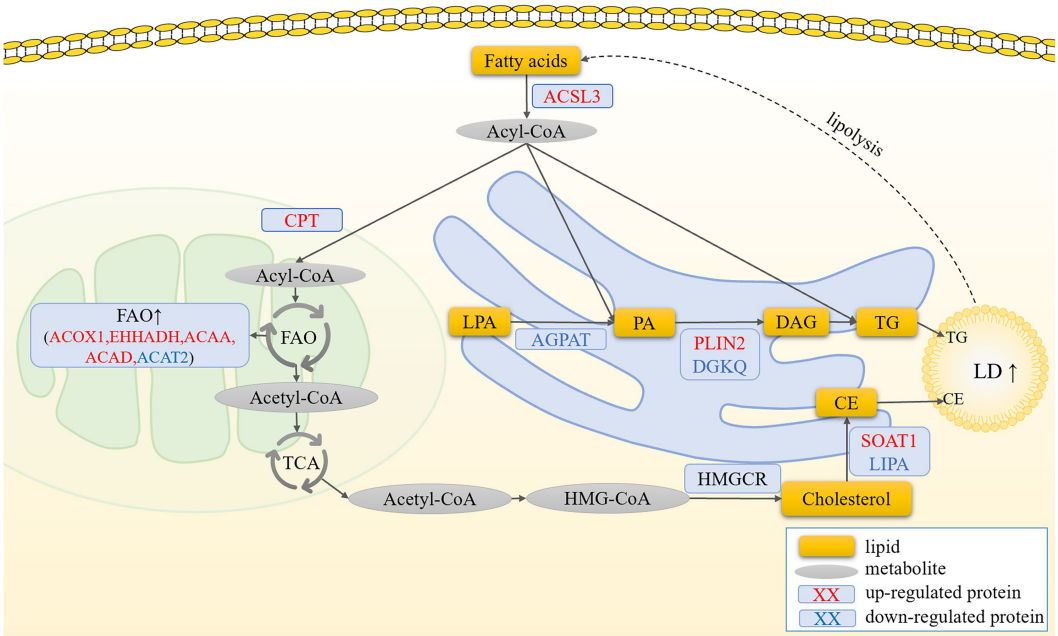

FIGURE 6
Prediction of the molecular mechanism by which ACSL3 regulates the synthesis of LDs in granulosa cells. In pre-hierarchical granulosa cells, fatty acids activated by ACSL3 are oxidized and enter the TCA cycle to meet the cells' energy demands. In contrast, in hierarchical granulosa cells, fatty acids activated by ACSL3 promote lipid droplet formation through the synthesis of TG and CE, leading to a significant increase in intracellular lipid deposition.

Data availability statement

The mass spectrometry proteomics data have been deposited in the ProteomeXchange Consortium through the PRIDE partner repository with the dataset identifier PXD061272.

Ethics statement

The animal study was approved by Approval for this research was granted by the Institutional Animal Care and Use Committee (IACUC) of Sichuan Agricultural University (Chengdu campus, Sichuan, China, Permit No. DKY20170913). The study was conducted in accordance with the local legislation and institutional requirements.

Author contributions

XY: Conceptualization, Funding acquisition, Writing – review & editing. XZ: Validation, Writing – original draft. YL: Validation, Writing – original draft. HX: Formal analysis, Visualization, Writing – original draft. ZW: Formal analysis, Visualization, Writing – original draft. XH: Formal analysis, Visualization, Writing – original draft. SH: Methodology, Supervision, Writing – original draft. LiaL: Methodology, Supervision, Writing – review & editing. HL: Data curation, Software, Writing – review & editing. HH: Data curation, Software, Writing – review & editing. CH: Data curation, Software, Writing – review & editing. XG: Investigation, Resources, Writing – review & editing. LinL: Methodology, Supervision, Writing – review & editing. LX: Methodology, Supervision, Writing – review & editing. JH: Conceptualization, Formal analysis, Writing – review & editing. JW: Conceptualization, Funding acquisition, Writing – review & editing.

Funding

The author(s) declare that financial support was received for the research and/or publication of this article. This study was financially supported by the National Natural Science Foundation of China (Grant Number: 32202676), the Guangxi Natural Science Foundation (Grant Number: 2022GXNSFBA035582), the Program for Waterfowl Industry Technology System Innovation Team of Sichuan Province (Project Number: SCCXTD-2024-25), the Innovation and Demonstration Project of Industry-Education Integration in Feed Industrial Chain Transformation and Upgrading of Sichuan Province (Project Number: 2212129406), the National Key R&D Program of China (Project Number: 2023YFD1300304), and another National Natural Science Foundation of China Grant (Grant Number: 32272882).

Conflict of interest

The authors declare that the research was conducted in the absence of any commercial or financial relationships that could be construed as a potential conflict of interest.

Generative AI statement

The author(s) declare that no Gen AI was used in the creation of this manuscript.

Publisher's note

Supplementary material

The Supplementary material for this article can be found online at: https://www.frontiersin.org/articles/10.3389/fvets.2025.1544718/full#supplementary-material

SUPPLEMENTARY FIGURE S1
The top 20 most significantly enriched GO terms and KEGG pathways.

SUPPLEMENTARY TABLE S1
Functional classification of DEPs.

SUPPLEMENTARY TABLE S2
The top 20 up and down-regulated proteins at five time points.

SUPPLEMENTARY TABLE S3
The GO terms and KEGG pathways at five time points.

References

1. Liu T, Qu J, Tian M, Yang R, Song X, Li R, et al. Lipid metabolic process involved in oocyte maturation during Folliculogenesis. *Front Cell Dev Biol*. (2022) 10:806890. doi: 10.3389/fcell.2022.806890

2. Eppig JJ, Wigglesworth K, Pendola FL. The mammalian oocyte orchestrates the rate of ovarian follicular development. *Proc Natl Acad Sci USA*. (2002) 99:2890–4. doi: 10.1073/pnas.052658699

3. Eppig JJ. Oocyte control of ovarian follicular development and function in mammals. *Reproduction*. (2001) 122:829–38. doi: 10.1530/rep.0.1220829

4. Zhu G, Fang C, Li J, Mo C, Wang Y, Li J. Transcriptomic diversification of granulosa cells during follicular development in chicken. *Sci Rep*. (2019) 9:5462. doi: 10.1038/s41598-019-41132-1

5. Yang S, Chen J, Ma B, Wang J, Chen J. Role of autophagy in Lysophosphatidylcholine-induced apoptosis of mouse ovarian granulosa cells. *Int J Mol Sci*. (2022) 23:1479. doi: 10.3390/ijms23031479

6. Chen Z, Lei L, Wen D, Yang L. Melatonin attenuates palmitic acid-induced mouse granulosa cells apoptosis via endoplasmic reticulum stress. *J Ovarian Res*. (2019) 12:43. doi: 10.1186/s13048-019-0519-z

7. Zhou X, Mo Z, Li Y, Huang L, Yu S, Ge L, et al. Oleic acid reduces steroidogenesis by changing the lipid type stored in lipid droplets of ovarian granulosa cells. *J Anim Sci Biotechnol*. (2022) 13:27. doi: 10.1186/s40104-021-00660-5

8. Zhang N, Wang L, Luo G, Tang X, Ma L, Zheng Y, et al. Arachidonic acid regulation of intracellular signaling pathways and target gene expression in bovine ovarian granulosa cells. *Animals*. (2019) 9:374. doi: 10.3390/ani9060374

9. Tu J, Chen Y, Li Z, Yang H, Chen H, Yu Z. Long non-coding RNAs in ovarian granulosa cells. *J Ovarian Res*. (2020) 13:63. doi: 10.1186/s13048-020-00663-2

10. Li L, Shi X, Shi Y, Wang Z. The signaling pathways involved in ovarian follicle development. *Front Physiol*. (2021) 12:730196. doi: 10.3389/fphys.2021.730196

11. Yao J, Ma Y, Lin X, Zhou S, Mi Y, Zhang C. The attenuating effect of the intraovarian bone morphogenetic protein 4 on age-related endoplasmic reticulum stress in chicken follicular cells. *Oxidative Med Cell Longev*. (2020) 2020:4175613. doi: 10.1155/2020/4175613

12. Gan X, Wang Y, Gao S, Chen X, Hu S, Wang J, et al. Exploration of the effects of goose TCs on GCs at different follicular stages using a co-culture model. *Biosci Rep*. (2020) 40:BSR20200445. doi: 10.1042/BSR20200445

13. Gao S, Gan X, He H, Hu S, Deng Y, Chen X, et al. Dynamic characteristics of lipid metabolism in cultured granulosa cells from geese follicles at different developmental stages. *Biosci Rep*. (2019) 39:BSR20192188. doi: 10.1042/BSR20192188

14. Wen R, Gan X, Hu S, Gao S, Deng Y, Qiu J, et al. Evidence for the existence of de novo lipogenesis in goose granulosa cells. *Poult Sci*. (2019) 98:1023–30. doi: 10.3382/ps/pey400

15. Yuan X, Hu S, Li L, Han C, Liu H, He H, et al. Lipidomics profiling of goose granulosa cell model of stearoyl-CoA desaturase function identifies a pattern of lipid droplets associated with follicle development. *Cell Biosci*. (2021) 11:95. doi: 10.1186/s13578-021-00604-6

16. Walther TC, Farese RV Jr. Lipid droplets and cellular lipid metabolism. *Annu Rev Biochem*. (2012) 81:687–714. doi: 10.1146/annurev-biochem-061009-102430

17. Farese RV Jr, Walther TC. Lipid droplets finally get a little R-E-S-P-E-C-T. *Cell*. (2009) 139:855–60. doi: 10.1016/j.cell.2009.11.005

18. Henne WM, Reese ML, Goodman JM. The assembly of lipid droplets and their roles in challenged cells. *EMBO J*. (2018) 37:e98947. doi: 10.15252/embj.201898947

19. Liu P, Ying Y, Zhao Y, Mundy DI, Zhu M, Anderson RG. Chinese hamster ovary K2 cell lipid droplets appear to be metabolic organelles involved in membrane traffic. *J Biol Chem*. (2004) 279:3787–92. doi: 10.1074/jbc.M311945200

20. Bartz R, Li WH, Venables B, Zehmer JK, Roth MR, Welti R, et al. Lipidomics reveals that adiposomes store ether lipids and mediate phospholipid traffic. *J Lipid Res*. (2007) 48:837–47. doi: 10.1194/jlr.M600413-JLR200

21. Li Z, Thiel K, Thul PJ, Beller M, Kühnlein RP, Welte MA. Lipid droplets control the maternal histone supply of Drosophila embryos. *Curr Biol*. (2012) 22:2104–13. doi: 10.1016/j.cub.2012.09.018

22. Klemm EJ, Spooner E, Ploegh HL. Dual role of ancient ubiquitous protein 1 (AUP1) in lipid droplet accumulation and endoplasmic reticulum (ER) protein quality control. *J Biol Chem*. (2011) 286:37602–14. doi: 10.1074/jbc.M111.284794

23. Saka HA, Thompson JW, Chen YS, Dubois LG, Haas JT, Moseley A, et al. *Chlamydia trachomatis* infection leads to defined alterations to the lipid droplet proteome in epithelial cells. *PLoS One*. (2015) 10:e0124630. doi: 10.1371/journal.pone.0124630

24. Khor VK, Ahrends R, Lin Y, Shen WJ, Adams CM, Roseman AN, et al. The proteome of cholesteryl-ester-enriched versus triacylglycerol-enriched lipid droplets. *PLoS One*. (2014) 9:e105047. doi: 10.1371/journal.pone.0105047

25. Mirza AH, Cui L, Zhang S, Liu P. Comparative proteomics reveals that lipid droplet-anchored mitochondria are more sensitive to cold in brown adipocytes. *Biochim Biophys Acta Mol Cell Biol Lipids*. (2021) 1866:158992. doi: 10.1016/j.bbalip.2021.158992

26. Tian JJ, Zhang JM, Yu EM, Sun JH, Xia Y, Zhang K, et al. Identification and analysis of lipid droplet-related proteome in the adipose tissue of grass carp (*Ctenopharyngodon idella*) under fed and starved conditions. *Comp Biochem Physiol Part D Genomics Proteomics*. (2020) 36:100710. doi: 10.1016/j.cbd.2020.100710

27. Sun Y, Heng J, Liu F, Zhang S, Liu P. Isolation and proteomic study of fish liver lipid droplets. *Biophys Rep*. (2023) 9:120–33. doi: 10.52601/bpr.2023.230004

28. Bersuker K, Peterson CWH, M. ToSahl SJ, Savikhin V, Grossman EA, et al. A proximity labeling strategy provides insights into the composition and dynamics of lipid droplet proteomes. *Dev Cell*. (2018) 44:97–112.e7. doi: 10.1016/j.devcel.2017.11.020

29. Tsai TH, Chen E, Li L, Saha P, Lee HJ, Huang LS, et al. The constitutive lipid droplet protein PLIN2 regulates autophagy in liver. *Autophagy*. (2017) 13:1130–44. doi: 10.1080/15548627.2017.1319544

30. Poppelreuther M, Rudolph B, Du C, Großmann R, Becker M, Thiele C, et al. The N-terminal region of acyl-CoA synthetase 3 is essential for both the localization on lipid droplets and the function in fatty acid uptake. *J Lipid Res*. (2012) 53:888–900. doi: 10.1194/jlr.M024562

31. Sathyanarayan A, Mashek MT, Mashek DG. ATGL promotes autophagy/Lipophagy via SIRT1 to control hepatic lipid droplet catabolism. *Cell Rep*. (2017) 19:1–9. doi: 10.1016/j.celrep.2017.03.026

32. Bell DJ, Freeman BM. Physiology and biochemistry of the domestic fowl, Volume 5. Cambridge: Academic Press (1971).

33. Gilbert AB, Evans AJ, Perry MM, Davidson MH. A method for separating the granulosa cells, the basal lamina and the theca of the preovulatory ovarian follicle of the domestic fowl (Gallus domesticus). *J Reprod Fertil*. (1977) 50:179–81. doi: 10.1530/jrf.0.0500179

34. Gan X, Chen D, Deng Y, Yuan J, Kang B, Qiu J, et al. Establishment of an in vitro culture model of theca cells from hierarchical follicles in ducks. *Biosci Rep*. (2017) 37:BSR20160491. doi: 10.1042/BSR20160491

35. Silva RC, Báo SN, Jivago JL, Lucci CM. Ultrastructural characterization of porcine oocytes and adjacent follicular cells during follicle development: lipid component evolution. *Theriogenology*. (2011) 76:1647–57. doi: 10.1016/j.theriogenology.2011.06.029

36. Dadarwal D, Adams GP, Hyttel P, Brogliatti GM, Caldwell S, Singh J. Organelle reorganization in bovine oocytes during dominant follicle growth and regression. *Reprod Biol Endocrinol*. (2015) 13:124. doi: 10.1186/s12958-015-0122-0

37. Sturmey RG, O'Toole PJ, Leese HJ. Fluorescence resonance energy transfer analysis of mitochondrial:lipid association in the porcine oocyte. *Reproduction*. (2006) 132:829–37. doi: 10.1530/REP-06-0073

38. Elis S, Desmarchais A, Maillard V, Uzbekova S, Monget P, Dupont J. Cell proliferation and progesterone synthesis depend on lipid metabolism in bovine granulosa cells. *Theriogenology*. (2015) 83:840–53. doi: 10.1016/j.theriogenology.2014.11.019

39. Liu H, Zhang W, Li Q, Liu J, Zhang T, Zhou T, et al. The comprehensive mechanisms underlying nonhierarchical follicular development in geese (*Anser cygnoides*). *Anim Reprod Sci*. (2015) 159:131–40. doi: 10.1016/j.anireprosci.2015.06.007

40. Yamasaki M, Hasegawa S, Suzuki H, Hidai K, Saitoh Y, Fukui T. Acetoacetyl-CoA synthetase gene is abundant in rat adipose, and related with fatty acid synthesis in mature adipocytes. *Biochem Biophys Res Commun*. (2005) 335:215–9. doi: 10.1016/j.bbrc.2005.07.053

41. Yu S, Wei W, Xia M, Jiang Z, He D, Li Z, et al. Molecular characterization, alternative splicing and expression analysis of ACSF2 and its correlation with egg-laying performance in geese. *Anim Genet*. (2016) 47:451–62. doi: 10.1111/age.12435

42. Tian W, Zheng H, Yang L, Li H, Tian Y, Wang Y, et al. Dynamic expression profile, regulatory mechanism and correlation with egg-laying performance of ACSF gene family in chicken (*Gallus gallus*). *Sci Rep*. (2018) 8:8457. doi: 10.1038/s41598-018-26903-6

43. Ellis JM, Li LO, Wu PC, Koves TR, Ilkayeva O, Stevens RD, et al. Adipose acyl-CoA synthetase-1 directs fatty acids toward beta-oxidation and is required for cold thermogenesis. *Cell Metab*. (2010) 12:53–64. doi: 10.1016/j.cmet.2010.05.012

44. Kassan A, Herms A, Fernández-Vidal A, Bosch M, Schieber NL, Reddy BJ, et al. Acyl-CoA synthetase 3 promotes lipid droplet biogenesis in ER microdomains. *J Cell Biol*. (2013) 203:985–1001. doi: 10.1083/jcb.201305142

45. Ran M, Hu S, Ouyang Q, Xie H, Zhang X, Lin Y, et al. miR-202-5p inhibits lipid metabolism and steroidogenesis of goose hierarchical granulosa cells by targeting ACSL3. *Animals*. (2023) 13:325. doi: 10.3390/ani13030325

46. Shirai Y, Saito N. Diacylglycerol kinase as a possible therapeutic target for neuronal diseases. *J Biomed Sci*. (2014) 21:28. doi: 10.1186/1423-0127-21-28

47. Shionoya T, Usuki T, Komenoi S, Isozaki T, Sakai H, Sakane F. Distinct expression and localization of the type II diacylglycerol kinase isozymes δ, η and κ in the mouse reproductive organs. *BMC Dev Biol*. (2015) 15:6. doi: 10.1186/s12861-015-0055-z

48. Simigdala N, Gao Q, Pancholi S, Roberg-Larsen H, Zvelebil M, Ribas R, et al. Cholesterol biosynthesis pathway as a novel mechanism of resistance to estrogen deprivation in estrogen receptor-positive breast cancer. *Breast Cancer Res*. (2016) 18:58. doi: 10.1186/s13058-016-0713-5

49. Grimsey N, Han GS, O'Hara L, Rochford JJ, Carman GM, Siniossoglou S. Temporal and spatial regulation of the phosphatidate phosphatases lipin 1 and 2. *J Biol Chem*. (2008) 283:29166–74. doi: 10.1074/jbc.M804278200

50. Brindley DN, Pilquil C, Sariahmetoglu M, Reue K. Phosphatidate degradation: phosphatidate phosphatases (lipins) and lipid phosphate phosphatases. *Biochim Biophys Acta*. (2009) 1791:956–61. doi: 10.1016/j.bbalip.2009.02.007

51. Zhang C, Wang R, Chen W, Kang X, Huang Y, Walker R, et al. Gene structure and spatio-temporal expression of chicken LPIN2. *Mol Biol Rep*. (2014) 41:4081–91. doi: 10.1007/s11033-014-3278-3

52. Panizza E, Zhang L, Fontana JM, Hamada K, Svensson D, Akkuratov EE, et al. Ouabain-regulated phosphoproteome reveals molecular mechanisms for Na(+), K(+)-ATPase control of cell adhesion, proliferation, and survival. *FASEB J*. (2019) 33:10193–206. doi: 10.1096/fj.201900445R

53. Liu Y, Zhou Z, He X, Tao L, Jiang Y, Lan R, et al. Integrated analyses of miRNA-mRNA expression profiles of ovaries reveal the crucial interaction networks that regulate the prolificacy of goats in the follicular phase. *BMC Genomics*. (2021) 22:812. doi: 10.1186/s12864-021-08156-2

54. Seals RC, Urban RJ, Sekar N, Veldhuis JD. Up-regulation of basal transcriptional activity of the cytochrome P450 cholesterol side-chain cleavage (CYP11A) gene by isoform-specific calcium-calmodulin-dependent protein kinase in primary cultures of ovarian granulosa cells. *Endocrinology*. (2004) 145:5616–22. doi: 10.1210/en.2003-1528

55. Backs J, Stein P, Backs T, Duncan FE, Grueter CE, McAnally J, et al. The gamma isoform of CaM kinase II controls mouse egg activation by regulating cell cycle resumption. *Proc Natl Acad Sci USA*. (2010) 107:81–6. doi: 10.1073/pnas.0912658106

56. Medvedev S, Stein P, Schultz RM. Specificity of calcium/calmodulin-dependent protein kinases in mouse egg activation. *Cell Cycle*. (2014) 13:1482–8. doi: 10.4161/cc.28432

57. Di Malta C, Siciliano D, Calcagni A, Monfregola J, Punzi S, Pastore N, et al. Transcriptional activation of RagD GTPase controls mTORC1 and promotes cancer growth. *Science*. (2017) 356:1188–92. doi: 10.1126/science.aag2553

58. Gao J, Zhang RL, Zhou CQ, Ma Y, Zhuang GL. RNA interference targeting of sphingomyelin phosphodiesterase 1 protects human granulosa cells from apoptosis. *J Obstet Gynaecol Res*. (2009) 35:421–8. doi: 10.1111/j.1447-0756.2008.00974.x

59. Li ZQ, Li JJ, Lin ZZ, Zhang DH, Zhang GF, Ran JS, et al. Knockdown of CPT1A induce chicken adipocyte differentiation to form lipid droplets. *Brazilian J Poultry Sci*. (2022) 24. doi: 10.1590/1806-9061-2021-1589

60. Wang Y, Li X, Cao Y, Xiao C, Liu Y, Jin H, et al. Effect of the ACAA1 gene on Preadipocyte differentiation in sheep. *Front Genet*. (2021) 12:649140. doi: 10.3389/fgene.2021.649140

61. Zhang Y, Wang Y, Wang X, Ji Y, Cheng S, Wang M, et al. Acetyl-coenzyme a acyltransferase 2 promote the differentiation of sheep precursor adipocytes into adipocytes. *J Cell Biochem*. (2019) 120:8021–31. doi: 10.1002/jcb.28080

62. Miltiadou D, Hager-Theodorides AL, Symeou S, Constantinou C, Psifidi A, Banos G, et al. Variants in the 3′ untranslated region of the ovine acetyl-coenzyme a acyltransferase 2 gene are associated with dairy traits and exhibit differential allelic expression. *J Dairy Sci*. (2017) 100:6285–97. doi: 10.3168/jds.2016-12326

63. Ma Z, Huang Z, Zhang C, Liu X, Zhang J, Shu H, et al. Hepatic Acat2 overexpression promotes systemic cholesterol metabolism and adipose lipid metabolism in mice. *Diabetologia*. (2023) 66:390–405. doi: 10.1007/s00125-022-05829-9

64. Li T, Li X, Meng H, Chen L, Meng F. ACSL1 affects triglyceride levels through the PPARγ pathway. *Int J Med Sci*. (2020) 17:720–7. doi: 10.7150/ijms.42248

65. Deng Y, Zhou C, Mirza AH, Bamigbade AT, Zhang S, Xu S, et al. Rab18 binds PLIN2 and ACSL3 to mediate lipid droplet dynamics. *Biochim Biophys Acta Mol Cell Biol Lipids*. (2021) 1866:158923. doi: 10.1016/j.bbalip.2021.158923

66. Fujimoto Y, Itabe H, Sakai J, Makita M, Noda J, Mori M, et al. Identification of major proteins in the lipid droplet-enriched fraction isolated from the human hepatocyte cell line HuH7. *Biochim Biophys Acta*. (2004) 1644:47–59. doi: 10.1016/j.bbamcr.2003.10.018

67. Klasson TD, LaGory EL, Zhao H, Huynh SK, Papandreou I, Moon EJ, et al. ACSL3 regulates lipid droplet biogenesis and ferroptosis sensitivity in clear cell renal cell carcinoma. *Cancer Metab*. (2022) 10:14. doi: 10.1186/s40170-022-00290-z

68. Santos PH, Franchi FF, Nunes SG, Fontes PK, Giroto AB, Mani F, et al. Is FSH combined with equine chorionic gonadotropin able to modify lipid metabolism in bovine superstimulated antral follicles? *Anim Reprod*. (2024) 21:e20230063. doi: 10.1590/1984-3143-ar2023-0063

69. Padanad MS, Konstantinidou G, Venkateswaran N, Melegari M, Rindhe S, Mitsche M, et al. DeBerardinis, and P.P. Scaglioni, fatty acid oxidation mediated by acyl-CoA Synthetase long chain 3 is required for mutant KRAS lung tumorigenesis. *Cell Rep*. (2016) 16:1614–28. doi: 10.1016/j.celrep.2016.07.009

70. Perez-Riverol Y, Bandla C, Kundu DJ, Kamatchinathan S, Bai J, Hewapathirana S, et al. The PRIDE database at 20 years: 2025 update. *Nucleic Acids Res*. (2025) 53:D543–d553. doi: 10.1093/nar/gkae1011

frontiers | Frontiers in Veterinary Science

TYPE Original Research
PUBLISHED 31 March 2025
DOI 10.3389/fvets.2025.1538990

OPEN ACCESS

EDITED BY
Manuel Garcia-Herreros,
National Institute for Agricultural and Veterinary Research (INIAV), Portugal

REVIEWED BY
Juan G. Maldonado-Estrada,
University of Antioquia, Colombia
Nélida Rodríguez-Osorio,
Universidad de la República, Uruguay

*CORRESPONDENCE
Yanan Yang
✉ yangyn@gsau.edu.cn
Shengguo Zhao
✉ zhaosg@gsau.edu.cn

RECEIVED 03 December 2024
ACCEPTED 06 March 2025
PUBLISHED 31 March 2025

CITATION
Xi B, An X, Yue Y, Shen H, Han G, Yang Y and Zhao S (2025) Identification and profiling of microRNAs during sheep's testicular development.
Front. Vet. Sci. 12:1538990.
doi: 10.3389/fvets.2025.1538990

Identification and profiling of microRNAs during sheep's testicular development

Binpeng Xi[1], Xuejiao An[2,3], Yaojing Yue[2,3], Haimiao Shen[4], Gaohui Han[5], Yanan Yang[1]* and Shengguo Zhao[1]*

[1]College of Animal Science and Technology, Gansu Agricultural University, Lanzhou, China, [2]Key Laboratory of Animal Genetics and Breeding on the Tibetan Plateau, Ministry of Agriculture and Rural Affairs, Lanzhou Institute of Husbandry and Pharmaceutical Sciences, Chinese Academy of Agricultural Sciences, Lanzhou, China, [3]Sheep Breeding Engineering Technology Research Center of Chinese Academy of Agricultural Sciences, Lanzhou, China, [4]Dongxiang County Mutton Sheep Industry Research Center, Linxia, China, [5]Dongxiang County Animal Husbandry Development Center, Linxia, China

The normal development of the testis is essential for male reproduction, as it is the site of sperm production and a prerequisite for spermatogenesis. MiRNAs play crucial roles in various testicular biological processes, including cell proliferation, spermatogenesis, hormone secretion, metabolism, and reproductive regulation. In this study, we utilized deep sequencing data to analyze the expression patterns of small RNAs in testicular tissues of Southern × Hu sheep F1 hybrids at 0, 3, 6 months, and 1 year of age, thereby exploring the functions of miRNAs in testicular development and spermatogenesis. A total of 787 known miRNAs and 415 novel miRNAs were identified. We identified 217, 254, 405, 130, 305, and 138 DE miRNAs in the testes of M0 vs. M3, M0 vs. M6, M0 vs. Y1, M3 vs. M6, M3 vs. Y1, and M6 vs. Y1, respectively. GO annotation and KEGG pathway analysis of DE miRNA target genes revealed that target genes such as *YAP1*, *ITGB1*, *DOT1L*, *SMAD4*, and *SOX9* may be involved in various biological processes, including reproductive pathways such as FOXO, Hippo, Wnt, cAMP, Rap1, and MAPK signaling pathways. The expression levels of 12 randomly selected miRNAs in testes at 0, 3, 6 months, and 1 year of age were detected by qRT-PCR, and the results were consistent with the sequencing data. This study characterized and investigated the differential expression of miRNAs in sheep testes at different developmental stages using deep sequencing technology. These findings will contribute to a deeper understanding of the functions of miRNAs in regulating testicular development and enhancing reproductive performance in male sheep.

KEYWORDS

testicular development, Southdown × Hu sheep hybrid F1 generation, microRNA, spermatogenesis, small RNA sequencing

Introduction

Hu sheep are mainly produced in Jiaxing and Taihu Lake regions of Zhejiang Province. As a unique breed of multi-parous sheep in our country, Hu sheep has many advantages such as perennial estrus, early sexual maturity, strong adaptability and suitability for crossing (1). The Southdown sheep, a short-wooled meat breed, is characterized by its dense, short, and light fleece, early maturity, ease of fattening, and tender meat, making it a preferred choice for crossbreeding sires (2). The enhancement of animal performance can be achieved through the introduction of breeds for crossbreeding improvement, a widely adopted strategy in animal production. Cross breeding can also combine the excellent characteristics of multiple varieties,

create new characteristics that the original parents do not have, and enhance the vitality of the offspring (3). The Southdown × Hu F1 hybrids enhanced meat quality and increased lambing rates, retaining the high productivity of Hu sheep while inheriting the superior meat yield, quality, and rapid growth traits of Southdown sheep (4). As an important reproductive organ of male animals, the testis is mainly responsible for the production of sperm and androgens (5). Because normal testicular development is essential for breeding, studying testicular development in sheep is crucial for enhancing semen quality and increasing lamb production.

MicroRNA (miRNA) is a non-coding RNA between 18 and 24 nucleotides in length, which controls post-transcriptional gene silencing by interacting with the 3′-untranslated region (3′-UTR) of target mRNA, stimulating mRNA degradation or blocking translation (6). In the past few decades, many studies have investigated miRNA expression profiles using microarray technology, small RNA sequencing and reported that many miRNAs are expressed in mouse and human germ cells. In mammals, miRNAs are key controllers of cell differentiation and function, mediate a variety of cellular processes, and play an indispensable role in testicular development and spermatogenesis (7). Substantial evidence indicates that microRNAs (miRNAs) play pivotal roles in various facets of reproductive physiology, encompassing testicular development, spermatogenesis, and the regulation of functional effects (8–10). In the study of miRNA in Tibetan sheep, 1,118 immune-related miRNAs were found and speculated to be related to testicular development and meiosis in Tibetan sheep. Similarly, a recent study showed that miR-301b-3p and miR-3584-5p could promote the proliferation of rat immature testicular Sertoli cells by targeted inhibition of *RASD1* gene expression (11). Yu et al. (12) found in mice that miR-34c could promote the differentiation and meiosis process of Spermatogonial stem cells (SSCs) by targeting *Nanos2* gene and up-regulating the expression of meiosis-related genes *Stra8* and *Dazl*. Smorag et al. (13) found that miR-34b-5p could regulate the meiotic process of mouse spermatocytes by targeting *IGFBP2* gene. Overexpression of miR-10a in human and mouse testicular germ cells can target and inhibit the expression of *Rad51* gene, leading to meiotic arrest and complete male infertility (14). Zhang et al. (15) found that miR-34b could target *MAP2K1* (also known as *MEK1*) to induce apoptosis of bovine testicular Sertoli cells through MEK/ERK signaling pathway. However, miRNAs involved in testicular development and their underlying molecular mechanisms have not been identified in Southdown × Hu F1 hybrids.

In this study, we used deep sequencing technology to characterize and study the differential expression of miRNAs in the testis of sheep at different stages of development, understand the molecular regulation mechanism, and identify the key miRNA targets involved in sheep testicular development and spermatogenesis. This study will help to further understand the function of miRNA in sheep testicular development and to identify key miRNAs that enhance reproductive performance in male sheep in the future.

Materials and methods

Animals and sample preparation

Twelve healthy Southdown × Hu F1 sheep were castrated in Qinghuan Mutton Sheep Breeding Company in Gansu Province. The age of the sheep was obtained from sheep breeding records. There were 3 sheep at 0 months old (newborn, namely M0–1, M0–2, M0–3), 3 sheep at 3 months old (sexually immature, namely M3–1, M3–2, M3–3), 3 sheep at 6 months old (sexually mature, namely M6–1, M6–2, M6–3), and 3 sheep at 1 year old (adult, namely Y1–1, Y1–2, Y1–3). We removed testes from 12 sheep after anesthesia and then stored them in an RNA/DNA sample protector (Servicebio, Wuhan, China). The testis of each sheep was dissected longitudinally, and the right testicular tissue of each sheep was collected, part of which was immediately frozen in liquid nitrogen and stored at −80°C for total RNA and protein extraction. The remaining portion will be fixed in a 2.5% glutaraldehyde solution and subsequently processed for paraffin embedding and sectioning.

Small RNA library construction and sequencing

After total RNA was extracted by Trizol reagent kit (Invitrogen, Carlsbad, CA, United States), the RNA molecules in a size range of 18–30 nt were enriched by polyacrylamide gelelectrophoresis (PAGE). Then the 3′ adapters were added and the 36–48 nt RNAs were enriched. The 5′ adapters were then ligated to the RNAs as well. The ligation products were reverse transcribed by PCR amplification and the 140–160 bp size PCR products were enriched to generate a cDNA library and sequenced using Illumina HiSeq Xten by Gene DenovoBiotechnology Co. (Guangzhou, China)

Bioinformatics analysis

Basic reads are converted to sequence raw data by base calling. Low-quality reads were filtered to remove reads containing 5′ primer contaminants and poly (A). Reads without 3′ adapters and insert tags, as well as Reads shorter than 15 nt or longer than 41 nt in the raw data, were filtered out to obtain clean Reads. For preliminary analysis, the length distribution of clean sequences in the reference genome was determined. Non-coding RNAs are labeled as RNAs, tRNAs, small nuclear RNAs (snRNAs), miRNA, gene, rep, miRNA and unannotation. These RNAs were aligned and subsequently Bowtie (16) searches were performed against Rfam v.10.1[1] (17). Known miRNAs were identified by aligning sequencing reads to the miRBase v22 database[2] and the sheep reference genome (Qar Rambouillet v1.0). The known miRNA expression patterns in different samples were analyzed (18). Subsequently, the unannotated reads were analyzed by mirdeep2 to predict novel miRNAs (19). The hairpin structure of pre-miRNA and the miRBase database were used to identify the corresponding miRNA star sequence and miRNA mature sequence. The expression of known and novel miRNAs was analyzed using TPM (transcripts per million; miRNAs normalized by TPM) (20). Differential expression analysis of miRNAs between the two groups was performed using the DEG algorithm in the R package (21). The P- values were adjusted by the method of Benjamini and Hoch-berg

1 http://www.sanger.a.uk/softare/Rfam
2 http://www.mirbase.org/

to control the false discovery rate (FDR). Differentially expressed miRNAs were defined when the adjusted FDR was <0.05. In addition, we used the mean TPM value to calculate fold change (FC) between groups, defining up-regulated (log2FC ≥ 1) and down-regulated (log2FC ≤ 1) miRNAs, respectively. The target of DE miRNA was predicted using Miranda software with the following parameters: single residue pair matching score ≥ 150, ΔG ≤ −30 kcal/mol, and strict 5′ seed pairing required (22). Considering the hypergeometric distribution, R was used for Gene ontology (GO) enrichment and Kyoto Encyclopedia of Genes and Genomes (KEGG) pathway enrichment analysis of DE miRNA-target-get genes (23–25).

Validation of RNA sequence data

Twelve known sheep miRNAs were randomly selected for analysis, and qRT-PCR was used to validate the RNA-seq data. Real-time PCR was performed using a LightCycler 480 II real-time PCR apparatus (Roche, Swiss). Each sample was analyzed in triplicate. microRNA specific primer sequences were designed and synthesized in the laboratory by Qingdao Biotechnology Company based on microRNA sequences obtained from the miRBase database (Release 20.0). Primer information is given in Supplementary Table S1.

Results

Overview of sequencing results

We used Illumina Hiseq 2500 sequencing to analyze small RNA populations in 12 libraries obtained from testis of 0-month-old (M0), 3-month-old (M3), 6-month-old (M6), and 1-year-old (Y1) sheep. The results of miRNA sequence quality control are presented in Supplementary Table S2. A total of 157.27 Mb raw reads were obtained. After removing low-quality sequences, aptamers and discarding sequences shorter than 18 nt, 35.58 Mb, 32.67 Mb, 34.01 Mb and 41.01 Mb clean reads were obtained from M0, M3, M6 and Y1 libraries, respectively, for further analysis. 922,960, 1,780,035, 3,372,847, and 4,070,428 unique srRNAs were extracted from M0, M3, M6, and Y1 testes and mapped to the sheep reference genome (Supplementary Table S3). All clean reads were aligned to the miRBase database and recorded as one of the known RNA categories based on their biogenesis and annotation (Figure 1A). As shown in Figure 1A, Y1(7.21%) accounted for the largest proportion of known miRNAs, while M0(6.56%) and M3(5.85%) accounted for the second, and M6(3.3%) accounted for the smallest. However, the highest proportion of unannotated small RNAs was found in the M6(96.13%) and Y1(91.89%) libraries, which represent other types of small RNAs such as piRNAs. A principal component analysis (PCA) of all mapped genes showed that M0, M3, M6, and Y1 group could be distinguished by part along the axis of the first principal component (Figure 1B). Analysis of the read length distribution of all small RNA libraries showed that the dominant length of small RNAs was 22 nt, accounting for at least 37.72% (Figure 1C).

Identification of known and novel miRNAs in sheep testes

To identify miRNAs in sheep testes, the sequences obtained after removal of small RNAs, including tRNA, snRNA, and rRNA, were compared with the miRBase database to obtain known miRNAs. Sequences that were not annotated into the miRBase database were predicted as novel miRNAs. A total of 787 known miRNAs and 415 novel miRNAs were identified across the 12 libraries (Supplementary Table S4). The frequency of expression of each miRNA in the 12 libraries varied widely, ranging from a few to hundreds of thousands of sequence reads. The expression of these

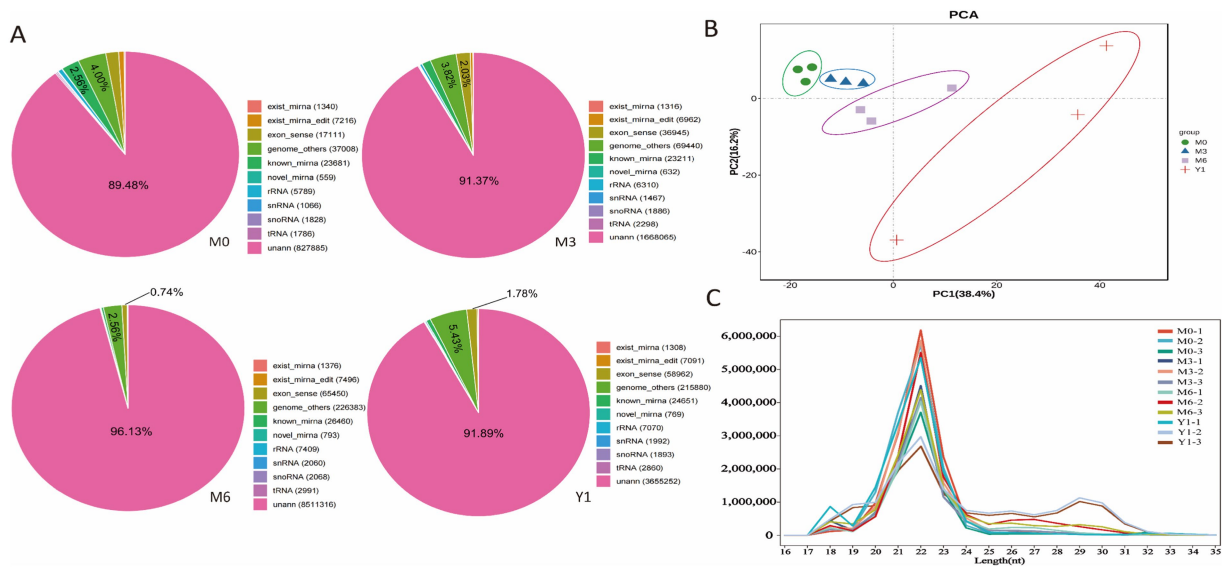

FIGURE 1
Identification and classification of miRNA in sheep testis. **(A)** Total number of unique sequences in libraries M0, M3, M6, and Y1. **(B)** PCA analysis of all mapped genes in M0, M3, M6, and Y1 groups. **(C)** Length distribution and abundance of sequences in the M0, M3, M6, and Y1 libraries.

novel miRNAs was very low, ranging from 18 to 25 nt in length with a distribution peak of 22 nt. Overall, the expression of most known miRNAs was highest in the testis of 3-month-old sheep, followed by 6-month-old and finally 0-month-old sheep (Figure 2A). The most highly expressed members in all libraries were members of the mir-199-x, mir-125-x, miR-99-z, miR-151-x, and miR-202-x families, each with more than 100,000 reads.

Differential expression of miRNAs in sheep testis tissue

Using the differential expression genes (DEGs) algorithm from an R package, the transcriptional changes of microRNAs (miRNAs) during sheep testis development were analyzed. Comparisons of miRNA expression profiles between different libraries were presented in Supplementary Tables S5–S10, visualized through scatter plots. Additionally, a scatter plot illustrated the pattern of DE miRNAs among all control groups, revealing that only 138 DE miRNAs were identified between M6 and Y1 testes, albeit with low expression levels (Figure 2B). Between M0 and M3, a total of 217 DE miRNAs were identified, with 139 upregulated and 78 downregulated. Between M0 and M6, 254 DE miRNAs were found, comprising 205 upregulated and 49 downregulated. From M0 to Y1, a remarkable change of 405 DE miRNAs was observed, with 319 upregulated and 86 downregulated. During the transition from M3 to M6, 130 DE miRNAs were identified, of which 97 were upregulated and 33 were downregulated. Lastly, between M3 and Y1, 305 DE miRNAs were detected, with 236 upregulated and 69 downregulated (Figure 2C).

Prediction of target genes for DE miRNAs

Using the Miranda software, the target genes of miRNAs were predicted. Subsequently, the potential functional roles of these differentially expressed miRNAs were investigated. Potential targets for the differentially expressed miRNAs were screened based on criteria of a minimum single-residue pair total match score of ≥150 and a total energy of ≤ − 30 kcal/mol. Among the 217, 254, 405, 130, 305, and 138 miRNAs identified between M0 vs. M3, M0 vs. M6, M0 vs. Y1, M3 vs. M6, M3 vs. Y1, and M6 vs. Y1, respectively, 5,233, 8,769, 23,588, 696, 8,021, and 180 targets were predicted in 885, 1,679, 2,679, 388, 2006, and 171 target genes, respectively. For the majority of differentially expressed miRNAs, multiple distinct target genes were present; however, for some differentially expressed

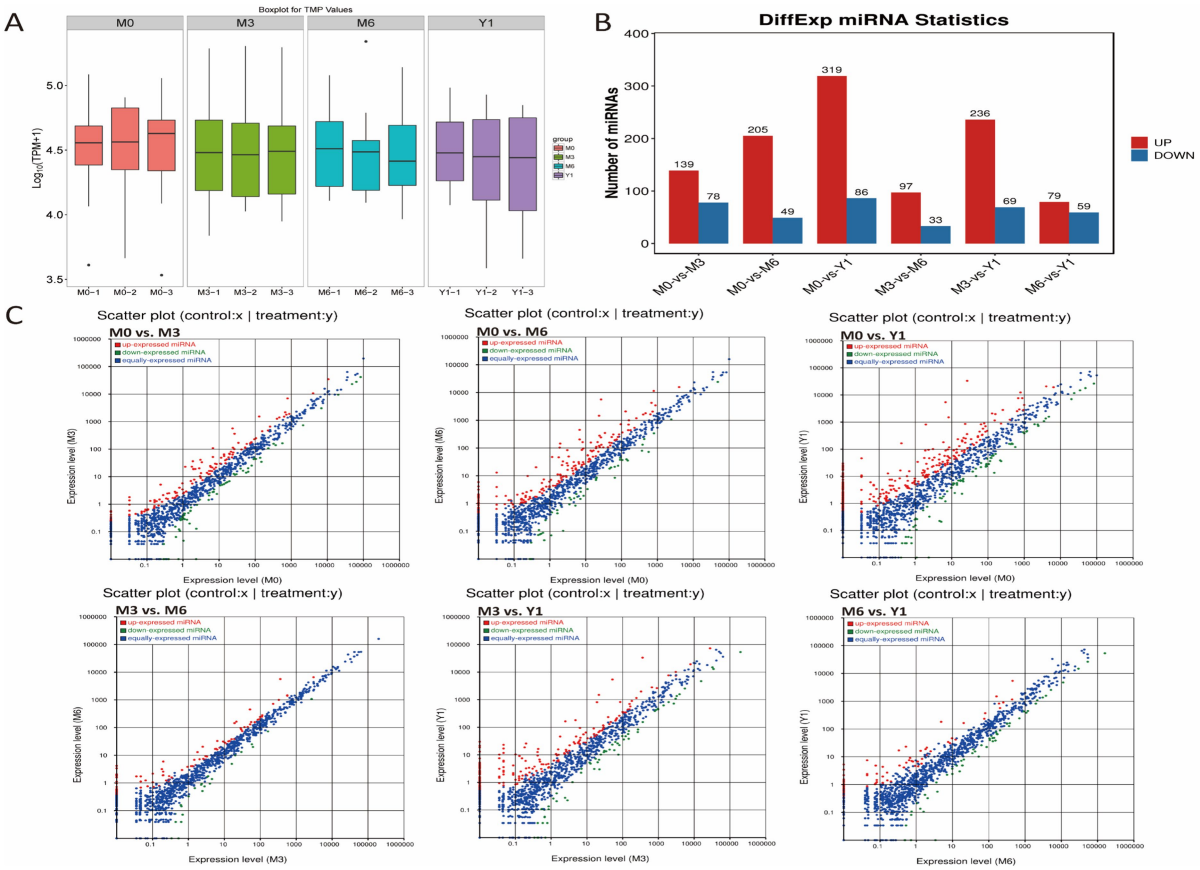

FIGURE 2
Comparative analysis of testicular miRNAs in sheep at different developmental stages. **(A)** miRNA expression levels in testis of 0, 3, 6 months and 1 year old sheep. **(B)** Barplot showing the number of up-and down-regulated DE miRNAs. **(C)** Scatter plot for differential comparison of miRNAs between pairs of groups; red, green, and blue dots indicate significantly up-regulated, down-regulated, and unchanged transcripts, respectively.

miRNAs, only a single target gene was identified. Additionally, certain target genes were targeted by multiple differentially expressed miRNAs. For instance, oar-miR-431 was predicted to target 914 genes, miR-199-y was predicted to target 1,510 genes, while *BMP4* was uniquely targeted by miR-142-y.

GO enrichment and KEGG pathway analysis of target genes

To gain a deeper understanding of the functions of DE miRNAs in sheep testis development, we performed Gene Ontology (GO) and Kyoto Encyclopedia of Genes and Genomes (KEGG) enrichment analyses on the candidate target genes of all DE miRNAs. The GO analysis results are presented in Figure 3. Between M0 and M3, target genes were significantly enriched in categories such as animal organ development, cell morphogenesis, cell part morphogenesis, and Rab GTPase binding (Figure 3A). Between M0 and M6, target genes were significantly enriched in regulation of cellular biosynthetic process, dendrite morphogenesis, tube development, organ morphogenesis, and cell–cell adherens junction (Figure 3B). Between M0 and Y1, target genes were notably enriched in reproductive process, apical junction complex, apical plasma membrane, and ATP binding (Figure 3D). Between M3 and M6, target genes were significantly enriched in cell differentiation, cell morphogenesis involved in differentiation, Wnt signaling pathway, and apical junction complex (Figure 3C). Between M3 and Y1, target genes were enriched in tube morphogenesis, regulation of organelle organization, plasma membrane, Golgi complex, and microtubule binding (Figure 3F). Lastly, between M6 and Y1, target genes were significantly enriched in cell migration, dendrite morphogenesis, organ morphogenesis, and cell–cell junction organization (Figure 3E).

KEGG Pathway Annotation identified significant enrichment of target genes of DE miRNAs in various comparisons. In M0 vs. M3, 30 pathways were enriched, including the Ras, MAPK, Rap1, cAMP, and Notch signaling pathways (Figure 4A). Four key pathways related to testis development were cAMP, MAPK, PI3K-Akt, and Wnt signaling. In M0 vs. M6, target genes were enriched in 30 pathways, such as adherens junction, tight junction, spinocerebellar ataxia, phospholipase D signaling, and endocytosis (Figure 4B). Four testis development-related pathways were MAPK, cAMP, FOXO, and GnRH signaling pathways. Between M3 and M6, 30 pathways were enriched, including Notch, Ras,

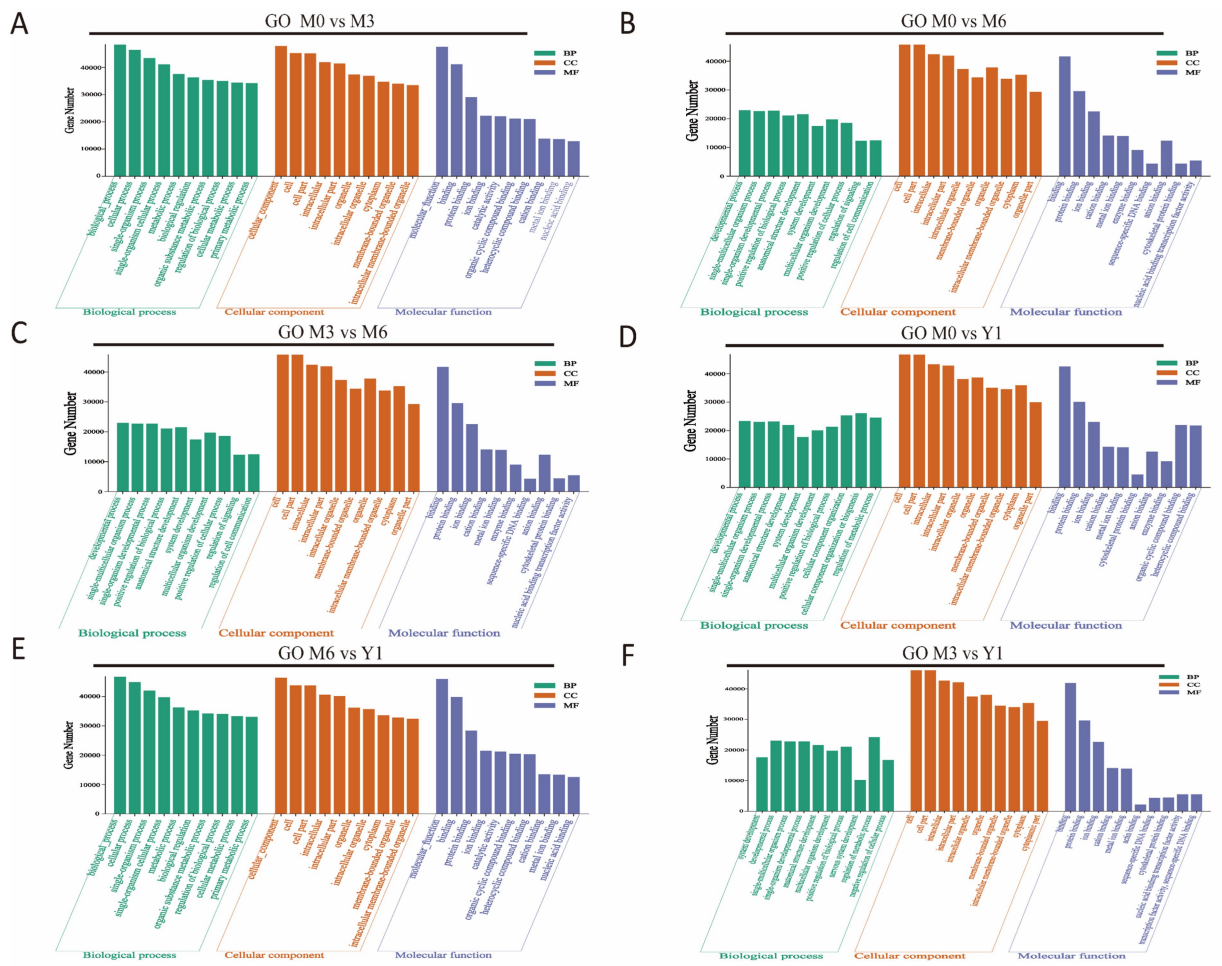

FIGURE 3
GO enrichment analysis of target genes of differentially expressed miRNAs. **(A)** M0 vs M3; **(B)** M0 vs M6; **(C)** M3 vs M6; **(D)** M0 vs Y1; **(E)** M6 vs Y1; **(F)** M3 vs Y1; M0 represents 0 months of age, M3 represents 3 months of age, M6 represents 6 months of age, and Y1 represents 1 year of age.

thyroid hormone, and ErbB signaling (Figure 4C). Five key pathways were Notch, ErbB, endocytosis, Ras, and thyroid hormone signaling.

In M0 vs. Y1, 49 pathways were enriched, including Notch, Ras, thyroid hormone, and ErbB signaling (Figure 4D). Five testis development-related pathways were FOXO, ErbB, endocytosis, Ras, and thyroid hormone signaling. Between M6 and Y1, 30 pathways were enriched, such as Hippo, adherens junction, cAMP, Notch, and Ras signaling (Figure 4E). Five key pathways were Notch, Hippo, cAMP, endocytosis, and FOXO signaling. Similarly, in M3 vs. Y1, 30 pathways were enriched, including tight junction, endocytosis, Ras, adherens junction, and spinocerebellar ataxia (Figure 4F). Four testis development-related pathways were Ras, MAPK, and cAMP signaling (Figure 5).

Cluster analysis of miRNA co-expression

We performed co-expression cluster analysis of the differentially expressed miRNAs screened from each comparison group and screened the top 5 miRNAs with degree values. After comparison, the number of miRNA target genes in M0 vs. M3 group, M0 vs. Y1 group and M0 vs. M6 group was higher than that in other groups. Notably, oar-miR-29b, oar-miR-143, oar-miR-370-3p, oar-miR-19b,

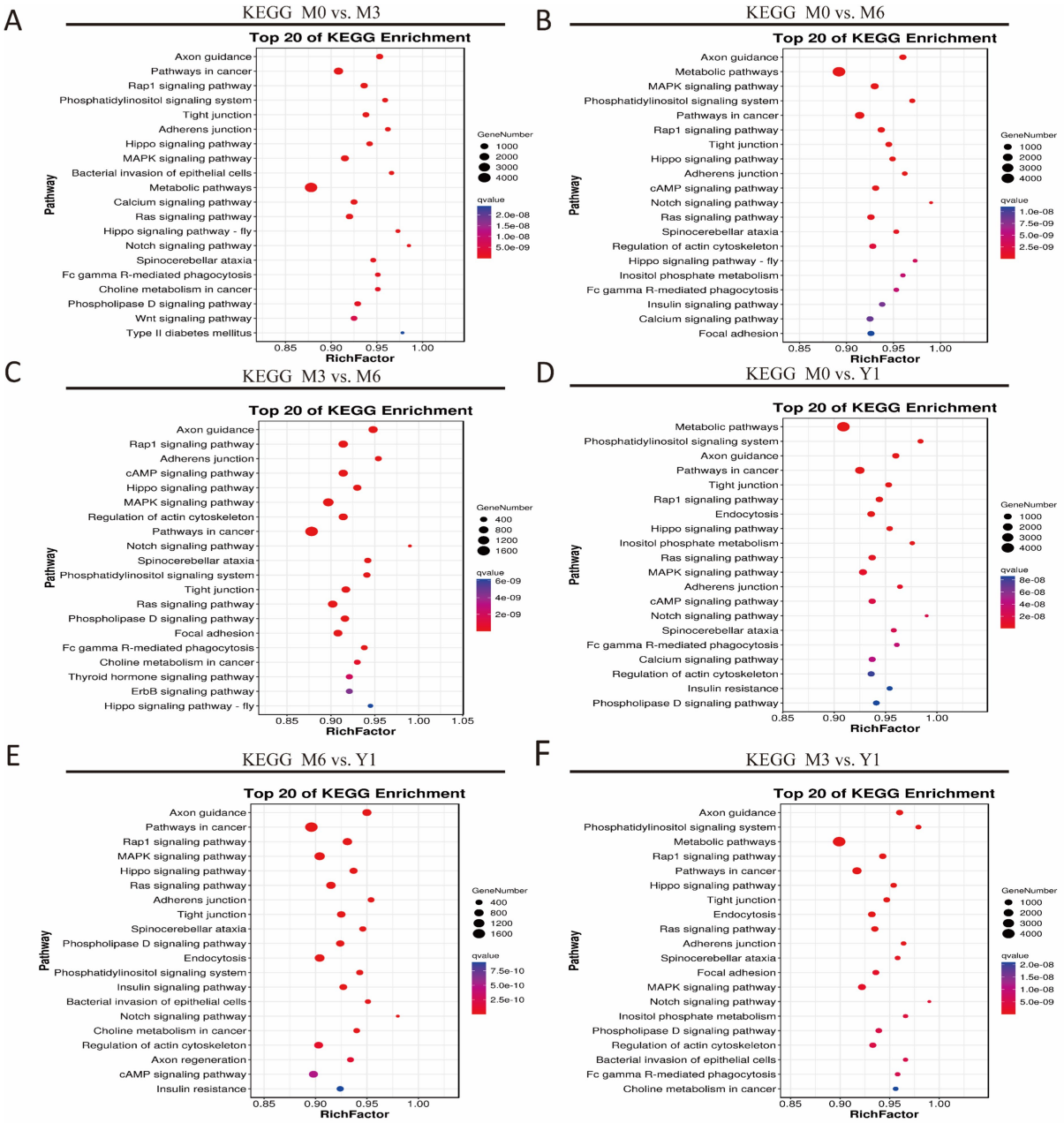

FIGURE 4
KEGG analysis of target genes of differentially expressed miRNAs. **(A)** M0 vs M3; **(B)** M0 vs M6; **(C)** M3 vs M6; **(D)** M0 vs Y1; **(E)** M6 vs Y1; **(F)** M3 vs Y1; M0 represents 0 months of age, M3 represents 3 months of age, M6 represents 6 months of age, and Y1 represents 1 year of age.

oar-miR-432, and oar-miR-29b were repeated for different times in the 6 comparison groups. TGF family genes related to testicular development were all regulated by differential miRNAs in the five comparison groups (Figure 5).

Quantitative RT-PCR validation

Randomly selected 12 known sheep miRNAs, including oar-miR-152, oar-miR-10b, oar-miR-21, oar-miR-22-3p, oar-miR-25, oar-miR-99a, oar-miR-379-3p, oar-miR-409-5p, oar-miR-1179, oar-miR-132, oar-miR-374a, and oar-miR-28-y, were used to validate the RNA-seq data. As shown in Figure 6, the qRT-PCR results exhibited similar expression trends compared to the small RNA-seq results.

Discussion

The production of sperm and androgens is the primary function of the testis, both of which play a vital role in the entire reproductive system. The differentiation of somatic cells into Sertoli cells initiates male-specific development and guides the development of germ cells toward the spermatogenic lineage (26). Consequently, testicular development and spermatogenesis are crucial processes that affect the reproductive efficiency of male sheep. Additionally, several functional genes have been reported to regulate testicular development and spermatogenesis in sheep (27–29). Recently, miRNAs have been found to regulate biological processes by inhibiting the translation or degradation of target mRNAs (30–32). Since the discovery of miRNAs and their role in gene expression regulation, numerous studies have delved into their involvement in testicular hormone synthesis, cell proliferation, meiosis of haploid spermatocytes, and spermatogenesis (33–35). However, only a few studies have characterized the miRNAs involved in testicular development during early puberty in sheep. In this study, we employed Illumina Solexa technology to sequence small RNAs in testicular tissues from 0-month, 3-month, 6-month, and 1-year-old male sheep, analyzed DE miRNAs, predicted novel miRNAs, and conducted GO enrichment and KEGG pathway analyses of target genes across four miRNA libraries.

The dynamic testicular development of male sheep at 0-month, 3-month, 6-month, and 1-year-old corresponds to the neonatal, pre-pubertal, pubertal, and adult stages, respectively. By comparing the reference genome, we identified 217, 254, 405, 130, 205, and 138 known DE miRNAs in comparisons between M0 vs. M3, M0 vs. M6, M0 vs. Y1, M3 vs. M6, M3 vs. Y1, and M6 vs. Y1, respectively. Notably, more novel DE miRNAs were identified compared to known DE sheep miRNAs, contributing to the identification of key miRNAs in sheep testicular development and enriching the sheep miRBase database. Previous studies have reported that miR-34c, miR-21, and miR-499b regulate the reproductive performance of male mammals, including promoting spermatogonial meiosis, inhibiting Sertoli cell

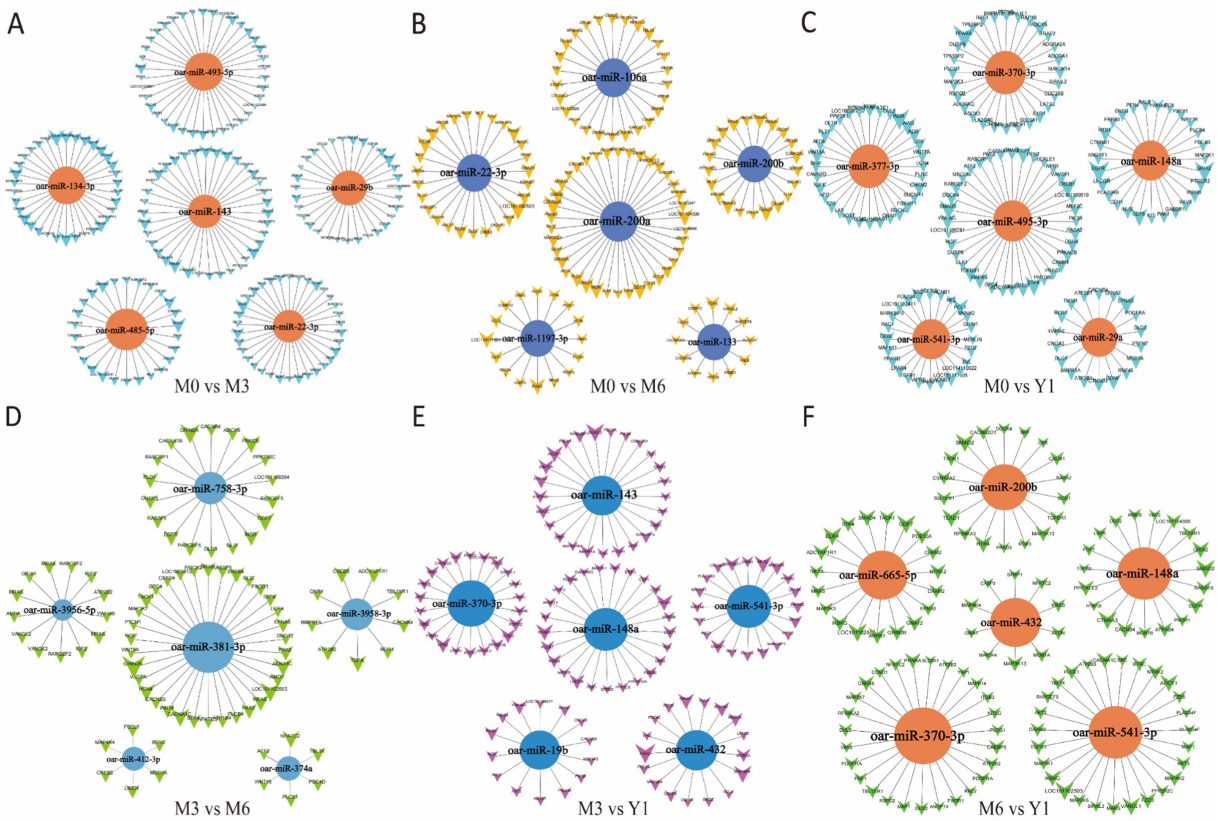

FIGURE 5
Cluster analysis of differential miRNA co-expression in pairwise comparison groups. **(A)** M0 vs M3; **(B)** M0 vs M6; **(C)** M0 vs Y1; **(D)** M3 vs M6; **(E)** M3 vs Y1; **(F)** M6 vs Y1; M0 represents 0 months of age, M3 represents 3 months of age, M6 represents 6 months of age, and Y1 represents 1 year of age.

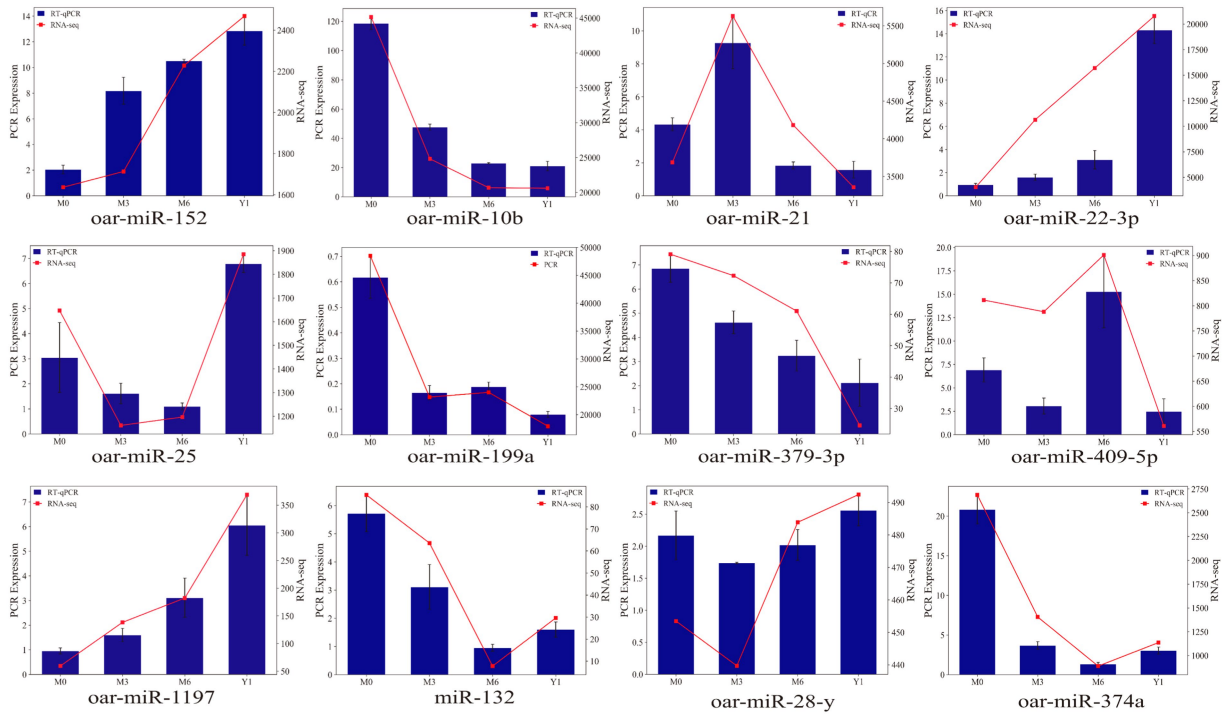

FIGURE 6
Validation of the expression of differentially expressed miRNAs by qRT-PCR. The blue bar graph represents RT-qPCR, the red broken line represents RNA-seq, the left ordinate is PCR Expression, and the right ordinate is RNA-seq.

apoptosis, and maintaining the necessary germ cell population of spermatogonial stem cells (SSCs) (36–38). In our study, miR-34c, miR-21, and miR-499b showed significantly higher expression in the Y1 group compared to the M6 group, suggesting their potential involvement in sheep testicular development. Additionally, miR-31-5p downregulation has been detected in the miRNA profiles of seminal exosomes from patients with asthenozoospermia and azoospermia (39) and in non-obstructive azoospermia testes (40), indicating its potential as a predictive marker for azoospermia. Accordingly, miR-155 targets genes involved in MAPK and Wnt signaling pathways, affecting sperm motility (41). Overexpression of miR-10a in testicular germ cells of humans and mice can target and inhibit Rad51 gene expression, leading to meiotic arrest and complete male infertility (42). Similarly, these miRNAs may be associated with sheep testicular development, albeit their specific functions in sheep testes require further exploration and validation.

GO annotation and KEGG pathway analysis can provide a detailed and comprehensive understanding of the functions of DE miRNA target genes from the aspects of cellular components, biological processes, molecular functions and related pathways. GO and KEGG analyses showed that the target genes of DE miRNAs were involved in different biological processes, including growth and development, reproduction, cell proliferation, hormone secretion, and several other metabolic processes. Interestingly, the cAMP, Hippo, MAPK, Wnt, and FOXO signaling pathways are widely recognized to regulate reproduction.

FOXO1 is mainly expressed in Sertoli cells (43), while *FOXO3a* is expressed in other cells of the testis, such as Leydig cells (44). This cell type specificity allows FOXO family members to regulate the development and function of different cell types in the testis. *FOXO* further regulates testicular development by promoting gonadotropin secretion and testosterone synthesis. The most multifunctional miRNAs controlling target genes in FOXO signaling pathways included oar-miR-19b, oar-miR-200a, oar-miR-369-3p, oar-miR-200b, and oar-miR-493-5p. Each of them regulates key genes in the FOXO signaling pathway such as *FOXO1* and *FOXO6*. The PI3K-Akt signaling pathway directly or indirectly maintains and promotes spermatogenesis by regulating the proliferation, survival, and anti-apoptosis of immature Sertoli cells, mature Sertoli cells, spermatogonial stem cells, and spermatogenic cells (45). In PI3K-Akt signaling pathway, oar-miR-1197-3p, oar-miR-136, oar-miR-199a-3p, oar-miR-410-5p, oar-miR-432 targeted *WT1* gene regulation, *WT1* can not only activate PI3K/Akt and other pathways to inhibit apoptosis, but also plays a crucial role in the assembly and maintenance of fetal testicular cords (46). The Wnt pathway affects the production and maturation of spermatogenic cells by regulating cell proliferation and differentiation. Studies have shown that abnormal activation or inhibition of *Wnt* may affect the normal proliferation and differentiation process of testicular cells, which in turn affects sperm production (47). As a key gene in this pathway, *DOT1L* is co-targeted by DE miRNAs such as oar-let-7f and oar-miR-22-3p. *DOT1L* promotes SSCs self-renewal by catalyzing Histone H3 lysine 79 methylation (H3K79me). It is essential for the maintenance of spermatogenesis (48). The expression of oar-miR-22-3p was found to be significantly changed from M0 to Y1, suggesting that oar-miR-22-3p plays an important role in spermatogenesis and testicular development in sheep. Evidence accumulated over the past few years has highlighted the major functions of MAPK, AMPK, and cAMP signaling pathways during spermatogenesis, with MAPK signaling regulating germ cell

proliferation, meiosis, and Sertoli cell proliferation (49). In addition, the AMPK and FOXO signaling pathways influence the proliferation of Sertoli cells (50). Among the MAPK, cAMP, PI3K-Akt, FOXO, Wnt, and AMPK pathways, oar-miR-133, oar-miR-1197-3p, oar-miR-758-3pr, and oar-let-7f are the most potent miRNAs that regulate multiple genes within various testicular development and spermatogenesis-related pathways. Each of these miRNAs plays a crucial role in modulating diverse targets in these signaling cascades. In this study, the downregulation of oar-miR-26a, oar-miR-99a, and oar-miR-148a during the development of sheep testes from neonatal to adult stages suggests their significant contribution to promoting testicular development and spermatogenesis in sheep.

Conclusion

In summary, we have characterized the miRNA transcriptome across four testicular developmental stages, from birth to adulthood, in the F1 offspring of a cross between Southdown sheep and Hu sheep. A total of 788 known miRNAs and 415 novel miRNAs were identified across the 12 libraries. GO and KEGG pathway analyses of all DE miRNA targets in the libraries revealed significant enrichment in MAPK signaling pathway, Rap1 signaling pathway, Wnt signaling pathway, and FOXO signaling pathway. We believe these results will contribute to a deeper understanding of the roles of miRNAs in sheep testicular development and potentially facilitate the discovery of miRNAs to enhance the reproductive performance of male sheep in the future.

Data availability statement

The data presented in the study are deposited in the NCBI SRA repository, accession number PRJNA1195695.

Ethics statement

The animal studies were approved by Animal Management and Ethics Committee of Lanzhou Institute of Animal Husbandry and Medicine, Chinese Academy of Agricultural Sciences and met the requirements of the Institutional Animal Care and Use Committee (license number: SYXK-2019-010). The studies were conducted in accordance with the local legislation and institutional requirements. Written informed consent was obtained from the owners for the participation of their animals in this study.

Author contributions

BX: Formal analysis, Methodology, Validation, Visualization, Writing – original draft, Writing – review & editing. XA: Formal analysis, Investigation, Methodology, Validation, Visualization, Writing – original draft, Writing – review & editing. YYu: Validation, Visualization, Writing – original draft. HS: Methodology, Writing – original draft. GH: Investigation, Software, Writing – original draft. YYa: Conceptualization, Data curation, Funding acquisition, Project administration, Resources, Supervision, Writing – review & editing. SZ: Conceptualization, Data curation, Funding acquisition, Project administration, Resources, Supervision, Writing – review & editing.

Funding

The author(s) declare that financial support was received for the research and/or publication of this article. This research was funded by the Gansu Province Science and Technology Plan Project Technology Innovation Guidance Program-LuGan Science and Technology Collaboration topic of 23CXNA0020.

Conflict of interest

The authors declare that the research was conducted in the absence of any commercial or financial relationships that could be construed as a potential conflict of interest.

Generative AI statement

The authors declare that no Gen AI was used in the creation of this manuscript.

Publisher's note

Supplementary material

The Supplementary material for this article can be found online at: https://www.frontiersin.org/articles/10.3389/fvets.2025.1538990/full#supplementary-material

SUPPLEMENTARY TABLE S1
Details of primer sequences of miRNAs used for RT-qPCR.

SUPPLEMENTARY TABLE S2
miRNA Sequence Quality Control.

SUPPLEMENTARY TABLE S3
Read mapping summary of sheep miRNA.

SUPPLEMENTARY TABLE S4
The novel miRNAs and known miRNAs identified in all libraries.

SUPPLEMENTARY TABLE S5
Differentially expressed miRNAs between M0 and M3.

SUPPLEMENTARY TABLE S6
Differentially expressed miRNAs between M0 and M6.

SUPPLEMENTARY TABLE S7
Differentially expressed miRNAs between M0 and Y1.

SUPPLEMENTARY TABLE S8
Differentially expressed miRNAs between M3 and M6.

SUPPLEMENTARY TABLE S9
Differentially expressed miRNAs between M3 and Y1.

SUPPLEMENTARY TABLE S10
Differentially expressed miRNAs between M6 and Y1.

References

1. Wang J. Analysis of factors affecting farly growth traits of Hu sheep and estimation of genetic parameters (D). *Xinjiang Agric Univ*. (2022). doi: 10.27431/d.cnki.gxnyu.2022.000762

2. Liu T, Lu Z, Shi H, Sun W, Zhang J, Zhu Z. Comparative study on mutton quality of F1 generation of different cross combinations. *Acta Ecol Anim Domast*. (2023) 44:46–52. doi: 10.3969/j.issn.1673-1182.2023.09.009

3. Zhang R, An X, Li J, Lu Z, Niu C, Xu Z. Comparative analysis of growth performance, meat productivity, and meat quality in Hu sheep and its hybrids. *Acta Pratacul Sin*. (2024) 33:186–97. doi: 10.11686/cyxb2023157

4. Kong L, Yue Y, Zhang C, Lu Z. Slaughtering performance and meat quality characteristics of Hu sheep and its hybrid offspring with Southdown sheep. *Food Sci*. (2023) 44:64–70. doi: 10.7506/spkx1002-6630-20221124-285

5. Marcon E, Babak T, Chua G, Hughes T, Moens PB. miRNA and piRNA localization in the male mammalian meiotic nucleus. *Chromosom Res*. (2008) 16:243–60. doi: 10.1007/s10577-007-1190-6

6. Afonso J, Lima AO, de Sousa MAP, de Athayde FRF, Fortes MRS. Transcription factors and miRNA act as contrary regulators of gene expression in the testis and epididymis of *Bos indicus* animals. *Gene*. (2024) 899:148133. doi: 10.1016/j.gene.2024.148133

7. Hossain MM, Sohel MM, Schellander K, Tesfaye D. Characterization and importance of microRNAs in mammalian gonadal functions. *Cell Tissue Res*. (2012) 349:679–90. doi: 10.1007/s00441-012-1469-6

8. McIver SC, Roman SD, Nixon B, McLaughlin EA. miRNA and mammalian male germ cells. *Hum Reprod Update*. (2012) 18:44–59. doi: 10.1093/humupd/dmr041

9. Kotaja N. MicroRNAs and spermatogenesis. *Fertil Steril*. (2014) 101:1552–62. doi: 10.1016/j.fertnstert.2014.04.025

10. Chen W, Cui Y, Ning M, Zhang H, Yin C, He Z. The mechanisms and functions of microRNAs in mediating the fate determinations of human spermatogonial stem cells and Sertoli cells. *Semin Cell Dev Biol*. (2022) 121:32–9. doi: 10.1016/j.semcdb.2021.05.003

11. Yin X, Ma T, Han R, Ding J, Zhang H, Han X, et al. MiR-301b-3p/3584-5p enhances low-dose mono-n-butyl phthalate (MBP)-induced proliferation by targeting Rasd1 in Sertoli cells. *Toxicol In Vitro*. (2018) 47:79–88. doi: 10.1016/j.tiv.2017.11.009

12. Yu M, Mu H, Niu Z, Zhu Z, Zhu H, Jin L. miR-34c enhances mouse spermatogonial stem cells differentiation by targeting Nanos2. *J Cell Biochem*. (2014) 115:232–42. doi: 10.1002/jcb.24655

13. Smorag L, Zheng Y, Nolte J, Zechner U, Engel W, Pantakani D. MicroRNA signature in various cell types of mouse spermatogenesis: evidence for stage-specifically expressed miRNA-221, −203 and -34b-5p mediated spermatogenesis regulation. *Biol Cell*. (2012) 104:677–92. doi: 10.1111/boc.201200014

14. Wang Z, Zhang X, Li Z, Abdalla BA, Chen Y, Nie Q. MiR-34b-5p mediates the proliferation and differentiation of myoblasts by targeting IGFBP2. *Cells*. (2019) 8:360. doi: 10.3390/cells8040360

15. Zhang L, Ma T, Tao Q, Tan W, Chen H, Liu W, et al. Bta-miR-34b inhibits proliferation and promotes apoptosis via the MEK/ERK pathway by targeting MAP2K1 in bovine primary Sertoli cells. *J Anim Sci*. (2020) 98:skaa313. doi: 10.1093/jas/skaa313

16. Langmead B, Trapnell C, Pop M, Salzberg SL. Ultrafast and memory-efficient alignment of short DNA sequences to the human genome. *Genome Biol*. (2009) 10:R25. doi: 10.1186/gb-2009-10-3-r25

17. Griffiths-Jones S, Bateman A, Marshall M, Khanna A, Eddy SR. Rfam: an RNA family database. *Nucleic Acids Res*. (2003) 31:439–41. doi: 10.1093/nar/gkg006

18. Griffiths-Jones S, Saini HK. Van Dongen, S Enright AJ. miRBase: tools for microRNA genomics. *Nucleic Acids Res*. (2008) 36:D154–8. doi: 10.1093/nar/gkm952

19. Friedlander MR, Mackowiak SD, Li N, Chen W, Rajewsky N. miRDeep2 accurately identifies known and hundreds of novel microRNA genes in seven animal clades. *Nucleic Acids Res*. (2012) 40:37–52. doi: 10.1093/nar/gkr688

20. Sun J, Wang S, Li C, Ren Y, Wang J. Novel expression profiles of microRNAs suggest that specific miRNAs regulate gene expression for the sexual maturation of female Schistosoma japonicum after pairing. *Parasite Vector*. (2014) 7:177. doi: 10.1186/1756-3305-7-177

21. Anders S, Huber W. Differential expression analysis for sequence count data. *Genome Biol*. (2010) 11:R106. doi: 10.1186/gb-2010-11-10-r106

22. Enright AJ, John B, Gaul U, Tuschl T, Sander C, Marks DS. MicroRNA targets in Drosophila. *Genome Biol*. (2003) 5:R1. doi: 10.1186/gb-2003-5-1-r1

23. Kanehisa M, Goto S. KEGG: Kyoto encyclopedia of genes and genomes. *Nucleic Acids Res*. (2000) 27:29–34. doi: 10.1093/nar/27.1.29

24. Kanehisa M. Toward understanding the origin and evolution of cellular organisms. *Protein Sci*. (2019) 28:1947–51. doi: 10.1002/pro.3715

25. Kanehisa M, Furumichi M, Sato Y, Kawashima M, Ishiguro-Watanabe M. KEGG for taxonomy-based analysis of pathways and genomes. *Nucleic Acids Res*. (2022) 51:D587–92. doi: 10.1093/nar/gkac963

26. Mäkelä JA, Koskenniemi JJ, Virtanen HE, Toppari J. Testis Development. *Endocr Rev*. (2019) 40:857–905. doi: 10.1210/er.2018-00140

27. Li S, Zhao B, Yang H, Dai K, Cai Y, Xu H, et al. Comprehensive transcriptomic analysis revealing the regulatory dynamics and networks of the pituitary-testis axis in sheep across developmental stages. *Front Vet Sci*. (2024) 11:1367730. doi: 10.3389/fvets.2024.1367730

28. Yang H, Wang F, Li F, Ren C, Pang J, Wan Y, et al. Comprehensive analysis of long noncoding RNA and mRNA expression patterns in sheep testicular maturation. *Biol Reprod*. (2018) 99:650–61. doi: 10.1093/biolre/ioy088

29. Xu H, Sun W, Pei S, Li W, Li F, Yue X. Identification of key genes related to postnatal testicular development based on transcriptomic data of testis in Hu sheep. *Front Genet*. (2022) 12:773695. doi: 10.3389/fgene.2021.773695

30. Yun Y, Wu R, He X, Qin X, Chen L, Sha L, et al. Integrated transcriptome analysis of miRNAs and mRNAs in the skeletal muscle of Wuranke sheep. *Genes (Basel)*. (2023) 14:2034. doi: 10.3390/genes14112034

31. Wang Q, Cao H, Su X, Liu W. Identification of key miRNAs regulating fat metabolism based on RNA-seq from fat-tailed sheep and F2 of wild argali. *Gene*. (2022) 834:146660. doi: 10.1016/j.gene.2022.146660

32. Han H, Chen Q, Gao Y, Li J, Li W, Dang R, et al. Comparative transcriptomics analysis of testicular miRNA from cryptorchid and normal horses. *Animals*. (2020) 10:338. doi: 10.3390/ani10020338

33. Pan C, Fei Q, Jin J, Zheng J, Wu D, Li H, et al. MicroRNA profiling reveals the role of miR-133b-3p in promoting apoptosis and inhibiting cell proliferation and testosterone synthesis in mouse TM3 cells. *In Vitro Cell Dev Biol Anim*. (2023) 59:63–75. doi: 10.1007/s11626-022-00745-z

34. Yu Z, Liu Y, Li Y, Zhang J, Peng J, Gong J, et al. miRNA-338-3p inhibits glioma cell proliferation and progression by targeting MYT1L. *Brain Res Bull*. (2022) 179:1–12. doi: 10.1016/j.brainresbull.2021.11.016

35. Walker WH. Regulation of mammalian spermatogenesis by miRNAs. *Semin Cell Dev Biol*. (2022) 121:24–31. doi: 10.1016/j.semcdb.2021.05.009

36. Niu Z, Goodyear SM, Rao S, Wu X, Tobias JW, Avarbock MR, et al. MicroRNA-21 regulates the self-renewal of mouse spermatogonial stem cells. *Proc Natl Acad Sci USA*. (2011) 108:12740–5. doi: 10.1073/pnas.1109987108

37. Bouhallier F, Allioli N, Lavial F, Chalmel F, Perrard MH, Durand P, et al. Role of miR-34c microRNA in the late steps of spermatogenesis. *RNA*. (2010) 16:720–31. doi: 10.1261/rna.1963810

38. Liu WM, Pang RT, Chiu PC, Wong BP, Lao K, Lee KF, et al. Sperm-borne microRNA-34c is required for the first cleavage division in mouse. *Proc Natl Acad Sci USA*. (2012) 109:490–4. doi: 10.1073/pnas.1110368109

39. Barcelo M, Mata A, Bassas L, Larriba S. Exosomal microRNAs in seminal plasma are markers of the origin of azoospermia and can predict the presence of sperm in testicular tissue. *Hum Reprod*. (2018) 33:1087–98. doi: 10.1093/humrep/dey072

40. Zhang HT, Zhang Z, Hong K, Tang WH, Liu DF, Mao JM, et al. Altered microRNA profiles of testicular biopsies from patients with nonobstructive azoospermia. *Asian J Androl*. (2020) 22:100–5. doi: 10.4103/aja.aja_35_19

41. Liu Y, Sun Y, Li Y, Bai H, Xu S, Xu H, et al. Identification and differential expression of microRNAs in the testis of chicken with high and low sperm motility. *Theriogenology*. (2018) 122:94–101. doi: 10.1016/j.theriogenology.2018.09.010

42. Gao H, Wen H, Cao C, Dong D, Yang C, Xie S, et al. Overexpression of MicroRNA-10a in germ cells causes male infertility by targeting Rad51 in mouse and human. *Front Physiol*. (2019) 10:765. doi: 10.3389/fphys.2019.00765

43. Javdan N, Ayatollahi SA, Iqbal Choudhary M, Al-Hasani S, Pazoki-Toroudi H. FOXO1 targeting by capsaicin reduces tissue damage after testicular torsion. *Andrologia*. (2018) 50:e13032. doi: 10.1111/and.13032

44. Zhao X, Liu F, Chen Z, Gao Y, Cui K, Shi D. Phenotypic study of foxo3a knockout mice created by TALEN-mediated gene targeting. *China Acad J Electr Publ House*. (2018) 31:23–4. doi: 10.1038/nbt.2477

45. Chen K, Wei B, Hao S, Yang W. The PI3K/AKT signaling pathway: how does it regulate development of Sertoli cells and spermatogenic cells? *Histol Histopathol*. (2022) 37:621–36. doi: 10.14670/HH-18-457

46. Wen Q, Wang Y, Tang J, Cheng C, Liu Y. Sertoli cell Wt1 regulates peritubular Myoid cell and fetal Leydig cell differentiation during fetal testis development. *PLoS One*. (2016) 11:e0167920. doi: 10.1371/journal.pone.0167920

47. Lundgaard Riis M, Delpouve G, Nielsen JE, Melau C, Langhoff Thuesen L, Juul Hare K, et al. Inhibition of WNT/β-catenin signalling during sex-specific gonadal differentiation is essential for normal human fetal testis development. *Cell Commun Signal*. (2024) 22:330. doi: 10.1186/s12964-024-01704-9

48. Lin H, Cossu IG, Leu NA, Deshpande AJ, Bernt KM, Luo M, et al. The DOT1L-MLLT10 complex regulates male fertility and promotes histone removal during spermiogenesis. *Development*. (2023) 150:dev201501. doi: 10.1242/dev.201501

49. La Y, Ma X, Bao P, Chu M, Guo X, Liang C, et al. Identification and profiling of microRNAs during yak's testicular development. *BMC Vet Res*. (2023) 19:53. doi: 10.1186/s12917-023-03602-7

50. Meroni SB, Galardo MN, Rindone G, Gorga A, Riera MF, Cigorraga SB. Molecular mechanisms and signaling pathways involved in Sertoli cell proliferation. *Front Endocrinol*. (2019) 10:224. doi: 10.3389/fendo.2019.00224

frontiers | Frontiers in Veterinary Science

TYPE Original Research
PUBLISHED 10 April 2025
DOI 10.3389/fvets.2025.1492135

OPEN ACCESS

EDITED BY
Regiane R. Santos,
Schothorst Feed Research, Netherlands

REVIEWED BY
Tarique Hussain,
Nuclear Institute for Agriculture and Biology, Pakistan
Danuza Leão,
Centro Nacional de Primatas, Brazil

*CORRESPONDENCE
Asep Gunawan
✉ agunawan@apps.ipb.ac.id

RECEIVED 06 September 2024
ACCEPTED 17 March 2025
PUBLISHED 10 April 2025

CITATION
Maulana T, Said S, Arifiantini RI, Jakaria J and Gunawan A (2025) Proteomic analysis of Toraya buffalo seminal plasma and sperm: uncovering insights to optimize reproductive success.
Front. Vet. Sci. 12:1492135.
doi: 10.3389/fvets.2025.1492135

Proteomic analysis of Toraya buffalo seminal plasma and sperm: uncovering insights to optimize reproductive success

Tulus Maulana[1,2], Syahruddin Said[2], Raden Iis Arifiantini[3], Jakaria Jakaria[4] and Asep Gunawan[4]*

[1]Graduate School of Animal Production and Technology, Faculty of Animal Science, IPB University, Bogor, Indonesia, [2]Research Center for Applied Zoology, National Research and Innovation Agency, Bogor, Indonesia, [3]Division of Veterinary Reproduction and Obstetrics, School of Veterinary Medicine and Biomedical Sciences, IPB University, Bogor, Indonesia, [4]Department of Animal Production and Technology, Faculty of Animal Science, IPB University, Bogor, Indonesia

The characterization of sperm and seminal plasma proteins is essential for understanding bull fertility and optimizing reproductive success in buffalo bulls. Despite its importance, the reproductive proteomic of Toraya buffalo, an indigenous breed in Indonesia, remains largely unexplored. This study aimed to examine the seminal plasma and sperm proteins of Toraya buffalo to uncover those critical for reproductive functions. Semen samples were collected from eight Toraya buffalo bulls aged 4 to 10 years. Protein profiling was performed using one-dimensional sodium dodecyl sulfate-polyacrylamide gel electrophoresis (1D-SDS-PAGE), followed by in-gel digestion and liquid chromatography-tandem mass spectrometry (LC-MS/MS) analysis. Bioinformatics tools, including UniProt, PANTHER, DAVID, and STRING, were utilized to identify and annotate the detected proteins. This study successfully identified four key reproductive proteins: ADAM32 in seminal plasma and ZPBP, SPACA3, and CCDC136 in sperm. These proteins are essential for sperm motility, energy production, and acrosome formation, which are critical processes for fertilization. Additionally, many identified proteins were associated with metabolic pathways, particularly the tricarboxylic acid (TCA) cycle, which plays a fundamental role in energy supply for sperm function. In conclusion, this study offers the first comprehensive proteomic identification of seminal plasma and sperm proteins associated with reproductive functions in the Toraya buffalo. The findings highlight the presence of key proteins in sperm, including ZPBP, SPACA3, and CCDC136, as well as the identification of ADAM32 in seminal plasma, contributing to a deeper understanding of buffalo reproductive biology.

KEYWORDS

proteome, seminal plasma, sperm, TCA cycle, Toraya buffalo

1 Introduction

The Toraya buffalo is an indigenous breed from Indonesia that plays a vital role in the agricultural and livestock systems of the region, particularly in Sulawesi (1). The breeding outcome of these buffaloes is essential for the efficiency and continuity of the livestock industry and local culture. In spite of their significance, issues concerning fertility and reproductive health are prevalent, underscoring the necessity for scientific methods to enhance breeding effectiveness and reproductive results.

Seminal plasma, a complex secretion from the testes, accessory sex glands, and epididymis, is essential for sperm fertility. It plays a critical role in sperm maturation, motility acquisition, capacitation, and the acrosome reaction (2). Sperm development is a complex process involving the proliferation and differentiation of male germ cells, with mature sperm undergoing final maturation and acquiring motility in the epididymis (3) Poor semen quality, particularly low sperm motility, is a primary indicator of this reproductive inefficiency and may be linked to an inadequate seminal microenvironment. Brohi et al. (4) reported, male infertility is a significant challenge, with underlying mechanisms that remain poorly understood.

Due to the essential function of proteins in these reproductive processes, comprehensive and systematic identification of sperm and seminal plasma proteins is vital for gaining new insights into sperm development, male fertility, and infertility. Proteomic analyses of sperm and seminal plasma have been conducted in various domestic animals, including buffalo (3, 5, 6), cattle (7–11), stallion (12) and sheep (13). To investigate the proteins involved in sperm development, we conducted an integrated proteomic study on buffalo sperm and seminal plasma. This approach enables the identification and characterization of key proteins that regulate sperm maturation, motility, and fertilization, offering insights into their roles in reproductive health. Understanding the protein profiles in sperm and seminal plasma is crucial, as variations can significantly impact fertility.

A comprehensive proteomic analysis by Gomes et al. (11) identified several key proteins in bovine seminal plasma, including BSPs (BSP1, BSP5, BSP3), spermadhesins, clusterin, osteopontin, and metalloproteinase inhibitor2. Similarly, Ashwita et al. (14) reported, proteomic profiling of spermatozoa and seminal plasma in *Bos indicus* bulls revealed proteins linked to semen quality, such as those involved in sperm protection, capacitation, and the acrosome reaction. These findings underscore the importance of identifying and characterizing proteins in sperm and seminal plasma, as their roles are critical to understanding and improving reproductive health and fertility outcomes. Despite their adaptability to hot and humid tropical climates, buffaloes exhibit low reproductive efficiency, a common issue among buffalo breeds (3).

By exploring the proteomic profiles of Toraya buffalo sperm and seminal plasma, this research represents a pioneering effort utilizing omics technology for the conservation of this important breed, which plays a crucial role in food security and local culture. The study aims to uncover valuable insights that can enhance reproductive biotechnology, optimize reproductive success, and characterize reproductive function proteins in the seminal plasma and sperm of Toraya buffalo through proteomic analysis.

2 Materials and methods

2.1 Experimental design and animal

The semen used in this study was collected from eight Toraya buffalo bulls, an endemic species native to Tanah Toraja Regency, South Sulawesi, Indonesia. The bulls were aged between four and ten years, with an average body weight of 400–600 kg. The experimental design and animal models used in this study were approved by the Animal Ethics Committee of the National Agency for Research and Innovation under certificate number 050/KE.02/SK/03/2023.

2.2 Semen collection and protein extraction

Semen samples were collected using an artificial vagina, a method that minimizes physiological alterations in the animals. The collection was conducted by experienced technicians to ensure proper handling and to maintain semen quality. Immediately after collection, semen quality was assessed through both macroscopic and microscopic evaluations. Only bulls with sperm motility exceeding 70% and a sperm concentration greater than 800×10^6 cells/mL were included in this study, following the Indonesian National Standard (SNI) for fresh semen (15). Due to the exploratory nature of this study and time constraints, semen collection was performed only once. Toraya buffalo is a unique species indigenous to Toraja Regency, and semen collection required approval from the owners or local community leaders. These factors made repeated collection unfeasible, and thus, a single collection was performed for the purposes of this initial investigation.

2.3 Protein extraction and protein molecular weight analysis using 1D SDS-Page

The semen was then centrifuged at 6500 rpm, 4°C for 30 min to separate the sperm from the seminal plasma. The supernatant (seminal plasma) and the pellet (sperm) were carefully collected and stored at −20°C for subsequent analysis. The sperm pellets were extracted using PRO-PREPTM Protein Extraction Solution (iNtRON Biotechnology, Korea) according to the manufacturer's instructions. A total of 400 μL of PRO-PREP solution was added to the sperm pellet and incubated at −20°C for 20 min. The mixture was then centrifuged at 13,000 rpm (4°C) for 5 min, and the supernatant was transferred into a sterile tube. The total soluble protein concentration of the seminal plasma and sperm samples was measured prior to SDS-PAGE analysis using the bicinchoninic acid (BCA) protein assay method (Thermo Scientific™, United States).

SDS-Page analysis was performed to determine the protein profile based on molecular weight, depicted in the form of bands on the gel. Protein separation was performed using SurePAGE™, Bis-Tris, 10 cm × 8 cm, 12 wells, 4–20% gradient gel (M00656; GenScript) (SurePAGE, GenScript Biotech Corp., Hong Kong), with running buffer Tris-MOPS-SDS (M00138; GenScript). Electrophoresis was performed at a voltage of 200 V and a current of 100–120 mA for 50 min. The gel was then stained using Coomassie Brilliant Blue stain (R-250; Bio-Rad, United States). The marker used was the Broad Multi Color Pre-Stained Protein Standard (M00624; GenScript) with a molecular weight range of ~5–270 kDa.

2.4 In gel tryptic digestion dan peptide clean up

The protein bands are excised into 1 mm × 1 mm pieces from an acrylamide gel and placed in sterile microcentrifuge tubes. Dye

removal is achieved by adding 200 μL of a destaining solution (80 mg ammonium bicarbonate in 20 mL ACN and 20 mL ultrapure water) and incubating at 37°C for 30 min with gentle agitation, repeating the process once more. Cysteine groups are reduced by adding 30 μL of reduction solution (3.3 μL TCEP in 30 μL digestion buffer) and incubating at 60°C for 10 min. After discarding the reduction solution, alkylation is performed by adding 30 μL of alkylation solution (iodoacetamide in digestion buffer) and incubating for 1 h at room temperature in the dark. The gel pieces are then washed twice with 200 μL destaining solution at 37°C for 15 min. For digestion, 50 μL of ACN is added to dry the gel pieces for 15 min, followed by a 5–10 min air dry. Then, 10 μL of active trypsin solution (10 ng/μL) is added, incubated for 15 min, and then 25 μL digestion buffer is added for a 4 h incubation at 37°C or overnight at 30°C with agitation. The digestion is stopped by adding 10 μL of 1% TFA or formic acid and incubating for 5 min. Peptide purification is performed using Pierce C18 Spin Columns, first activating the resin with 200 μL of 50% ACN and equilibrating with 200 μL of 0.5% TFA in 5% ACN. A 150 μL sample is added, followed by centrifugation at 1500 g for 5 min to allow peptides to bind. The column is washed with 200 μL equilibration buffer and centrifuged, and peptides are eluted with 20 μL of 70% ACN. Eluted peptides are dried in a vacuum centrifuge (SpeedVac) and ready for LC–MS/MS analysis.

2.5 Peptide fractionation and LC–MS/MS analysis

The dried peptide sample was dissolved in 50 μL of a dissolving solution consisting of 2% ACN, 98% ultrapure water, and 0.1% formic acid. After that, the peptide sample was centrifuged at 12,000 rpm for 10 min. Next, 2.5 μL of the peptide was fractionated using the Nano LC Ultimate 3,000 Series System Tandem Q Exactive Plus Orbitrap HRMS (Thermo Scientific). The trap column used had a diameter of 30 μm and a length of 5 mm (Thermo Scientific™ 164,649), combined with a PepMap RSLC C18 capillary column (75 μm inner diameter X 15 cm, 3 μm particle size, 100 pore size, part number ES 800, Thermo Scientific) and a flow rate of 300 nL/min. The eluents used were H2O + 0.1% formic acid and Acetonitrile (A) + 0.1% formic acid (B). The elution process involved a gradient from 2 to 35% solvent B over 27 min, followed by a gradient from 35 to 99% solvent B over 10 min, then 99% solvent B for 15 min, and finally 2% solvent B for 30 min. Signal peptide was obtained using the LTQ-Orbitrap mass spectrometer (Thermo Scientific, Bremen, Germany) with a mass range of 200–2000 m/z.

2.6 Database analysis, protein classification, and bioinformatics

The data obtained from the LC–MS/MS instrument were analyzed using Proteome Discoverer 2.2 software with the Sequest HT search engine (16). The analysis was performed using the *Bos taurus* proteome database available at UniProt,[1] applying false discovery rates of 1% (strict) and 5% (relaxed). The theoretical isoelectric point (pI) was calculated based on the amino acid sequences present in the database. The HT score, representing the sum of all Xcorr peptide values exceeding the defined threshold, was used for protein identification, Xcorr (cross-correlation) is a metric used to assess the alignment between experimentally derived peptide fragments and the theoretical spectrum, which consists of a series of b and y ions. Proteins were required to have an HT sequence score greater than 1 and at least two unique peptides, with a mass tolerance of 10 ppm. To further analyze the functions of the identified proteins, the PANTHER classification system[2] and the Database for Annotation, Visualization, and Integrated Discovery (DAVID) v6.8[3] were utilized. Venn analysis for group comparisons was conducted using the web-based tool available at https://bioinformatics.psb.ugent.be/webtools/Venn/. Additionally, protein–protein interactions were analyzed using STRING version 11.0.[4]

TABLE 1 Number of identified seminal plasma and sperm proteins of Toraya buffalo.

Protein	Toraya buffalo (n = 8)	
	Seminal plasma	Sperm
Proteome discover 2.2	1893	1913
Selection results	311	260

Proteome discover 2.2: expressed proteins from software analysis; Selection result: proteins that have been selected from protein duplication, unique protein ≥ 2, HT > 1.

3 Results

3.1 Profiling and distribution of proteins in seminal plasma and sperm

The LC–MS/MS analysis, processed using Proteome Discoverer 2.2 software, identified a total of 1,893 proteins in seminal plasma and 1,913 proteins in sperm from eight Toraya buffalo bulls (Table 1). Protein identification in sperm and seminal plasma was based on the Xcorr value of peptides exceeding the predefined threshold (Sequest HT score). The most abundant proteins identified in sperm (Table 2) were TUBB4B (139.6), ATP5F1B (114.72), CCIN (72.62), RAB2A (67.07), and GAPDHS (69.27). In seminal plasma (Table 2), the five most abundant proteins were CLU (513.38), ALB (229.36), HSP90AA1 (161.9), A2M (127.57), and GPI (116.61) (Figure 1).

Venn diagram analysis using Venny software (Figure 2) revealed that 37 proteins (6.9%) were expressed in both seminal plasma and sperm, while 274 proteins (51.3%) were uniquely expressed in seminal plasma and 223 proteins (41.8%) were uniquely expressed in sperm. The distribution of the proteome in seminal plasma and sperm of Toraya buffalo is illustrated in Figure 2, based on molecular weight (kDa), isoelectric point (pI), and the number of unique peptides. The highest proportion of proteins in both seminal plasma and sperm was observed within the molecular weight range of

1 https://www.uniprot.org/proteomes/

2 http://pantherdb.org/

3 https://david.ncifcrf.gov/home.jsp

4 https://version-11-0.string-db.org/

TABLE 2 Summary of high abundant proteins in sperm and seminal plasma.

Protein name	Xcorr value	Gene name	Uniprot-ID	Molecular function
Sperm				
Tubulin beta-4B	139.96	TUBB4B	Q3MHM5	Major constituent of microtubules
ATP synthase subunit beta	114.72	ATP5F1B	A0A452DII8	Mitochondrial membrane ATP synthase
Calicin	72.62	CCIN	Q28068	Possible morphogenic cytoskeletal
GADPH	69.27	GAPDHS	A0A4W2CEF3	Energy production during spermatogenesis
Ras-related protein Rab-2A	67.07	RAB2A	A0A4W2I9W7	Vesicle transport leading to acrosome formation
Seminal plasma				
Clusterin	513.38	CLU	A0A4W2D277	Prevents aggregation of nonnative proteins
Albumin	229.36	ALB	A0A4W2D8T3	Main protein of plasma
HSP 90-alpha	161.9	HSP90AA1	A0A4W2G0N7	Key role in the cellular response to stress
Alpha-2-macroglobulin	127.57	A2M	Q7SIH1	Regulate immune responses
Glucose-6-phosphate isomerase	116.61	GPI	A0A4W2CDD2	Providing the energy

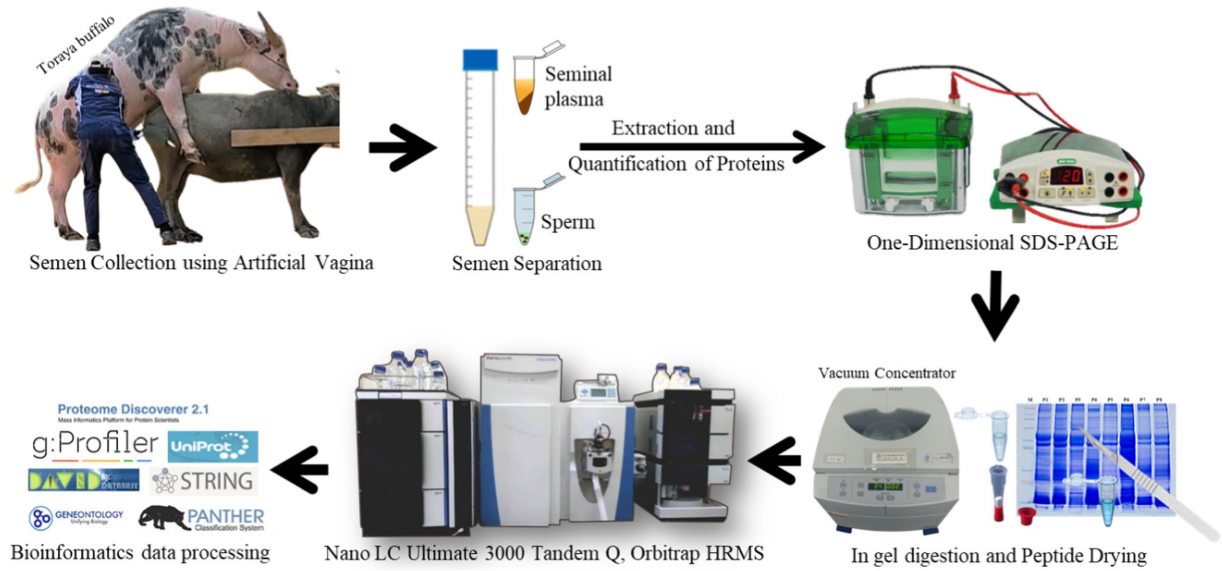

FIGURE 1
Scheme of proteomic analysis of Toraya buffalo seminal plasma and sperm.

41–60 kDa, while the lowest was detected at molecular weights ≤10 kDa and ≥ 200 kDa.

When analyzed based on isoelectric point (pI), seminal plasma proteins were most abundant within the pI range of 6–7, with the lowest abundance at pI values ≥11. In contrast, sperm proteins were predominantly found within the pI range of 8–9, with the lowest abundance at pI values ≥11 (Figures 3A,B).

Regarding the number of unique peptides, the highest proportion was observed in proteins with a single unique peptide, comprising 275 proteins (46.93%) in seminal plasma and 260 proteins (50.10%) in sperm. Conversely, proteins with 10 unique peptides were the least represented, with only 5 proteins (0.85%) in seminal plasma and 2 proteins (0.39%) in sperm (Figures 3C,D). Additionally, several proteins containing more than 14 unique peptides were identified, including Tubulin beta-4B chain (Q3MHM5), ATP synthase subunit beta (A0A452DII8), and Calicin (Q28068) in sperm, as well as Alpha-2-macroglobulin (Q7SIH1), Cullin-associated NEDD8-dissociated protein (A0A6P5BT66), and Heat shock protein HSP 90-alpha (A0A4W2G0N7) in seminal plasma.

3.2 Gene ontology analysis of the proteins

The classification of proteins from PANTHER GO analysis of seminal plasma and sperm in Toraya buffalo revealed that there were proteins that remained unclassified or did not have any assigned category. This could be due to the limitations of the buffalo database, which still follows the *Bos taurus* database. Biological processes based on GO analysis revealed that cellular process (GO:0009987) and metabolic process (GO:0008152) were the most dominant in the seminal plasma and sperm of Toraya buffalo. The seminal plasma proteins were associated with

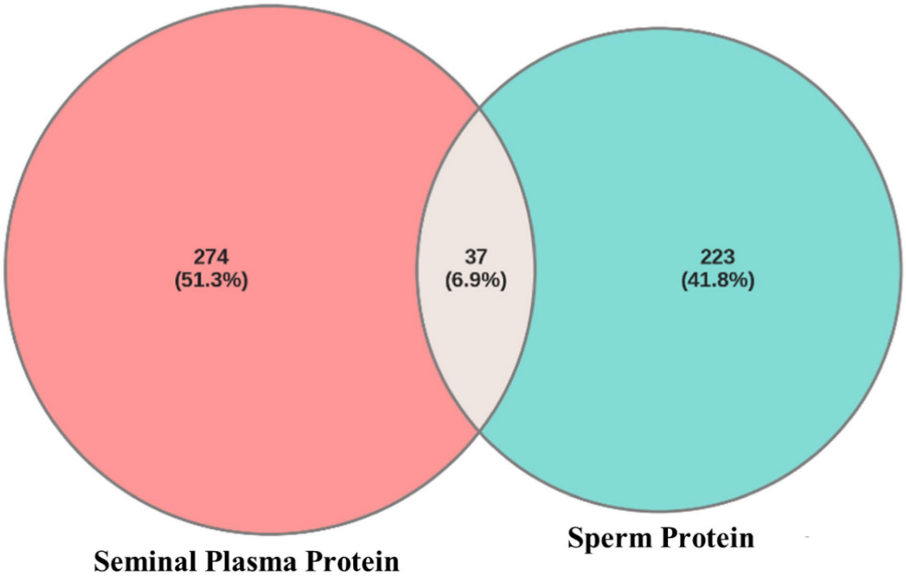

FIGURE 2
Venn diagram of proteins from Toraya buffalo seminal plasma and sperm.

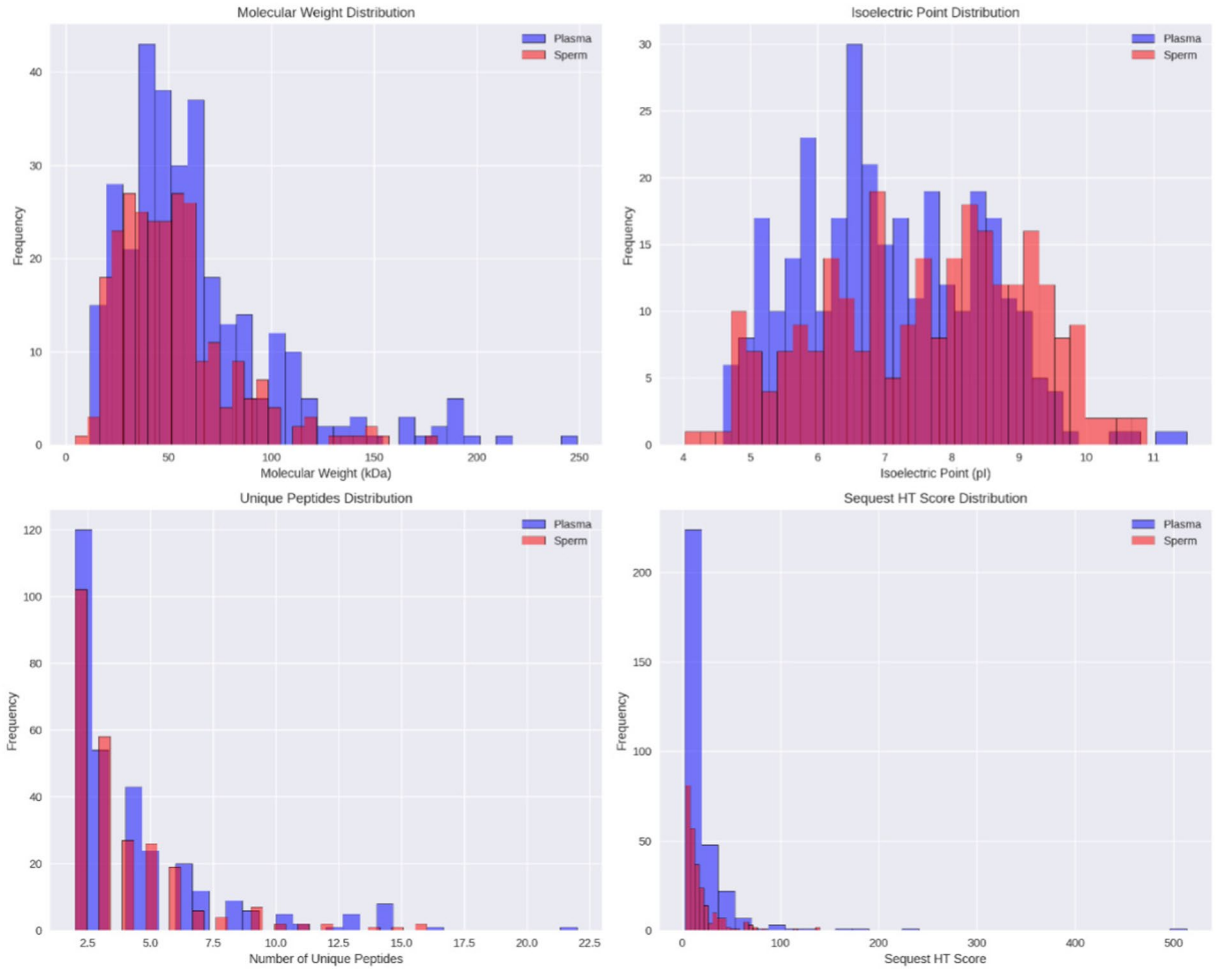

FIGURE 3
Distribution of identified proteins in Toraya buffalo sperm and seminal plasma. **(A)** molecular weight, **(B)** isoelectric point (pI), **(C)** number of unique peptides, **(D)** and sequest HT score.

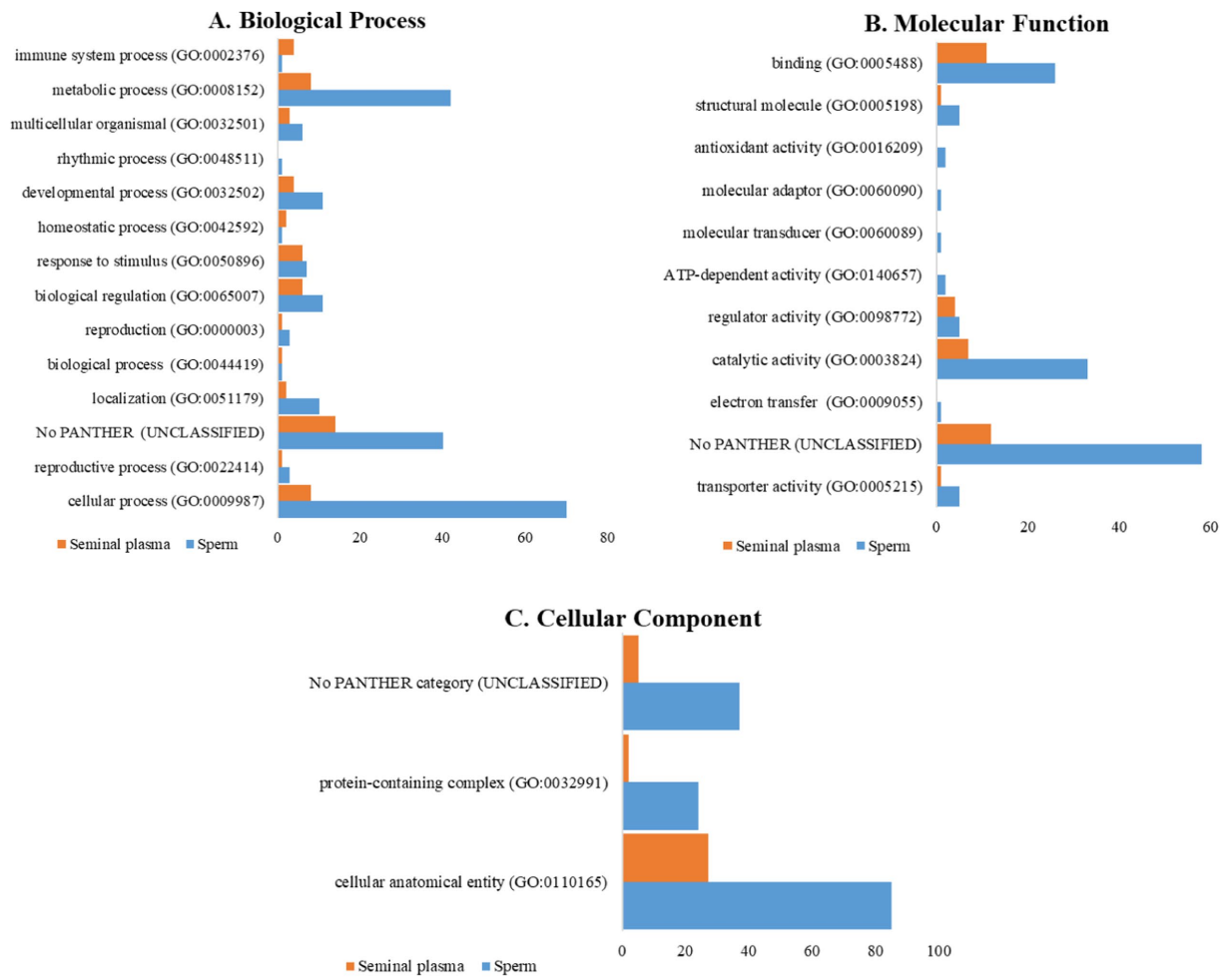

FIGURE 4
Comparison of proteins involved in **(A)** biological processes, **(B)** molecular functions, **(C)** and cellular components, in seminal plasma and sperm of Toraya buffalo.

reproduction (GO:0000003) and reproductive processes (GO:0022414), including ADAM32 (A0A3Q1LZ36), while the sperm proteins included ZPBP (F1N369), SPACA3 (A6QQ77), and CCDC136 (F1N343) (Figure 4A). The predominant molecular functions identified in seminal plasma were binding (GO:0005488) and catalytic activity (GO:0003824), as shown in Figure 4B. Additionally, the most dominant cellular component in both seminal plasma and sperm was the cellular anatomical entity (GO:0110165), as depicted in Figure 4C.

3.3 Seminal plasma and sperm protein interaction and pathway enrichment analysis

STRING analysis of expressed proteins related to reproductive function (GO:0000003) and reproductive process (GO:0022414) in seminal plasma (Figure 5A) showed that ADAM32 protein interacted with HTRA4, PLEKHA2, STXBP4, TUBGCP5, IQCG, AMER3, PRSS54, TEX55, SPATA21, and LSM1 proteins. The interaction between ZPBP proteins and other proteins is essential for spermatogenesis and sperm function. The proteins that interact with ZPBP include ACRBP, SSMEM1, SPATA48, TSACC, ARMH4, SPA17, TEX30, ROPN1, and SPACA1. These interactions indicate that ZPBPs have a central role in the protein network involved in zona pellucida binding during fertilization, as well as in different aspects of sperm development and function (Figure 5B).

The SPACA3 protein interacts with several other proteins that are crucial for spermatogenesis and sperm function. These proteins include IZUMO4, ACRBP, SPACA1, IZUMO1, TMEM190, IZUMO2, TSGA10, TCEA2, PRM3, and SPAG11B (Figure 5C). Furthermore, the proteins that interact with CCDC136 in this network are CCDC184, CCDC7, PROCA1, DHRS7B, ALMS1, FAM205A, FAM71B, NT5C1B, ESR2, and CCDC151. The CCDC136 protein as a central node, likely played a significant role in regulating cellular functions and participating in various biochemical pathways and biological processes (Figure 5D).

STRING analysis was conducted on sperm proteins that are related to reproduction (Table 3). The ZPBP protein plays a crucial role in processes like acrosome assembly and spermatid development.

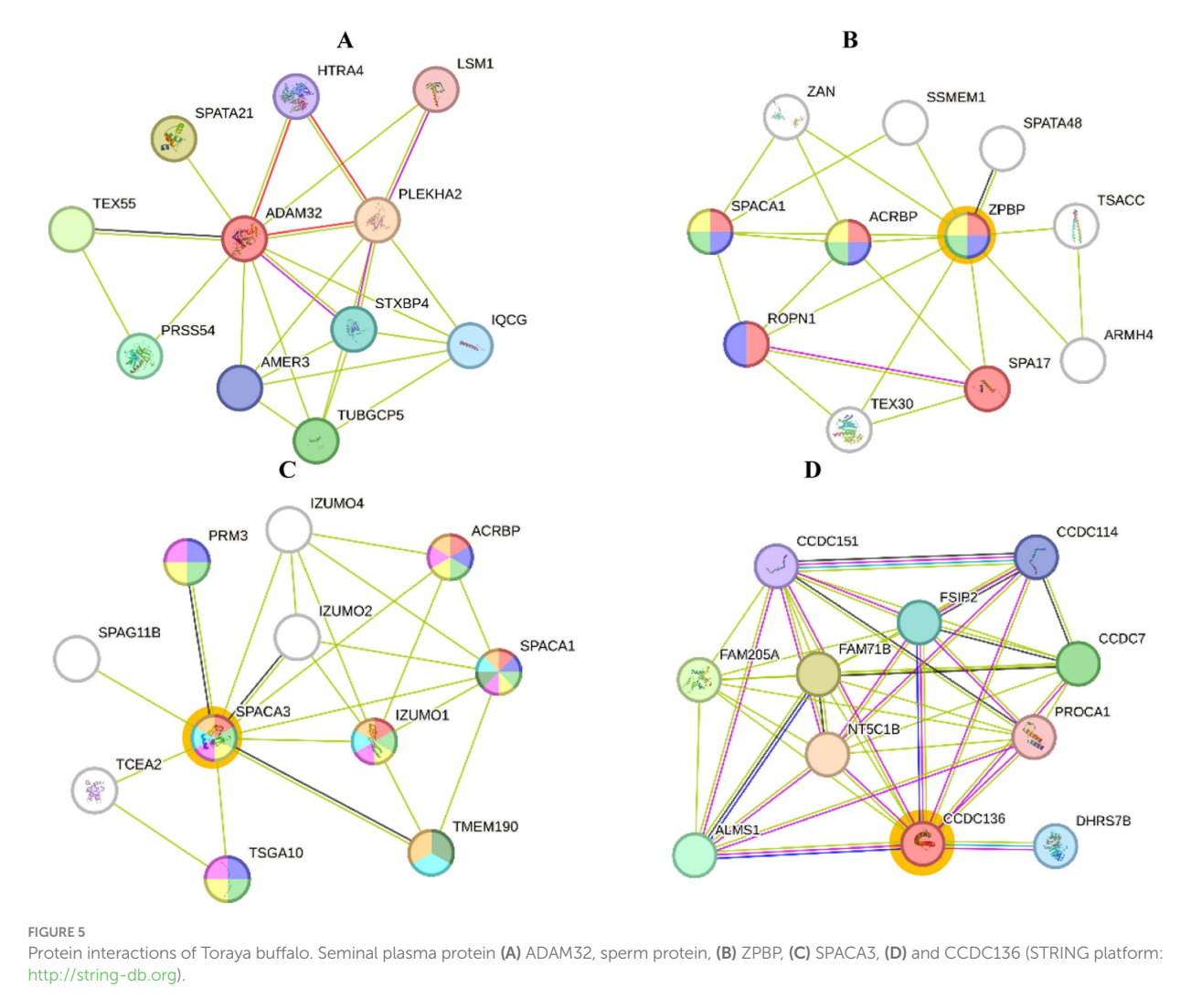

FIGURE 5
Protein interactions of Toraya buffalo. Seminal plasma protein **(A)** ADAM32, sperm protein, **(B)** ZPBP, **(C)** SPACA3, **(D)** and CCDC136 (STRING platform: http://string-db.org).

In the case of acrosome assembly (GO:0001675), ZPBP is one of three out of twenty proteins involved, with a very low false discovery rate (FDR) of 0.0021, indicating its high significance. ZPBP is also associated with sexual reproduction and acrosomal vesicles. The counts and FDR values further highlight its significant role in relevant networks.

Similarly, SPACA3 protein is involved in various reproductive processes and cellular components. For example, in the context of multicellular organism reproduction (GO:0032504), SPACA3 interacts with proteins such as IZUMO1 and ACRBP, and it is present in 6 out of 575 relevant proteins, with an extremely low FDR of 0.0018, indicating high statistical significance. SPACA3 is also associated with the acrosomal membrane and vesicle, with counts and FDR values showing strong significance, particularly for the acrosomal membrane with an FDR of 7.60e-07. CCDC136 is involved in the outer dynein arm docking complex (GO:0120228), with CCDC136 and its interacting partners constituting 2 out of 5 proteins in this complex, and an FDR of 0.0084. Although the FDR for CCDC136 is slightly higher compared to some other proteins, the results still indicate significance in its structural function within ciliary complexes.

The results showed that there are enzymes in the TCA cycle pathway that play an important role in energy metabolism. In sperm, namely Aconitase (4.2.1.3), α-Ketoglutarate Dehydrogenase (1.2.4.2), Succinyl-CoA Synthetase (6.2.1.4) and Succinate Dehydrogenase (1.3.51). In seminal plasma, Citrate Synthase (2.3.3.1) while the enzymes found in seminal plasma and sperm are malate dehydrogenase (1.1.1.37) and fumarase (4.2.1.2) (Figure 6).

4 Discussion

The characterization of proteomes in ejaculated sperm and seminal plasma is essential for understanding their functional roles in male fertility. In this study, LC–MS/MS was employed to identify the total protein composition of seminal plasma and sperm (Table 1), with findings that are consistent with previous research. Fu et al. (3) identified 864 proteins in buffalo seminal plasma and 2,147 proteins in mature buffalo sperm using LC–MS/MS. Additionally, a study utilizing shotgun proteomics identified 1,695 proteins on the surface of buffalo sperm, with nearly half of these proteins involved in key reproductive processes, including spermatogenesis, sperm maturation, and gamete interaction (17).

The most abundant proteins identified in seminal plasma and sperm in this study play critical roles in motility, energy metabolism,

TABLE 3 STRING analysis of sperm proteins related to the reproduction.

Protein (accession)	GO-term	Protein function	Count in network	FD rate	Interaction proteins
ZPBP	GO:0001675	Acrosome assembly (BP)	3 of 20	0.0021	ZPBP, ACRBP, SPACA
	GO:0007286	Spermatid development (BP)	4 of 151	0.0047	ZPBP, ACRBP, ROPN1, SPACA1
	GO:0019953	Sexual reproduction (BP)	5 of 602	0.0140	ZPBP, ACRBP, SPACA1, ROPN1, SPA17
	GO:0001669	Acrosomal vesicle (CC)	3 of 92	0.0223	ZPBP, ACRBP, SPACA1
SPACA3	GO:0001675	Cellular process involved in reproduction (BP)	4 of 317	0.0357	SPACA3, IZUMO1, SPACA1, ACRBP
	GO:0032504	Multicellular organism reproduction (BP)	6 of 575	0.0018	SPACA3, IZUMO1, SPACA1, ACRBP, TSGA10, PRM3
	GO:0022414	Reproductive process (BP)	6 of 1,033	0.0183	SPACA3, IZUMO1, SPACA1, ACRBP, TSGA10, PRM3
	GO: 0019953	Sexual reproduction (BP)	6 of 602	0.0018	SPACA3, IZUMO1, SPACA1, ACRBP, TSGA10, PRM3
	GO:0007283	Spermatogenesis (BP)	4 of 362	0.0498	SPACA1, ACRBP, PRM3, TSGA10
	GO:0002080	Acrosomal membrane (CC)	4 of 21	7.60e-	SPACA3, IZUMO1, SPACA1, MEM190
	GO:0001669	Acrosomal vesicle (CC)	5 of 92	7.60e-	SPACA3, IZUMO1, SPACA1, MEM190, ACRBP
	GO:0002079	Inner acrosomal membrane (CC)	2 of 6	0.0019	SPACA1, MEM190
CCDC136	GO: 0120228	Outer dynein arm docking complex (CC)	2 of 5	0.0084	CCDC151, CCDC114

False discovery (FD); Biological process (BP); Cellular component (CC).

sperm protection, and structural integrity (Table 2). The predominant proteins in sperm TUBB4B, ATP5F1B, CCIN, RAB2A, and GAPDHS are crucial for motility, energy metabolism, and cytoskeletal stability (18–20). Meanwhile, the most abundant proteins in seminal plasma CLU, ALB, HSP90AA1, A2M, and GPI are primarily involved in sperm protection, molecular transport, protein stabilization, energy provision, and enzymatic regulation (21, 22). These findings align with previous studies, which reported that the most abundant seminal plasma proteins (ALB, CLU, and AZGP1) and sperm proteins (TUBB, AKAP4, and ODF2) are associated with enhanced fertility in buffalo bulls (3). In buffalo, sperm quality has been identified as a major factor contributing to male infertility. Previous research has demonstrated that a substantial proportion of reproductive failures can be attributed to poor semen quality (23). These findings highlight the importance of understanding the seminal plasma and sperm proteome as a means to improve fertility outcomes in buffalo breeding programs.

Mass spectrometry techniques, such as LC–MS/MS, facilitate the identification of unique peptides in seminal plasma and sperm, enabling a comprehensive analysis of protein compositions in complex biological fluids. This approach is instrumental in identifying potential biomarkers associated with male fertility. For instance, specific proteins in seminal plasma linked to sperm motility and male infertility have been identified as potential diagnostic markers (24, 25). Gene ontology (GO) annotations of the buffalo sperm and seminal plasma proteomes allowed for the prediction of protein functions, providing valuable insights into key biological processes, including energy metabolism, fertilization, the acrosomal reaction, antioxidant activity, and sperm capacitation (26).

The classification of proteins using PANTHER GO analysis involves several hierarchical stages. Initially, proteins are categorized based on their molecular functions, including catalytic activity, binding affinity, and structural roles. Subsequently, proteins are classified according to their involvement in specific biological processes, such as metabolism, cellular regulation, and reproduction. Lastly, proteins are grouped based on their cellular localization, including the cytoplasm, nucleus, and other reproductive structures (8, 27).

The STRING database serves as a powerful tool for elucidating protein–protein interaction networks, which are essential for understanding the functional roles of proteins in reproductive processes (Figures 5, 6). Among these, ADAM32, a protein found in bull seminal plasma, plays a critical role in sperm quality and function. Proteomic analyses have demonstrated a correlation between its molecular weight and semen quality parameters, including motility, viability, and plasma membrane integrity factors that collectively influence fertility (8, 28). ADAM family proteins, including ADAM32, are implicated in sperm-egg interactions and fertility in both bulls and humans. Additionally, metalloproteinase inhibitor 2, a key regulator of ADAMs, has been linked to bull fertility and sperm DNA integrity (11).

STRING analysis of sperm proteins related to reproduction provides a comprehensive understanding of interaction networks involved in various reproductive mechanisms. One such protein, zona pellucida-binding protein (ZPBP), is crucial for spermatozoa-zona pellucida binding and subsequent fertilization. Notably, ZPBP is more abundant in high-fertility (HF) bulls, making it a potential biomarker for fertility. Proper ZPBP function is essential for sperm-zona pellucida interactions, and its dysfunction can result in compromised fertility (26, 29). ZPBP, with a molecular weight of 36.8 kDa and an isoelectric point (pI) of 9.13, exists in two isoforms: ZPBP1, expressed in spermatids and sperm, and ZPBP2, expressed in the testis. ZPBP1 interacts with ZP2, triggering the acrosome reaction required for fertilization. Disruption of either ZPBP1 or ZPBP2 has been linked to infertility due to abnormal sperm morphology and function (30, 31).

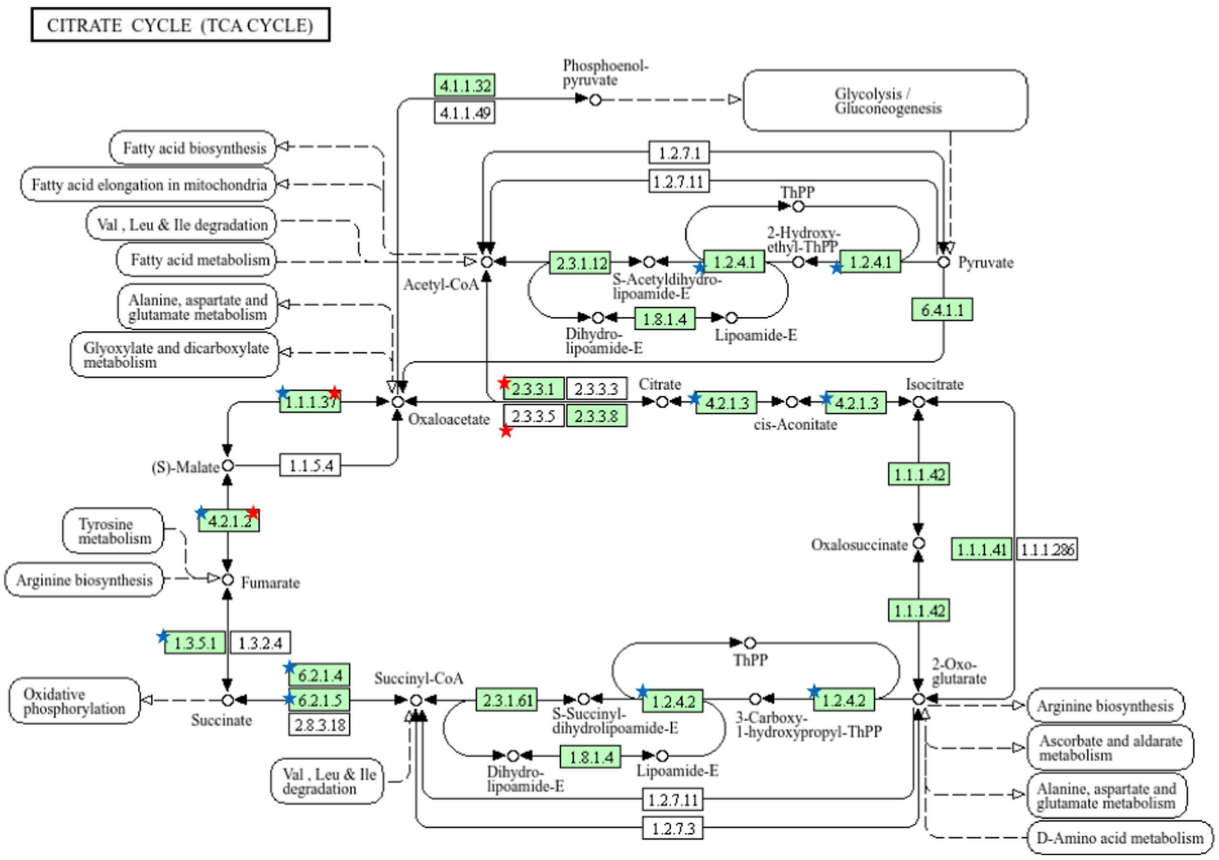

FIGURE 6
Pathway analysis using the KEGG pathway database identified proteins involved in the TCA cycle. The red star denotes the detected proteins in seminal plasma and the blue star notes the detected proteins in sperm.

Another crucial protein, SPACA3 (also known as SPRASA or SLLP1), is essential for bovine spermiogenesis and sperm-egg interactions. It plays a significant role in the acrosome reaction and oocyte plasma membrane adhesion (32). SPACA3 interacts with other sperm proteins, including equatorin (EQTN), which facilitates sperm-oocyte fusion through the acrosome reaction (33, 34). Additionally, CCDC136, a testis-specific gene, is critical for acrosome formation and fertilization. Knockout studies in mice have shown that the absence of CCDC136 results in severe acrosome defects, leading to infertility. As a member of the coiled-coil domain-containing (CCDC) protein family, CCDC136 is vital for sperm motility and capacitation. Its importance is further demonstrated *in vitro*, where anti-CCDC136 antibodies significantly inhibit fertilization (35, 36).

Pathway analysis using the Kyoto Encyclopedia of Genes and Genomes (KEGG) database enables the identification of proteins involved in the tricarboxylic acid (TCA) cycle by mapping them to specific metabolic pathways. Kumanresen et al. (29) reported that GO annotations facilitate the characterization of biological processes, cellular components, and molecular functions of differentially expressed proteins. Proteins involved in glycolytic pathways, the mitochondrial respiratory chain, and the TCA cycle are essential for sperm motility and energy metabolism. Recent studies have identified two key enzymes related to the TCA cycle, pyruvate dehydrogenase E1 component subunit alpha-2 (PDHA2) and aconitase 2 (ACO2), which are crucial for ATP production in sperm mitochondria (9).

Proteomic studies on buffalo seminal plasma and sperm have also revealed proteins involved in energy metabolism, including those associated with glycolysis and the pentose phosphate pathway—both of which are functionally linked to the TCA cycle (3, 11, 36, 37). The TCA cycle, also referred to as the citric acid or Krebs cycle, serves as a central metabolic pathway in cellular respiration, generating ATP to meet the high energy demands of sperm cells. This cycle is particularly vital for spermatids, as it fuels sperm motility, which is essential for successful fertilization (38, 39).

Key enzymes such as malate dehydrogenase (EC 1.1.1.37) and fumarase (EC 4.2.1.2) play crucial roles in the TCA cycle. Malate dehydrogenase catalyzes the oxidation–reduction reaction that generates NADH, which subsequently contributes to ATP production via the electron transport chain (40, 41). Given that sperm require substantial energy for motility and fertilization, the TCA cycle serves as one of the primary pathways for ATP synthesis in sperm mitochondria. Additionally, enzymes present in seminal plasma contribute to metabolite availability and redox balance, which are essential for maintaining sperm quality. ATP is particularly critical for microtubule activity, which supports multiple sperm functions, including acrosome formation and activation—both of which are energy-intensive processes (42).

Fumarase is another key enzyme in the TCA cycle, catalyzing the reversible hydration of fumarate to malate, thereby ensuring the continuity of the metabolic pathway (40). In addition to these

enzymes, other metabolic components of seminal plasma provide valuable insights into sperm health and function. The findings of this study offer a crucial reference for future research on buffalo sperm function and seminal plasma proteomics, particularly in the context of fertility biomarkers. Moreover, these insights pave the way for the development of molecular tools for bull selection, contributing to the conservation of indigenous Indonesian buffalo breeds and enhancing reproductive efficiency.

5 Conclusion

This study presents the first comprehensive proteomic identification of seminal plasma and sperm proteins associated with reproductive functions in the Toraya buffalo. The research underscores the identification of key proteins, such as ZPBP, SPACA3, and CCDC136 in sperm, and ADAM32 in seminal plasma, which are potential biomarkers for fertility. These proteins play significant roles in reproductive processes and their presence could offer new avenues for fertility evaluation and enhancement in buffalo breeding programs.

Data availability statement

The data supporting the conclusions of this research can be obtained from the corresponding author upon a reasonable request.

Ethics statement

The animal study was approved by the Animal Ethics Commission of the National Research and Innovation Agency with certificate number 050/KE.02/SK/03/2023. The study was conducted in accordance with the local legislation and institutional requirements.

Author contributions

TM: Conceptualization, Data curation, Writing – original draft, Writing – review & editing, Formal analysis, Project administration, Investigation, Methodology. SS: Funding acquisition, Validation, Writing – original draft, Writing – review & editing, Formal analysis, Investigation, Methodology, Visualization. RIA: Conceptualization, Supervision, Writing – review & editing. JJ: Conceptualization, Supervision, Writing – review & editing. AG: Methodology, Supervision, Formal analysis, Validation, Investigation, Writing – review & editing.

Funding

The author(s) declare that financial support was received for the research and/or publication of this article. This study was financially supported by the Riset dan Inovasi Indonesia Maju (RIIM) batch 3 partnership BRIN and LPDP (letter of appointment number: 12/II.7/HK/2023).

Acknowledgments

The authors sincerely thank to IPB University for its support and thanks to Kana and Tian for their invaluable assistance in field sample collection.

Conflict of interest

The authors declare that the research was conducted in the absence of any commercial or financial relationships that could be construed as a potential conflict of interest.

Publisher's note

All claims expressed in this article are solely those of the authors and do not necessarily represent those of their affiliated organizations, or those of the publisher, the editors and the reviewers. Any product that may be evaluated in this article, or claim that may be made by its manufacturer, is not guaranteed or endorsed by the publisher.

References

1. Maulana T, Iskandar H, Said S, Gunawan A. The current status and potential development of genetic resources of indigenous toraya spotted buffalo in Indonesia: a systematic review. *World Vet J*. (2023) 13:617–25. doi: 10.54203/SCIL.2023.WVJ66

2. Bromfield JJ. Seminal fluid and reproduction: much more than previously thought. *J Assist Reprod Genet*. (2014) 31:627–36. doi: 10.1007/s10815-014-0243-y

3. Fu Q, Pan L, Huang D, Wang Z, Hou Z, Zhang M. Proteomic profiles of buffalo spermatozoa and seminal plasma. *Theriogenology*. (2019) 134:74–82. doi: 10.1016/j.theriogenology.2019.05.013

4. Brohi RD, Huo LJ. Posttranslational modifications in spermatozoa and effects on male fertility and sperm viability. *OMICS*. (2017) 21:245–56. doi: 10.1089/omi.2016.0173

5. Huang Y, Fu Q, Yang L, Guan J, Pan H, Chen F, et al. Differences between high- and low-motility buffalo sperm identified by comparative proteomics. *Reprod Domest Anim*. (2015) 50:443–51. doi: 10.1111/rda.12511

6. Hou Z, Fu Q, Huang Y, Zhang P, Chen F, Li M, et al. Comparative proteomic identification buffalo spermatozoa during in vitro capacitation. *Theriogenology*. (2019) 126:303–9. doi: 10.1016/j.theriogenology.2018.12.025

7. Westfalewicz B, Słowińska M, Judycka S, Ciereszko A, Dietrich MA. Comparative proteomic analysis of young and adult bull (*bos taurus*) cryopreserved semen. *Animals*. (2021) 11:2013. doi: 10.3390/ani11072013

8. Iskandar H, Andersson G, Sonjaya H, Arifiantini RI, Said S, Hasbi H, et al. Protein identification of seminal plasma in Bali bull (*Bos javanicus*). *Animals*. (2023) 13:514. doi: 10.3390/ani13030514

9. Rosyada ZNA, Pardede BP, Kaiin EM, Gunawan M, Maulana T, Said S, et al. A proteomic approach to identifying spermatozoa proteins in indonesian native madura bulls. *Front Vet Sci*. (2023) 10:1287676. doi: 10.3389/fvets.2023.1287676

10. Ramesha KP, Mol P, Kannegundla U, Thota LN, Gopalakrishnan L, Rana E, et al. Deep proteome profiling of semen of indian indigenous malnad gidda (*bos indicus*) cattle. *J Proteome Res*. (2020) 19:3364–76. doi: 10.1021/acs.jproteome.0c00237

11. Gomes FP, Park R, Viana AG, Fernandez-Costa C, Topper E, Kaya A, et al. Protein signatures of seminal plasma from bulls with contrasting frozen–thawed sperm viability. *Sci Rep*. (2020) 10:14661–14. doi: 10.1038/s41598-020-71015-9

12. Swegen A, Curry BJ, Gibb Z, Lambourne SR, Smith ND, Aitken RJ. Investigation of the stallion sperm proteome by mass spectrometry. *Reproduction*. (2015) 149:235–44. doi: 10.1530/REP-14-0500

13. Soleilhavoup C, Tsikis G, Labas V, Harichaux G, Kohnke PL, Dacheux JL, et al. Ram seminal plasma proteome and its impact on liquid preservation of spermatozoa. *J Proteome*. (2014) 109:245–60. doi: 10.1016/j.jprot.2014.07.007

14. Ashwitha A, Ramesha KP, Ramesh P, Kootimole CN, Devadasan MJ, Ammankallu S, et al. Quantitative proteomics profiling of spermatozoa and seminal plasma reveals proteins associated with semen quality in *Bos indicus* bulls. *J Proteome*. (2023) 273:104794. doi: 10.1016/j.jprot.2022.104794

15. Badan Standardisasi Nasional. Frozen semen part-1: Buffalo. Indonesian National Standard. Jakarta (Indonesia): Badan Standardisasi Nasional (2021).

16. Orsburn BC. Proteome discoverer—a community enhanced data processing suite for protein informatics. *Proteomes*. (2021) 9:15. doi: 10.3390/proteomes9010015

17. Batra V, Dagar K, Diwakar MP, Kumaresan A, Kumar R, Datta TK. The proteomic landscape of sperm surface deciphers its maturational and functional aspects in buffalo. *Front Physiol*. (2024) 22:1–17. doi: 10.1186/s12864-021-07640-z

18. Yan W. Calicin is a key sperm head-shaping factor essential for male fertility. *Sci Bull*. (2022) 67:2395–7. doi: 10.1016/j.scib.2022.11.022

19. Li C, Chen J, Mu S, Zhang H, Guo M, Li Y, et al. Rab2 and Rab6 are implicated in acrosome formation during spermatogenesis in eriocheir sinensis: based on sperm proteome. *Front Biosci*. (2023) 28:160. doi: 10.31083/j.fbl2808160

20. Sanzhaeva U, Wonsettler NR, Rhodes SB, Ramamurthy V. TUBB4B is essential for the expansion of differentiating spermatogonia. *Sci Rep*. (2024) 14:20889. doi: 10.1038/s41598-024-71303-8

21. Wei H, Zhang Y, Jia Y, Chen X, Niu T, Chatterjee A, et al. Heat shock protein 90: biological functions, diseases, and therapeutic targets. *MedComm*. (2024) 5:e470. doi: 10.1002/mco2.470

22. Saewu A, Kadunganattil S, Raghupathy R, Kongmanas K, Diaz-Astudillo P, Hermo L, et al. Clusterin in the mouse epididymis: possible roles in sperm maturation and capacitation. *Reproduction*. (2017) 154:867–80. doi: 10.1530/REP-17-0518

23. Soggiu A, Piras C, Hussein HA, De Canio M, Gaviraghi A, Galli A, et al. Unravelling the bull fertility proteome. *Mol BioSyst*. (2013) 9:1188–95. doi: 10.1039/c3mb25494a

24. Barrachina F, Jodar M, Delgado-Dueñas D, Soler-Ventura A, Estanyol JM, Mallofré C, et al. Stable-protein pair analysis as a novel strategy to identify proteomic signatures: application to seminal plasma from infertile patients. *Mol Cell Proteomics*. (2019) 18:S77–90. doi: 10.1074/mcp.RA118.001248

25. Wu Y, Yuan Y, Chen L, Wang M, Yang Y, Wang Y, et al. Quantitative proteomic analysis of human seminal plasma from normozoospermic and asthenozoospermic individuals. *Biomed Res Int*. (2019) 2019:1–10. doi: 10.1155/2019/2735038

26. Karanwal S, Pal A, Chera JS, Batra V, Kumaresan A, Datta TK, et al. Identification of protein candidates in spermatozoa of water buffalo (*Bubalus bubalis*) bulls helps in predicting their fertility status. Front cell. *Dev Biol*. (2023) 11:11. doi: 10.3389/fcell.2023.1119220

27. Fernandez-Encinas A, García-Peiró A, del Rey J, Ribas-Maynou J, Abad C, Amengual MJ, et al. Proteomic analysis in seminal plasma of fertile donors and infertile patients with sperm dna fragmentation. *Int J Mol Sci*. (2020) 21:5046. doi: 10.3390/ijms21145046

28. Leahy T, Rickard JP, Bernecic NC, Druart X, de Graaf SP. Ram seminal plasma and its functional proteomic assessment. *Reproduction*. (2019) 157:R243–56. doi: 10.1530/REP-18-0627

29. Kumaresan A, Sinha MK, Paul N, Nag P, Ebenezer Samuel King JP, Kumar R, et al. Establishment of a repertoire of fertility associated sperm proteins and their differential abundance in buffalo bulls (*Bubalus bubalis*) with contrasting fertility. *Sci Rep*. (2023) 13:2272. doi: 10.1038/s41598-023-29529-5

30. Lin YN, Roy A, Yan W, Burns KH, Matzuk MM. Loss of zona Pellucida binding proteins in the Acrosomal matrix disrupts acrosome biogenesis and sperm morphogenesis. *Mol Cell Biol*. (2007) 27:6794–805. doi: 10.1128/MCB.01029-07

31. Yatsenko AN, O'Neil DS, Roy A, Arias-Mendoza PA, Chen R, Murthy LJ, et al. Association of mutations in the zona pellucida binding protein 1 (ZPBP1) gene with abnormal sperm head morphology in infertile men. *Mol Hum Reprod*. (2012) 18:14–21. doi: 10.1093/molehr/gar057

32. Li X, Duan C, Li R, Wang D. Insights into the mechanism of bovine spermiogenesis based on comparative transcriptomic studies. *Animals*. (2021) 11:80. doi: 10.3390/ani11010080

33. Pang WK, Amjad S, Ryu DY, Adegoke EO, Rahman MS, Park YJ, et al. Establishment of a male fertility prediction model with sperm RNA markers in pigs as a translational animal model. *J Anim Sci Biotechnol*. (2022) 13:84. doi: 10.1186/s40104-022-00729-9

34. Zheng H, Mandal A, Shumilin IA, Chordia MD, Panneerdoss S, Herr JC, et al. Sperm lysozyme-like protein 1 (SLLP1), an intra-acrosomal oolemmal-binding sperm protein, reveals filamentous organization in protein crystal form. *Andrology*. (2015) 3:756–71. doi: 10.1111/andr.12057

35. Geng Q, Ni L, Ouyang B, Hu Y, Zhao Y, Guo J. A novel testis-specific gene, ccdc136, is required for acrosome formation and fertilization in mice. *Reprod Sci*. (2016) 23:1387–96. doi: 10.1177/1933719116641762

36. Urizar-Arenaza I, Osinalde N, Akimov V, Puglia M, Candenas L, Pinto FM, et al. Phosphoproteomic and functional analyses reveal sperm-specific protein changes downstream of kappa opioid receptor in human spermatozoa. *Mol Cell Proteomics*. (2019) 18:S118–31. doi: 10.1074/mcp.RA118.001133

37. Viana AGA, Martins AMA, Pontes AH, Fontes W, Castro MS, Ricart CAO, et al. Proteomic landscape of seminal plasma associated with dairy bull fertility. *Sci Rep*. (2018) 8:16323–13. doi: 10.1038/s41598-018-34152-w

38. Almadaly EA, Abdel-Salam ABS, Sahwan FM, Kahilo KA, Abouzed TK, El-Domany WB. Fertility-associated biochemical components in seminal plasma and serum of buffalo (*Bubalus bubalis*) bulls. *Front Vet Sci*. (2023) 9:9. doi: 10.3389/fvets.2022.1043379

39. Kang W, Harada Y, Yamatoya K, Kawano N, Kanai S, Miyamoto Y, et al. Extra-mitochondrial citrate synthase initiates calcium oscillation and suppresses age-dependent sperm dysfunction. *Lab Investig*. (2020) 100:583–95. doi: 10.1038/s41374-019-0353-3

40. Martínez-Reyes I, Chandel NS. Mitochondrial TCA cycle metabolites control physiology and disease. *Nat Commun*. (2020) 11:102. doi: 10.1038/s41467-019-13668-3

41. Arnold PK, Finley LWS. Regulation and function of the mammalian tricarboxylic acid cycle. *J Biol Chem*. (2023) 299:102838. doi: 10.1016/j.jbc.2022.102838

42. Magdanz V, Boryshpolets S, Ridzewski C, Eckel B, Reinhardt K. The motility-based swim-up technique separates bull sperm based on differences in metabolic rates and tail length. *PLoS One*. (2019) 14:e0223576. doi: 10.1371/journal.pone.0223576

frontiers | Frontiers in Veterinary Science

TYPE Original Research
PUBLISHED 30 April 2025
DOI 10.3389/fvets.2025.1552045

OPEN ACCESS

EDITED BY
Manuel Garcia-Herreros,
National Institute for Agricultural and Veterinary Research (INIAV), Portugal

REVIEWED BY
Karima Mahmoud,
National Research Centre, Egypt
Aykut Gram,
Erciyes University, Türkiye

*CORRESPONDENCE
Lei Yang
✉ leiyang@imu.edu.cn
Guanghua Su
✉ suguanghua0707@163.com

†These authors have contributed equally to this work

RECEIVED 27 December 2024
ACCEPTED 03 April 2025
PUBLISHED 30 April 2025

CITATION
Su X, Gao G, Chen L, Zhang L, Liu G, Bian C, Su G and Yang L (2025) Identification of candidate blood biomarkers through metabolomics analysis in bovine superovulation.
Front. Vet. Sci. 12:1552045.
doi: 10.3389/fvets.2025.1552045

Identification of candidate blood biomarkers through metabolomics analysis in bovine superovulation

Xiaohu Su[1†], Guangqi Gao[2†], Liqiang Chen[1], Liguo Zhang[3], Guangnan Liu[3], Chao Bian[4], Guanghua Su[1*] and Lei Yang[1*]

[1]State Key Laboratory of Reproductive Regulation and Breeding of Grassland Livestock, School of Life Sciences, Inner Mongolia University, Hohhot, Inner Mongolia Autonomous Region, China, [2]Key Laboratory of Dairy Products Processing, Ministry of Agriculture and Rural Affairs, Inner Mongolia Agricultural University, Hohhot, Inner Mongolia Autonomous Region, China, [3]Ulanqab Animal Husbandry Workstation, Ulanqab Agriculture and Animal Husbandry Bureau, Ulanqab, Inner Mongolia Autonomous Region, China, [4]Tumor Radiotherapy Department, Inner Mongolia People's Hospital, Hohhot, Inner Mongolia Autonomous Region, China

Superovulation and embryo transfer technologies provide strong support for improving the productivity of cattle population. A non-invasive diagnostic method for superovulation prediction is necessary to improve its efficiency. Compared to macromolecular substances, there has been an increasing number of studies on small molecular metabolites as biomarkers. This study aimed to identify key biomarkers associated with superovulation outcomes in cows through serum metabolomics analysis. In this study, 36 induced estrus cows were selected, and the blood samples were collected at three time points: before FSH injection, before artificial insemination, and before embryo collection. Then, the cows were classified into high embryonic yield (HEY) and low embryonic yield (LEY) groups based on the total number of embryos. Furthermore, a serum untargeted metabolomics analysis of the two groups was conducted using liquid chromatography with tandem mass spectrometry (LC–MS/MS). A total of 372 embryos were collected. The metabolomics analysis revealed that 1,158 metabolites were detected, and 617 were annotated. In the before FSH injection samples, 121 differential metabolites were identified between the two groups. In the before artificial insemination samples, 129 differential metabolites were identified. In the before embryo collection samples, 201 differential metabolites were identified. A total of 11 differential metabolites were shared between the before FSH injection and before artificial insemination samples, while five differential metabolites were shared across all three samples. The majority of the differential metabolites were significantly enriched in pathways related to amino acid and fatty acid metabolism, digestive system secretion, and ovarian steroidogenesis. This study showed that phosphatidylcholine [PC; 14:0/22:1(13Z)], phosphatidylethanolamine [PE; DiMe (11, 3)], triacylglycerol [TG; 15:0/16:0/22:4 (7Z, 10Z, 13Z, 16Z)], phosphatidylinositol [PI; 16:0/22:2 (13Z, 16Z)], and phosphatidylserine [PS; 18:0/20:4(8Z, 11Z, 14Z, 17Z)] were differentially expressed in the serum during the superovulation period. These could serve as potential biomarkers for embryonic yield prediction in bovine superovulation. The lipid and amino acid metabolic pathways may have an impact on the ovarian response. The results of this study could provide novel screening indexes of donors for bovine superovulation, although the accuracy of the relevant factors requires further investigation.

KEYWORDS

cow, superovulation, metabolome, serum, biomarker

Introduction

The cattle industry is an important part of animal husbandry. Superovulation and embryo transfer technologies provide powerful support for improving the productivity of cattle population. However, the efficiency of bovine superovulation is affected by multiple factors, including genetics, age, body condition, diseases, and management, likely through their influence on the uterine environment, oocyte quality, and embryo development (1). To improve the screening efficiency of donors for bovine superovulation, several strategies have been established, including small follicle detection by ultrasound (2), genotype analysis (3–5), reproductive hormone detection (AMH, P4, E2, and FSH) (6–13), blood vitamin levels (14), paraoxonase-1 (15), serum biochemical parameters (16), and partial metabolic parameters (17, 18). However, the ovarian antral follicle count does not have a linear correlation with the outcome of embryo production (19). The prediction efficiency of reproductive hormone levels varies with age (11). In addition, the detection time is also important. Compared to macromolecular substances, there have been an increasing number of studies on small molecule metabolites as biomarkers.

Metabolites are the end products of various biochemical reactions in cells. Their composition and activity are influenced by both internal and external factors. Many studies have been conducted on the metabolome and bovine reproduction, including reproductive performance (17, 18, 20), pregnancy prediction (21–24), and reproductive disorders (1, 25–27). In the research by Horn et al., the preovulatory serum metabolome was analyzed in cows with different body condition scores to explain the mechanisms by which extreme body conditions affect reproductive capacity (18). However, more studies are necessary to identify reliable metabolic biomarkers related to bovine superovulation and to more comprehensively reveal the regulatory mechanisms, as metabolites are affected by many factors.

In this study, differences in serum reproductive hormones and metabolites between high embryonic yield (HEY) and low embryonic yield (LEY) HuaXi cows were analyzed during the superovulation period to identify key biomarkers related to superovulation outcomes. The study results may provide novel screening indexes of donors for bovine superovulation.

Results

Embryo production

In this study, 36 cows were selected and treated using the standard superovulation process (Figure 1). The results are shown in Table 1. A total of 372 embryos were collected, with an average of 10.33 ± 1.25 embryos per cow. Of these, 286 embryos were viable, with an average of 7.94 ± 1.16 embryos per cow. Finally, 11 cows were assigned to the HEY group, while 9 cows were assigned to the LEY group.

Untargeted metabolic profiling of the cows' serum during superovulation

To explore the serum metabolic differences between HEY and LEY groups, untargeted metabolomics analysis was performed. In total, 13,222 features were detected, of which 5,654 metabolites were annotated (Supplementary Table S1). According to the Human Metabolome Database (HMDB) analysis, the most enriched category was lipids and lipid-like molecules (353 metabolites), followed by organic acids and derivatives (75 metabolites) and benzenoids (69 metabolites; Supplementary Figure S1A). According to the Kyoto Encyclopedia of Genes and Genomes (KEGG) analysis, the most enriched pathway was metabolic pathways (206 metabolites), followed by glycerophospholipid metabolism (135 metabolites) and the biosynthesis of secondary metabolites (75 metabolites; Supplementary Figure S1B).

Multivariate statistical analysis

Principal component analysis (PCA) was conducted to determine the separation and aggregation of samples between HEY and LEY groups. The first principal component (PC1) and the second principal component (PC2) were 12.3 and 8.2%, respectively (Figure 2A). Orthogonal partial least squares discriminant analysis (OPLS-DA) was performed to further investigate the variables responsible for classification and to achieve better group separation. For the before FSH injection samples, the R2 of the OPLS-DA model was 0.996 and the Q2 was 0.736 (Figure 2B). In the before artificial insemination samples, the R2 and Q2 were 0.996 and 0.796, respectively (Figure 2C). In the before embryo collection samples, the R2 and Q2 were 0.988 and 0.553,

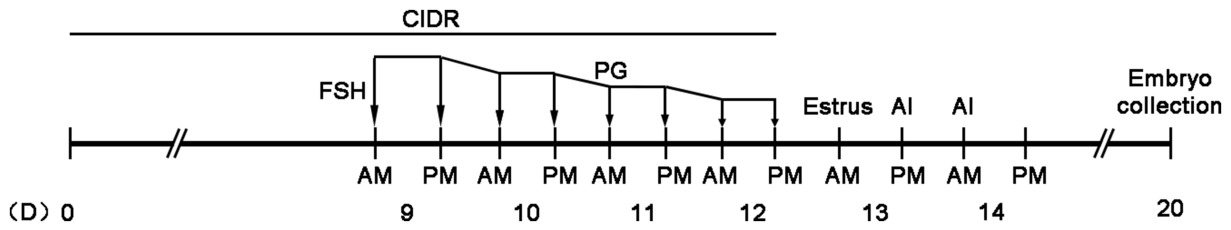

FIGURE 1
CIDR (Zoetis, New Zealand) was inserted into the vagina on day 0 (D0). Between days 9 and 12, a total of 500 μg of FSH (Stimufol®, Belgium) was injected in eight doses, with each dose decreasing by 10%. On the fifth FSH injection (morning of D11), 300 μg of PG (Reprobiol, New Zealand) was injected synchronously. The CIDR was removed at the time of the final FSH injection. Estrus detection occurred on D13, and AI was performed twice (12 h interval). On D20, embryos were collected via uterus flushing after the cows were anesthetized with a caudal spinal injection of lidocaine hydrochloride.

TABLE 1 Statistics of embryonic production after superovulation in cows (mean ± S.D.).

Donor number	Total embryos	Average total embryos	Total viable embryos	Average viable embryos	HEY donor number	Average total embryos of HEY	Average viable embryos of HEY	LEY donor number	Average total embryos of LEY	Average viable embryos of LEY
36	372	10.33 ± 1.25	286	7.94 ± 1.16	11	18.64 ± 2.15	14.91 ± 2.35	9	2.78 ± 0.46	2.22 ± 0.36

respectively (Figure 2D). The results showed that serum metabolites could be used to distinguish between the two groups.

Identification of differential metabolites

The liquid chromatography with tandem mass spectrometry (LC–MS/MS) data were used to analyze the metabolites of different substances. Differential metabolites were screened based on the following criteria: VIP ≥ 1, FC > 1.2 or < 0.83, and $p \leq 0.05$. A comprehensive statistical analysis was performed.

In the before FSH injection samples, 121 differential metabolites were identified, of which 23 were upregulated in the HEY group and 98 were upregulated in the LEY group (Figure 3A; Supplementary Table S2). In the before artificial insemination samples, 129 differential metabolites were identified, of which 28 were upregulated in the HEY group and 101 were upregulated in the LEY group (Figure 3B; Supplementary Table S3). In the before embryo collection samples, 201 differential metabolites were identified, of which 53 were upregulated in the HEY group and 148 were upregulated in the LEY group (Figure 3C; Supplementary Table S4).

Among the differential metabolites at three sampling time points, there were 11, 16, and 66 shared differential metabolites between the before FSH injection and before artificial insemination samples, the before artificial insemination and before embryo collection samples, and the before FSH injection and before embryo collection samples, respectively (Figure. 3D; Supplementary Tables S5–S7). In addition, five shared differential metabolites were identified across all three sampling time points. Among them, phosphatidylcholine [PC; 14:0/22:1(13Z)] was upregulated in the HEY group, while phosphatidylethanolamine [PE; DiMe (11, 3)], triacylglycerol [TG; 15:0/16:0/22:4 (7Z, 10Z, 13Z, 16Z)], phosphatidylinositol [PI; 16:0/22:2 (13Z, 16Z)], and phosphatidylserine [PS; 18:0/20:4(8Z, 11Z, 14Z, 17Z)] were upregulated in the LEY group at all three time points (Figure 3D; Table 2).

Functional enrichment of the differential metabolites

The functional enrichment of differential metabolites was performed following the method described by Kanehisa et al. (28). The results showed that 21 pathways were enriched in the before FSH injection samples. Among these, nine pathways were significantly enriched, including inositol phosphate metabolism, phosphatidylinositol signaling system, and glycosylphosphatidylinositol (GPI)-anchored biosynthesis, among others (Figure 4A). A total of 24 pathways were enriched in the before artificial insemination samples. Among these, three pathways were significantly enriched, including fatty acid biosynthesis, phototransduction–fly, and shigellosis (Figure 4B). A total of 24 pathways were enriched in the before embryo collection samples. Among these, 13 pathways were significantly enriched, including inositol phosphate metabolism, fat digestion and absorption, and regulation of lipolysis in adipocytes, among others (Figure 4C).

Discussion

In bovine superovulation, the physiological status of the donor plays an important role in the outcome. Metabolites in the blood can reflect the physiological status of the body (29). Here, we found that there were distinct serum metabolites between bovine donors with different embryo yields at the time points before FSH injection, before artificial insemination, and before embryo collection. Phosphatidylcholine [PC; 14:0/22:1(13Z)], phosphatidylethanolamine [PE; DiMe (11, 3)], triacylglycerol [TG; 15:0/16:0/22:4 (7Z, 10Z, 13Z, 16Z)], phosphatidylinositol [PI; 16:0/22:2 (13Z, 16Z)], and phosphatidylserine [PS; 18:0/20:4(8Z, 11Z, 14Z, 17Z)] were the shared differential metabolites. The functions of these differential metabolites include fatty acid and protein metabolism and GPI-anchor biosynthesis, among others.

Several studies have shown that lipids present in follicular fluid are associated with the development of oocyte, and the concentration of lipids in the blood can reflect the concentration of follicular fluid. Furthermore, obesity is associated with irregular reproductive cycles. In obese horses, oocytes had lower concentrations of lipids consistent with PC and PE, while lipids consistent with TG tended to be higher (30). In patients with polycystic ovary syndrome, lipid profiling of follicular fluid showed differences in PC, PS, PI, and PE, strongly suggesting that these lipids may serve as biomarkers for pregnancy outcomes (31). In a study comparing human lipid profiles of follicular fluid between young poor ovarian responders and normal responders, lipids related to PC, PE, and PI were differentially expressed. These lipids may be involved in hormonal responses and oocyte development processes (32). PE, a glycerophospholipid, plays a role in the biosynthesis of PC (33). In this study, PE-NMe(11D3/11D3) was identified as a differential metabolite and may serve as a biomarker for the ovarian response during bovine ovulation.

A study on PC in bovine follicular fluid found variations during superovulation and estrous synchronization treatments, indicating that superovulation could increase the phospholipid content in follicular fluid (34). Additionally, a human superovulation study showed that some PC-related lipids in follicular fluid had higher concentrations in the successful group (32). In an ovine superovulation study, we found that certain PC-related metabolites in donor serum were significantly different between HEY and LEY populations (35). In this study, we found that PC [14:0/22:1(13Z)] was significantly higher in the HEY group than in the LEY group at all three time points. PC [14:0/22:1(13Z)] is a

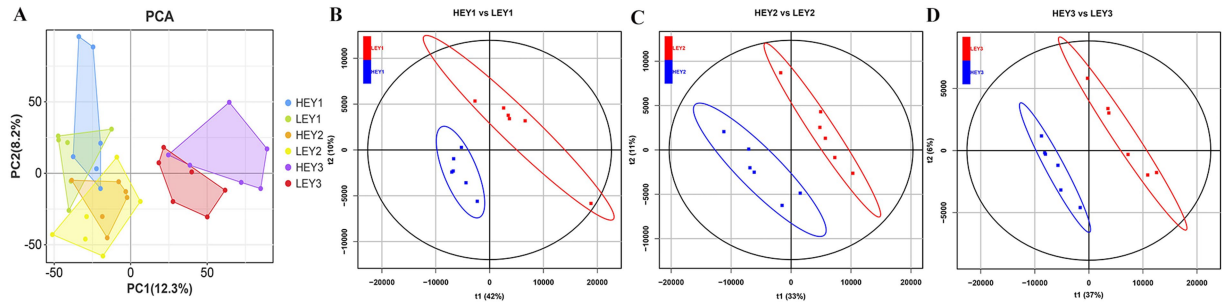

FIGURE 2
Multivariate statistical analysis results of the metabolome. **(A)** PCA results. B–D: OPLS-DA results from three sampling time points: **(B)** before FSH injection; **(C)** before artificial insemination; and **(D)** before embryo collection. HEY1: High embryonic yield group at the sampling before FSH injection. LEY1: Low embryonic yield group at the sampling before FSH injection. HEY2: High embryonic yield group at the sampling before artificial insemination. LEY2: Low embryonic yield group at the sampling before artificial insemination. HEY3: High embryonic yield group at the sampling before embryo collection. LEY3: Low embryonic yield group at the sampling before embryo collection.

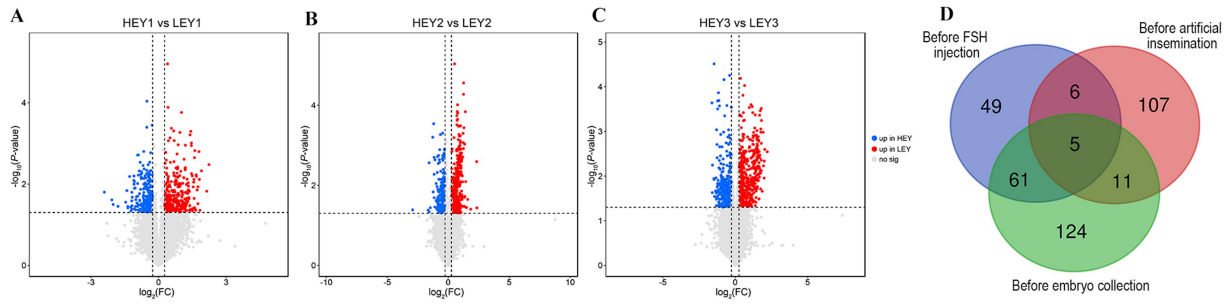

FIGURE 3
Differential metabolite analysis results. **(A–C)** Volcano plots for three sampling time points: **(A)** Before FSH injection; **(B)** before artificial insemination; and **(C)** before embryo collection. **(D)** Venn diagram of the differential metabolites across three sampling time points. HEY1: High embryonic yield group at the sampling before FSH injection. LEY1: Low embryonic yield group at the sampling before FSH injection. HEY2: High embryonic yield group at the sampling before artificial insemination. LEY2: Low embryonic yield group at the sampling before artificial insemination. HEY3: High embryonic yield group at the sampling before embryo collection. LEY3: Low embryonic yield group at the sampling before embryo collection.

glycerophospholipid in which a PC moiety occupies the glycerol substitution site. Phospholipids are ubiquitous in nature and are key components of the lipid bilayer in cells. They also play crucial roles in metabolism and signaling (36). Taken together, PC [14:0/22:1(13Z)] may serve as a serum biomarker for bovine superovulation.

Lipid metabolism provides the energy source during oocyte maturation. Lipids in oocytes are primarily triglycerides composed of specific fatty acids, which differ by species (37). In cumulus–oocyte complexes (COCs), TG are metabolized by lipases and through β-oxidation in mitochondria for ATP production (37). In dairy cows, follicular fluid TG levels were lower than those in serum, but there was a significant correlation between the two (38). In humans, studies have indicated that the majority of serum metabolites, including TG, are also present in follicular fluid, albeit at reduced levels (39). In adult zebrafish, high blood TG levels had negative effects on their offspring (40). Interestingly, Calonge et al. (41) found that the lipid profiles in follicular fluid and plasma inversely and significantly influenced ovarian response and the number of matured oocytes recovered. In this study, we found that TG composition [15:0/16:0/22:4(7Z,10Z,13Z,16Z)] was higher in the LEY group comparted to the HEY group. This suggests that excessively high blood TG levels affect the ovarian response during bovine superovulation.

PI could help maintain the low activity levels of the Hippo pathway (42). Emerging studies have discovered that the Hippo pathway plays an important role in regulating ovarian physiology and fertility (43). The process of oocyte maturation depends on follicle development. Previous studies have demonstrated that the Hippo pathway regulates the activation and growth of follicles (44–47). Related research has suggested that the upstream Hippo component, SAV1/MST1/2, contributes to the suppression of ovarian granulosa cell proliferation, while the Hippo effector YAP1 is essential for the proliferation of these granulosa cells (48). In summary, the serum metabolites related to PI may regulate follicle development through the Hippo pathway. In this study, we found that the level of PI [16:0/22:2 (13Z, 16Z)] was significantly higher in the HEY group than in the LEY group at all three sampling time points. This finding may be associated with the outcome of embryo production.

Conclusion

Serum metabolomics analysis provides a feasible approach to explore the predictors of superovulation in bovine. This study showed that PC [14:0/22:1(13Z)], PE [DiMe (11, 3)], TG [15:0/16:0/22:4 (7Z, 10Z, 13Z, 16Z)], PI [16:0/22:2 (13Z, 16Z)], and PS [18:0/20:4(8Z, 11Z, 14Z, 17Z)] were differentially expressed in the serum during the superovulation period. These could serve as potential biomarkers for embryonic yield prediction in bovine superovulation. The lipid and amino acid metabolic

TABLE 2 Shared differential metabolites across three sampling time points.

Metabolite ID	MS1 name	MZ	Sampling time	Relative abundance of HEY group	Relative abundance of LEY group	Fold change[a]	*p* value[b]	VIP[c]	Up. down[d]
POS_788.6168_5.679	PC[14:0/22:1(13Z)]	788.62	Before FSH injection	1661555.38	1179292.10	1.41	0.0220	9.05	up
			Before artificial insemination	1940812.82	1320729.14	1.47	0.0222	8.94	up
			Before embryo collection	2104757.61	1350278.94	1.56	0.0240	8.33	up
NEG_811.5229_7.6312	PE [DiMe(11,3)]	811.52	Before FSH injection	19015.44	52112.66	0.36	0.0011	2.38	down
			Before artificial insemination	31786.16	61470.94	0.52	0.0347	1.88	down
			Before embryo collection	16952.03	52399.75	0.32	0.0036	2.11	down
NEG_884.7788_7.6502	TG[15:0/16:0/22:4(7Z,10Z,13Z,16Z)]	884.78	Before FSH injection	11372.16	21573.02	0.53	0.0315	1.25	down
			Before artificial insemination	15427.56	37777.81	0.41	0.0332	1.78	down
			Before embryo collection	9420.85	25223.36	0.37	0.0025	1.40	down
NEG_889.575_7.8226	PI[16:0/22:2(13Z,16Z)]	889.57	Before FSH injection	533499.10	1606997.01	0.33	0.0022	14.04	down
			Before artificial insemination	907624.75	2356853.26	0.39	0.0348	12.79	down
			Before embryo collection	482513.64	1404412.95	0.34	0.0060	10.55	down
NEG_810.5216_7.6216	PS[18:0/20:4(8Z,11Z,14Z,17Z)]	810.52	Before FSH injection	55926.94	147153.83	0.38	0.0006	4.07	down
			Before artificial insemination	85709.53	170426.08	0.50	0.0446	3.14	down
			Before embryo collection	51423.13	152406.47	0.34	0.0037	3.57	down

[a]The fold change between the high embryonic yield group and the low embryonic yield group (a higher ratio indicates a higher level of expression of a compound in the high embryonic yield group).
[b]*p*-value represents the significance level of the difference between the two groups.
[c]Variable importance in projection of the two groups.
[d]Compared to the low embryonic yield group, the high embryonic yield group showed upregulated or downregulated expression of this metabolite.

10.3389/fvets.2025.1552045

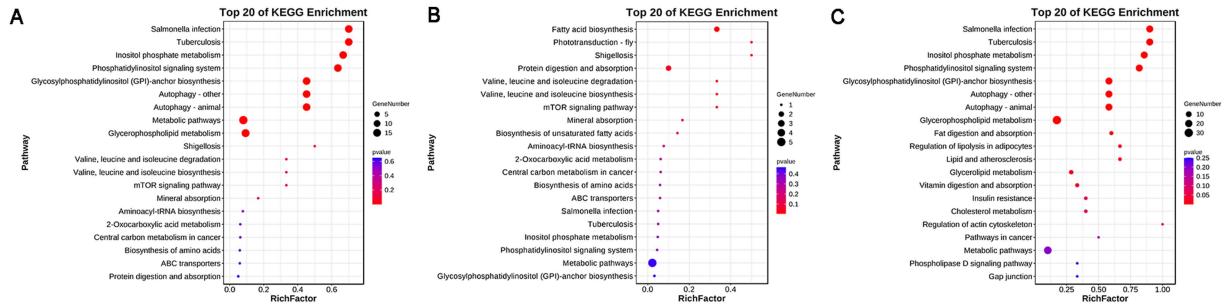

FIGURE 4
KEGG enrichment results of differential metabolites. **(A)** Before FSH injection; **(B)** before artificial insemination; **(C)** before embryo collection.

pathways may have an impact on the ovarian response. The study results may provide novel screening indexes of donors for bovine superovulation, although the accuracy of the relevant factors requires further investigation.

Methods

Experimental location and cows' management

This study was conducted at the Livestock Experimental Base of Inner Mongolia University in Hohhot (Inner Mongolia, China). This region has a tropical mid-temperate, semi-arid continental monsoon climate, characterized by long dry winters and short rainy summers.

A total of 36 sexually mature and clinically healthy Huaxi cows, aged 2 to 4 years, were used in this study. The cows' diet was designed to meet their nutritional needs, with unified management during feeding in the barn. The cows were fed a total mixed ration consisting of 15.00% alfalfa hay, 50.00% whole corn silage, and 35.00% cow concentrate supplement, resulting in a forage-to-concentrate ratio of 65:35.

Superovulation protocols

The cows were treated as follows (Figure 1): A CIDR (Zoetis, New Zealand) was inserted into the vagina on day 0 (D0). Between days 9 and 12, a total of 500 μg of FSH (Stimufol®, Belgium) was injected in eight doses, with each dose decreasing by 10%. On the fifth FSH injection (morning of D11), 300 μg of PG (Reprobiol, New Zealand) was injected synchronously. The CIDR was removed at the time of the final FSH injection. Estrus detection occurred on D13, and artificial insemination (AI) was performed twice (12 h interval). On D20, embryos were collected via uterus flushing after the cows were anesthetized with a caudal spinal injection of lidocaine hydrochloride.

Blood sampling

Blood samples were collected in the mornings on D9, before FSH injection; on D13, before artificial insemination; and on D20, before embryo collection. The samples were collected in vacuum blood collection tubes. Then, the samples were centrifuged at 10000 × g for 10 min to obtain the serum. All serum samples were stored in liquid nitrogen until further use.

LC–MS/MS measurements for serum metabolomics

Based on the total embryonic yield, the cows with ≥ 13 embryos were classified into the high embryonic yield (HEY) group, and the cows with ≤ 5 embryos were classified into the low embryonic yield (LEY) group. Six cows from each group ($n = 6$) were selected for serum metabolomics analysis. The LC–MS/MS-based serum metabolomics analysis was performed by LC-Bio Co. Ltd. (Hangzhou, China), following the methodology described by Xu et al. (35).

Briefly, the serum samples were purified with methanol and diluted in LC–MS grade water. UHPLC–MS/MS analyses were performed using a Vanquish UHPLC system (Thermo Fisher Scientific, Germany) coupled with an Orbitrap Q Exactive™ HF mass spectrometer (Thermo Fisher Scientific, Germany). The solvent gradient was set as follows: 2% B, 1.5 min; 2–85% B, 3 min; 100% B, 10 min; 100–2% B, 10.1 min; and 2% B, 12 min. The Q Exactive™ HF mass spectrometer was operated in both positive and negative polarity modes, with a spray voltage of 3.5 kV, a capillary temperature of 320°C, a sheath gas flow rate of 35 psi, an auxiliary gas flow rate of 10 L/min, an S-lens RF level of 60, and an auxiliary gas heater temperature of 350°C.

Data processing and metabolite identification

Briefly, raw data files generated through UHPLC–MS/MS were processed using Compound Discoverer 3.1 (CD3.1, Thermo Fisher Scientific, Germany). Then, the peaks were matched with mzCloud,[1] mzVault, and MassList databases to obtain accurate qualitative and relative quantitative results. Statistical analyses were performed using R statistical software (version R-3.4.3), Python (Python 2.7.6 version), and CentOS (CentOS release 6.6).

Data analysis

The Kyoto Encyclopedia of Genes and Genomes (KEGG),[2] the LIPID MAPS (Lipidmaps),[3] and the Human Metabolome Database

1 https://www.mzcloud.org/
2 http://www.kegg.com
3 www.lipidmaps.org

(HMDB)[4] were used to annotate the biological functions of the metabolites. Bioinformatic analysis was performed using R software (v.4.0.2) or the OmicStudio tools available at https://www.omicstudio.cn/tool. The metabolism data were statistically analyzed using the two-sided Wilcoxon rank sum test and finally visualized using the ggpubr package (version 0.6.0). The metabolites with a variable importance in projection (VIP) > 1, a p-value < 0.05, and a fold change (FC) ≥ 1.2 or ≤ 0.83 were considered differential metabolites. Volcano plots were used to filter the metabolites of interest based on $\log_2$(FoldChange) and -$\log_{10}$(p-value) of metabolites using ggplot2 in R language. A Venn diagram of the differential metabolites was created at http://bioinformatics.psb.ugent.be/webtools/Venn/. The functions of differential metabolites were analyzed using the KEGG database.

Data availability statement

The original contributions presented in the study are publicly available. This data can be found here: https://db.cngb.org/search/project/CNP0006676/.

Ethics statement

The animal study was approved by Inner Mongolia University Research Ethics Committee. The study was conducted in accordance with the local legislation and institutional requirements.

Author contributions

XS: Data curation, Methodology, Writing – original draft, Writing – review & editing. GG: Data curation, Funding acquisition, Methodology, Writing – original draft. LC: Methodology, Writing – original draft. LZ: Methodology, Writing – original draft. GL: Methodology, Writing – original draft. CB: Data curation, Writing – original draft. GS: Conceptualization, Investigation, Methodology, Validation, Writing – original draft. LY: Conceptualization, Formal analysis, Funding acquisition, Project administration, Resources, Supervision, Validation, Visualization, Writing – review & editing.

Funding

The author(s) declare that financial support was received for the research and/or publication of this article. This study was supported by the Scientific and Technological Innovation 2030: 2023ZD0404803; National Natural Science Foundation of China: 32360837, 32341052; Inner Mongolia Science and Technology Leading Team: 2022LJRC0006; Inner Mongolia Science and Technology Major Projects: to leiyang; Xinjiang Uygur Science and Technology Major Project: 2023A02011-1; Research support funds for high-level talents in public institutions at the autonomous region level in Inner Mongolia in 2022 (2022110).

4 http://www.hmdb.ca

Acknowledgments

We would like to express our sincere gratitude to LC-Bio Co. Ltd. (Hangzhou, China) for their assistance with metabolomics processing.

Conflict of interest

The authors declare that the research was conducted in the absence of any commercial or financial relationships that could be construed as a potential conflict of interest.

Generative AI statement

The author(s) declare that no Gen AI was used in the creation of this manuscript.

Publisher's note

Supplementary material

The Supplementary material for this article can be found online at: https://www.frontiersin.org/articles/10.3389/fvets.2025.1552045/full#supplementary-material

SUPPLEMENTARY FIGURE S1
Classification of cows' serum metabolites during superovulation **(A)** Classification result of annotated metabolites by HMDB analysis. **(B)** KEGG pathway enrichment analysis result of annotated metabolites.

References

1. Kasimanickam R, Kasimanickam V, Kastelic JP, Ramsey K. Metabolic biomarkers, body condition, uterine inflammation and response to superovulation in lactating Holstein cows. *Theriogenology*. (2020) 146:71–9. doi: 10.1016/j.theriogenology.2020.02.006

2. Kawamata M. Relationships between the number of small follicles prior to superovulatory treatment and superovulatory response in Holstein cows. *J Vet Med Sci*. (1994) 56:965–7. doi: 10.1292/jvms.56.965

3. Yang W-C, Yang LG, Riaz H, Tang KQ, Chen L, Li SJ. Effects in cattle of genetic variation within the IGF1R gene on the superovulation performance and pregnancy rates after embryo transfer. *Anim Reprod Sci*. (2013) 143:24–9. doi: 10.1016/j.anireprosci.2013.10.008

4. Hirayama H. Effects of genetic background on responses to superovulation in Japanese black cattle. *J Vet Med Sci*. (2019) 81:373–8. doi: 10.1292/jvms.18-0537

5. Rasheed ST, Younis LS, Aboud QM. Association between bovine GDF9 SNPs and calving rate (superovulation) in Holstein-Friesian cows. *Archives of Razi Institute*. (2021) 76:1035–45. doi: 10.22092/ari.2021.354310.1632

6. Testart J, Kann G, Saumande J, Thibier M. Oestradiol-17beta, progesterone, FSH and LH in prepubertal calves induced to superovulate. *J Reprod Fertil*. (1977) 51:329–36. doi: 10.1530/jrf.0.0510329

7. Callesen H, Greve T, Hyttel P. Preovulatory evaluation of the superovulatory response in donor cattle. *Theriogenology*. (1988) 30:477–88. doi: 10.1016/0093-691X(88)90197-5

8. Guilbault LA, Lussier JG, Grasso F. Interrelationships of hormonal and ovarian responses in superovulated heifers pretreated with FSH-P at the beginning of the estrous cycle. *Theriogenology*. (1992) 37:1029–40. doi: 10.1016/0093-691X(92)90101-V

9. Kitahara G, Kamimura S, Hamana K. Relationship between the peripheral concentrations of estradiol-17β ($E_{₂}$) and Preovulatory characteristics of cumulus-oocyte complexes (COCs) during superovulation treatment in Japanese black cows. *J Reprod Dev*. (2011) 57:159–62. doi: 10.1262/jrd.09-155T

10. Kafi M, McGowan MR. Relationship between different concentrations of the plasma progesterone at the time of FSH-P treatment and the Superovulatory response in Holstein dairy heifers. *Reprod Domest Anim*. (2012) 47:e75–8. doi: 10.1111/j.1439-0531.2011.01966.x

11. Fushimi Y, Monniaux D, Takagi M. Efficacy of a single measurement of plasma anti-Miillerian hormone concentration for ovum pick-up donor selection of Japanese black heifers in herd breeding programs. *J Reprod Dev*. (2019) 65:369–74. doi: 10.1262/jrd.2019-003

12. Karl KR, Jimenez-Krassel F, Gibbings E, Ireland JLH, Clark ZL, Tempelman RJ, et al. Negative impact of high doses of follicle-stimulating hormone during superovulation on the ovulatory follicle function in small ovarian reserve dairy heifers. *Biol Reprod*. (2021) 104:695–705. doi: 10.1093/biolre/ioaa210

13. Karl KR, Ireland JLH, Clark ZL, Tempelman RJ, Latham KE, Ireland JJ. Limitations in use of ovarian reserve biomarkers to predict the superovulation response in small ovarian reserve heifers. *Theriogenology*. (2022) 182:53–62. doi: 10.1016/j.theriogenology.2022.01.033

14. Sekizawa F. Relationship between embryo collection results after superovulation treatment of Japanese black cows and their plasma β-carotene and vitamin concentrations. *J Reprod Dev*. (2012) 58:377–9. doi: 10.1262/jrd.11-075H

15. Alkan H. Evaluation of the relationship between serum paraoxonase-1 activity and superovulation response/embryo yield in Holstein cows. *J Vet Med Sci*. (2021) 83:535–41. doi: 10.1292/jvms.20-0578

16. Chorfi Y, Lanevschi A, Dupras R, Girard V, Tremblay A. Serum biochemical parameters and embryo production during superovulatory treatment in dairy cattle. *Res Vet Sci*. (2007) 83:318–21. doi: 10.1016/j.rvsc.2007.01.010

17. Watanabe U, Takagi M, Yamato O, Otoi T, Okamoto K. Retrospective surveillance of metabolic parameters affecting reproductive performance of Japanese black breeding cows. *J Vet Sci*. (2014) 15:283–8. doi: 10.4142/jvs.2014.15.2.283

18. Horn EJ, Read CC, Edwards JL, Schrick FN, Rhinehart JD, Payton RR, et al. Preovulatory follicular fluid and serum metabolome profiles in lactating beef cows with thin, moderate, and obese body condition. *J Anim Sci*. (2022) 100:1–14. doi: 10.1093/jas/skac152

19. Alward KJ, Cockrum RR, Ealy AD. Associations of antral follicle count with fertility in cattle: a review. *JDS communications*. (2023) 4:132–7. doi: 10.3168/jdsc.2022-0283

20. Silva F. Peri-estrus ovarian, uterine, and hormonal variables determine the uterine luminal fluid metabolome in beef heifers. *Biol Reprod*. (2021) 105:1140–53. doi: 10.1093/biolre/ioab149

21. Gimeno I, Salvetti P, Carrocera S, Gatien J, le Bourhis D, Gómez E. The recipient metabolome explains the asymmetric ovarian impact on fetal sex development after embryo transfer in cattle. *J Anim Sci*. (2024) 102:skae081. doi: 10.1093/jas/skae081

22. Gómez E, Salvetti P, Gatien J, Carrocera S, Martín-González D, Muñoz M. Blood plasma metabolomics predicts pregnancy in Holstein cattle transferred with fresh and vitrified/warmed embryos produced in vitro. *J Proteome Res*. (2020) 19:1169–82. doi: 10.1021/acs.jproteome.9b00688

23. Guo YS, Tao JZ. Metabolomics and pathway analyses to characterize metabolic alterations in pregnant dairy cows on D 17 and D 45 after AI. *Sci Rep*. (2018) 8:8. doi: 10.1038/s41598-018-23983-2

24. Phillips KM, Read CC, Kriese-Anderson LA, Rodning SP, Brandebourg TD, Biase FH, et al. Plasma metabolomic profiles differ at the time of artificial insemination based on pregnancy outcome, in *Bos taurus* beef heifers. *Sci Rep*. (2018) 8:8. doi: 10.1038/s41598-018-31605-0

25. Funeshima N, Miura R, Katoh T, Yaginuma H, Kitou T, Yoshimura I, et al. Metabolomic profiles of plasma and uterine luminal fluids from healthy and repeat breeder Holstein cows. *BMC Vet Res*. (2021) 17:54. doi: 10.1186/s12917-021-02755-7

26. Jawor P, Ząbek A, Wojtowicz W, Król D, Stefaniak T, Młynarz P. Metabolomic studies as a tool for determining the post-mortem interval (PMI) in stillborn calves. *BMC Vet Res*. (2019) 15:15. doi: 10.1186/s12917-019-1935-4

27. Ji G, Zhang J, Feng X, Sheng H, Hu H, Li F, et al. Analysis of blood biochemistry and non-targeted metabolomics of endometritis in dairy cows. *Anim Reprod Sci*. (2024) 264:107460. doi: 10.1016/j.anireprosci.2024.107460

28. Kanehisa M, Furumichi M, Sato Y, Ishiguro-Watanabe M, Tanabe M. KEGG: integrating viruses and cellular organisms. *Nucleic Acids Res*. (2021) 49:D545–d551. doi: 10.1093/nar/gkaa970

29. Jensch R, Baber R, Körner A, Kiess W, Ceglarek U, Garten A, et al. Association of Whole Blood Amino Acid and Acylcarnitine Metabolome with anthropometry and IGF-I serum levels in healthy children and adolescents in Germany. *Meta*. (2024) 14:489. doi: 10.3390/metabo14090489

30. Sessions-Bresnahan DR, Schauer KL, Heuberger AL, Carnevale EM. Effect of obesity on the Preovulatory follicle and lipid fingerprint of equine oocytes. *Biol Reprod*. (2016) 94:15. doi: 10.1095/biolreprod.115.130187

31. Cordeiro FB, Cataldi TR, do Vale Teixeira da Costa L, de Lima CB, Stevanato J, Zylbersztejn DS, et al. Follicular fluid lipid fingerprinting from women with PCOS and hyper response during IVF treatment. *J Assist Reprod Genet*. (2015) 32:45–54. doi: 10.1007/s10815-014-0375-0

32. Cataldi T, Cordeiro FB, da Costa LDVT, Pilau EJ, Ferreira CR, Gozzo FC, et al. Lipid profiling of follicular fluid from women undergoing IVF: young poor ovarian responders versus normal responders. *Hum Fertil (Camb)*. (2013) 16:269–77. doi: 10.3109/14647273.2013.852255

33. Chang W. Lipidomics and spatial metabolomics reveal the heterogeneity in lipid distribution within pecan kernels. *Food Chem*. (2024) 467:142368. doi: 10.1093/jas/skae081

34. Santos PH, Fontes PK, Franchi FF, Nogueira MFG, Belaz KRA, Tata A, et al. Lipid profiles of follicular fluid from cows submitted to ovarian superstimulation. *Theriogenology*. (2017) 94:64–70. doi: 10.1016/j.theriogenology.2017.02.002

35. Xu Q, Wang C, Wang L, Feng R, Guo Y, Feng S, et al. Correlation analysis of serum reproductive hormones and metabolites during multiple ovulation in sheep. *BMC Vet Res*. (2022) 18:290. doi: 10.1186/s12917-022-03387-1

36. Scholpa NE. Evolution of lipid metabolism in the injured mouse spinal cord. *J Neurotrauma*. (2024) 42:182–196. doi: 10.1089/neu.2024.0385

37. Dunning KR, Russell DL, Robker RL. Lipids and oocyte developmental competence: the role of fatty acids and β-oxidation. *Reproduction*. (2014) 148:R15–27. doi: 10.1530/REP-13-0251

38. Leroy JL. Metabolite and ionic composition of follicular fluid from different-sized follicles and their relationship to serum concentrations in dairy cows. *Anim Reprod Sci*. (2004) 80:201–11. doi: 10.1016/S0378-4320(03)00173-8

39. Valckx S. BMI-related metabolic composition of the follicular fluid of women undergoing assisted reproductive treatment and the consequences for oocyte and embryo quality. *Hum Reprod*. (2012) 27:3531–9. doi: 10.1093/humrep/des350

40. Virote B, Moreira AMS, Silva Souza JGD, Castro TFD, Melo N, Carneiro WF, et al. Obesity induction in adult zebrafish leads to negative reproduction and offspring effects. *Reproduction*. (2020) 160:833–42. doi: 10.1530/REP-20-0119

41. Núñez Calonge R, Guijarro JA, Andrés C, Cortés S, Saladino M, Caballero P, et al. Relationships between lipids levels in blood plasma, follicular fluid and seminal plasma with ovarian response and sperm concentration regardless of age and body mass index. *Rev Int Androl*. (2022) 20:178–88. doi: 10.1016/j.androl.2021.02.004

42. Li FL, Fu V, Liu G, Tang T, Konradi AW, Peng X, et al. Hippo pathway regulation by phosphatidylinositol transfer protein and phosphoinositides. *Nat Chem Biol*. (2022) 18:1076–86. doi: 10.1038/s41589-022-01061-z

43. Clark KL, George JW, Przygrodzka E, Plewes MR, Hua G, Wang C, et al. Hippo signaling in the ovary: emerging roles in development, fertility, and disease. *Endocr Rev*. (2022) 43:1074–96. doi: 10.1210/endrev/bnac013

44. Grosbois J, Demeestere I. Dynamics of PI3K and hippo signaling pathways during in vitro human follicle activation. *Hum Reprod*. (2018) 33:1705–14. doi: 10.1093/humrep/dey250

45. Kawamura K, Cheng Y, Suzuki N, Deguchi M, Sato Y, Takae S, et al. Hippo signaling disruption and Akt stimulation of ovarian follicles for infertility treatment. *Proc Natl Acad Sci USA*. (2013) 110:17474–9. doi: 10.1073/pnas.1312830110

46. Hu LL, Su T, Luo RC, Zheng YH, Huang J, Zhong ZS, et al. Hippo pathway functions as a downstream effector of AKT signaling to regulate the activation of primordial follicles in mice. *J Cell Physiol*. (2019) 234:1578–87. doi: 10.1002/jcp.27024

47. Devos M, Grosbois J, Demeestere I. Interaction between PI3K/AKT and hippo pathways during in vitro follicular activation and response to fragmentation and chemotherapy exposure using a mouse immature ovary model. *Biol Reprod*. (2020) 102:717–29. doi: 10.1093/biolre/ioz215

48. Sun X, Niu X, Qin N, Shan X, Zhao J, Ma C, et al. Novel insights into the regulation of LATS2 kinase in prehierarchical follicle development via the hippo pathway in hen ovary. *Poult Sci*. (2021) 100:101454. doi: 10.1016/j.psj.2021.101454

frontiers | Frontiers in Veterinary Science

TYPE Original Research
PUBLISHED 03 July 2025
DOI 10.3389/fvets.2025.1565807

OPEN ACCESS

EDITED BY
Manuel Garcia-Herreros,
National Institute for Agricultural and Veterinary Research (INIAV), Portugal

REVIEWED BY
Regiane R. Santos,
Schothorst Feed Research, Netherlands
Xiaoyun He,
Chinese Academy of Agricultural Sciences, China

*CORRESPONDENCE
Jun Luo
✉ luojun@nwafu.edu.cn

RECEIVED 23 January 2025
ACCEPTED 13 June 2025
PUBLISHED 03 July 2025

CITATION
Shi C, Liu Q, Wang W, He Q, Zhao J, Zhang F, Zhu L and Luo J (2025) Transcriptome and proteome of ovarian tissues revealed the differences in the ovaries of dairy goats during the breeding and non-breeding seasons.
Front. Vet. Sci. 12:1565807.
doi: 10.3389/fvets.2025.1565807

Transcriptome and proteome of ovarian tissues revealed the differences in the ovaries of dairy goats during the breeding and non-breeding seasons

Chenbo Shi, Qingqing Liu, Wei Wang, Qiuya He, Jianqing Zhao, Fuhong Zhang, Lu Zhu and Jun Luo*

Shaanxi Key Laboratory of Molecular Biology for Agriculture, College of Animal Science and Technology, Northwest A&F University, Yangling, China

Dairy goats represent a crucial species within global dairy livestock. In temperate regions with distinct seasons, dairy goats exhibit reduced reproductive activity under long photoperiod conditions—a phase termed the non-breeding season. This poses a significant challenge to sustaining year-round goat milk production. As the pivotal organ for reproduction, the molecular regulatory mechanisms of the ovary in seasonal breeding remain incompletely characterized. This study investigated the variations in gonadotropin levels in dairy goats across breeding and non-breeding seasons, alongside an evaluation of follicle size and quantity. Furthermore, ovarian differences were explored at the molecular level using transcriptomic and proteomic methodologies. The findings indicate that follicle-stimulating hormone (FSH) and luteinizing hormone (LH) levels in dairy goats are significantly reduced during the non-breeding season compared to the breeding season ($p < 0.05$). Furthermore, follicle sizes in dairy goats are notably larger during the breeding season relative to the non-breeding season ($p < 0.05$). A total of 1,115 differentially expressed genes (DEGs) were identified, comprising 749 upregulated and 366 downregulated genes. Additionally, 520 differentially expressed proteins (DEPs) were identified, with 162 upregulated and 358 downregulated. The identified common DEGs and DEPs exhibiting consistent expression patterns include *TMEM205*, *TM7SF2*, *SLC35G1*, *GSTM1*, and *ABHD6*. These DEGs and DEPs suppress follicular development during the non-breeding season by regulating steroid hormone biosynthesis. In conclusion, this study reveals the molecular basis underlying seasonal reproductive differences at the ovarian level in dairy goats, offering new insights into the mechanisms of their seasonal reproduction.

KEYWORDS

dairy goat, transcriptome, proteome, ovary, seasonal reproduction

Introduction

As a breed specifically developed for dairy production, the dairy goat holds a significant role within the livestock industry and the dairy sector across numerous countries (1). Goat milk is rich in essential fatty acids, abundant milk proteins, and vitamins, all of which positively influence human health (2). In regions of low latitude, such as northwestern China, dairy goats demonstrate a significant decrease in reproductive activity from spring to summer (February to August). This seasonal decline often results in fluctuations in milk supply, posing challenges in consistently meeting market and consumer demands throughout the year.

The seasonal reproductive cycle of animals is a multifaceted physiological process regulated by multiple factors, primarily including photoperiod and temperature changes, with photoperiod serving as the dominant determinant (3–6). Extended daylight periods during the non-breeding season induce inactive reproductive status in dairy goats. The photoperiod modulates melatonin secretion by the pineal gland, with light cues being relayed to the pineal gland through the suprachiasmatic nucleus in the brain. This process governs the release of thyroid stimulating hormone (TSH) from the pituitary gland via melatonin, subsequently influencing the secretion of gonadotropin-releasing hormone (GnRH) by the hypothalamus. As a result, ovarian function is affected through the actions of luteinizing hormone (LH) and follicle-stimulating hormone (FSH) secreted by the pituitary gland (7). In certain mammalian species, alterations in photoperiod can modulate the activity of kisspeptin and RFRP-3 neurons within the hypothalamus, which are integral to the regulation of GnRH release. Consequently, photoperiodic changes influence the functionality of these neurons, thereby impacting the reproductive axis and dictating the timing of seasonal reproduction (8).

Estrogen (E2) and progesterone (P4) secreted by the ovaries play a central role in regulating the reproductive cycle and supporting pregnancy, while the ability of the ovaries to store oocytes directly affects female fertility (9). Notable differences exist in ovarian biological function between breeding and non-breeding seasons. Research indicates that reduced LH levels during the non-breeding season can result in slower follicular development (10). In Boer goats, the size and number of follicles during the non-breeding season are diminished compared to the breeding season (11). However, the alterations in ovarian function during the non-breeding season are intricate and necessitate further investigation into their underlying causes.

RNA sequencing (RNA-seq) provides valuable insights into genetic information at the transcriptional level. Furthermore, proteomic analysis of functional proteins enables more comprehensive elucidation of underlying molecular mechanisms. In this study, we investigated follicular development and reproductive hormone levels in dairy goats during both the breeding and non-breeding seasons to enhance our understanding of their reproductive status. Additionally, RNA-seq was employed to compare the ovarian transcriptomic profiles of dairy goats, while a 4D-DIA proteomic approach was utilized to examine the ovarian proteomic data. This dual analysis offers insights into the transcriptomic and proteomic variations in ovarian expression patterns across different seasons. The findings provide a foundation for elucidating the specific characteristics of seasonal reproduction in dairy goats and for exploring potential underlying molecular mechanisms.

Materials and methods

The experiment was performed under approval by the Animal Ethical and Welfare Committee at the Northwest Agriculture and Forestry University, China.

Animals

This study was conducted in region, Shaanxi, China (34° 16′N, 108° 4′E). The region has distinct four seasons, characterized by a continental monsoon climate, with an average annual temperature of 12°C. Following the summer solstice, the duration of daylight diminishes, prompting the dairy goats in the region to enter the breeding season. Conversely, post the winter solstice, the daylight duration increases, leading the dairy goats in the area to transition into the non-breeding season. The peak breeding season for dairy goats in the region is from August (14 h of daylight) to October (12 h of daylight), while clearly exhibit anestrus status from March (12 h of daylight) to May (14 h of daylight).

The goat breed is Xinnong Saanen dairy goats, all females were multiparous and ranged in age from 2.5 to 3.5 years, with an average body weight of 47.29 ± 7.45 kg. The diet consists of corn silage and alfalfa hay for roughage. The concentrate includes soybean meal, corn grain, bran, trace mineral salt, and vitamin-mineral premix. The concentrate-to-roughage ratio is 4:6, and they have ad libitum access to water.

Experimental design

Forty dairy goats were divided into two experimental groups, with studies conducted during the non-breeding season group (NBS group) from March to May and the breeding season group (BS group) from August to October, each lasting 6 weeks. Weekly blood samples were obtained from the goats via jugular venipuncture. Upon the conclusion of the experiment, ovarian samples from the goats were procured for subsequent analysis.

Ovaries collection and follicle counting

The ovaries were harvested under general anesthesia with xylazine hydrochloride (Administer a muscular injection at a dose of 2.5 μL/kg in accordance with the instructions; Huamu Animal Health Products Corporation), and the ovaries were collected in a sterile operating room. Following the surgery, the goats were placed in quiet and clean pens for 7 days, with daily iodine disinfection of the wounds. The follicle count was recorded, and the diameter of each follicle was measured using a ruler. Follicles with a diameter smaller than 2.5 mm and larger than 2.5 mm were categorized as small-sized and large-sized follicles, respectively. The ovarian tissues were preserved in liquid nitrogen for subsequent transcriptomic and proteomic sequencing analyses.

RNA sequencing

The total RNA of the ovaries was extracted by Trizol reagent (Invitrogen, United States), according to the instructions of the manufacturer. The purity and concentration of the extracted RNA were detected by NanoDrop 2000A Spectrophotometer (Thermo Fisher Scientific, United States). According to the manufacturer's manual, cDNA libraries and sequencing were performed at Allwegene Company (Beijing, China). Briefly, mRNAs were extracted from total RNA using oligo (dT) magnetic beads and then broken into short fragments. The fragmented mRNAs were reverse-transcribed into cDNAs which were then amplified by PCR.

The cDNA libraries were sequenced using Illumina HiSeq 2000. Clean data were obtained by removing reads containing adapters and low-quality reads from the raw data. Subsequent analyses were performed using the clean data. The clean redas were mapped to the *Capra hircus* reference genome Capra_hircus. ARS1.[1] Calculate the number of clean reads mapped to each gene, and standardize gene expression using the RPKM (Reads per kilobase per million mapped reads) method. Based on RPKM-normalized results, gene expression levels are evaluated, with genes satisfying $p < 0.05$ and |FoldChange| > 2identified as differentially expressed genes (DEGs). CPM (Counts per million mapped reads) data are used to assess the quality and accuracy of transcriptomic analyses.

R software (Ggplot2 R package) was used for plot, and Kyoto Encyclopedia of Genes and Genomes (KEGG) enrichment analysis was performed using the OmicShare tool.[2] Gene Ontology (GO) enrichment analysis was performed and the results visualized with the OmicShare tool, an online platform for data analysis.[3] KEGG pathways or GO terms with $p < 0.05$ were considered significantly enriched in DEGs.

4D-DIA proteomics

Ovarian samples were retrieved from liquid nitrogen storage and pulverized using liquid nitrogen. Subsequently, 200 mg of the pulverized sample was transferred to a centrifuge tube, and 300 μL of RIPA buffer solution was added and mixed thoroughly. Cryogenic grinding was performed using steel beads at 70 Hz for 4 min, followed by centrifugation at 12,000 rpm for 10 min at 4°C. The samples then underwent ultrasonic treatment in an ice-water bath for 15 min to ensure complete lysis. A second centrifugation was conducted at 12,000 rpm for 10 min at 4°C, and the supernatant was collected for further analysis.

The protein concentration was quantified utilizing the Bicinchoninic Acid (BCA) assay. Subsequently, peptide samples were prepared for instrumental analysis. In summary, proteins underwent precipitation via acetone, followed by reconstitution, reduction, and alkylation. Trypsin was then employed for enzymatic digestion of the proteins. Subsequently, trifluoroacetic acid (TFA) was used to remove sodium deoxycholate (SDC) from the peptide samples. Following desalting, the samples were prepared for instrumental analysis.

For each sample, 200 ng of total peptides were separated and analyzed with a nano-UPLC (nanoElute2) coupled to a timsTOF Pro2 instrument (Bruker) with a nano-electrospray ion source. Vendor's raw MS files were processed using SpectroMine software (4.2.230428.52329) and the built-in Pulsar search engine.

The statistical analysis of the dataset was primarily executed utilizing R software (version 4.0). Protein raw intensity values underwent normalization via the median. The identification of significantly different proteins was conducted using the R package metaX, applying a filtration based on two criteria: a p-value < 0.05 from the T-test and a fold change > 1.2. Enrichment analyses for GO and KEGG Pathways of the differentially expressed proteins were performed using hypergeometric tests, with functional terms deemed significantly enriched if they exhibited a p-value < 0.05. The subcellular localization of proteins was analyzed using the WoLF PSORT software.[4]

Real-time quantitative PCR

Extract total RNA using the previously described method. Subsequently, 1,000 ng of RNA was reverse transcribed into cDNA utilizing the PrimeScript™ RT reagent Kit with gDNA Eraser (Takara, China). The sequences and GenBank accession numbers of the primers employed for target gene amplification are presented in Table 1. Quantitative detection of the target genes was performed using the SYBR Green PCR Master Mix (Takara, China). The relative gene expression was analyzed using the $2 - \Delta\Delta Ct$ method.

Elisa assay

Centrifuge the blood samples at 3000 rpm for 5 min to collect the serum. Use the ELISA kit (Fankew, China) according to the manufacturer's instructions to detect FSH and LH in the serum.

Statistical analyses

Statistical analyses were conducted utilizing SPSS software version 17.0 (SPSS Inc., Chicago, IL, United States), incorporating a minimum of three independent replicates. Independent sample t-tests were employed to compare the two groups, with all data expressed as mean ± standard error of the mean (S. E. M.). A p-value of less than 0.05 was deemed statistically significant. The levels of significance are denoted as follows: * indicates $p < 0.05$, ** indicates $p < 0.01$, and *** indicates $p < 0.001$.

Results

Reproductive hormone levels and follicle counts

During the six-week experimental period, the levels of FSH and LH in dairy goats were assessed weekly. Serum FSH levels during weeks 1, 3, 4, and 6 of the breeding season were significantly higher than those in the non-breeding season ($p < 0.05$), while serum LH levels during weeks 1, 2, and 5 of the breeding season were significantly higher than those in the non-breeding season ($p < 0.05$; Figures 1A,B). Despite these findings, FSH levels at weeks 2 and 5 showed no significant difference ($p > 0.05$), and LH levels at weeks 3, 4, and 6 also exhibited no significant difference ($p > 0.05$; Figures 1A,B). Additionally, an analysis of follicular size and quantity indicated that, relative to the non-breeding season, dairy goats in the breeding season exhibited a greater number of large-sized follicles ($p < 0.05$) and fewer

1 https://ftp.ensembl.org/pub/release-111/fasta/capra_hircus
2 https://www.omicshare.com/tools/home/report/koenrich.html
3 https://www.omicshare.com/tools/home/soft/enrich_circle
4 https://wolfpsort.hgc.jp/

TABLE 1 Primers used for the qRT-PCR validation.

Gene name	Primer sequence (5′-3′)	Product size (bp)	Accession number
FASN	F: GCACACAATATGGACCCCCA	183	NM_001285629.1
	R: CATGCTGTAGCCTACGAGGG		
LDLR	F: TTTGAACGCACGAAAGCAGG	165	XM_005682375.3
	R: GTTTGATCCTGACCAGGGGG		
FSHR	F: ATGCGGTCGAACTGAGGTTT	146	NM_001285636.1
	R: GGGCAGGTTGGAGAACACAT		
TMEM206	F: ACTGAGCAGCCACCTACCTA	116	XM_018060751.1
	R: TGAGGAGGGACCTACTCTGC		
TM7SF2	F: CCTACCGAATCGTGCCCTAC	176	XM_005699882.3
	R: CCTATCAGGCCGTTCATCCC		
SLC35G1	F: CTGTCCTGGACTTGGCTTGT	192	XM_018041634.1
	R: CGTTGACCTTTGGGGCCTAT		
ABHD6	F: GAGGTCAGCCCCTCTAGGTA	175	XM_018038385.1
	R: TCCTCCGCCAGTACCAGTAA		

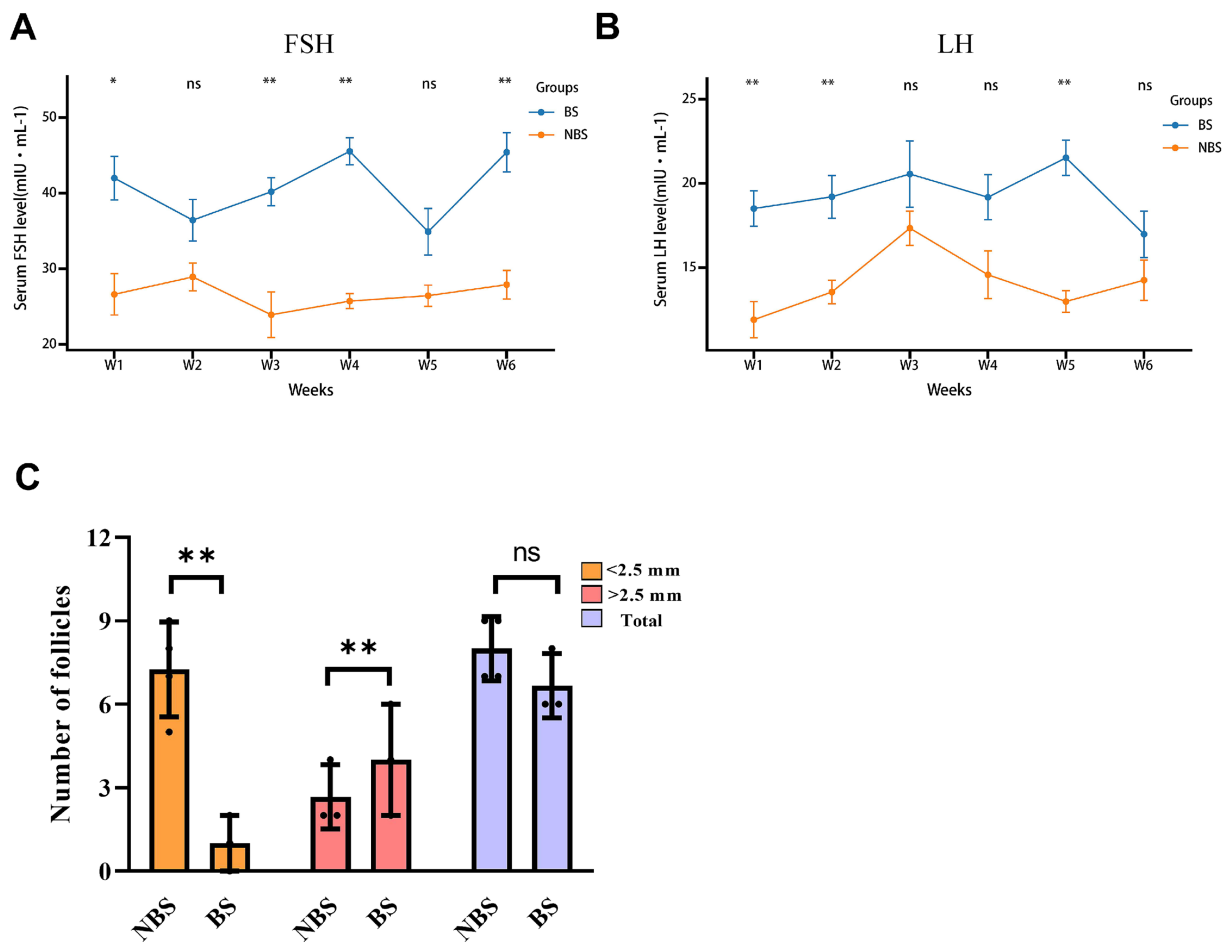

FIGURE 1
Levels of FSH and LH in the serum and follicle count in dairy goats during the breeding and non-breeding seasons. The contents of FSH **(A)** and LH **(B)** in serum were measured by ELISA. **(C)** Size and number of ovarian follicles.*$p < 0.05$, **$p < 0.01$, ns > 0.05.

small-sized follicles ($p < 0.05$), while the total follicle count remained statistically unchanged ($p > 0.05$; Figure 1C).

Transcriptome analysis

The principal component analysis (PCA) results illustrate the distribution of samples across the first two principal components (PC1 and PC2), with PC1 accounting for 37.5% of the variance and PC2 accounting for 24.7% (Figure 2A). A total of 954 DEGs were identified between the NBS and BS groups, with 749 genes upregulated in the NBS group and 366 genes upregulated in the BS group (Figures 2B,C). A comprehensive analysis of the top 20 DEGs revealed that the log2(fc) values for integrin subunit beta 6 (ITGB6), fibrous sheath interacting protein 2 (FSIP2), and acid phosphatase 3 (ACP3) were upregulated by factors of 10.9, 10.7, and 10.5, respectively (Table 2). Conversely, the log2(fc) values for G protein-coupled Receptor 22 (GPR22) and pyroglutamylated RFamide peptide receptor (QRFPR) were downregulated by factors of 10.6 and 10.0, respectively (Table 2).

KEGG enrichment analysis identified the top 20 pathways significantly enriched with DEGs (Figure 2D). Among these, 120 DEGs were significantly enriched in metabolic pathways, 8 DEGs in steroid biosynthesis, 8 DEGs in glutathione metabolism, and 12 DEGs in ovarian steroidogenesis. The enriched pathways are predominantly annotated in categories such as metabolism, genetic information processing, environmental information processing, cellular processes, organizational systems, and human diseases (Figure 2E). Notably, metabolism accounts for the highest number of annotated pathways (12 pathways), whereas environmental information processing accounts for the fewest (only 3 pathways; Figure 2E).

GO analysis identified the top 20 terms that are significantly enriched among the DEGs, categorizing them into three primary domains: biological process, molecular function, and cellular component (Figures 2F,G). The terms exhibiting the highest distribution of DEGs include cellular anatomical entity, cellular process, binding, and biological regulation (Figures 2F,G).

Proteomic analysis

The results of 4D-DIA proteomics analysis showed that principal component analysis (PCA) revealed the distribution of principal components, with PC1 accounting for 73.1% of the variance and PC2 for 8.2% (Figure 3A). In comparison to NBS group, the BS group exhibited 162 upregulated and 358 downregulated differential expressed proteins(DEPs), as illustrated in the volcano plot and heatmap

TABLE 2 The top 20 upregulated or downregulated DEGs in NBS vs. BS.

Ensemble ID	Symbol	Description	Log2(fc)	*p*-value	UP/DOWN
ENSCHIG00000004135	–	–	11.5	0.048	UP
ENSCHIG00000013972	ITGB6	Integrin beta-6	10.9	0.002	UP
ENSCHIG00000020565	-	-	−10.8	0.001	DOWM
ENSCHIG00000016918	-	-	10.8	0.005	UP
ENSCHIG00000016003	FSIP2	Fibrous sheath interacting protein 2	10.7	0.006	UP
ENSCHIG00000010247	GPR22	G protein-coupled receptor 22	−10.6	0.001	DOWM
ENSCHIG00000016695	ACP3	Acid phosphatase 3	10.5	0.023	UP
ENSCHIG00000010784	RNASE12	Ribonuclease A family member 12	10.5	0.024	UP
ENSCHIG00000026746	-	-	10.5	0.024	UP
ENSCHIG00000021440	CNNM1	Cyclin-M1	10.3	0.005	UP
ENSCHIG00000016148	ANO2	Anoctamin 2	10.3	0.000	UP
ENSCHIG00000022191	ERN2	Endoplasmic reticulum nucleotide receptor 2	10.2	0.011	UP
ENSCHIG00000004467	-	-	10.2	0.035	UP
ENSCHIG00000002414	ACTL7A	Actin like 7A	10.2	0.025	UP
ENSCHIG00000015989	-	-	10.1	0.001	UP
ENSCHIG00000007733	GJB1	Gap junction protein beta 1	10.0	0.004	UP
ENSCHIG00000015444	SCGN	Secretagogin	10.0	0.045	UP
ENSCHIG00000022770	P2RX2	Purinergic receptor P2X 2	10.0	0.020	UP
ENSCHIG00000026596	QRFPR	Pyroglutamylated RFamide peptide receptor	−10.0	0.005	DOWM
ENSCHIG00000008489	FGFBP1	Fibroblast growth factor binding protein 1	10.0	0.006	UP

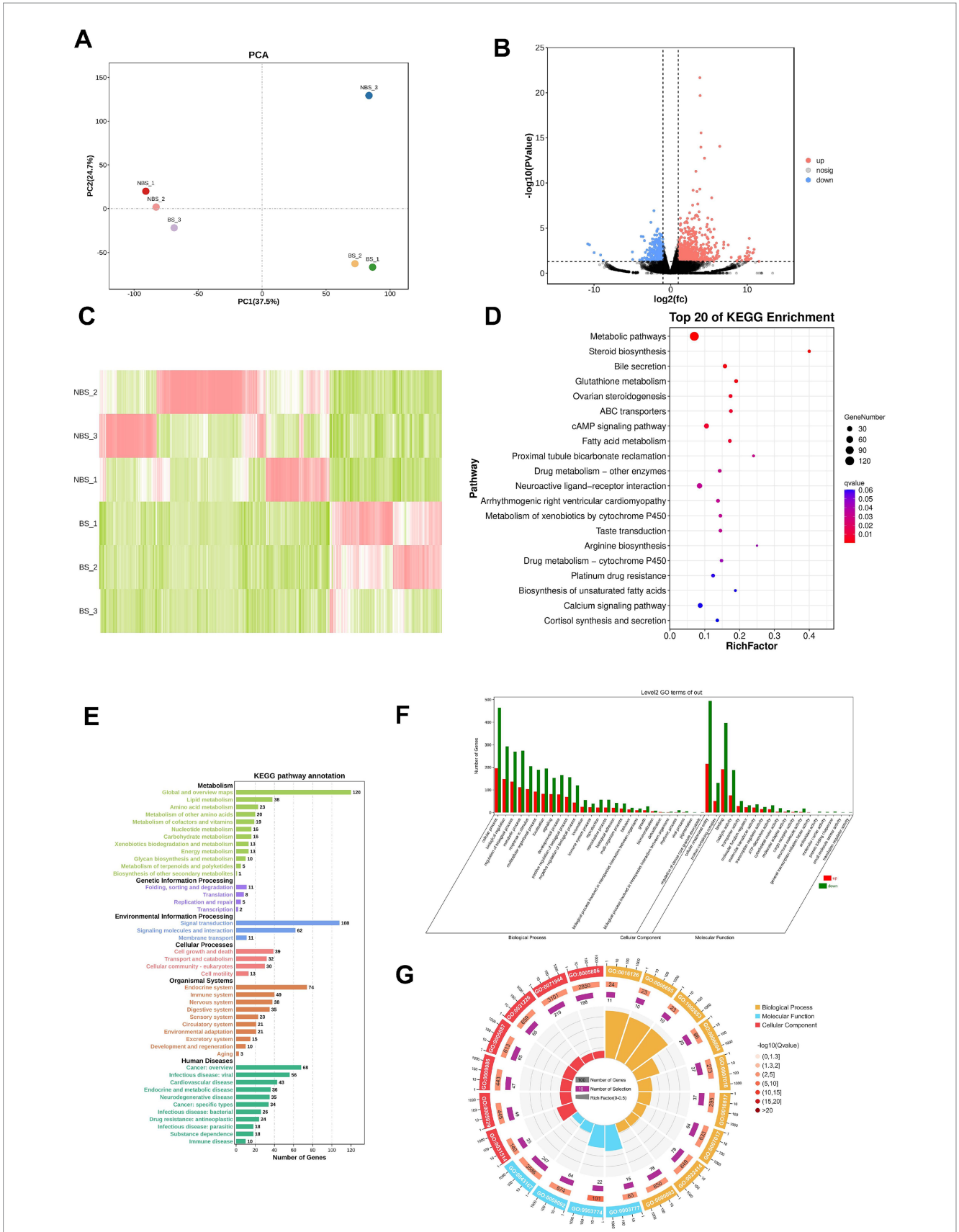

FIGURE 2
Transcriptome sequencing and bioinformatics analysis. **(A)** PCA analysis. **(B)** Volcano plot. **(C)** Heatmap of DEGs. **(D)** Top 20 pathways obtained from KEGG pathway enrichment. **(E)** KEGG pathway annotation. **(F)** GO terms enrichment analysis. **(G)** Enrichment circle plot of GO terms.

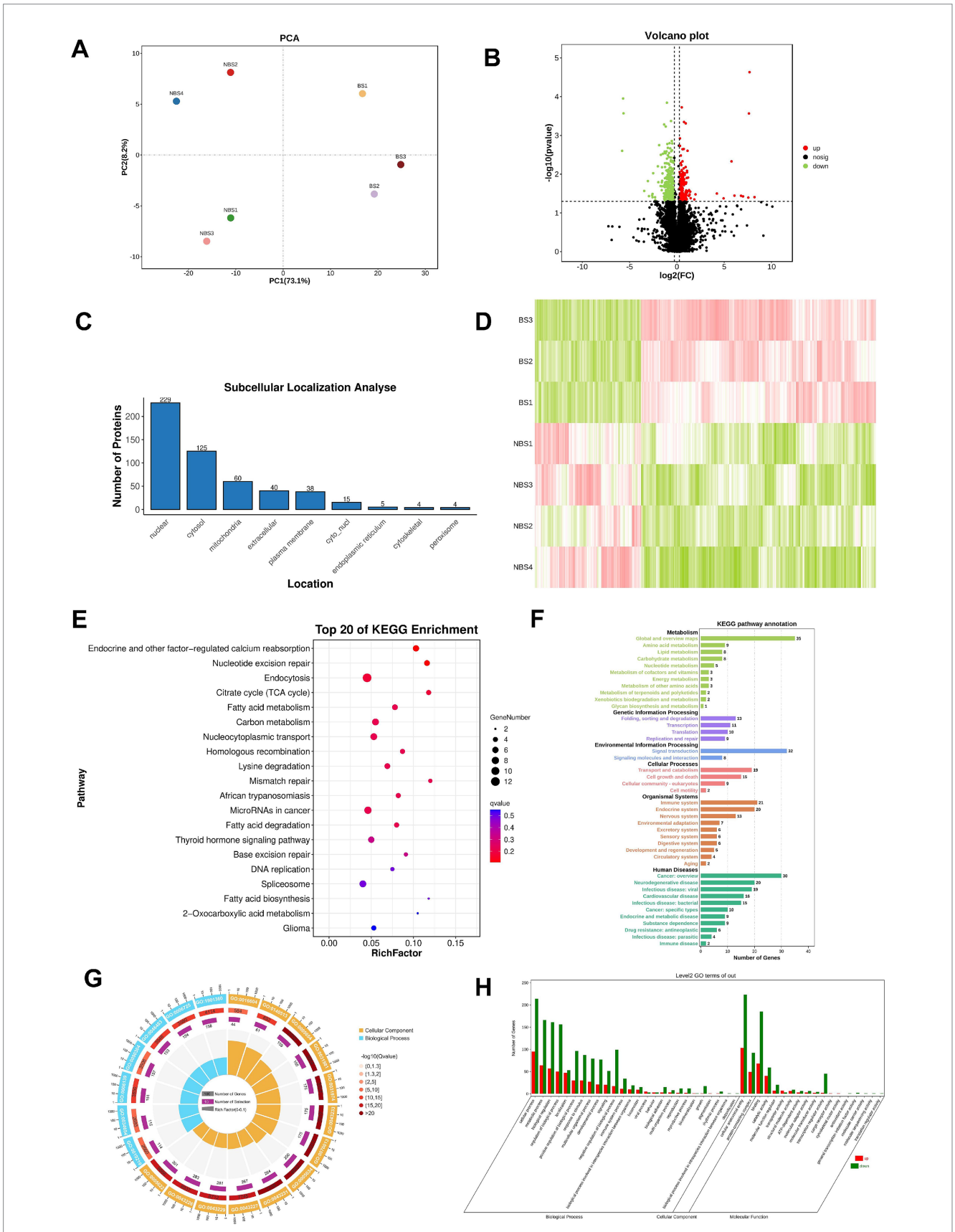

FIGURE 3
Proteomic sequencing and bioinformatics analysis. **(A)** PCA analysis. **(B)** Volcano plot. **(C)** Subcellular localization of DEPs. **(D)** Heatmap of DEPs. **(E)** Top 20 pathways obtained from KEGG pathway enrichment. **(F)** KEGG pathway annotation. **(G)** Enrichment circle plot of GO terms. **(H)** GO terms enrichment analysis.

TABLE 3 The top 20 upregulated or downregulated DEPs in NBS vs. BS.

UniProt	Gene name	Description	Log2(fc)	P-Value	UP/DOWN
A0A452E5B3	LOC108633460	-	8.20	0.039	UP
A0A452EUQ3	SLC35G1	Solute carrier family 35 member G1	7.67	<0.0001	UP
A0A452G0K2	GCA	Grancalcin	7.61	<0.0001	UP
A0A452FHU2	-	-	7.55	0.040	UP
A0A452ET71	MPC1	Mitochondrial pyruvate carrier	6.98	0.037	UP
A0A452FW07	AMDHD1	Amidohydrolase domain-containing protein 1	6.78	0.036	UP
A0A097ITJ2	DSG4	Desmoglein 4	6.08	0.036	UP
A0A8C2S393	-	-	−5.79	0.003	DOWN
A0A452EFZ7	-	-	5.77	0.005	UP
A0A452DPQ3	LYSMD3	LysM domain containing 3	−5.69	<0.0001	DOWN
A0A452FHR7	KAT2A	Lysine acetyltransferase 2A	−5.64	0.000	DOWN
A0A452F5C7	LPIN1	Phosphatidate phosphatase	4.93	0.042	UP
A0A452F944	ABLIM2	Actin binding LIM protein family member 2	4.22	0.032	UP
A0AAJ7P8Z1	MAP4	Microtubule-associated protein	−3.45	0.027	DOWN
A0A452G561	YAF2	YY1 associated factor 2	−3.07	0.015	DOWN
A0A452FBP5	VGLL4	Vestigial like family member 4	−2.96	0.037	DOWN
A0A452FRZ1	LOC108638216	-	−2.62	0.035	DOWN
A0A8C2S6S3	RAB34	RAB34, member RAS oncogene family	−2.58	0.032	DOWN
A0A452G1X2	UBE2S	E2 ubiquitin-conjugating enzyme	−2.58	0.039	DOWN
A0A452FDM1	-	-	−2.51	0.009	DOWN

(Figures 3B,D). Subcellular localization analysis revealed that the DEPs are predominantly situated in the nucleus, cytoplasm, and mitochondria (Figure 3C). Table 3 presents the log2 fold change (fc) values for the top 20 DEPs, highlighting that LOC108633460, solute carrier family 35 member (SLC35G1), and grancalcin (GCA) were upregulated by 8.20, 7.67, and 7.71 times, respectively. Conversely, the log2 (fc) values for LysM domain containing 3 (LYSMD3) and histone acetyltransferase (KAT2A) were reduced by 5.69 and 5.64 times, respectively (Table 3).

KEGG enrichment analysis identifies the top 20 enriched pathways, with the five most significant being endocrine and other factor-regulated calcium reabsorption, nucleotide excision repair, endocytosis, citrate cycle (TCA Cycle), and fatty acid metabolism. Additionally, the thyroid hormone signaling pathway, associated with steroid hormone synthesis, is also enriched (Figure 3E). Pathway annotation results indicate that there are 11 pathways each annotated to metabolism and human diseases (Figure 3F).

Furthermore, Gene Ontology (GO) analysis identifies the top 20 significantly enriched terms among the DEPs, with cellular anatomical entity, cellular process, and binding exhibiting the highest distribution of DEPs. These top 20 terms are categorized exclusively under cellular component and biological process, with no classification under molecular function (Figures 3G,H).

Conjoint analysis of DEGs and DEPs

To overcome the constraints of analyzing a single omics dataset and to improve the precision and dependability of bioinformatics analysis, a joint analysis of DEGs and DEPs was conducted. Seven common DEGs/DEPs were identified, with transmembrane protein 205 (TMEM205), transmembrane 7 superfamily member 2 (TM7SF2), solute carrier family 35 member G1 (SLC35G1), glutathione S-transferase (GSTM5), abhydrolase domain containing 6, acylglycerol lipase (ABHD6), E2 ubiquitin-conjugating enzyme (UBE2S) and insulin-like growth factor-binding protein 2 (IGFBP2)exhibiting similar expression patterns in both DEGs and DEPs (Figure 4).

Validation of selected DEGs by qRT-PCR

qRT-PCR validation was conducted on genes associated with ovarian hormone synthesis, in addition to the four shared genes identified from DEGs and DEPs. In the ovarian tissues of dairy goats during the breeding season, the expression levels of fatty acid synthase (FASN) ($p < 0.01$), low-density lipoprotein receptor (LDLR) ($p < 0.05$), follicle stimulating hormone receptor (FSHR) ($p < 0.05$), TMEM205

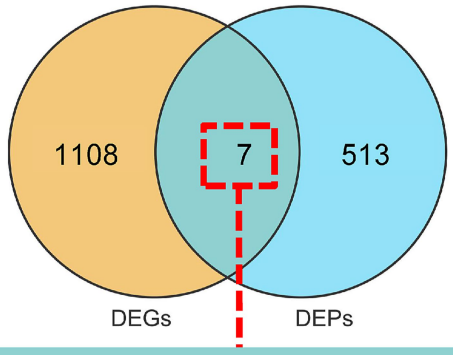

Name	Description	DEGs	DEPs	Consistency
TMEM205	Transmembrane protein 205	Up	Up	Yes
TM7SF2	Transmembrane 7 superfamily member 2	Up	Up	Yes
SLC35G1	Solute carrier family 35 member G1	Up	Up	Yes
GSTM5	Glutathione S-transferase	Down	Down	Yes
ABHD6	Abhydrolase domain containing 6, acylglycerol lipase	Up	Up	Yes
UBE2S	E2 ubiquitin-conjugating enzyme	Up	Down	No
IGFBP2	Insulin-like growth factor-binding protein 2	Up	Down	No

FIGURE 4
Conjoint Analysis of DEGs and DEPs. There are 7 shared DEGs/DEPs (green).

($p < 0.05$), TM7SF2 ($p < 0.05$), ABHD6 ($p < 0.01$) and SLC35G1 ($p < 0.05$) were significantly increased (Figures 5A–G), and the fold change showed a trend similar to the corresponding counts per million (CPM) values in the RNA sequencing results, indicating the accuracy of the RNA sequencing data (Figure 5H).

Discussion

The regulation of reproductive hormones, including FSH and LH, is a multifaceted process influenced by a range of factors, encompassing environmental cues and intrinsic physiological mechanisms. In seasonally breeding species such as goats, the secretion of these hormones is typically downregulated during the non-breeding season, resulting in diminished reproductive activity. The seasonality of goat reproduction is primarily governed by alterations in photoperiod, which modulate the negative feedback exerted by estradiol on LH secretion. Specifically, during extended photoperiods, the negative feedback of E2 is enhanced, leading to reduced LH secretion and the suppression of ovulation (12, 13). Similarly, during the non-breeding season, goats exhibit decreased levels of FSH (14). The administration of PMSG or other pharmacological agents that stimulate FSH release can induce ovulation in goats during this period. In this study, we observed that the overall concentrations of FSH and LH in the bloodstream of dairy goats during the non-breeding season are significantly lower than those observed during the breeding season. FSH and LH are pivotal gonadotropins that regulate various dimensions of ovarian follicular development, including follicular growth, maturation, and ovulation. FSH is particularly critical for follicle maturation and development, whereas LH plays a significant role in follicular development and oocyte maturation (15, 16). Furthermore, existing research suggests that follicular development is subject to seasonal influences (17, 18). Our study reveals that follicle size in dairy goats is reduced during the non-breeding season compared to the breeding season, which we attribute to diminished levels of FSH and LH during the non-breeding period. Consequently, the analysis of hormone concentrations and follicle counts indicates that the ovarian activity of dairy goats is in a quiescent state during the non-breeding season relative to the breeding season.

To further investigate the potential genetic factors underlying the differences in seasonal reproductive status, we conducted transcriptomic analysis and 4D-DIA proteomic analysis, identifying several DEGs and DEPs that may be related to ovarian function. In the study of ovarian aging, *ITGB6* is associated with the remodeling of the extracellular matrix, which may affect the fibrotic process of the ovary. Studies have shown that *ITGB6* is highly expressed in the stromal cells of aged ovaries and is associated with the cell-stromal junction process (19). In addition, previous studies have indicated that ITGB6 promotes lipid metabolism in ovarian cancer through its interaction with the PI3K signaling pathway (20). GPR22 is classified as a G protein-coupled receptor. Although research on the role of GPR22 in ovarian function is still limited, existing evidence indicates the involvement of G protein-coupled receptors in follicular development, ovulation, and ovarian steroid hormone metabolism. Within the ovarian context, the activation of the G protein-coupled estrogen receptor (GPER) is intimately associated with critical processes such as cell proliferation, differentiation, and apoptosis, all of which are essential for oocyte growth and ovulation (21). Additionally, G protein-coupled receptor 30 (GPR30) has been identified as a regulatory factor in the secretion of gonadotropins in cattle, underscoring its potential importance in reproductive regulation (22). *SLC35G1* was significantly upregulated in granulosa cells of different sizes of follicles compared to follicular membrane cells (23). It was found that the

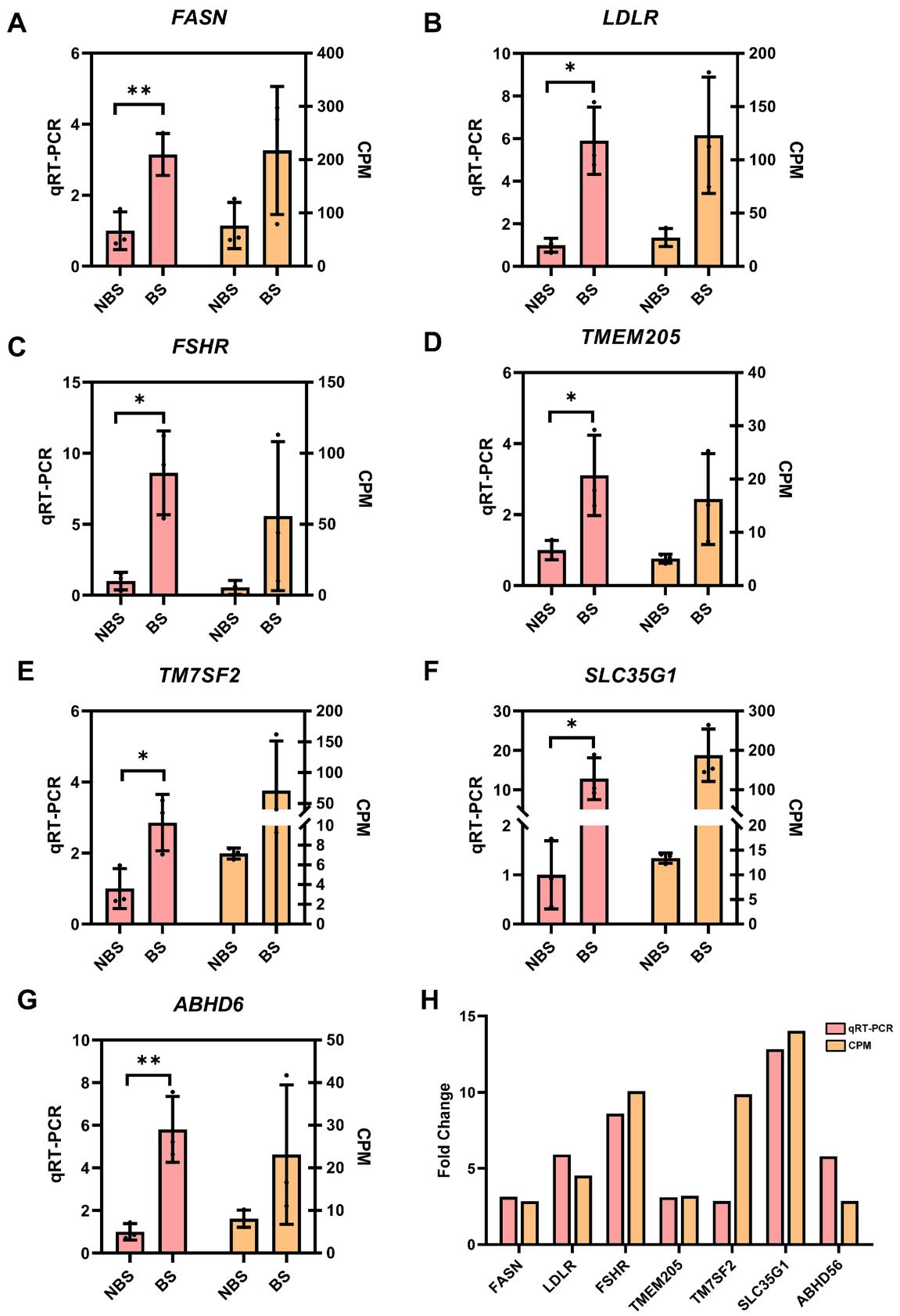

FIGURE 5
The expression of some DEGs were verified by qRT-PCR. The CPM value(right Y-axis) was taken as the relative expression level of DEGs(left Y-axiss). **(A)** *FASN*. **(B)** *LDLR*. **(C)** *FSHR*. **(D)** *TMEM205*. **(E)** *TM7SF2*. **(F)** *SLC35G1*. **(G)** *ABHD6*. **(H)** Fold change between qRT-PCR and CPM. The relative expression level of DEGs were analyzed with independent sample t-tests.*$p < 0.05$, **$p < 0.01$.

leukemia inhibitory factor promoted the expression of *KAT2A in vitro* maturation of bovine oocytes (24). The KEGG enrichment analysis reveals that the DEGs and DEPs are predominantly associated with metabolic pathways and pathways related to steroid synthesis. Metabolic pathways are integral to ovarian hormone secretion and follicular development, with metabolic status exerting a significant influence on ovarian function. This is particularly pertinent as metabolic pathways are intrinsically linked to follicle maturation (25). During follicular development, the synthesis of steroid hormones, such as estradiol and progesterone, is facilitated by both granulosa and theca cells, with secretion levels being directly modulated by FSH and LH (26). In the initial stages of follicular development, FSH enhances the expression of the steroidogenic acute regulatory protein (StAR) in granulosa cells via its receptors, thereby augmenting the transport of cholesterol to the mitochondria—a critical step in steroid synthesis (27). Concurrently, LH, through its receptors in theca cells, upregulates the expression of steroidogenic enzymes, thereby promoting the synthesis of steroid hormones (26). Our GO analysis reveals a significant enrichment of terms related to cellular processes and biological regulation among the differentially expressed genes, with a particular emphasis on those associated with ovarian development and hormone secretion. In the context of follicular development, ovarian granulosa cells engage in bidirectional communication with oocytes, a process that is crucial for the development and functionality of both cell types. Current research suggests that the interactiono between granulosa cells and oocytes can elucidate changes in gene expression during follicle maturation, as evidenced by transcriptomic analyses (28).

The integration of multi-omics analyses offers insights into various tiers of biological systems. Our comprehensive analysis of DEGs and DEPs revealed 5 common DEGs/DEPs, which demonstrated consistent expression patterns in both the transcriptomic data and RT-qPCR validation. This concordance underscores the reliability of the transcriptomic findings. The *TMEM205* gene, which encodes the transmembrane protein 205, is a member of the transmembrane protein family (29). Although research on this gene is currently limited, evidence suggests that mutations in *TMEM205* may be associated with chemotherapy resistance in ovarian cancer (30). Research has shown that *TM7SF2* is involved in the steroidogenic biosynthetic pathways of ovarian granulosa cells (31). Combining this with our results, it can be inferred that TM7SF2 may influence follicle maturation by affecting hormone synthesis in granulosa cells. Additionally, *SLC35G1* is expressed in granulosa cells, with expression levels in follicles of varying sizes surpassing those in theca cells (23). This suggests that SLC35G1 may contribute to the functional differences in synthesis between granulosa and theca cells, functions that are tightly regulated by FSH and LH, potentially due to seasonal variations in LH and FSH levels in dairy goats. Research has demonstrated that human subjects possessing the *GSTM1* deletion genotype exhibit significantly reduced testosterone levels (32). This phenomenon may be attributed to the role of GSTM1 as a steroid-binding protein, implying that GSTM1 potentially regulates steroid synthesis and thereby influences the seasonal reproductive status of dairy goats. Conversely, limited research exists regarding the role of ABHD6 in ovarian function. Research on *ABHD6* and ovarian function is scarce; however, some studies have confirmed that estrogen can promote high expression of *ABHD6* in women immune cells (33). There is a wealth of research indicating that estrogen can influence estrus in goats (34, 35). This suggests that the secretion of ovarian estrogen may differ between the breeding and non-breeding seasons.

Conclusion

In conclusion, this study utilized transcriptomic and proteomic sequencing to investigate the molecular basis of seasonal reproductive differences in dairy goats. We, respectively, identified 1,115 DEGs and 520 DEPs in ovarian tissue between the breeding and non-breeding seasons. Critically, our results demonstrate reduced FSH and LH levels and impaired follicular development during the non-breeding season. Furthermore, functional analyses strongly suggest that the genes *TMEM205*, *TM7SF2*, *SLC35G1*, *GSTM1*, and *ABHD6* contribute to suppressed ovarian function in the non-breeding season, through regulating specific roles in steroid hormone synthesis pathways. These findings offer new insights into the molecular mechanisms underlying seasonal variations in dairy goat ovaries, presenting innovative strategies to mitigate seasonal anestrus and enhance year-round milk production.

Data availability statement

The transcriptomics datasets generated during the current study are available in NCBI SRA (PRJNA1280907), https://www.ncbi.nlm.nih.gov/bioproject/PRJNA1280907. The mass spectrometry proteomics data have been deposited to the ProteomeXchange Consortium, https://proteomecentral.proteomexchange.org, via the iProX partner repository with the dataset identifier PXD065416.

Ethics statement

The animal study was approved by the Institutional Animal Care and Use Committee of Northwest A&F University. The study was conducted in accordance with the local legislation and institutional requirements.

Author contributions

CS: Data curation, Writing – original draft. QL: Supervision, Writing – review & editing. WW: Writing – review & editing. QH: Resources, Writing – review & editing. JZ: Writing – review & editing. FZ: Methodology, Writing – review & editing. LZ: Methodology, Writing – review & editing. JL: Conceptualization, Funding acquisition, Writing – review & editing.

Funding

The author(s) declare that financial support was received for the research and/or publication of this article. This research was jointly

supported by the National Key Research and Development Program of China (no. 2021YFD1600704). Shaanxi Livestock and Poultry Breeding Double-chain Fusion Key Proiect of China (2022GD-TSLD-46-0201), Hohhot City Science and Technology Plan Project (Major Science and Technology Special Project) in China (no. 2023150103000025). This work received support from the high-performance computing (HPC) resources at Northwest A&F University (NWAFU).

Conflict of interest

The authors declare that the research was conducted in the absence of any commercial or financial relationships that could be construed as a potential conflict of interest.

Generative AI statement

The authors declare that no Gen AI was used in the creation of this manuscript.

Publisher's note

All claims expressed in this article are solely those of the authors and do not necessarily represent those of their affiliated organizations, or those of the publisher, the editors and the reviewers. Any product that may be evaluated in this article, or claim that may be made by its manufacturer, is not guaranteed or endorsed by the publisher.

References

1. Zhao JQ, Mu YP, Gong P, Liu BL, Zhang FH, Zhu L, et al. Whole-genome resequencing of native and imported dairy goat identifies genes associated with productivity and immunity. *Front Vet Sci*. (2024) 11:11. doi: 10.3389/fvets.2024.1409282

2. Cabiddu A, Delgadillo-Puga C, Decandia M, Molle AG. Extensive ruminant production systems and Milk quality with emphasis on unsaturated fatty acids, volatile compounds, antioxidant protection degree and phenol content. *Animals (Basel)*. (2019) 9:771. doi: 10.3390/ani9100771

3. Liddle TA, Stevenson TJ, Majumdar G. Photoperiodic regulation of avian physiology: from external coincidence to seasonal reproduction. *J Exp Zool A Ecol Integr Physiol*. (2022) 337:890–901. doi: 10.1002/jez.2604

4. Nakane Y, Yoshimura T. Photoperiodic regulation of reproduction in vertebrates. *Annu Rev Anim Biosci*. (2019) 7:173–94. doi: 10.1146/annurev-animal-020518-115216

5. Poissenot K, Chorfa A, Moussu C, Trouillet AC, Brachet M, Chesneau D, et al. Photoperiod is involved in the regulation of seasonal breeding in male water voles (*Arvicola terrestris*). *J Exp Biol*. (2021) 224. doi: 10.1242/jeb.242792

6. Simonneaux V. A kiss to drive rhythms in reproduction. *Eur J Neurosci*. (2020) 51:509–30. doi: 10.1111/ejn.14287

7. Henningsen JB, Franois G, Valérie S. Rfrp neurons – the doorway to understanding seasonal reproduction in mammals. *Front Endocrinol*. (2016) 7:36. doi: 10.3389/fendo.2016.00036

8. Weems PW, Goodman RL, Lehman MN. Neural mechanisms controlling seasonal reproduction: principles derived from the sheep model and its comparison with hamsters. *Front Neuroendocrinol*. (2015) 37:43–51. doi: 10.1016/j.yfrne.2014.12.002

9. Mossa F, Ireland JJ. Physiology and endocrinology symposium: anti-Müllerian hormone: a biomarker for the ovarian reserve, ovarian function, and fertility in dairy cows. *J Anim Sci*. (2019) 97:1446–55. doi: 10.1093/jas/skz022

10. Evans ACO. Characteristics of ovarian follicle development in domestic animals. *Reprod Domest Anim*. (2003) 38:240–6. doi: 10.1046/j.1439-0531.2003.00439.x

11. Nogueira DM, Cavalieri J, Gummow B, Parker AJ. Comparison of follicular dynamics and hormone profiles in Boer goats examined during the breeding and non-breeding seasons in the tropics of Queensland, Australia. *Small Rum Res*. (2015) 125:93–100. doi: 10.1016/j.smallrumres.2015.02.014

12. Muñoz AL, Chesneau D, Hernández H, Bedos M, Duarte G, Vielma J, et al. Sexually active bucks counterbalance the seasonal negative feedback of estradiol on Lh in Ovariectomized goats. *Domest Anim Endocrin*. (2017) 60:42–9. doi: 10.1016/j.domaniend.2017.03.004

13. Karsch FJ, Bittman EL, Foster DL, Goodman RL, Legan SJ, Robinson JE. Neuroendocrine basis of seasonal reproduction. *Recent Prog Horm Res*. (1984) 40:185. doi: 10.1016/B978-0-12-571140-1.50010-4

14. Decourt C, Robert V, Anger K, Galibert M, Madinier JB, Liu X, et al. A synthetic Kisspeptin analog that triggers ovulation and advances puberty. *Sci Rep*. (2016) 6:6. doi: 10.1038/srep26908

15. Chaves RN, Duarte AB, Rodrigues GQ, Celestino JJ, Silva GM, Lopes CA, et al. The effects of insulin and follicle-simulating hormone (Fsh) during in vitro development of ovarian goat Preantral follicles and the relative Mrna expression for insulin and Fsh receptors and cytochrome P450 aromatase in cultured follicles. *Biol Reprod*. (2012) 87:69. doi: 10.1095/biolreprod.112.099010

16. Silva CM, Castro SV, Faustino LR, Rodrigues GQ, Brito IR, Saraiva MV, et al. Moment of addition of Lh to the culture medium improves in vitro survival and development of secondary goat pre-antral follicles. *Reprod Domest Anim*. (2011) 46:579–84. doi: 10.1111/j.1439-0531.2010.01704.x

17. Horoz H, Kasikçi G, Ak K, Alkan S, Sönmez C. Controlling the breeding season using melatonin and Progestagen in Kivircik ewes. *Turk J Vet Anim Sci*. (2003) 27:301–5.

18. Arikan MS, Mat B, Alkan H, Cevrimli MB, Akin AC, Sahin TS, et al. A Meta-analysis of the effects of synchronization protocols applied to sheep in Turkey on pregnancy rates during breeding and non-breeding seasons. *Vet Med Sci*. (2021) 7:2280–9. doi: 10.1002/vms3.610

19. Wei Y, Yu R, Cheng S, Zhou P, Mo S, He C, et al. Single-cell profiling of mouse and primate ovaries identifies high levels of Egfr for stromal cells in ovarian aging. *Mol Ther Nucleic Acids*. (2023) 31:1–12. doi: 10.1016/j.omtn.2022.11.020

20. Lin F, Li X, Wang X, Sun H, Wang Z, Wang X. Stanniocalcin 1 promotes metastasis, lipid metabolism and cisplatin Chemoresistance via the Foxc2/Itgb6 signaling Axis in ovarian Cancer. *J Exp Clin Cancer Res*. (2022) 41:129. doi: 10.1186/s13046-022-02315-3

21. Pavlik R, Wypior G, Hecht S, Papadopoulos P, Kupka M, Thaler C, et al. Induction of G protein-coupled estrogen receptor (Gper) and nuclear steroid hormone receptors by gonadotropins in human granulosa cells. *Histochem Cell Biol*. (2011) 136:289–99. doi: 10.1007/s00418-011-0846-7

22. Kadokawa H. Discovery of new receptors regulating luteinizing hormone and follicle-stimulating hormone secretion by bovine Gonadotrophs to explore a new paradigm for mechanisms regulating reproduction. *J Reprod Dev*. (2020) 66:291–7. doi: 10.1262/jrd.2020-012

23. Hatzirodos N, Hummitzsch K, Irving-Rodgers HF, Rodgers RJ. Transcriptome comparisons identify new cell markers for Theca Interna and granulosa cells from small and large antral ovarian follicles. *PLoS One*. (2015) 10:e0119800. doi: 10.1371/journal.pone.0119800

24. Vendrell-Flotats M, García-Martínez T, Martínez-Rodero I, López-Béjar M, LaMarre J, Yeste M, et al. In vitro maturation in the presence of leukemia inhibitory factor modulates gene and Mirna expression in bovine oocytes and embryos. *Sci Rep*. (2020) 10:961. doi: 10.1038/s41598-020-74961-6

25. Mantri M, Zhang HH, Vlaminck RID. A spatiotemporal molecular atlas of the ovulating mouse ovary. *Proc Natl Acad Sci U S A*. (2024) 121:18121. doi: 10.1073/pnas.2317418121

26. Zheng M, Poulsen LC, Wang NF, Mamsen LS, Johannsen ML, Styrishave B, et al. Progesterone and 17-Hydroxy-progesterone concentrations in follicular fluid and serum reflect their production in granulosa and Theca cells. *Reprod Biomed Online*. (2024) 49:103853. doi: 10.1016/j.rbmo.2024.103853

27. Fang L, Guo Y, Li Y, Jia Q, Han X, Liu B, et al. Epigallocatechin-3-Gallate stimulates Star expression and progesterone production in human granulosa cells through the 67-Kda laminin receptor-mediated Creb signaling pathway. *J Cell Physiol*. (2022) 237:687–95. doi: 10.1002/jcp.30538

28. Regassa A, Rings F, Hoelker M, Cinar U, Tholen E, Looft C, et al. Transcriptome dynamics and molecular cross-talk between bovine oocyte and its companion cumulus cells. *BMC Genomics*. (2011) 12:57. doi: 10.1186/1471-2164-12-57

29. Gallenito MJ, Qasim TS, Tutol JN, Prakash V, Dodani SC, Meloni G. A recombinant platform to characterize the role of transmembrane protein Htmem205 in Pt(ii)-drug resistance and extrusion. *Metallomics*. (2020) 12:1542–54. doi: 10.1039/d0mt00114g

30. Li LY, Kim HJ, Park SA, Lee SH, Kim LK, Lee JY, et al. Genetic profiles associated with Chemoresistance in patient-derived xenograft models of ovarian Cancer. *Cancer Res Treat*. (2019) 51:1117–27. doi: 10.4143/crt.2018.405

31. Liu ZL, Rudd MD, Hernandez-Gonzalez I, Gonzalez-Robayna I, Fan HY, Zeleznik AJ, et al. Fsh and Foxo1 regulate genes in the sterol/steroid and lipid biosynthetic pathways in granulosa cells. *Mol Endocrinol*. (2009) 23:649–61. doi: 10.1210/me.2008-0412

32. Savic-Radojevic A, Mazibrada I, Djukic T, Stankovic ZB, Pljesa-Ercegovac M, Sedlecky K, et al. Glutathione S-transferase (Gst) polymorphism could be an early marker in the development of polycystic ovary syndrome (Pcos) - an insight from non-obese and non-insulin resistant adolescents. *Endokrynol Pol*. (2018) 69:366–74. doi: 10.5603/EP.a2018.0034

33. Drehmer MN, Muniz YCN, Marrero AR, Löfgren SE. Gene expression of Abhd6, a key factor in the endocannabinoid system, can be modulated by female hormones in human immune cells. *Biochem Genet*. (2019) 57:35–45. doi: 10.1007/s10528-018-9871-8

34. Nagai K, Endo N, Tanaka T, Kamomae H. Exposure to estrogen mimicking the level of late pregnancy suppresses estrus subsequently induced by estrogen at the level of the follicular phase in Ovariectomized Shiba goats. *J Reprod Dev*. (2013) 59:123–30. doi: 10.1262/jrd.2012-140

35. Sun S, Lv M, Niu H, Luo J. Influence of repeated estrus synchronization treatment on hormone secretion, growth, and development of dairy goats. *Front Vet Sci*. (2023) 10:1333633. doi: 10.3389/fvets.2023.1333633

frontiers | Frontiers in Veterinary Science

TYPE Original Research
PUBLISHED 13 August 2025
DOI 10.3389/fvets.2025.1573093

OPEN ACCESS

EDITED BY
Pedro Aponte,
Universidad San Francisco de Quito, Ecuador

REVIEWED BY
Regiane R. Santos,
Schothorst Feed Research, Netherlands
Ke Wang,
Northwest A&F University, China

*CORRESPONDENCE
Yong Han
✉ 2642900225@qq.com

RECEIVED 08 February 2025
ACCEPTED 22 July 2025
PUBLISHED 13 August 2025

CITATION
Zhao Y, Han Y, Yuan C, Yang Y, Long Y and Xiao W (2025) Genome-wide selection signal analysis reveals copy number variation associated with litter size in Guizhou Black goat.
Front. Vet. Sci. 12:1573093.
doi: 10.3389/fvets.2025.1573093

Genome-wide selection signal analysis reveals copy number variation associated with litter size in Guizhou Black goat

Yanpin Zhao[3], Yong Han[2,1]*, Chao Yuan[2], Yang Yang[2], Yong Long[3] and Wen Xiao[3]

[1]Guizhou University of Traditional Chinese Medicine, Guiyang, China, [2]Institute of Animal Husbandry and Veterinary Sciences, Guizhou Academy of Agricultural Sciences, Guiyang, China, [3]College of Animal Science, Guizhou University, Guiyang, China

Introduction: Copy number variation (CNV) is a common form of genomic structural variation arising from genome sequence rearrangements, which primarily involves variations in the copy number of large genomic segments. This study focuses on performing selection signal analysis of CNVs to identify candidate loci and genes associated with litter size in Guizhou Black goat.

Methods: Sample selection: 30 Guizhou Black goats were divided into high-lambing and low-lambing groups based on their continuous lambing records. Genetic analysis: Phylogenetic tree construction and principal component analysis (PCA) were performed to assess genetic differences between the two groups. Selection signal indicators: Genetic differentiation index (FST) and nucleotide diversity ($\theta\varpi$) were used as indicators for identifying selection signals. CNV identification: 180 CNVs associated with litter size were identified through selection signal analysis. Functional annotation: Candidate genes within these CNVs were annotated, and further analysis was conducted using Gene Ontology (GO) and KEGG pathway enrichment methods.

Results: Genetic differentiation: Phylogenetic tree construction and PCA revealed significant differences in genetic structure between the high-lambing and low-lambing groups. CNV identification: 180 CNVs were found to be associated with litter size. Candidate genes: Functional annotation of the CNVs identified 49 candidate genes. Pathway enrichment: GO and KEGG pathway analysis revealed significant enrichment of these genes in several reproduction-related biological pathways, including the Hippo signaling pathway, steroid hormone biosynthesis, and retinol metabolism.

Discussion: This study provides novel insights into the genetic mechanisms underlying prolificacy in Guizhou Black goats. The identification of CNVs associated with litter size offers potential targets for genomic selection breeding, which could be used to improve reproductive traits in this breed. The enriched pathways, such as the Hippo signaling pathway, steroid hormone biosynthesis, and retinol metabolism, suggest that these biological processes may play a critical role in regulating fertility and reproductive efficiency in goats. The findings highlight the potential for utilizing CNVs as markers for improving reproductive performance in livestock breeding programs.

KEYWORDS

CNV, goats, litter size, whole genome sequencing, select signal

1 Introduction

As economically significant livestock, goats contribute substantially to the global production of meat, milk, and hides. Increasing production volume alone is insufficient to meet the growing global demand for goat-derived products. Enhancing goat reproductive performance is a pressing concern, as litter size is a critical trait influencing reproductive efficiency and overall productivity. Consequently, enhancing litter size has become a primary objective in goat breeding programs. While factors such as maternal nutrition and dietary supplements (e.g., folic acid) play roles in determining litter size, genetic factors are also crucial. Recently, many studies have focused on identifying genetic variants and genes associated with litter size in goats. For instance, a genome-wide association study (GWAS) identified single nucleotide polymorphism (SNP) variants associated with litter size at birth (LSB) in Markhoz goats. Candidate genes annotated from these variants include GABRA5, AKAP13, and SV2B (1). Similarly, when analyzing SNPs associated with litter size in Chuanzhong Black goats, Guo et al. utilized FST and θπ analyses to examine population selection signals. Their findings annotated 506 and 528 genes in high-litter and low-litter groups, respectively. Additionally, polymorphism analysis revealed a significant association between the g.89172108 T > G variant in the exon of the AMH gene and litter size, suggesting its potential as a marker for selecting high-fertility individuals (2). As a complex trait, litter size is influenced by multiple genetic factors. Focusing exclusively on SNPs may not provide a comprehensive understanding of their genetic basis. Copy number variation (CNV), an essential form of structural variation involving changes in the copy number of large genomic segments, can significantly impact gene expression and function. Increasing evidence indicates that CNVs play a vital role in animal reproduction. For example, a CNV-based GWAS in Canadian Holstein cattle identified two CNVRs linked to three reproductive traits: calf survival rate, interval from first service to conception, and non-return rate (3).

The Guizhou Black Goat is a local meat-type breed native to the southwestern region of Guizhou Province, China. It is characterized by a moderate body size, tender meat with a mild odor, and strong adaptability to cold climates and low-quality forage. However, its relatively low reproductive performance has become a limiting factor for the breed's development and widespread utilization. This study aims to identify copy number variations (CNVs) associated with lambing traits by analyzing whole-genome sequencing data of high- and low-litter-size Guizhou Black goat groups. We conducted selection signal analysis of CNVs between these groups to identify candidate genes potentially linked to litter size. These genes contribute to elucidating the genetic mechanisms underlying lambing traits and serve as valuable molecular markers for genetic improvement and enhanced reproductive performance in goats.

2 Materials and methods

2.1 Sample collection and whole genome resequencing

The 30 Guizhou Black goats used in this study were all sourced from Maiping Town, Huaxi District, Guizhou Province. The selected goats were healthy females aged 2–3 years, raised under uniform management conditions, and underwent annual disease screening. All experimental goats were fed a semi-grazing system, provided with the same basic diet (including silage corn, hay and concentrate) during the dry season, and allowed to eat natural pasture freely during the green season. Based on lambing records from the past 2 years, 15 high-litter-size individuals (average litter size ≥ 2) were selected to form the high-lambing group (HL), while 15 low-litter-size individuals (average litter size = 1) were chosen as the low-lambing group (LL) for whole-genome resequencing. Blood samples were collected using vacuum blood collection tubes between 8:00 and 9:00 in the morning. The studies involving animals were reviewed and approved by Guizhou University Subcommittee of Experimental Animal Ethics [eae-gzu-2024-e054]. Blood samples were collected for DNA extraction, and high-quality DNA samples were subsequently used to construct sequencing libraries. The DNBSEQ-T7 sequencer was employed to sequence, producing raw sequencing data with an average coverage depth of 33.3X.

2.2 CNV detection and annotation

To minimize errors caused by human factors during sequencing, the raw data were first filtered using Fastp (v0.23.4), and reads containing adapters were removed based on the following criteria. Paired reads were discarded if the proportion of "N" bases in a sequencing read exceeded 1% of the total bases. Additionally, paired reads were excluded if the number of low-quality bases (Q ≤ 5) in a sequencing read exceeded 50% of the total bases. Subsequently, BWA (v0.7.17) was used to align the clean reads to the reference genome (GCF_001704415.2_ARS1.2_genomic.chr), and SAMtools (v1.17) was employed to calculate basic metrics, such as sequencing depth and genome coverage, to prepare for subsequent variant detection. For structural variant (SV) detection, Manta was used to identify SVs for each individual. SVs of the same type were merged across individuals based on genomic position and variant length to remove redundancy. Paragraph genotyping was employed to genotype each individual using the deduplicated SV results. At the population level, further deduplication was performed based on positional overlap criteria (50% for deletions; 90% for insertions, inversions, and duplications) and genotype consistency (population genotype consistency ≥ 0.95).

Quality control was conducted on the deduplicated SVs using the following filtering criteria: variant length (ABS (INFO/SVLEN) ≤ 10,000,000), allelic frequency heterozygosity (INFO/ExcHet) ≥ 0.05, missing rate (F_MISSING) ≤ 0.2, and minor allele frequency (INFO/MAF) > 0. The Plink software was used to calculate CNV frequencies across all individuals, and R (v4.2.0) was used for visualization. Custom Perl scripts were employed for CNV analyses specific to different groups. Finally, all CNVs were annotated using Annovar.

2.3 Population structure analysis and selective feature detection

The experimental animals were divided into high-litter-size (HL, $n = 15$) and low-litter-size (LL, $n = 15$) groups based on their lambing records. Selection signature detection was then performed on these two groups. To understand the genetic structure of the HL and LL

groups, principal component analysis (PCA) was conducted using the GCTA software (4) with the make-grm and pca commands. The PCA results were visualized using R software.

Next, two methods, genetic differentiation index (FST) and nucleotide diversity (θπ), were employed for selection signature analysis using VCFtools (v0.1.17). For FST analysis, a sliding window approach was applied with a 100 kb chromosome interval and a 10 kb step size. Subsequently, nucleotide diversity (π) values were calculated separately for each group, and the relative difference in nucleotide diversity between the groups was determined as $\log_2(\pi HL/\pi LL)$. Candidate loci were identified by selecting those present in the top 1% of windows from both the FST sliding window analysis and the $\log_2(\pi HL/\pi LL)$ sliding window analysis.

2.4 Functional annotation and pathway enrichment of candidate gene

The resulting data were filtered further after identifying candidate CNV loci within the selected regions based on the top 1% of FST sliding window analysis and $\log_2(\pi HL/\pi LL)$. Goat gene annotation files were downloaded from the ENSEMBL database, and bedtools was used to annotate the candidate CNVs to their corresponding genes. Loci that were not enriched for genes or had negative FST values were excluded. Differential gene sets were then subjected to Gene Ontology (GO) and KEGG pathway enrichment analysis using the clusterProfiler package in R (v4.4.0). This analysis aimed to identify significantly enriched biological processes and pathways associated with the candidate CNVs.

3 Results

3.1 Identification and distribution of CNVs

Following variant detection and filtering, a total of 2,083 CNV sites were retained. All detected CNVs were deletions, and the identification statistics are presented in Figure 1. A length distribution analysis of all CNVs revealed that most loci fell within the 1–5 kb range. Functional annotation of CNV regions indicated that approximately 60.5% were located in intergenic regions, 23.8% in intronic regions, and only 10.9% in exonic regions. The proportions of CNVs in downstream (0.4%) and upstream (0.3%) regions were relatively low. CNVs related to non-coding RNA were also uncommon, with ncRNA exons accounting for 1.9% and ncRNA introns for 1.2%. Additionally, CNVs were identified in 3′ untranslated regions (3′ UTR, 0.4%), 5′ untranslated regions (5′ UTR, 0.2%), splicing sites (0.2%), and overlapping upstream and downstream regions (0.05%).

We analyzed the chromosomal distribution of CNVs and the number of CNVs at different frequencies in the HL and LL groups, and the results are shown in Figure 2. For statistical evaluation of the CNV distribution, we performed a chi-square test for the CNV distribution of each chromosome in both groups with a Bonferroni correction for multiple testing. The results, summarized in Supplementary Tables S1, S2, indicated no significant differences in CNV distribution at the chromosomal level between the HL and LL groups. Furthermore, the frequency statistics of CNVs showed no significant differences between the two groups. It is worth noting that, the results of Fisher's exact test showed that the frequencies of deletion CNVs were significantly different between the HL and LL groups in the frequency ranges of 0–0.1 and 0.2–0.3.

3.2 Analysis of group structure

The results of the principal component analysis (PCA) are presented in Figure 3. Despite some overlap between individuals from the HL and LL groups, the two groups display a distinct differentiation trend. This observation is corroborated by the phylogenetic tree in Figure 3, where all individuals are predominantly clustered into two separate branches, this also indicates that there is a clear differentiation between the two groups.

3.3 Selective signal analysis of HL and LL

The results of the selection signal analysis are presented in Figure 4. A total of 180 CNV loci were selected based on the relative difference in π values, $\log_2(\pi HL/\pi LL)$, and the top 1% of FST. After annotation, 49 candidate genes (Table 1) were identified.

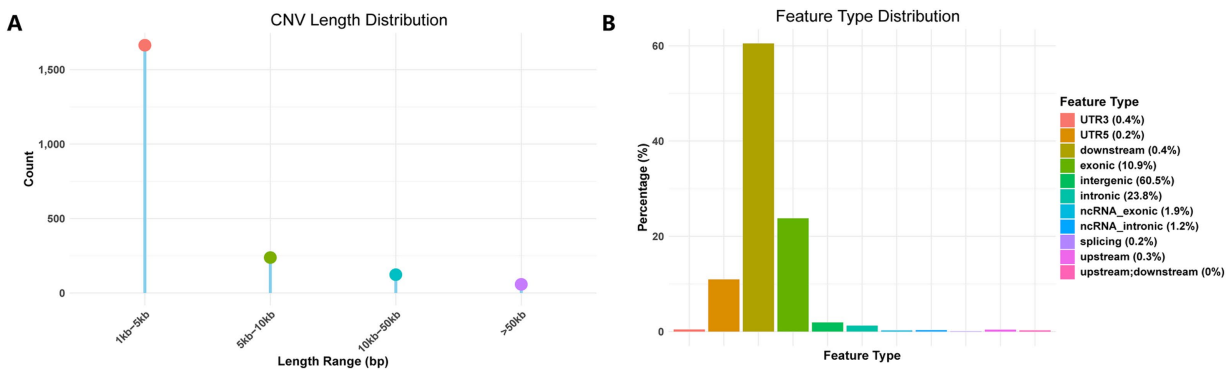

FIGURE 1
Identification statistics of CNVs. **(A)** CNV depth distribution. **(B)** Feature type distribution.

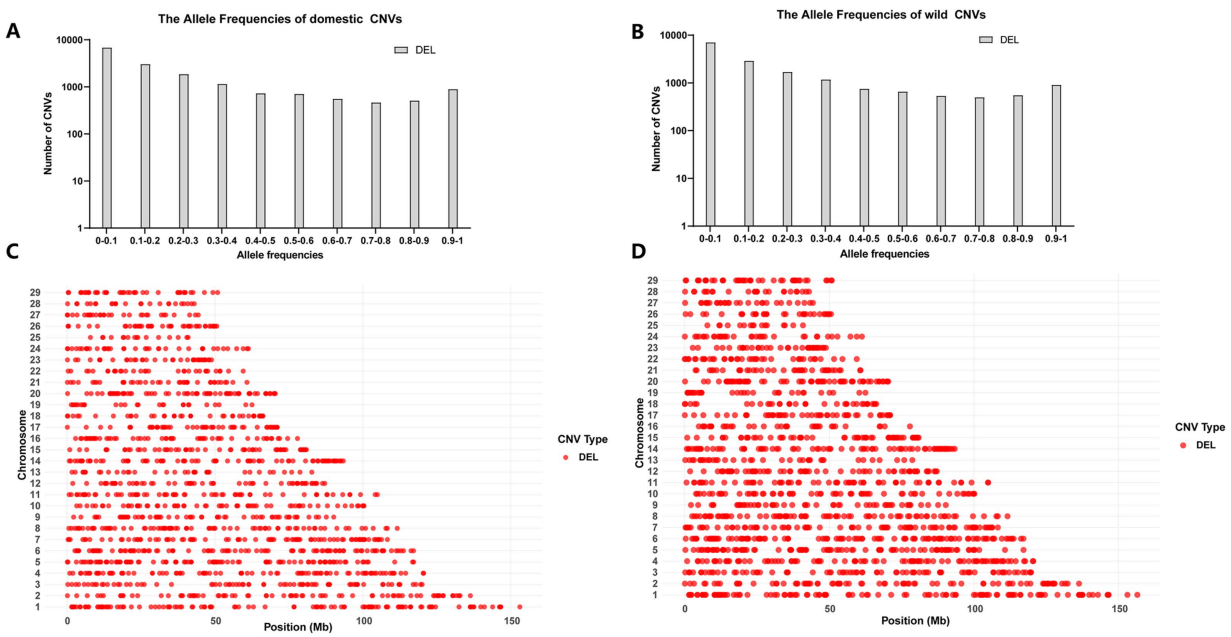

FIGURE 2
Distribution statistics of CNVs. **(A)** The number of CNVs at different frequencies in the HL group. **(B)** The number of CNVs at different frequencies in the LL group. **(C)** The distribution of chromosome CNVs in the HL group. **(D)** The distribution of chromosome CNVs in the LL group.

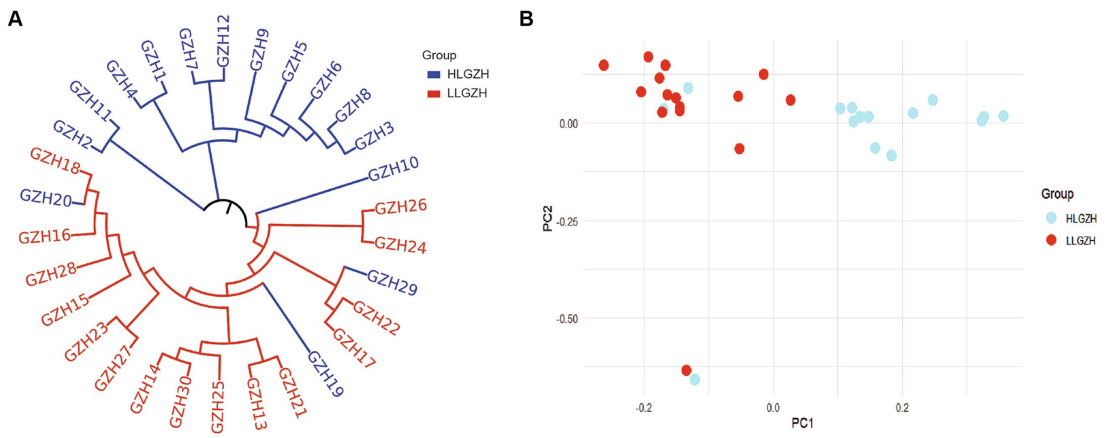

FIGURE 3
(A) Phylogenetic tree. **(B)** Principal component analysis.

3.4 GO and KEGG enrichment analysis of candidate genes

The primary significantly enriched pathways identified by GO and KEGG analyses are presented in Figure 5. A total of 59 KEGG pathways were enriched, including 14 significant pathways ($p < 0.05$), primarily associated with metabolism, hormones, signaling, and chemical carcinogenesis. The most significantly enriched pathway was ascorbate and aldate metabolism (chx00053). In the GO enrichment analysis, 532 pathways were identified, of which 134 were significant ($p < 0.05$). Among these, 453 biological processes (BP), 24 cellular components (CC), and 55 molecular functions (MF) were enriched, primarily related to apoptosis, stress response, lipid metabolism, development and regeneration, signal transduction, protein interactions, gene expression, and repair. The most significantly enriched biological process was positive regulation of cell death (GO:0010942), the most significantly enriched cellular component was connexin complex (GO:0005922), and the most significantly enriched molecular function was glucuronosyltransferase activity (GO:0015020).

4 Discussion

4.1 Distribution of CNV

We conducted a statistical analysis of the distribution and types of CNVs between the HL and LL populations. The results indicated that only deletion CNVs showed a significant difference, suggesting

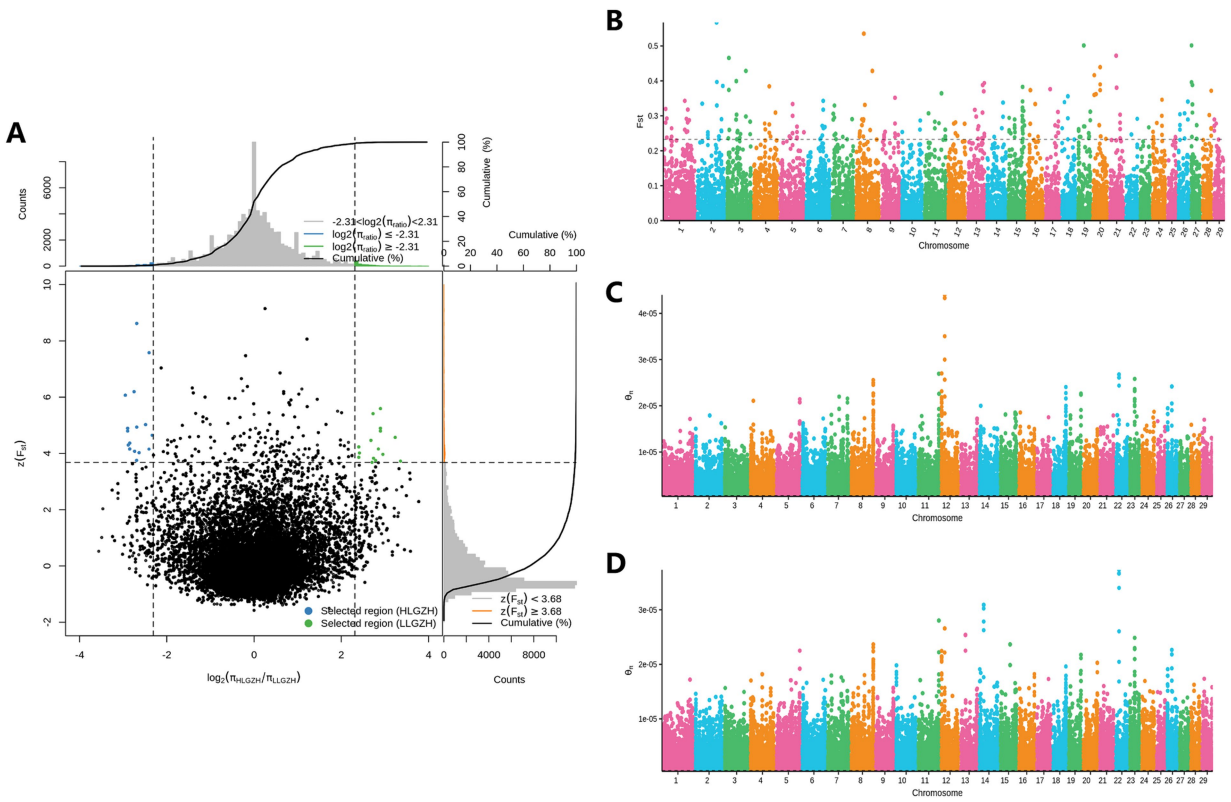

FIGURE 4
Selection of signal analysis. **(A)** Fst and $\log_2(\pi HL/\pi LL)$ for the top 1%. **(B)** Manhattan plot of all CNVs (Fst). **(C)** Manhattan plot of CNVs (π) for the LL group. **(D)** Manhattan plot of CNVs (π) for the HL group.

that the deletion copy number may be associated with lambing traits. Previous studies have demonstrated that CNV deletions are linked to animal reproductive performance. For example, Zhang Ruiqian (5) conducted a comparative analysis of CNVs in goats with different litter size trait groups. They found that in the deletion CNV analysis of high-yield and low-yield groups, 173 genes were unique to the high-yield group, indicating that the missing CNV may be related to the high litter size of goats. Similarly, Ting Sun et al. (6) found that a CNV deletion in SPAG16 was associated with reproductive ability (semen motility) in bulls.

4.2 Population structure analysis and selection signal analysis

The phylogenetic tree and principal component analysis results revealed clear genetic differentiation between the HL and LL groups, indicating structural genetic differences between the high-yield and low-yield groups, warranting further investigation. We reviewed the relevant literature and compiled statistics for the 49 selected genes (Table 1). Among them, 16 genes were classified as unknown, with no relevant studies identified. Of the remaining 33 genes, 16 have been identified in the literature as being associated with animal reproduction, while the others are linked to diseases, organ development, and cell differentiation. Notably, TRNAC-GCA was selected as a candidate gene for fertility in Katahdin ewes through whole-genome selection signal analysis (7), while STXBP6 was identified as a candidate gene in a meta-analysis of key SNPs related to pig litter size. Additionally, several candidate genes have been implicated in the regulation of ovulation-related processes in animals. For instance, GJA4 (8) supports oocyte maturation, while the roles of LINGO1 (9) and PTGER3 (10) appear more complex and may involve regulatory or inhibitory functions during follicular development and angiogenesis. Half of the 33 known candidate genes have been implicated in reproduction, further supporting the accuracy of the results in this study.

4.3 GO and KEGG enrichment

During the enrichment analysis, we identified three GO pathways directly related to placental development: "placenta development," "embryonic placenta morphogenesis," and "cell differentiation involved in embryonic placenta development." Previous studies have shown that placental traits in sheep are associated with litter size (11), and alterations in litter size can lead to a reduction in placental weight (12). Abnormal placental development also can result in the death of some embryos, thereby reducing litter size. Furthermore, the placenta secretes various hormones that regulate pregnancy maintenance and fetal development, which influence litter size. For example, the placenta secretes progesterone (13), and research has shown that progesterone plays a role in determining bovine oocyte quality and embryo development (14). Oocyte quality and embryo development are closely linked to litter size. The two most significant GO terms in

TABLE 1 Candidate gene functions (References (8–10, 21–48) are all listed in the table in top and bottom order).

Gene		Functionality	Reference
GJA4	Reproduction	Maturation and developmental competence of bovine oocytes	(8)
LINGO1		Bovine oocyte development	(9)
PTGER3		Promotes the onset of ovulation in monkeys	(10)
ZNF131		Inhibits estrogen signaling	(21)
MIR186		Regulates Follicle Stimulating Hormone (FSH) Expression	(22)
GJB3		Gene expression affects mouse embryo survival	(23)
HNF4A		Human Embryonic Stem Cell Differentiation	(24)
KDM4C		Mouse Embryonic Stem Cell Identity	(25)
PCDH15		Mouse Embryonic Development	(26)
SOX5		Involvement in mouse gonadal development	(27)
AXIN2		Human Embryonic Stem Cell Self-Renewal	(28)
STXBP6		Candidate Genes for Littering Traits in Pigs	(29)
TRNAC-GCA		Candidate genes for fertility in sheep	(7)
STK17B		Causes severe defects in porcine sperm acrosomes	(30)
CEP112		Coordinate spermatogenesis	(5)
DNAH7		Male reproductive disorders (sperm motility)	(32)
ALDH5A1	Disease	Good predictor of ovarian cancer	(33)
DGKE		Causes kidney related diseases	(34)
DLGAP3		Brain disorders	(35)
GPLD1		New therapeutic target for chronic diseases	(36)
PPP2R2B		Inhibitors of Triple Negative Breast Cancer (TNBC)	(37)
SERINC3		Limits HIV-1 Infectivity	(38)
TRNAG-CCC		Involved in inflammatory process of mastitis	(39)
TTPAL		Promotes gastric tumorigenesis	(40)
UTRN		Potential Biomarkers for Breast Cancer	(41)
ZNF438		Polycystic Ovary Syndrome (PCOS) Candidate Genes	(42)
ZRANB2		Involved in Adriamycin Resistance in Breast Cancer Cells	(43)
BET1	Other	Regulates protein transport between the endoplasmic reticulum and the Golgi apparatus	(44)
GJB4, GJB5		Mouse Epididymis Development	(45)
KIAA0319		Human neuroepithelial cell development	(46)
PKIG		Osteoblast differentiation	(47)
R3HDML		Satellite cell proliferation and differentiation	(48)
C19H17orf67, LOC102168522, LOC102179380, LOC102180243, LOC102180519, LOC102180784, LOC102183140, LOC102187692, LOC102188962, LOC102189228, LOC102189502, LOC102189778, LOC106501965, LOC108633190, LOC108638409, SMIM12			NA

the enrichment analysis were "connexin complex" and "gap junction," both of which are critical components of cell-to-cell communication and closely linked to reproductive function. Studies on gap junction proteins in the female reproductive organs of mice have shown that certain connexins (such as CX43, CX37, and CX26) are vital for female reproductive function (15).

In the KEGG enrichment analysis, we identified several pathways directly related to animal reproduction, such as the Hippo Signaling Pathway, Steroid Hormone Biosynthesis, and Retinol Metabolism. Studies have shown that the Hippo signaling pathway plays a critical role in ovarian development, follicular development, and oocyte maturation (16). Steroid hormones, including estrogen, progesterone, and testosterone, are directly involved in regulating the reproductive system and serve as core pathways for reproduction, controlling follicular development, ovulation, and pregnancy maintenance (17). Additionally, retinol (vitamin A) plays a vital role in the reproductive system, particularly in regulating embryonic development (18), follicular maturation, and spermatogenesis (19).

Notably, when we created Sankey bubble plots for the GO and KEGG enrichment results, we identified three genes common to both plots: LOC102168522, LOC102183140, and LOC108633190. A review of the relevant literature revealed that, while the overexpression of

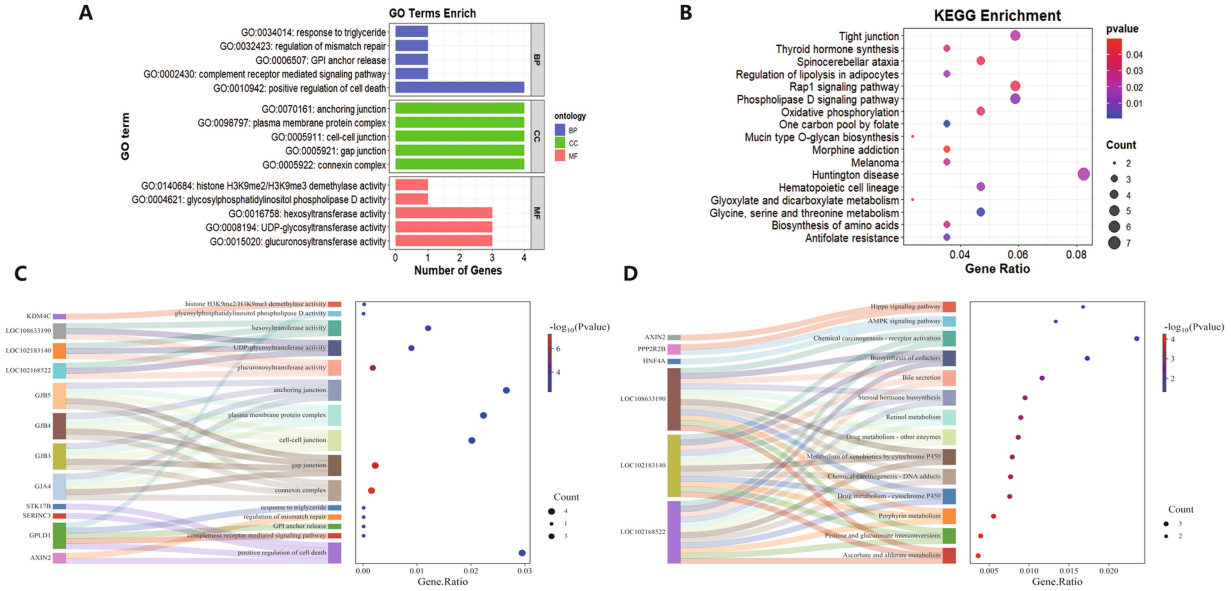

FIGURE 5
GO and KEGG enrichment. **(A)** GO-enriched PB, CC, and MF top 5. **(B)** KEGG top 17 significant pathways. **(C)** GO top 15 Sankey bubble plots. **(D)** KEGG top 14 Sankey bubble plots.

LOC102168552 has been shown to promote the growth of mammary epithelial cells (20), no studies have reported on the functional roles of the other two genes. We hypothesize that these three genes may be associated with lambing performance in Guizhou Black goats; however, definitive conclusions can only be drawn through further in-depth investigation of these genes.

5 Conclusion

In this study, we conducted a genome-wide selection signal analysis using the genetic differentiation index (Fst) and nucleotide diversity ($\theta\pi$) to identify CNVs associated with lambing performance in Guizhou Black goats. A total of 2083 CNVs were detected in the HL and LL groups, and 180 CNVs were selected as potentially associated with lambing performance. Furthermore, we identified 49 candidate genes, including TRNAC-GCA, STXBP6, and GJA4, which may be linked to lambing traits.

Data availability statement

The original sequence data of Guizhou Black Goat used in this paper have been deposited in the National Genome Science Data Center (Nucleic Acids Research 2022) and are publicly accessible at the following URL: https://bigd.big.ac.cn/gsa/browse/CRA019130.

Ethics statement

The studies involving animals were reviewed and approved by Guizhou University Subcommittee of Experimental Animal Ethics [eae-gzu-2024-e055].

Author contributions

YZ: Conceptualization, Data curation, Writing – original draft, Writing – review & editing. YH: Investigation, Methodology, Writing – original draft, Writing – review & editing. CY: Supervision, Validation, Writing – review & editing. YY: Project administration, Software, Writing – review & editing. YL: Methodology, Project administration, Writing – review & editing. WX: Validation, Formal analysis, Writing – review & editing.

Funding

The author(s) declare that financial support was received for the research and/or publication of this article. The sources of funding for this study were Innovative Utilization of Livestock and Poultry Germplasm Resources and Construction of Basic Science and Technology Platform (Qiannongke Technology Innovation [2023] 04) and Major Special Projects of the Guizhou Province Department of Science and Technology provided funding for this work (Qianke Service Enterprise [2020] 4009).

Acknowledgments

Thanks to everyone who helped with this article.

Conflict of interest

The authors declare that the research was conducted in the absence of any commercial or financial relationships that could be construed as a potential conflict of interest.

Generative AI statement

The authors declare that no Gen AI was used in the creation of this manuscript.

Publisher's note

Supplementary material

The Supplementary material for this article can be found online at: https://www.frontiersin.org/articles/10.3389/fvets.2025.1573093/full#supplementary-material

References

1. Mahmoudi P, Rashidi A, Nazari-Ghadikolaei A, Rostamzadeh J, Razmkabir M, Huson HJ. Genome-wide association study reveals novel candidate genes for litter size in Markhoz goats. *Front Vet Sci*. (2022) 9:1045589. doi: 10.3389/fvets.2022.1045589

2. Guo C, Ye J, Liu J, Li Z, Deng M, Guo Y, et al. Whole-genome sequencing identified candidate genes associated with high and low litter size in Chuanzhong black goats. *Front Vet Sci*. (2024) 11:1420164. doi: 10.3389/fvets.2024.1420164

3. Rojas DOH, Chud T, Oliveira GJ, Hermisdorff IC, Narayana SG, Rochus CM, et al. Genome-wide association analyses reveal copy number variant regions associated with reproduction and disease traits in Canadian Holstein cattle. *J Dairy Sci*. (2024) 107:7052–63. doi: 10.3168/jds.2023-24295

4. Yang J, Lee SH, Goddard ME, Visscher PM. GCTA: A tool for genome-wide complex trait analysis[J]. *Am J Hum Genet*. (2011) 88:76–82. doi: 10.1016/j.ajhg.2010.11.011

5. Zhang RQ, Wang JJ, Zhang T, Zhai HL, Shen W. Copy-number variation in goat genome sequence: a comparative analysis of the different litter size trait groups. *Gene*. (2019) 696:40–6. doi: 10.1016/j.gene.2019.02.027

6. Sun T, Pei S, Liu Y, Hanif Q, Xu H, Chen N, et al. Whole genome sequencing of simmental cattle for SNP and CNV discovery. *BMC Genomics*. (2023) 24:179. doi: 10.1186/s12864-023-09248-x

7. Sanchez-Ramos R, Trujano-Chavez MZ, Gallegos-Sanchez J, Becerril-Perez CM, Cadena-Villegas S, Cortez-Romero C. Detection of candidate genes associated with fecundity through genome-wide selection signatures of Katahdin ewes. *Animals*. (2023) 13:272. doi: 10.3390/ani13020272

8. Hao T, Xu X, Hao H, Du W, Pang Y, Zhao S, et al. Melatonin improves the maturation and developmental ability of bovine oocytes by up-regulating GJA4 to enhance gap junction intercellular communication. *Reprod Fertil Dev*. (2021) 33:760–71. doi: 10.1071/RD21145

9. Janowski D, Salilew-Wondim D, Torner H, Tesfaye D, Ghanem N, Tomek W, et al. Incidence of apoptosis and transcript abundance in bovine follicular cells is associated with the quality of the enclosed oocyte. *Theriogenology*. (2012) 78:656–669.e5. doi: 10.1016/j.theriogenology.2012.03.012

10. Trau HA, Davis JS, Duffy DM. Angiogenesis in the primate ovulatory follicle is stimulated by luteinizing hormone via prostaglandin E2. *Biol Reprod*. (2015) 92:15. doi: 10.1095/biolreprod.114.123711

11. Ocak S, Emsen E, Koycegiz F, Kutluca M, Onder H. Comparison of placental traits and their relation to litter size and parity weight in sheep. *J Anim Sci*. (2009) 87:3196–201. doi: 10.2527/jas.2009-1913

12. Mesa H, Safranski TJ, Johnson RK, Lamberson WR. Correlated response in placental efficiency in swine selected for an index of components of litter size 1,2. *J Anim Sci*. (2003) 81:74–9. doi: 10.2527/2003.81174x

13. Tuckey RC. Progesterone synthesis by the human placenta. *Placenta*. (2005) 26:273–81. doi: 10.1016/j.placenta.2004.06.012

14. Lonergan P. Influence of progesterone on oocyte quality and embryo development in cows. *Theriogenology*. (2011) 76:1594–601. doi: 10.1016/j.theriogenology.2011.06.012

15. Winterhager E, Kidder GM. Gap junction connexins in female reproductive organs: implications for women's reproductive health. *Hum Reprod Update*. (2015) 21:340–52. doi: 10.1093/humupd/dmv007

16. Clark KL, George JW, Przygrodzka E, Plewes MR, Hua G, Wang C, et al. Hippo signaling in the ovary: emerging roles in development, fertility, and disease. *Endocr Rev*. (2022) 43:1074–96. doi: 10.1210/endrev/bnac013

17. Drummond AE. The role of steroids in follicular growth. *Reprod Biol Endocrinol*. (2006) 4:16. doi: 10.1186/1477-7827-4-16

18. Clagett-Dame M, Deluca HF. The role of vitamin a in mammalian reproduction and embryonic development. *Annu Rev Nutr*. (2002) 22:347–81. doi: 10.1146/annurev.nutr.22.010402.102745E

19. Hogarth CA, Griswold MD. The key role of vitamin a in spermatogenesis. *J Clin Invest*. (2010) 120:956–62. doi: 10.1172/JCI41303

20. Xuan R, Zhao X, Li Q, Zhao Y, Wang Y, Du S, et al. Characterization of long noncoding RNA in nonlactating goat mammary glands reveals their regulatory role in mammary cell involution and remodeling. *Int J Biol Macromol*. (2022) 222:2158–75. doi: 10.1016/j.ijbiomac.2022.09.291

21. Oh Y, Chung KC. Zinc finger protein 131 inhibits estrogen signaling by suppressing estrogen receptor α homo-dimerization. *Biochem Biophys Res Commun*. (2013) 430:400–5. doi: 10.1016/j.bbrc.2012.11.031

22. Han DX, Xiao Y, Wang CJ, Jiang H, Gao Y, Yuan B, et al. Regulation of FSH expression by differentially expressed miR-186-5p in rat anterior adenohypophyseal cells. *PLoS One*. (2018) 13:e0194300. doi: 10.1371/journal.pone.0194300

23. Plum A, Hallas G, Willecke K. Expression of the mouse gap junction gene Gjb3 is regulated by distinct mechanisms in embryonic stem cells and keratinocytes. *Genomics*. (2002) 79:24–30. doi: 10.1006/geno.2001.6671

24. Delaforest A, Nagaoka M, Si-Tayeb K, Noto FK, Konopka G, Battle MA, et al. HNF4a is essential for specification of hepatic progenitors from human pluripotent stem cells. *Development*. (2011) 138:4143–53. doi: 10.1242/dev.062547

25. Das PP, Shao Z, Beyaz S, Apostolou E, Pinello L, De Los AA, et al. Distinct and combinatorial functions of Jmjd2b/Kdm4b and Jmjd2c/Kdm4c in mouse embryonic stem cell identity. *Mol Cell*. (2014) 53:32–48. doi: 10.1016/j.molcel.2013.11.011

26. Murcia CL, Woychik RP. Expression of Pcdh15 in the inner ear, nervous system and various epithelia of the developing embryo. *Mech Dev*. (2001) 105:163–6. doi: 10.1016/s0925-4773(01)00388-4

27. Schartl M, Schories S, Wakamatsu Y, Nagao Y, Hashimoto H, Bertin C, et al. Sox5 is involved in germ-cell regulation and sex determination in medaka following co-option of nested transposable elements. *BMC Biol*. (2018) 16:16. doi: 10.1186/s12915-018-0485-8

28. Kim H, Wu J, Ye S, Tai CI, Zhou X, Yan H, et al. Modulation of β-catenin function maintains mouse epiblast stem cell and human embryonic stem cell self-renewal. *Nat Commun*. (2013) 4:2403. doi: 10.1038/ncomms3403

29. Sell-Kubiak E, Dobrzanski J, Derks M, Lopes MS, Szwaczkowski T. Meta-analysis of SNPs determining litter traits in pigs. *Genes*. (2022) 13:1730. doi: 10.3390/genes13101730

30. Sironen A, Uimari P, Nagy S, Paku S, Andersson M, Vilkki J. Knobbed acrosome defect is associated with a region containing the genes STK17b and HECW2 on porcine chromosome 15. *BMC Genomics*. (2010) 11:699. doi: 10.1186/1471-2164-11-699

31. Zhang X, Huang G, Jiang T, Meng L, Li T, Zhang G, et al. CEP112 coordinates translational regulation of essential fertility genes during spermiogenesis through phase separation in humans and mice. *Nat Commun*. (2024) 15:8465. doi: 10.1038/s41467-024-52705-8

32. Whitfield M, Thomas L, Bequignon E, Schmitt A, Stouvenel L, Montantin G, et al. Mutations in DNAH17, encoding a sperm-specific axonemal outer dynein arm heavy chain, cause isolated male infertility due to Asthenozoospermia. *Am J Hum Genet*. (2019) 105:198–212. doi: 10.1016/j.ajhg.2019.04.015

33. Shen T, Wang H, Tang B, Zhu G, Wang X. The impact of RNA binding proteins and the associated long non-coding RNAs in the TCA cycle on cancer pathogenesis. *RNA Biol*. (2023) 20:223–34. doi: 10.1080/15476286.2023.2216562

34. Ozaltin F, Li B, Rauhauser A, An SW, Soylemezoglu O, Gonul II, et al. DGKE variants cause a glomerular microangiopathy that mimics membranoproliferative GN. *J Am Soc Nephrol*. (2013) 24:377–84. doi: 10.1681/ASN.2012090903

35. Rasmussen AH, Rasmussen HB, Silahtaroglu A. The DLGAP family: neuronal expression, function and role in brain disorders. *Mol Brain*. (2017) 10:43. doi: 10.1186/s13041-017-0324-9

36. Cao J, Zhou A, Zhou Z, Liu H, Jia S. The role of GPLD1 in chronic diseases. *J Cell Physiol*. (2023) 238:1407–15. doi: 10.1002/jcp.31041

37. Li Z, Li Y, Wang X, Yang Q. PPP2R2B downregulation is associated with immune evasion and predicts poor clinical outcomes in triple-negative breast cancer. *Cancer Cell Int*. (2021) 21:13. doi: 10.1186/s12935-020-01707-9

38. Usami Y, Wu Y, Gottlinger HG. SERINC3 and SERINC5 restrict HIV-1 infectivity and are counteracted by Nef. *Nature*. (2015) 526:218–23. doi: 10.1038/nature15400

39. Silva AA, Silva DA, Silva FF, Costa CN, Silva HT, Lopes PS, et al. GWAS and gene networks for milk-related traits from test-day multiple lactations in Portuguese Holstein cattle. *J Appl Genet*. (2020) 61:465–76. doi: 10.1007/s13353-020-00567-3

40. Liu W, Gou H, Wang X, Li X, Hu X, Su H, et al. TTPAL promotes gastric tumorigenesis by directly targeting NNMT to activate PI3K/AKT signaling. *Oncogene*. (2021) 40:6666–79. doi: 10.1038/s41388-021-01838-x

41. Li H, Zhang W, Liu Y, Cai Z, Lan A, Shu D, et al. UTRN as a potential biomarker in breast cancer: a comprehensive bioinformatics and in vitro study. *Sci Rep*. (2024) 14:7702. doi: 10.1038/s41598-024-58124-5

42. Wu X, Wang CC, Cao Y, Li J, Li Z, Ma H, et al. Novel genetic risk and metabolic signatures of insulin signaling and Androgenesis in the anovulation of polycystic ovary syndrome. *Engineering*. (2023) 23:103–11. doi: 10.1016/j.eng.2022.08.013

43. Tanaka I, Chakraborty A, Saulnier O, Benoit-Pilven C, Vacher S, Labiod D, et al. ZRANB2 and SYF2-mediated splicing programs converging on ECT2 are involved in breast cancer cell resistance to doxorubicin. *Nucleic Acids Res*. (2020) 48:2676–93. doi: 10.1093/nar/gkz1213

44. Newman AP, Graf J, Mancini P, Rossi G, Lian JP, Ferro-Novick S. SEC22 and SLY2 are identical. *Mol Cell Biol*. (1992) 12:3663–4. doi: 10.1128/mcb.12.8.3663-3664.1992

45. Cyr DG, Adam C, Dufresne J, Gregory M. Regulation of the gap junction interplay during postnatal development in the rat epididymis. *Cell Tissue Res*. (2024) 398:191–206. doi: 10.1007/s00441-024-03919-1

46. Paniagua S, Cakir B, Hu Y, Kiral FR, Tanaka Y, Xiang Y, et al. Dyslexia associated gene KIAA0319 regulates cell cycle during human neuroepithelial cell development. *Front Cell Dev Biol*. (2022) 10:967147. doi: 10.3389/fcell.2022.967147

47. Chen X, Hausman BS, Luo G, Zhou G, Murakami S, Rubin J, et al. Protein kinase inhibitor γ reciprocally regulates osteoblast and adipocyte differentiation by downregulating leukemia inhibitory factor. *Stem Cells*. (2013) 31:2789–99. doi: 10.1002/stem.1524

48. Sakamoto K, Furuichi Y, Yamamoto M, Takahashi M, Akimoto Y, Ishikawa T, et al. R3hdml regulates satellite cell proliferation and differentiation. *EMBO Rep*. (2019) 20:e47957. doi: 10.15252/embr.201947957

Frontiers in Veterinary Science

Transforms how we investigate and improve animal health

The third most-cited veterinary science journal, bridging animal and human health with a comparative approach to medical challenges. It explores innovative biotechnology and therapy for improved health outcomes.

Discover the latest Research Topics

See more →

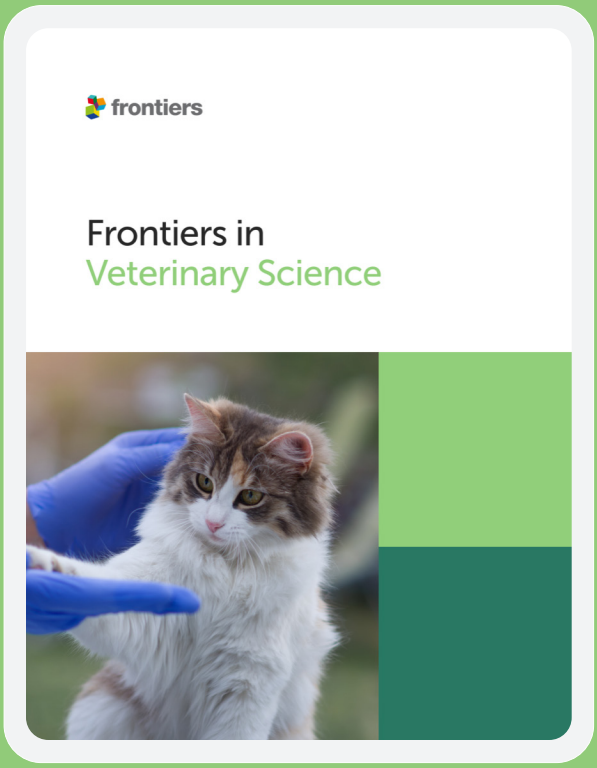

Frontiers

Avenue du Tribunal-Fédéral 34
1005 Lausanne, Switzerland
frontiersin.org

Contact us

+41 (0)21 510 17 00
frontiersin.org/about/contact